

# **Design and Syntheses of Neutral N-donor Linker Based Metal-Organic Frameworks (MOFs) Towards Environmental Applications**

A Thesis

Submitted in Partial Fulfillment of the Requirements for the  
Degree of

**Doctor of Philosophy**

by

**Aamod V. Desai**

ID: 20112011



**Indian Institute of Science Education and Research (IISER), Pune**

**2018**

Dedicated to

*Aaj, Baba and Shalmalee*



Indian Institute of Science Education and Research (IISER), Pune

---

## Certificate

---

It is hereby certified that the work described in this thesis entitled "*Design and Syntheses of Neutral N-donor Linker Based Metal-Organic Frameworks (MOFs) Towards Environmental Applications*" submitted by *Mr. Aamod V. Desai* was carried out by the candidate, under my supervision. The work presented here or any part of it has not been included in any other thesis submitted previously for the award of any degree or diploma from any other university or institution.

Date: 31<sup>st</sup> May, 2018

A handwritten signature in blue ink, appearing to read "Sujit K. Ghosh", written over a horizontal line.

**Dr. Sujit K. Ghosh**

Research Supervisor

Email: [sghosh@iiserpune.ac.in](mailto:sghosh@iiserpune.ac.in)

Contact No.: +91 (20) 25908076

## Declaration

I declare that this written submission represents my ideas in my own words and wherever other's ideas have been included; I have adequately cited and referenced the original sources. I also declare that I have adhered to all principles of academic honesty and integrity and have not misrepresented or fabricated or falsified any idea/data/fact/source in my submission. I understand that violation of the above will cause for disciplinary action by the Institute and can also evoke penal action from the sources which have thus not been properly cited or from whom proper permission has not been taken when needed.

Date: 31<sup>st</sup> May, 2018



**Aamod V. Desai**

ID: 20112011



## Acknowledgement

I take this opportunity to express my deep gratitude towards my PhD supervisor Dr. Sujit K. Ghosh, for shaping my research over the last five years. He has been a source of constant motivation and a diligent mentor who imbibed work ethics required for developing scientific temper and aptitude. I joined the lab as the first integrated-PhD student and despite tight deadlines or delays at different steps in the process, his contribution in all aspects have helped me progress and endure the journey with wholesome learning and assimilation of various skills and traits. Thank you sir for being an encouraging supervisor, believing in me and for keeping a positive outlook in all situations.

I deeply acknowledge the first director of IISER, Pune Prof. K. N. Ganesh and the current director Prof. J. B. Udgaonkar for providing a state-of-art institute having a vibrant research environment. I am extremely grateful to my research advisory committee (RAC) members, Dr. Amitava Das (CSIR-CSMCRI, Bhavnagar), Dr. Sakya Sen (NCL, Pune) and Dr. Partha Hazra (IISER, Pune) for their insights and suggestions during the annual meetings and during informal discussions. I thank Prof. M. Jayakannan (Chair, Chemistry department) and all the faculty members of the department for fostering a stimulating research environment in the department and being approachable for any queries. Being a part of the first batch of the integrated-PhD program in the institute, I wish to thank all the co-ordinators - Dr. A. Mukherjee, Dr. P. Mandal, Dr. S. G. Srivatsan, Dr. S. Chaudhury, Dr. R. Vaidhyanathan, who assisted throughout the program and made it a smooth journey to experience. I thank all the collaborators - especially Dr. Jing Li (Rutgers, USA), Dr. Rajamani Krishna (University of Amsterdam, Netherlands), Dr. Ravichandar Babarao (CSIRO, Australia), Dr. Mandar M. Shirolkar (University of Technology of China), Dr. Pablo Serra Crespo (TU Delft, Netherlands), who assisted in completion of different projects.

I would like to express my sincere regards towards Dr. A. D. Natu (MES Abasaheb Garware College), Dr. R. C. Chikate (MES Abasaheb Garware College), Dr. A. A. Natu (IISER Pune) and Dr. B. S. M. Rao (IISER Pune) for pushing me to pursue a PhD degree. I am grateful to Dr. Partha Hazra (IISER Pune), Dr. R. G. Bhat (IISER Pune) and Dr. Anirban Hazra (IISER Pune) and the senior students in their lab (Dr. Abhigyan Sengupta, Dr.

Tushar Khopade) who mentored me during the lab rotations which directly helped me shape my research aptitude and scope and prepared me for the long vigil ahead. I express my sincere gratitude to Ma'am (Dr. Sudarshana Mukherjee) for her friendly advices; and I wish Suvan all the best for his future.

The PhD experience has been enriched by each and every member (present and alumni) of the 'Microporous Materials Lab' group (Dr. Sanjog Nagarkar, Dr. Biplab Joarder, Dr. Biplab Manna, Dr. Soumya Mukherjee, Dr. Avishek Karmakar, Dr. Abhijeet Chaudhari, Dr. Partha Chowdhury, Dr. Tarak Nath Mandal, Dr. Sreenu Bhanoth, Dinesh Mullangi, Arif Inamdar, Shilpa Sonar, Partha Samanta, Shivani Sharma, Samraj Mollick, Yogeshwar More, Prateek Agrawal, Arunabha Sen, Subhajit Dutta, Sumanta Let, Writakshi Mandal, Sahel Fajal, Amrit Kumar, Shweta Singh, Naveen Kumar, Priyanshu Chandra) who have contributed significantly at different stages in varied capacities. I wish to thank all my seniors - Sanjog, Biplab bhaiyya, Manna, Abhijeet, Somu bhaiyya and Avishek bhaiyya for guiding, assisting, mentoring during my formative days as a PhD student and being there and helping me out in times of difficulties at all stages thereafter. Apart from their mentorship, I have been fortunate to have developed a strong personal equation with each of them. I wish to specially thank the N-donor team of the lab (Manna, Avishek bhaiyya, Shivani) for constructive discussions and providing insights in every project. Partha and I had the maximum overlap in my time in this lab, which was a long, memorable partnership of sharing highs and lows and driving each other to achieve full potential. I would consider myself fortunate to have shared a strong bond with a such skilled co-worker and a wonderful friend. I would like to specially mention about two undergraduate students who worked with me over a long period - Amit and Arkendu, for their enthusiastic involvement and optimistic ideas. I wish to acknowledge the prompt and unconditional assistance from Samraj, Arunabha, Subhajit, Sumanta, Sahel and Writakshi whenever required. I thank Tarak da and Sreenu ji for providing a timely advice and perspective. I especially thank Partha and Shivani for their invaluable support during the last phase of my PhD.

For the smooth progress in a long course, the support of technical and administrative staff is equally important. I thank Dr. Umeshreddy Kacherki and Anuradha for library assistance, technical staff of the institute - Parveen Nasa, Archana, Mahesh Jadhav, Nilesh Dumbre, Swati, Anil, Yatish, Ganesh Dimbar, Suresh Prajapat, Sandeep, Nitin,

Megha, Deepali and administrative staff - Mayuresh, Nayana, Tushar, Vrushali, Suresh, Prabhas, Priyadarshani for their prompt assistance at multiple occasions. I had the opportunity to attend several national (CRSI-2015; IUCr-2017; MTIC-2017; Inter-IISER Chemistry Meet-2017) and international conferences (EuroMOF-2017), for which I thank DST-SERB, Infosys Foundation and IISER-Pune for funding. I also express my deep gratitude to IISER Pune for research fellowship for the entire tenure in IISER. I thank Royal Society of Chemistry (RSC), John Wiley & Sons (Wiley-VCH), American Chemical Society (ACS), Cell Press, Elsevier, Nature Publishing Group (NPG) for publishing several research and review articles.

I particularly wish to thank my batchmates (Santosh and Anindita) for long discussion over tea and coffee throughout the last 7 years during both highs and lows, which kept driving the motivation to sustain the long terrain. I also wish to thank my other batchmates (Naresh, Ajay and Aakash) who had enrolled into the program at the same time. I was fortunate to have many good friends in IISER (especially Neeraj Maheshwari, Amrit, Vivek Kumar, Rupal Bhaisare, Nilesch Deshpande, Himani Rawat) who kept the ship sailing steadily in all weather. I was a part of the inaugural batch of Chemphilic Team (Departmental Club) which was indeed a memorable experience. Although indirectly connected, the support from friends outside IISER (Akhil, Nachiket Bapat, Swaraj, Varun, Nachiket Joshi) was precious and invaluable. I am indebted to my family (Aai, Baba, Shalmalee, Mama, Mami, Nani, Ninad, Jayesh, Ninad) for being the invisible backroom support, without whom this could not have been completed.

- Aamod V. Desai

# Contents

<b>1</b>	<b>Introduction</b>	
1.1	Metal-Organic Frameworks (MOFs)	1.1
1.2	Applications of MOFs	1.5
1.3	Environmental applications of MOFs	1.6
1.4	Overview of thesis	1.7
1.5	References	1.8
<b>2.</b>	<b>Probing the Influence of Anions in Directing the Structures and Functions of Neutral N-donor Ligand based MOFs</b>	
2.1	Introduction	2.1
2.2	Experimental	2.2
2.3	Results and discussion	2.5
2.4	Conclusions	2.11
2.5	Appendix Section	2.11
2.6	References	2.41
<b>3.</b>	<b>Water Stable Cationic MOF for Heavy Metal Oxoanion Pollutant Capture</b>	
3.1	Introduction	3.1
3.2	Experimental	3.2
3.3	Results and discussion	3.4
3.4	Conclusions	3.9
3.5	Appendix Section	3.10
3.6	References	3.25
<b>4.</b>	<b>Multifunctional Sulfonate-based Isostructural MOFs for CO<sub>2</sub> Capture</b>	
4.1	Introduction	4.1
4.2	Experimental	4.3
4.3	Results and discussion	4.6
4.4	Conclusions	4.10

4.5	Appendix Section	4.11
4.6	References	4.39
<b>5.</b>	<b>Base-resistant Cationic MOF as Ion-exchanger of Organic Dyes over Wide pH Range</b>	
5.1	Introduction	5.1
5.2	Experimental	5.2
5.3	Results and discussion	5.6
5.4	Conclusions	5.13
5.5	Appendix Section	5.14
5.6	References	5.49
<b>6.</b>	<b>Summary and Perspectives</b>	

## Synopsis

The primary motivation of the work in this thesis is to develop neutral N-donor linker based metal-organic frameworks (MOFs) towards their application for the recognition and capture of environmental pollutants. Metal-organic frameworks (MOFs) have emerged as a distinguished subset in the domain of porous materials owing to several advantages over conventional porous solids. The facile access to tune pore character, modulate physical/chemical characteristics on demand and examine host-guest chemistry on the basis of structure-property correlation has rendered MOFs as a unique class of polymeric crystalline solid material. The features of MOFs have been tapped for suitability in several applications such as gas storage, separation of industrially important mixtures, catalysis, sensing, ion-conduction etc.; but hitherto these compounds have not been explored profoundly for their utility as solid sorbents/sensory probes of environmental pollutants. Broadly, MOFs are classified into neutral and ionic on the basis of the residual charge on the framework backbone. Different donor groups have been evaluated for the preparation of MOFs such as carboxylates, sulfonates, phosphonates, N-heterocyclic aromatic rings etc. Although relatively unexplored, neutral N-donor based linkers offer several advantages alike other donor groups and in some cases can render unique features to the resulting frameworks. Typically N-donor ligand based MOFs have been found to be vulnerable to dissociation under humid conditions and hence very few applications have been evaluated using standalone neutral N-donor linker based MOFs. Thus the factors governing the stability of such frameworks were sought to be investigated as hydrolytic stability is a pre-requisite for any material seeking environmental applications. Further the insights gained from these studies were applied to synthesize MOFs as ion-exchange materials for the capture of heavy metal contaminants and highly absorbing organic dyes, or as solid adsorbents for the capture of air pollutants such as greenhouse gas CO<sub>2</sub>.

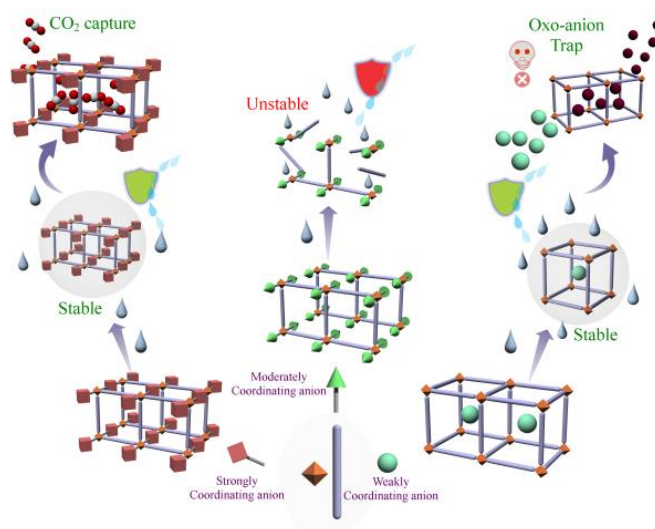
### *Chapter 1. Introduction*

At the outset, a brief discussion regarding metal-organic frameworks (MOFs) is included. The scope of MOFs with regard to structural diversity which is regulated by the myriad choice of the building blocks has been presented. The different types of linker systems used for the preparation of MOFs have been briefly discussed and the scope for detailed exploration for neutral N-donor linker based MOFs is provided. Further, the broad classification of MOFs on the basis of structural character (3 generations of MOFs) and the framework components (neutral and ionic) is discussed with representative examples of benchmark compounds. A short summary of the diverse applications presented by MOF compounds has been included. As the focus of the current work is on environmental applications of MOFs, a brief state-of-art overview has been provided. In particular, as stability is of prime importance while seeking

practical utility, the strategies for synthesis of stable MOFs along-with other key parameters necessary for real-time implementation have been briefly summarized.

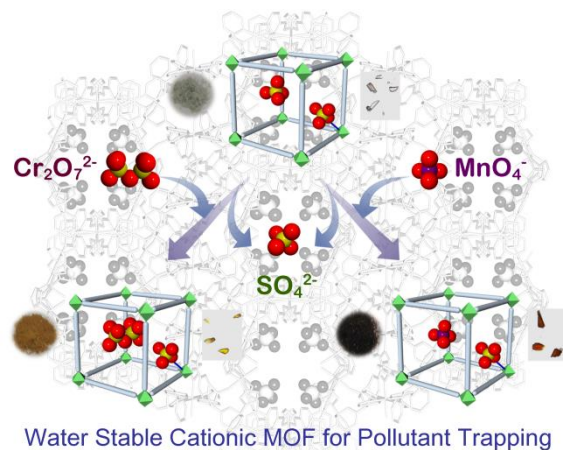
### *Chapter 2. Probing the Influence of Anions in Directing the Structures and Functions of Neutral N-donor Ligand based MOFs*

In this chapter, a library of compounds have been synthesized by keeping the metal ion and ligand fixed and varying the anion used in the reaction. The compounds were screened for the influence of anion in directing the structures of the compounds. Initially the hydrolytic stability of the compounds was evaluated which further provided insights into the influence of anions. The cationic MOF constructed from a weakly coordinating anion was tested for its ability to capture radioactive pollutant pertechnetate ( $\text{TcO}_4^-$ ) (via model anions perrhenate- $\text{ReO}_4^-$  and permanganate- $\text{MnO}_4^-$ ) via ion-exchange approach in aqueous medium. Another MOF having polar sites aligned along the pore surface was examined for the function of adsorption of greenhouse gas  $\text{CO}_2$ . (*Manuscript submitted*)



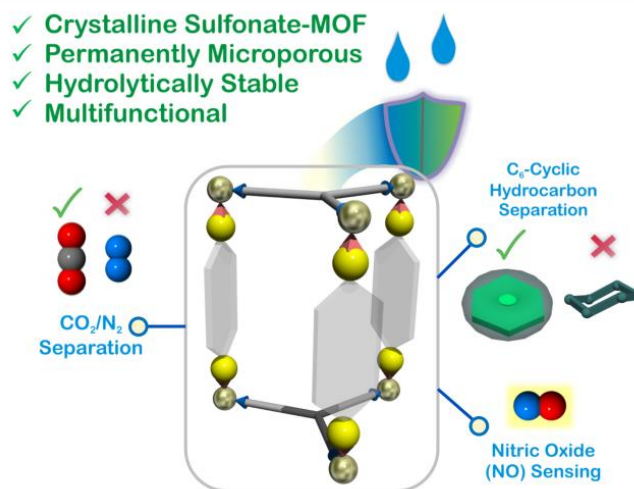
### *Chapter 3. Water Stable Cationic MOF for Heavy Metal Oxoanion Pollutant Capture*

In this chapter, a water-stable cationic MOF has been synthesized based on rational choice of building blocks to afford stability as well as ionic character. The 3-dimensional MOF bearing free sulfate anions was sought for the capture of heavy metal oxoanions having tetrahedral geometry via ion-exchange pathway. The ion-exchange process leads to naked-eye aqueous phase capture of dichromate and pertechnetate (via surrogate anion permanganate) in a selective manner. The compound was found to have relatively high uptake capacity and could be used for ion-exchange over multiple cycles. (*Angew. Chem. Int. Ed.* **2016**, *55*, 7811-7815)



#### Chapter 4. Multifunctional Sulfonate-based Isostructural MOFs for CO<sub>2</sub> Capture

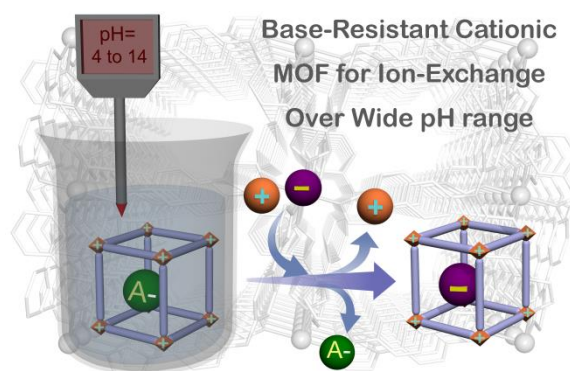
Extending the idea of stability afforded by sulfate anions, an isostructural pair of sulfonate-based MOFs having permanent porosity were synthesized. A disulfonate linker along with tridentate neutral N-donor ligand resulted in the formation of a porous structure having pore surfaces aligned with polar groups. The compounds exhibited high uptake of CO<sub>2</sub> over other gases and the extra functionalities bestowed by the choice of the building blocks resulted in multifunctional character of the MOFs, which hitherto has not been tapped for sulfonate-based systems. The compound bearing pendant amine groups exhibited selective detection of neurotransmitter gas nitric oxide (NO), whereas the second compound having 1D porous channel with naphthalene backbone was found to show adsorptive separation of benzene over cyclohexane. The stability afforded by the choice of the building blocks resulted in the MOFs retaining structure and pore character over a wide pH range. (*Manuscript under revision*)





## Chapter 5. Base-resistant Cationic MOF as Ion-exchanger of Organic Dyes over Wide pH Range

As sulfonate based molecules have binding tendencies with first row transition metals with smaller ionic radii, their role as a bulky anionic template was presented in the synthesis of a cationic MOF having porous channels with sulfonate functioning as bulky anion. The Ni(II)-centered cationic MOF was found to have unusual resistance in water and over wide pH range, even under high basic conditions. The features of stability and high porosity were tapped for the function of size-selective capture of hazardous organic dyes over wide pH range. The capture of dyes was found to be recyclable and the compound retained its structural integrity and performance of dye capture. (*iScience* **2018**, 3, 21-30)



## Chapter 6. Summary and Perspectives

In conclusion, a brief summary of the insights gained by the library of compounds reported in chapters 2-5 has been provided. An overview on the influence of anions/co-ligands in directing the structures and subsequent application features have been discussed. Apart from the outline proposing the factors affecting the stability of compounds built from neutral N-donor linkers, the design approaches yielding porous cationic MOFs based on neutral N-donor linkers have been summarized. The outcomes from the current work in the domain of MOFs for remediation of environmental pollutants has been discussed with regard to state-of-art. The systematic development of neutral N-donor MOFs as stable materials towards practical implementation can pave way for these compounds to find suitability for environmental applications.

## Acronyms

Anal.	Analysis
Calc.	Calculated
CCDC	Cambridge Crystallographic Data Centre
DMF	N,N'-dimethylformamide
DCM	Dichloromethane
EtOH	Ethanol
FT-IR	Fourier transform infra-red spectroscopy
g	Gram
MeOH	Methanol
mg	Milligram
min	Minutes
mL	Milliliter
mM	Millimolar
mmol	Milli moles
MOF	Metal-Organic Framework
PCP	Porous Coordination Polymer
PXRD	Powder X-Ray Diffraction
RT	Room Temperature
SCXRD	Single-Crystal X-Ray Diffraction
TGA	Thermogravimetric Analysis
UV	Ultraviolet
FE-SEM	Field Emission Scanning Electron Microscopy
MeCN	Acetonitrile
NMR	Nuclear Magnetic Resonance
iMOF	Ionic Metal-Organic Framework
EDX	Energy Dispersive X-ray Analysis
ICP-AES	Inductively Coupled Plasma Atomic Emission Spectroscopy

## Rights and Permissions

### Chapter 1:

Reprinted (adapted) with permission from *Dalton Trans.* **2016**, 45, 4060-4072. Copyright 2016: Royal Society of Chemistry. The article is licensed under a Creative Commons Attribution 3.0 Unported Licence.

### Chapter 3:

Reprinted (adapted) with permission from *Angew. Chem. Int. Ed.* **2016**, 55, 7811-7815. Copyright 2016: John Wiley and Sons. Licence number 4353661215995 dated 21<sup>st</sup> May 2018.

### Chapter 5:

Reprinted (adapted) with permission from *iScience* **2018**, 3, 21-30. Copyright Elsevier. This work is licensed under a Creative Commons Attribution (CC-BY-4.0).

## Research Publications

(† - indicates equal contribution)

### Included in thesis

1. Neutral N-donor ligand based flexible metal–organic frameworks (Perspective).  
Biplab Manna,† **Aamod V. Desai**† and Sujit K. Ghosh.  
*Dalton Trans.* **2016**, 45, 4060-4072.
2. Metal-Organic Frameworks (MOFs) for Recognition, Trapping and Sequestration of Toxic Anionic Pollutants.  
*Book Chapter. (Manuscript Submitted).*  
**Aamod V. Desai**, Shivani Sharma and Sujit K. Ghosh.
3. Probing the influence of anions in directing the structures and functions of neutral N-donor ligand based MOFs. (*Manuscript Submitted*).  
**Aamod V. Desai**, Shivani Sharma, Arkendu Roy and Sujit K. Ghosh.
4. A Water-Stable Cationic Metal-Organic Framework as a Dual Adsorbent of Oxoanion Pollutants.  
**Aamod V. Desai**, Biplab Manna, Avishek Karmakar, Amit Sahu and Sujit K. Ghosh.  
*Angew. Chem. Int. Ed.* **2016**, 55, 7811-7815.
5. Multifunctional Behavior of Sulfonate-based Hydrolytically Stable Microporous Metal-Organic Frameworks.  
(*Manuscript Under Revision*).  
**Aamod V. Desai**, Biplab Joarder, Arkendu Roy, Partha Samanta, Ravichandar Babarao and Sujit K. Ghosh.
6. Base-Resistant Ionic Metal-Organic Framework as a Porous Ion-Exchange Sorbent.  
**Aamod V. Desai**, Arkendu Roy, Partha Samanta, Biplab Manna and Sujit K. Ghosh.  
*iScience* **2018**, 3, 21-30.

### Not included in thesis

7. Aqueous Phase Nitric Oxide Detection by an Amine Decorated Metal-Organic Framework.  
**Aamod V. Desai**,† Partha Samanta,† Biplab Manna and Sujit K. Ghosh.  
*Chem. Commun.* **2015**, 51, 6111-6114.
8. Enhanced Proton Conduction by Post-Synthetic Covalent Modification in a Porous Coordination Framework.  
Partha Samanta,† **Aamod V. Desai**,† Bihag Anothumakkool, Mandar M. Shirolkar, Avishek Karmakar, Sreekumar Kurungot and Sujit K. Ghosh.  
*J. Mater. Chem. A* **2017**, 5, 13659-13664.
9. Ultrahigh Ionic Conduction in Water Stable Close-Packed Metal-Carbonate Frameworks.  
Biplab Manna,† **Aamod V. Desai**,† Rajith Illathvalappil, Kriti Gupta, Arunabha Sen, Sreekumar Kurungot and Sujit K. Ghosh.  
*Inorg. Chem.* **2017**, 56, 9710-9715.
10. Chemically stable ionic viologen-organic network: an efficient scavenger of toxic oxo-anions from water  
Partha Samanta, Priyanshu Chandra, Subhajit Dutta, **Aamod V. Desai** and Sujit K. Ghosh.  
*Chem. Sci.* **2018**, doi: 10.1039/C8SC02456A.
11. Selective Recognition of Hg(II) ion in Water by a Functionalized Metal-Organic Framework (MOF) Based Chemodosimeter.  
Partha Samanta, **Aamod V. Desai**, Shivani Sharma, Priyanshu Chandra and Sujit K. Ghosh.  
*Inorg. Chem.* **2018**, 57, 2360-2364.

12. Toxic Aromatics Induced Responsive Facets for a Pore Surface Functionalized Luminescent Coordination Polymer.  
Biplab Manna, Shivani Sharma, Soumya Mukherjee, **Aamod V. Desai** and Sujit K. Ghosh.  
*Inorg. Chem.* **2017**, *56*, 6864-6869.
13. Polar Pore Surface Guided Selective CO<sub>2</sub> Adsorption in a Pre-Functionalized Metal-Organic Framework.  
Soumya Mukherjee, Ravichandar Babarao, **Aamod V. Desai**, Bi-plab Manna and Sujit K. Ghosh.  
*Cryst. Growth Des.* **2017**, *17*, 3581-3587.
14. Aqueous Phase Sensing of Cyanide Ion Using a Hydrolytically Stable Metal-Organic Framework.  
Avishek Karmakar, Bi-plab Joarder, Abhik Mallick, Partha Samanta, **Aamod V. Desai**, Sudipta Basu and Sujit K. Ghosh.  
*Chem. Commun.* **2017**, *53*, 1253-1256.
15. Chemically Stable Microporous Hyper-Cross-linked Polymer (HCP): An Efficient Selective Cationic Dye Scavenger from Aqueous Medium.  
Partha Samanta, Priyanshu Chandra, **Aamod V. Desai** and Sujit K. Ghosh.  
*Mater. Chem. Front.* **2017**, *1*, 1384-1388.
16. Hydrogen-Bonded Organic Frameworks: A New Class of Porous Crystalline Proton Conducting Materials.  
Avishek Karmakar, Rajith Illathvalappil, Bihag Anothumakkool, Arunabha Sen, Partha Samanta, **Aamod V. Desai**, Sreekumar Kurungot and Sujit K. Ghosh.  
*Angew. Chem. Int. Ed.* **2016**, *55*, 10667-10671.
17. An Ultrahydrophobic Fluorous Metal-Organic Frameworks As A Promising Platform To Tackle Marine Oil Spills.  
Soumya Mukherjee, Ankit M. Kansara, Rajesh Gonnade, Dinesh Mullangi, Bi-plab Manna, **Aamod V. Desai**, Shridhar H. Thorat, Puyam S. Singh, Arnab Mukherjee and Sujit K. Ghosh.  
*Chem. Eur. J.* **2016**, *22*, 10937-10943.
18. High Hydroxide Conductivity in a Chemically Stable Metal-Organic Framework Containing Water-Hydroxide Supramolecular Chain.  
Sanjog S. Nagarkar, Bihag Anothumakkool, **Aamod V. Desai**, Mandar M. Shirolkar, Sreekumar Kurungot and Sujit K. Ghosh.  
*Chem. Commun.* **2016**, *52*, 8459-8462.
19. Harnessing Lewis Acidic Open Metal Sites of Metal-Organic Frameworks: Foremost Route to Achieve Highly Selective Benzene Sorption over Cyclohexane.  
Soumya Mukherjee, Bi-plab Manna, **Aamod V. Desai**, Yuefeng Yin, Rajamani Krishna, Ravichandar Babarao and Sujit K. Ghosh.  
*Chem. Commun.* **2016**, *52*, 8215-8218.
20. A Bifunctional Metal-Organic Framework: Striking CO<sub>2</sub> Selective Sorption Features with Guest-Induced Luminescence Tuning Behavior.  
Soumya Mukherjee, **Aamod V. Desai**, Yogeshwar D. More and Sujit K. Ghosh.  
*ChemPlusChem* **2016**, *81*, 702-707.

21. Bimodal Functionality in a Porous Covalent Triazine Framework by Rational Integration of Electron Rich and Deficient Pore Surface.  
Avishek Karmakar, Amrit Kumar, Abhijeet K. Chaudhari, Partha Samanta, **Aamod V. Desai**, Rajamani Krishna and Sujit K. Ghosh.  
*Chem. Eur. J.* **2016**, *22*, 4931-4937.
22. A Post-Synthetically Modified MOF for Selective and Sensitive Aqueous Phase Detection of Highly Toxic Cyanide Ion.  
Avishek Karmakar, Naveen Kumar, Partha Samanta, **Aamod V. Desai** and Sujit K. Ghosh.  
*Chem. Eur. J.* **2016**, *22*, 864-868.
23. A  $\pi$ -electron Deficient Diaminotriazine Functionalized MOF for Selective Sorption of Benzene over Cyclohexane.  
Biplab Manna, Soumya Mukherjee, **Aamod V. Desai**, Shivani Sharma, Rajamani Krishna and Sujit K. Ghosh.  
*Chem. Commun.* **2015**, *51*, 15386-15389.
24. Coherent Fusion of Water Array and Protonated Amine in a Metal-Sulphate Based Coordination Polymer for Proton Conduction.  
Biplab Manna, Bihag Anothumakkool, **Aamod V. Desai**, Partha Samanta, Sreekumar Kurungot and Sujit K. Ghosh.  
*Inorg. Chem.* **2015**, *54*, 5366-5371.
25. Nitro (-NO<sub>2</sub>) Functionalized Metal-Organic Framework as a Reaction based Fluorescence Turn-On Probe for Rapid and Selective H<sub>2</sub>S Detection.  
Sanjog S. Nagarkar, **Aamod V. Desai** and Sujit K. Ghosh.  
*Chem. Eur. J.* **2015**, *21*, 9994-9997.
26. Amide Functionalized Dynamic Metal-Organic Framework Exhibiting Visual Colorimetric Anion Exchange and Selective Uptake of Benzene and Cyclohexane.  
Avishek Karmakar, **Aamod V. Desai**, Biplab Manna, Biplab Joarder and Sujit K. Ghosh.  
*Chem. Eur. J.* **2015**, *21*, 7071-7076.
27. Exploiting Framework Flexibility of a Metal-Organic Framework for Selective Adsorption of Styrene over Ethylbenzene.  
Soumya Mukherjee, Biplab Joarder, **Aamod V. Desai**, Biplab Manna, Rajamani Krishna and Sujit K. Ghosh.  
*Inorg. Chem.* **2015**, *54*, 4403-4408.
28. Selective Detection of 2,4,6-trinitrophenol (TNP) by a  $\pi$ -stacked Organic Crystalline Solid in Water.  
Soumya Mukherjee, **Aamod V. Desai**, Arif I. Inamdar, Biplab Manna and Sujit K. Ghosh.  
*Cryst. Growth Des.* **2015**, *15*, 3493-3497.
29. Exploitation of Guest Accessible Aliphatic Amine Functionality of a Metal-Organic Framework for Selective Detection of 2,4,6-trinitrophenol (TNP) in Water.  
Soumya Mukherjee, **Aamod V. Desai**, Biplab Manna, Arif I. Inamdar and Sujit K. Ghosh.  
*Cryst. Growth Des.* **2015**, *15*, 4627-4634.
30. Aqueous Phase Selective Detection of 2,4,6-trinitrophenol using a Fluorescent Metal-Organic Framework with a Pendant Recognition Site.  
Sanjog S. Nagarkar, **Aamod V. Desai**, Partha Samanta and Sujit K. Ghosh.  
*Dalton Trans.* **2015**, *44*, 15175-15180.

31. Single-Crystal-to-Single-Crystal Transformation of an Anion Exchangeable Dynamic Metal-Organic Framework.  
Biplab Manna, **Aamod V. Desai**, Naveen Kumar, Avishek Karmakar and Sujit K. Ghosh.  
*CrystEngComm* **2015**, *17*, 8796-8800.
32. Selective Anion Exchange and Tunable Luminescent Behavior of MOF based Supramolecular Isomers.  
Biplab Manna, Shweta Singh, Avishek Karmakar, **Aamod V. Desai** and Sujit K. Ghosh.  
*Inorg. Chem.* **2015**, *54*, 110-116.
33. Selective and Sensitive Aqueous Phase Detection of TNP (2,4,6-trinitrophenol) by an Amine Functionalized Metal-Organic Framework.  
Biplab Joarder, **Aamod V. Desai**, Partha Samanta, Soumya Mukherjee and Sujit K. Ghosh.  
*Chem. Eur. J.* **2015**, *21*, 965-969.
34. Metal-Organic Framework based Highly Selective Fluorescence Turn-On Probe for Hydrogen Sulphide.  
Sanjog S. Nagarkar, Tanmoy Saha, **Aamod V. Desai**, Pinaki Talukdar and Sujit K. Ghosh.  
*Sci. Rep.* **2014**, *4*, 7053.
35. Guest-Responsive Function of a Dynamic Metal-Organic Framework with  $\pi$ -Lewis Acidic Pore Surface.  
Biplab Joarder, Soumya Mukherjee, Abhijeet K. Chaudhari, **Aamod V. Desai**, Biplab Manna and Sujit K. Ghosh.  
*Chem. Eur. J.* **2014**, *20*, 15303-15308.
36. Framework-flexibility driven Selective Sorption of p-Xylene over other Isomers by a Dynamic Metal-Organic Framework.  
Soumya Mukherjee, Biplab Joarder, Biplab Manna, **Aamod V. Desai**, Abhijeet K. Chaudhari and Sujit K. Ghosh.  
*Sci. Rep.* **2014**, *4*, 5761.
37. Anion-Responsive Tunable Bulk Phase Homochirality and Luminescence of a Cationic Framework.  
Biplab Manna, Biplab Joarder, **Aamod V. Desai**, Avishek Karmakar and Sujit K. Ghosh.  
*Chem. Eur. J.* **2014**, *20*, 12399-12404.
38. Dynamic Metal-Organic Framework with Anion-Triggered Luminescence Modulation Behavior.  
Avishek Karmakar, Biplab Manna, **Aamod V. Desai**, Biplab Joarder and Sujit K. Ghosh.  
*Inorg. Chem.* **2014**, *53*, 12225-12227.
39. A Fluorescent Metal-Organic Framework for Highly Selective Detection of Nitro-explosive in Aqueous Phase.  
Sanjog S. Nagarkar, **Aamod V. Desai** and Sujit K. Ghosh.  
*Chem. Commun.* **2014**, *50*, 8915-8918.

## Reviews

40. Potential of Metal-Organic Frameworks for Adsorptive Separation of Industrially and Environmentally Relevant Liquid Mixtures.  
Soumya Mukherjee,<sup>†</sup> **Aamod V. Desai**<sup>†</sup> and Sujit K. Ghosh.  
*Coord. Chem. Rev.* **2018**, *367*, 82-126.

41. Guest Responsive Metal-Organic Frameworks as Scaffolds for Separation and Sensing Applications.  
Avishek Karmakar, Partha Samanta, **Aamod V. Desai** and Sujit K. Ghosh.  
*Acc. Chem. Res.* **2017**, *50*, 2457-2469.
42. Metal-Organic Frameworks: Functional Luminescent and Photonic Materials for Sensing Applications.  
William P. Lustig, Soumya Mukherjee, Nathan D. Rudd, **Aamod V. Desai** and Sujit K. Ghosh.  
*Chem. Soc. Rev.* **2017**, *46*, 3242-3285.
43. Ionic Metal-Organic Frameworks (iMOFs): Design Principles and Applications.  
Avishek Karmakar, **Aamod V. Desai** and Sujit K. Ghosh.  
*Coord. Chem. Rev.* **2016**, *307*, 313-341.
44. Engineering Metal-Organic Frameworks for Aqueous Phase 2,4,6-trinitrophenol (TNP) Sensing.  
Sanjog S. Nagarkar, **Aamod V. Desai** and Sujit K. Ghosh.  
*CrystEngComm* **2016**, *18*, 2994-3007.
45. Stimulus-Responsive Metal-Organic Frameworks.  
Sanjog S. Nagarkar, **Aamod V. Desai** and Sujit K. Ghosh.  
*Chem. Asian J.* **2014**, *9*, 2358-2376.



---

# *Chapter 1*

---

## **Introduction**

## 1 Introduction

### 1.1 Metal-organic frameworks (MOFs):

The domain of porous materials has witnessed a remarkable rise over the last few decades owing to them commanding remarkable attention across several disciplines.<sup>1</sup> Among its sub-classes, metal-organic frameworks (MOFs) have commanded substantial research interest over congener materials like zeolites and activated carbon on account of their distinct advantages.<sup>2</sup> MOFs are porous crystalline solids having an extended coordination network built via bi-/multi-dentate organic linkers and held by metal ions/clusters in a periodic manner (Figure 1.1). Typically the solvent molecules used during the synthesis occupy the voids in the coordination space of the compounds. The myriad choice of building blocks affords liberty and control to prepare compounds for specific application demands. The ability to tune the pore character and ascribe precise structure-property correlation equips MOFs to find potential applicability for a range of functions.<sup>3</sup>

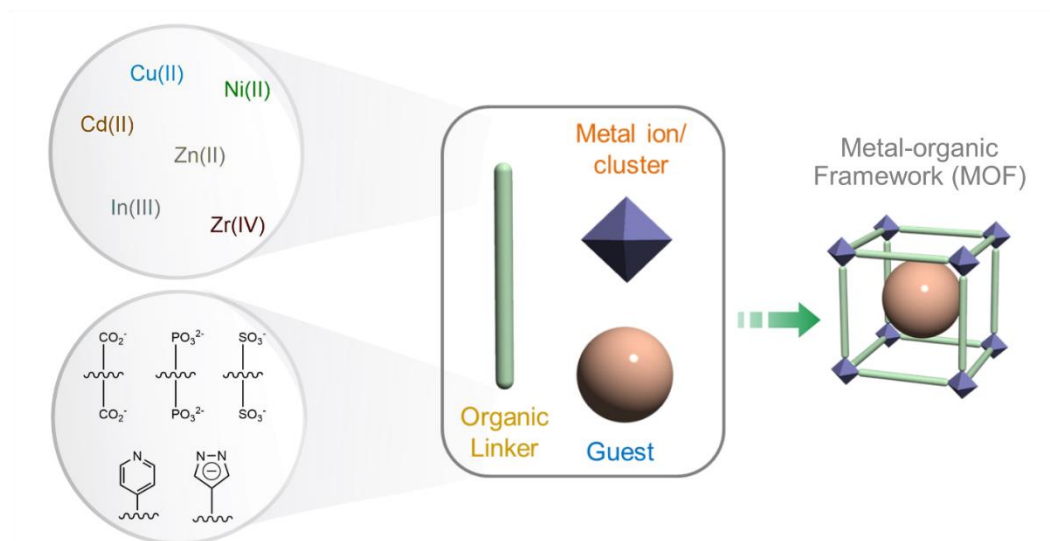


Figure 1.1 Schematic representation showing the general approach to synthesize metal-organic frameworks (MOFs).

#### 1.1.1 Building blocks:

The ample opportunity to have plethora of combinations affords MOFs a distinct advantage of tunability of properties and affordance of architectures with specific character of pore surfaces and pore dimensions.

Typically, first row transition metal cations have been employed for the preparation of MOFs with different kinds of linker systems. In certain cases, the characteristic features bestowed by the metal ion such as Fe(II) for magnetism or  $d^{10}$  cations [Zn(II) or Cd(II)] for ability to fluoresce directs the selection of the metal ion.<sup>4</sup> Apart from the application-specific features, certain metal ions such as Cu(II) (for Jahn-Teller distortion) or Zn(II) (for flexible coordination environments) are well suited in cases where dynamic compounds are sought after.<sup>5</sup> In pursuit of developing new compounds, stability has become an essential objective both in terms of material synthesis and for seeking practical implementation. In case of MOFs, the stability of the compounds is found to be directly correlated to the bond strength between the metal and ligand, and hence the choice of the metal ion is also influenced by the nature of binding ability.<sup>6</sup>

Unlike metal ions the wide array of organic linkers, both in terms of binding moieties and nature of the backbone, renders remarkable tool to explore the diversity of MOF compounds. Generally, carboxylate-based linkers have been utilized for the preparation of MOFs, as they have strong binding ability with majority of the transition metal ions.<sup>7</sup> Also, such linkers have diverse binding modes and depending upon the backbone, the binding geometries of the structures can be varied. In literature, sulfonate-based or phosphonate-terminal linkers have been proposed for the synthesis of MOFs but with very limited exploration relative to the carboxylate counterparts.<sup>8</sup> Another class of ligand system which has commanded attention is N-heterocyclic aromatic groups such as pyridine or azolate rings.<sup>9</sup> Although standalone compounds based on N-donor linkers have not been investigated thoroughly, they have been commonly employed as co-linkers to carboxylate-terminal ligands. Ligands having N-donor groups can be broadly segregated as neutral or ionic based on the charge. Typically ionic N-donor ligands such as imidazolate, pyrazolate or tetrazolate have higher  $pK_a$  resulting in stronger coordination bonds which offer higher resistance to hydrolysis. Neutral donor groups such as pyridine, imidazole have been typically employed for the preparation of cationic MOFs and also used as a co-linker to enhance the porosity or provide access to the functional sites. Despite understanding of different structures, the development of standalone neutral N-donor linker based MOFs is commanding attention as very few application studies have been evaluated with such systems.

### 1.1.2 Types of MOFs:

MOFs have been broadly classified into 3 generations based on the fate of the compound after the removal of guest molecules occluded during the synthesis (Figure 1.2).<sup>10</sup> 1<sup>st</sup> generation MOFs comprise of compounds which undergo complete breakdown of polymeric nature upon desolvation. Rigid MOFs which retain structural integrity after guest removal constitute the 2<sup>nd</sup> generation of MOFs.

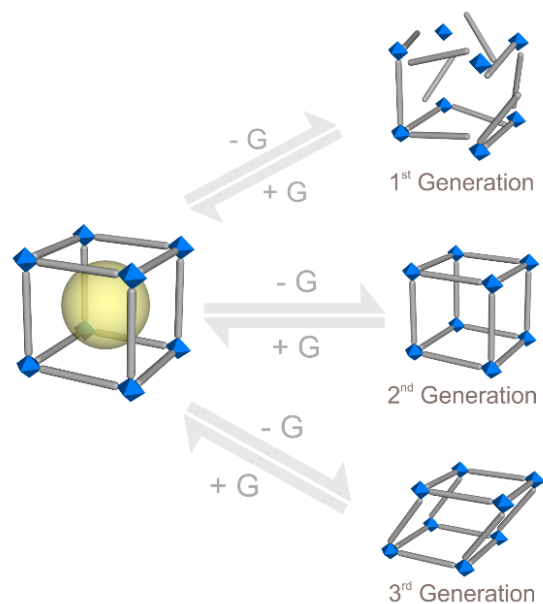


Figure 1.2 Classification of MOFs into 3 generations on the basis of fate of the compound after the removal of guest molecules.

The 3<sup>rd</sup> generation of MOFs include compounds which change their structure upon release of guest molecules and can revert back to original form upon antagonistic stimulus. Apart from this classification, MOFs are also segregated on the basis of charge of the polymeric framework, into neutral and ionic (Figure 1.3).<sup>11</sup>

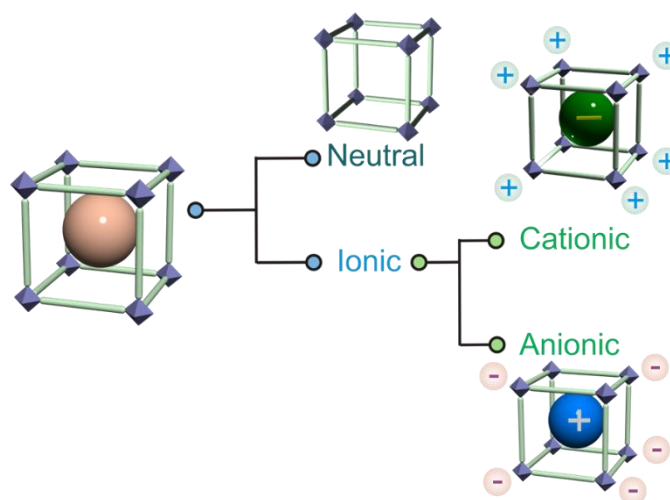


Figure 1.3 Classification of MOFs on the basis of the charge of the framework backbone.

Neutral MOFs have no residual charge on the framework whereas ionic MOFs (i-MOFs) have a net charge on the framework and the maintenance of the ionic equilibrium is satisfied by the counter-ions occupying the coordination space.

### 1.1.1.1 Neutral MOFs:

Majority of the frameworks reported in the literature have an electronically neutral framework where the charge balance is completed by the constituents of the coordination backbone itself. In such cases the electronic neutrality is achieved by the coordination of anionic ligands, typically carboxylates, to positive charge bearing metal ions/clusters (Figure 1.4a). In some cases though, the presence of secondary reaction sites associated with building blocks can lead to conversion of a neutral framework into an ionic framework associated with change in either coordination environment of the metal node or structural character of the ligand.<sup>12</sup>

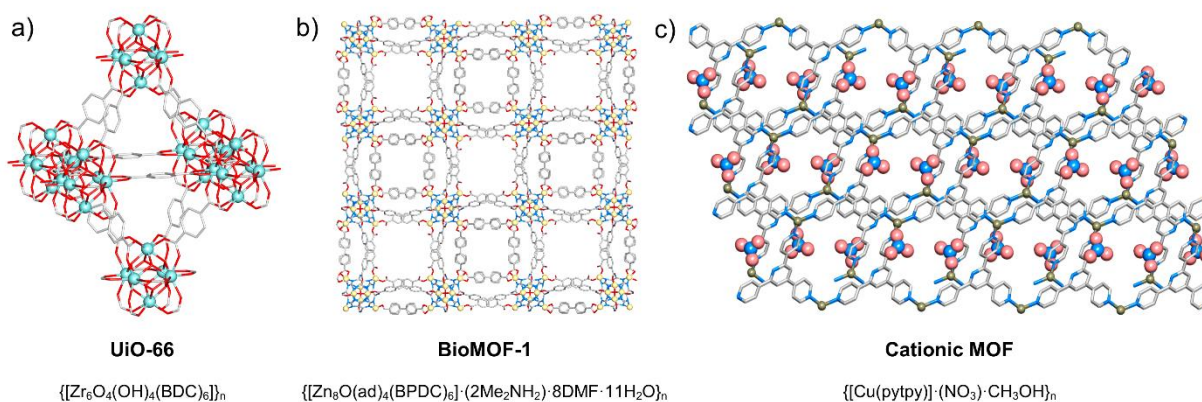


Figure 1.4 Packing diagram for some benchmark MOFs based on the charge of the framework, a) neutral MOF, b) anionic MOF and c) cationic MOF. The corresponding crystal structure data have been adapted from ref. 6c, 6d and 14d respectively. (Color code: C, grey; O, red; N, blue; Zr, light blue; Zn, orange; Cu, dark green. H-atoms have been omitted for clarity).

### 1.1.1.2 Ionic-MOFs (i-MOFs):

Ionic MOFs are classified into cationic and anionic, on the basis of the charge of the framework backbone. For cationic MOFs the framework has a net positive charge, while anionic MOFs bear a net negative charge, and the charge is balanced by uncoordinated anions and cations respectively (Figure 1.4b-1.4c). The presence of free ions in the coordination space affords intrinsic functionality to such compounds which has

been tapped for several applications.<sup>13</sup> Unlike neutral MOFs, the presence of extra framework ions necessitates the partial occupation of the voids by the charge-balancing species; which in certain cases can compromise with the surface area or hinder complete accessibility to the pore surface. Yet, ionic-MOFs have commanded much attention as they offer intrinsic ionic functionality which is highly suited for certain applications.

#### **1.1.1.2.a Cationic-MOFs:**

Broadly, cationic MOFs are synthesized by neutral linkers where the extra framework anion is included by the appropriate choice of the metal salt (Figure 1.4c). The most popular choice of donor group in this regard has been the bi-/multi-dentate pyridyl terminal linkers, such as 4,4'-bipyridine.<sup>14</sup> Apart from 6-member heterocyclic donor groups, 5-membered rings such as imidazole, triazole, pyrazole etc. too have been employed to prepare cationic MOFs.<sup>15</sup>

#### **1.1.1.2.b Anionic-MOFs:**

Although the preparation of anionic MOFs does not have broad design principles, unlike cationic MOFs, these compounds are generally prepared by metal ions having higher coordination numbers. As the ionic character is bestowed by higher concentration of the ligand around the metal nodes, they invariably protect the metal node from the influence of foreign species giving rise to higher stability.<sup>16</sup>

### **1.2 Applications of MOFs:**

On account of these advantages, MOFs have been found to present suitability for diverse applications (Figure 1.5),<sup>17</sup> such as:

- Gas storage and separation
- Separation of industrially relevant liquid mixtures
- Fuel cell applications (proton/hydroxide conduction)
- Sensing of toxic and hazardous species
- Heterogeneous catalysis
- Magnetism

The facile access to structure-property correlation has resulted in rapid advancement of MOFs for the aforementioned applications. Also the ability to tune the pore architecture and pore character results in tailoring the compounds for target-specific applications. In addition the ability to transduce the host-guest interactions via different signals affords remarkable advantage of using MOFs or MOF-based materials for

several applications. Based on these aspects, MOFs continue to progress as distinguished solid-state crystalline materials which will seek greater relevance towards practical implementation in the coming years. Among the different applications suitable using MOF-based materials, the current work focuses on development of MOFs towards environmental applications.

### 1.3 Environmental applications of MOFs:

Among different applications proposed by employment of MOFs, remediation of environmental pollutants has not been focused significantly yet. MOFs can mainly be applied for these applications as solid-state adsorbents of toxic gases ( $\text{CO}_2$ ,  $\text{SO}_2$ , nerve gas agents etc.) or as sorbents for the capture of hazardous pollutants (such as heavy metals, herbicides, organic dyes etc.) in water streams.<sup>18</sup>

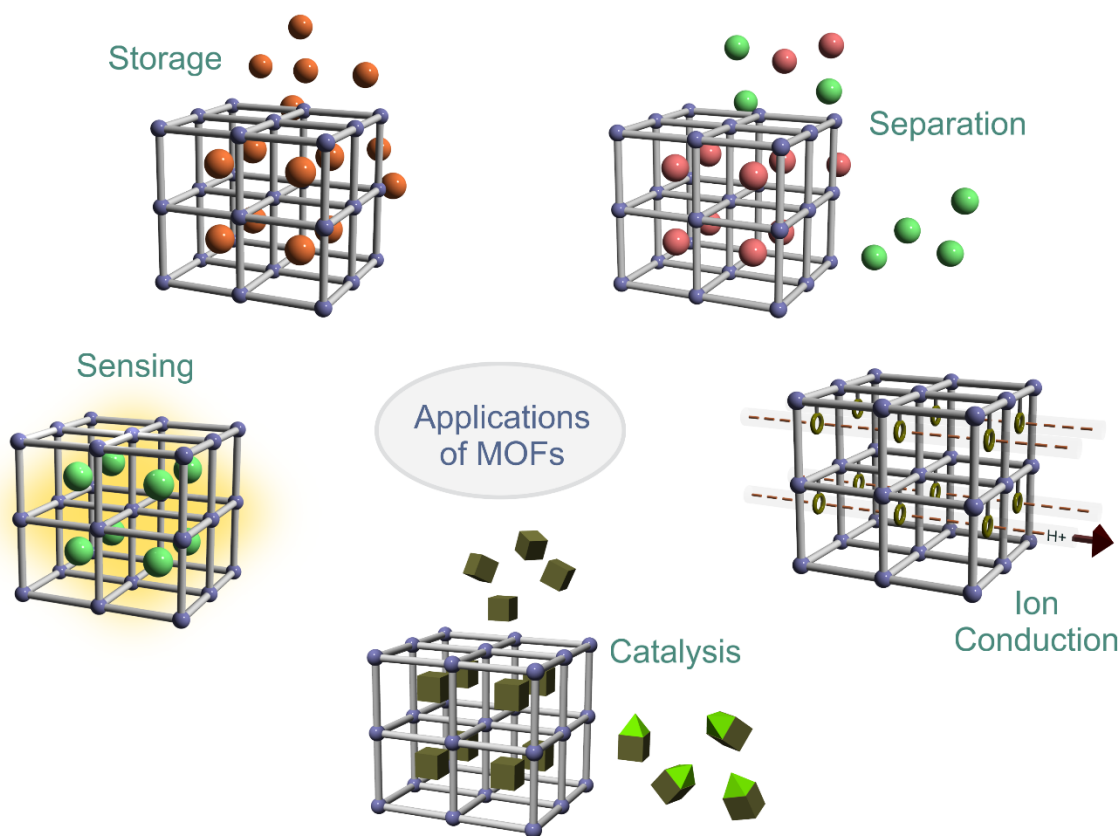


Figure 1.5 Schematic illustration of the potential diverse applications using MOFs.

Capture of toxic gases via adsorption has been found to be an energy efficient process in which the sorbent can be regenerated at low energy costs. Generally, neutral MOFs with pendant secondary functional groups such as  $\text{-NH}_2$ ,  $\text{-OH}$  have been found to enhance the adsorption ability of MOFs and in some cases improve the affinity of gases from a mixture.<sup>19</sup> As described in previous sub-sections, ionic-MOFs having extra framework ions can be much suitable as ion-exchange materials. In certain cases, the non-structural ligands having relatively weaker ligation to the metal nodes can function as the recognition site for the capture of ionic pollutants.<sup>20</sup>

One of the major limitations retarding the progress of MOFs is the lack of hydrolytic stability.<sup>21</sup> Also MOFs cannot be directly applied as solid-state materials for real-time application as they are obtained as highly dispersed powders and hence development of composites is much desired.<sup>22</sup> To overcome these issues simultaneous efforts are being devoted to prepare new MOFs which can expand the scope for environmental remediation or push the limits of existing compounds, and prepare new composite materials which can pave way for screening the utility of the compounds in real-time scenario. Also, certain other parameters required for seeking practical implementation such as toxicity of the compound, durability, performance over multiple cycles and performance under varying environments are necessary to be evaluated for optimizing MOFs for these applications.<sup>23</sup>

#### 1.4 Overview of thesis

Herein, the work carried out in this thesis has focused on developing neutral N-donor based MOFs and examining their ability to capture environmental pollutants. Generally, carboxylate-based MOFs have been tested for capture of toxic air contaminants whereas standalone N-donor linker based compounds are scarcely evaluated owing to lack of porous, rigid structures. Likewise, neutral and anionic MOFs have been studied for the capture of environmental pollutants from water streams but cationic MOFs which are synthesized from neutral N-donor linkers have not been thoroughly investigated owing to weak stability of such compounds in operating conditions. Typically pyridyl terminal molecules as neutral donor groups have been investigated for the preparation of MOFs, but owing to smaller size and stronger binding ability, 5-membered heterocyclic systems such as imidazole, triazole can be better alternatives as neutral donor ligands. Also higher dentate linkers assist in formation of higher dimensional networks and afford kinetic stability to the systems. Thus we narrowed our interest on a neutral tridentate organic linker by rational selection and developed several MOFs based on specific demands of the targeted applications.

Initially, the factors directing the structures based on neutral N-donor based ligand were screened (**Chapter 2**). A series of MOFs were prepared by fixing the ligand and metal cation and varying the anion. The influence of the coordinating tendencies of the anions on the overall structure and the consequent influence



on the application perspectives were thoroughly examined. Two compounds were found to be hydrolytically stable and their application studies were performed for CO<sub>2</sub> adsorption and ion-exchange of radioactive pertechnetate (TcO<sub>4</sub><sup>-</sup>) anions (via surrogate permanganate - MnO<sub>4</sub><sup>-</sup> and perrhenate - ReO<sub>4</sub><sup>-</sup> ions).

The knowledge gained from the library of compounds was then applied to prepare a cationic, water-stable MOF based on a rational design strategy (**Chapter 3**). The MOF could function as an efficient ion-exchange sorbent of heavy-metal oxoanions such as dichromate and pertechnetate, the latter studied using permanganate as a model ion. The ion-exchange selectivity and uptake capacities were thoroughly investigated and the recycling ability of the MOF was examined.

The ability of strongly coordinating anions to afford stable MOFs was extended to utilize disulfonate based linkers in addition to the neutral N-donor linker to afford hydrolytically stable porous MOFs (**Chapter 4**). Two isostructural MOFs bearing polar sites were found to have high adsorption for CO<sub>2</sub>. Both the compounds having a 1D porous channel were studied for their multifunctional behavior for C<sub>6</sub>-cyclic hydrocarbon separation and detection of neurotransmitter gas nitric oxide (NO). Both the compounds were found to be stable over a wide pH range, further endorsing the choice of the building blocks.

From the inputs gained from the previous chapters, we employed disulfonate as a bulky anion to prepare a porous cationic MOF (**Chapter 5**). The compound bearing high density of ligands around metal nodes resulted in unusual stability of the MOF over a wide pH range and under high basic conditions. Owing to the features of stability and porosity, ion-exchange of bulky organic dyes over wide pH range was carried out.

## 1.5 References

1. Slater, A. G.; Cooper, A. I., *Science* **2015**, *348*, aaa8075.
2. Kitagawa, S.; Kitaura, R.; Noro, S.-i., *Angew. Chem. Int. Ed.* **2004**, *43*, 2334-2375.
3. (a) Yaghi, O. M.; O'Keeffe, M.; Ockwig, N. W.; Chae, H. K.; Eddaoudi, M.; Kim, J., *Nature* **2003**, *423*, 705-714. (b) Lin, C.-K.; Zhao, D.; Gao, W.-Y.; Yang, Z.; Ye, J.; Xu, T.; Ge, Q.; Ma, S.; Liu, D.-L., *Inorg. Chem.* **2012**, *51*, 9039-9044. (c) Dhakshinamoorthy, A.; Asiri, A. M.; Garcia, H., *Chem. Commun.* **2017**, *53*, 10851-10869.
4. (a) Liu, X.; Zhou, Y.; Zhang, J.; Tang, L.; Luo, L.; Zeng, G., *ACS Appl. Mater. Interfaces* **2017**, *9*, 20255-20275. (b) Allendorf, M. D.; Bauer, C. A.; Bhakta, R. K.; Houk, R. J. T., *Chem. Soc. Rev.* **2009**, *38*, 1330-1352. (c) Lustig, W. P.; Mukherjee, S.; Rudd, N. D.; Desai, A. V.; Li, J.; Ghosh, S. K., *Chem. Soc. Rev.* **2017**, *46*, 3242-3285. (d) Espallargas, G. M.; Coronado, E., *Chem. Soc. Rev.* **2018**, *47*, 533-557.

5. (a) Schneemann, A.; Bon, V.; Schwedler, I.; Senkovska, I.; Kaskel, S.; Fischer, R. A., *Chem. Soc. Rev.* **2014**, *43*, 6062-6096. (b) Chang, Z.; Yang, D.-H.; Xu, J.; Hu, T.-L.; Bu, X.-H., *Adv. Mater.* **2015**, *27*, 5432-5441.
6. (a) Burtch, N. C.; Jasuja, H.; Walton, K. S., *Chem. Rev.* **2014**, *114*, 10575-10612. (b) Yuan, S.; Feng, L.; Wang, K.; J. Pang, Bosch, M.; Lollar, C.; Sun, Y.; Qin, J.; Yang, X.; Zhang, P.; Wang, Q.; Zou, L.; Zhang, Y.; Zhang, L.; Fang, Y.; Li, J.; Zhou, H.-C., *Adv. Mater.* **2018**, DOI: 10.1002/adma.201704303. (c) Cavka, J. H.; Jakobsen, S.; Olsbye, U.; Guillou, N.; Lamberti, C.; Bordiga, S.; Lillerud, K. P., *J. Am. Chem. Soc.* **2008**, *130*, 13850-13851. (d) An, J.; Geib, S. J.; Rosi, N. L., *J. Am. Chem. Soc.* **2009**, *131*, 8376-8377.
7. (a) Rao, C. N. R.; Natarajan, S.; Vaidhyanathan, R., *Angew. Chem. Int. Ed.* **2004**, *43*, 1466-1496. (b) Gu, J.; Wen, M.; Liang, X.; Shi, Z.; Kirillova, M. V.; Kirillov, A. M., *Crystals* **2018**, DOI: 10.3390/cryst8020083. (c) Schoedel, A.; Li, M.; Li, D.; O’Keeffe, M.; Yaghi, O. M. *Chem. Rev.* **2016**, *116*, 12466-12535.
8. (a) Shimizu, G. K. H.; Vaidhyanathan, R.; Taylor, J. M., *Chem. Soc. Rev.* **2009**, *38*, 1430-1449. (b) Reynolds, J. E.; Dunning, S. G.; McCulley, C. M.; Humphrey, S. M., *A Survey of Metal-Organic Frameworks Based on Phosphorus and Sulfur-Containing Building Blocks* (Elaboration and Applications of Metal-Organic Frameworks; Eds. Ma, S.; Perman, J. A.), **2018**, 37-141, DOI: 10.1142/9789813226739\_0002.
9. (a) Zhang, J.-P.; Zhang, Y.-B.; Lin, J.-B.; Chen, X.-M., *Chem. Rev.* **2012**, *112*, 1001-1033. (b) Manna, B.; Desai, A. V.; Ghosh, S. K., *Dalton Trans.* **2016**, *45*, 4060-4072.
10. Horike, S.; Shimomura, S.; Kitagawa, S., *Nat. Chem.* **2009**, *1*, 695-704.
11. (a) Karmakar, A.; Desai, A. V.; Ghosh, S. K., *Coord. Chem. Rev.* **2016**, *307*, 313-341. (b) Johnson, J. A.; Zhang, X.; Zhang, X.; Zhang, J., *Current Organic Chemistry*, **2014**, *18*, 1973-2001.
12. (a) Mao, C.; Kudla, R. A.; Zuo, F.; Zhao, X.; Mueller, L. J.; Bu, X.; Feng, P., *J. Am. Chem. Soc.* **2014**, *136*, 7579-7582. (b) Chen, T.; Zhang, C.; Qin, Y.; Yang, H.; Zhang, P.; Ye, F., *Materials*, **2017**, DOI: 10.3390/ma10080879. (c) Wiers, B. M.; Foo, M.-L.; Balsara, N. P.; Long, J. R., *J. Am. Chem. Soc.* **2011**, *133*, 14522-14525.
13. (a) Oliver, S. R. J., *Chem. Soc. Rev.* **2009**, *38*, 1868-1881. (b) Banerjee, D.; Kim, D.; Schweiger, M. J.; Kruger, A. A.; Thallapally, P. K., *Chem. Soc. Rev.* **2016**, *45*, 2724-2739. (c) Kumar, P.; Pournara, A.; Kim, K.-H.; Bansal, V.; Rapti, S.; Manos, M. J., *Prog. Mater. Sci.* **2017**, *86*, 25-74.

14. (a) Noro, S.-i.; Kitaura, R.; Kondo, M.; Kitagawa, S.; Ishii, T.; Matsuzaka, H.; Yamashita, M., *J. Am. Chem. Soc.* **2002**, *124*, 2568-2583. (b) Fei, H.; Paw U, L.; Rogow, D. L.; Bresler, M. R.; Abdollahian, Y. A.; Oliver, S. R. J., *Chem. Mater.* **2010**, *22*, 2027-2032. (c) Colinas, I. R.; Inglis, K. K.; Blanc, F.; Oliver, S. R. J., *Dalton Trans.* **2017**, *46*, 5320-5325. (d) Chen, Y.-Q.; Li, G.-R.; Chang, Z.; Qu, Y.-K.; Zhang, Y.-H.; Bu, X.-H., *Chem. Sci.* **2013**, *4*, 3678-3682.
15. (a) Li, X.; Xu, H.; Kong, F.; Wang, R., *Angew. Chem. Int. Ed.* **2013**, *52*, 13769-13773. (b) Li, X.; Gong, Y.; Zhao, H.; Wang, R., *Inorg. Chem.* **2014**, *53*, 12127-12134. (c) Guo, M.; Guo, H.; Liu, S.; Sun, Y.; Guo, X., *RSC Adv.* **2017**, *7*, 51021-51026. (d) Sheng, D.; Zhu, L.; Xu, C.; Xiao, C.; Wang, Y.; Wang, Y.; Chen, L.; Diwu, J.; Chen, J.; Chai, Z.; Albrecht-Schmitt, T. E.; Wang, S., *Environ. Sci. Technol.* **2017**, *51*, 3471-3479.
16. (a) An, J.; Shade, C. M.; Chengelis-Czegán, D. A.; Petoud, S.; Rosi, N. L., *J. Am. Chem. Soc.* **2011**, *133*, 1220-1223. (b) Li, L.; Wang, X.; Liang, J.; Huang, Y.; Li, H.; Lin, Z.; Cao, R., *ACS Appl. Mater. Interfaces* **2016**, *8*, 9777-9781. (c) Li, P.; Vermeulen, N. A.; Gong, X.; Malliakas, C. D.; Stoddart, J. F.; Hupp, J. T.; Farha, O. K., *Angew. Chem. Int. Ed.* **2016**, *55*, 10358-10362. (d) Ma, H.-F.; Liu, Q.-Y.; Wang, Y.-L.; Yin, S.-G., *Inorg. Chem.* **2017**, *56*, 2919-2925.
17. (a) Cui, Y.; Yue, Y.; Qian, G.; Chen, B., *Chem. Rev.* **2012**, *112*, 1126-1162. (b) Coronado, E.; Espallargas, G. M.; *Chem. Soc. Rev.* **2013**, *42*, 1526-1539. (c) Zhang, Z.; Yao, Z.-Z.; Xiang, S.; Chen, B., *Energy Environ. Sci.* **2014**, *7*, 2868-2899. (d) Ramaswamy, P.; Wong, N. E.; Shimizu, G. K. H., *Chem. Soc. Rev.* **2014**, *43*, 5913-5932. (e) Barea, E.; Montoro, C.; Navarro, J. A. R., *Chem. Soc. Rev.* **2014**, *43*, 5419-5430. (f) Wang, C.; Liu, X.; Demir, N. K.; Chen, J. P.; Li, K., *Chem. Soc. Rev.* **2016**, *45*, 5107-5134. (g) Bao, Z.; Chang, G.; Xing, H.; Krishna, R.; Ren, Q.; Chen, B., *Energy Environ. Sci.* **2016**, *9*, 3612-3641. (h) Wang, W.; Xu, X.; Zhou, W.; Shao, Z., *Adv. Sci.* **2017**, *4*, 1600371. (i) Wang, H.; Zhu, Q.-L.; Zou, R.; Xu, Q., *Chem* **2017**, *3*, 822-833. (j) Huang, Y.-B.; Liang, J.; Wang, X.-S.; Cao, R., *Chem. Soc. Rev.* **2017**, *46*, 126-157.
18. (a) DeCoste, J. B.; Peterson, G. W., *Chem. Rev.* **2014**, *114*, 5695-5727. (b) Liu, J.; McGrail, B. P.; Strachan, D. M.; Liu, J.; Tian, J.; Thallapally, P. K., *Metal-Organic Frameworks: Harmful Gas Removal*, (Encyclopedia of Inorganic and Bioinorganic Chemistry), **2014**, DOI: 10.1002/9781119951438.eibc2198. (c) Gao, Q.; Xu, J.; Bu, X.-H., *Coord. Chem. Rev.* **2018**, DOI: 10.1016/j.ccr.2018.03.015. (d) Mon, M.; Bruno, R.; Ferrando-Soria, J.; Armentano, D.; Pardo, E., *J. Mater. Chem. A* **2018**, *6*, 4912-4947. (e) Li, J.; Wang, X.; Zhao, G.; Chen, C.; Chai, Z.; Alsaedi, A.; Hayat, T.; Wang, X., *Chem. Soc. Rev.* **2018**, *47*, 2322-2356.

- 
19. (a) Lin, Y.; Kong, C.; Zhang, Q.; Chen, L.; *Adv. Energy Mater.* **2017**, *7*, 1601296. (b) Yu, J.; Xie, L.-H.; Li, J.-R.; Ma, Y.; Seminario, J. M.; Balbuena, P. B., *Chem. Rev.* **2017**, *117*, 9674-9754.
20. Howarth, A. J.; Liu, Y.; Hupp, J. T.; Farha, O. K., *CrystEngComm* **2015**, *17*, 7245-7253.
21. (a) Gelfand, B. S.; Shimizu, G. K. H., *Dalton Trans.* **2016**, *45*, 3668-3678. (b) Duan, J.; Jin, W.; Kitagawa, S., *Coord. Chem. Rev.* **2017**, *332*, 48-74.
22. (a) Stock, N.; Biswas, S., *Chem. Rev.* **2012**, *112*, 933-969. (b) Zhu, Q.-L.; Xu, Q., *Chem. Soc. Rev.* **2014**, *43*, 5468-5512. (c) Rubio-Martinez, M.; Avci-Camur, C.; Thornton, A. W.; Imaz, I.; MasPOCH, D.; Hill, M. R., *Chem. Soc. Rev.* **2017**, *46*, 3453-3480.
23. (a) Grande, C. A.; Blom, R.; Spjelkavik, A.; Moreau, V.; Payet, J., *Sus. Mater. Technol.* **2017**, *14*, 11-18. (b) Julien, P. A.; Mottillo, C.; Friscic, T., *Green Chem.* **2017**, *19*, 2729-2747.

---

## *Chapter 2*

---

# **Probing the Influence of Anions in Directing the Structures and Functions of Neutral N-donor Ligand based MOFs**

## 2.1 Introduction

Metal-organic frameworks (MOFs) or porous coordination polymers (PCPs) are infinitely extended crystalline polymers having voids built from coordination bonds between bi-/multi-dentate organic linkers and metal ions/clusters.<sup>1</sup> The functional character and architectures of these compounds can be modified by easily regulating the building blocks. Broadly, MOFs have been divided into neutral and ionic-MOFs (iMOFs) based on the charge of the coordination network.<sup>2</sup> Owing to the intrinsic functionality bestowed by the characteristics, iMOFs have recently emerged as an important subset of MOF-materials which have found applicability for certain important applications such as capture of environmental pollutants.<sup>3</sup> Typically, this application has been based on the ion-exchange phenomenon wherein the residual charge-balancing ion is exchanged with the incoming anionic species of interest. In this regard, cationic MOFs which bear free substitutable anions have shown promise as anion-exchange sorbents towards remediation of anionic species which are detrimental to the environment.<sup>4</sup> Generally, neutral N-donor linkers have been employed for the synthesis of cationic MOFs, apart from their participation as co-linkers in other MOFs, as the resulting coordination bond renders the presence of residual charge on the framework backbone.<sup>5</sup> Despite the understanding of design strategies to afford cationic MOFs, the development of MOFs constructed from N-donor ligands is still in rudimentary stages, as the relatively weaker metal-ligand coordination bond is susceptible to dissociation upon exposure to moisture or water. In general, the progress of MOFs towards practical implementation has been severely retarded on account of lack of stability, which is seeking much research attention in recent years.<sup>6</sup>

Among the different donor groups as neutral donor linkers, pyridyl terminal molecules have been much studied but the weak binding tendencies results in rapid dissociation under operational conditions. As suitable substitutes, 5-membered molecules such as imidazole/triazole have found affirmative research interest owing to the higher pKa/greater basicity relative to pyridyl donor moieties, which can lead to formation to stable MOFs.<sup>7</sup> Further, on account of relative smaller size of the terminal groups, these linkers afford the benefit of lower steric crowding and higher concentration of independent linkers around the metal node. Such donor groups have been found to impart local hydrophobicity and thus the resulting coordination network can lead to enhancement of chemical stability.<sup>8</sup> In addition to these aspects, the denticity of the linkers determines the stability of the resulting frameworks; wherein higher dentate ligands can undergo rapid repair and hence higher dentate ligands have found to impart higher kinetic stability.<sup>9</sup> With regard to structural aspects, the flexibility of the backbone too can influence the overall framework formation as the linker can accommodate the presence of other building blocks. In the synthesis of MOFs based on neutral N-donor linkers, the coordination ability of the counter anions strongly affects the nature of the resulting MOF, both in case of ionic and neutral MOFs. Generally, it has been observed that the use of non-/weakly-

coordinating anions leads to the formation of cationic MOFs with the anion occupying the voids, whereas strongly coordinating anions are favored for the preparation of neutral MOFs as charge-balancing species in the presence of neutral ligands. As discussed earlier, the characteristics of the building blocks directly influence the function of the resulting compounds. In this regard, the choice of the metal ion can affect the properties of the compound and direct its usage for specific applications. For instance, MOFs constructed from  $d^{10}$  transition metals (e.g.  $Zn^{2+}$ ,  $Cd^{2+}$ ) can yield luminescent MOFs,<sup>10</sup> which can be utilized for sensing applications. In addition, larger coordination sphere in case of Cd(II) and higher coordination numbers can lead to formation of diverse binding modes or coordination from different kinds of donor groups.

Despite the several advantages presented by neutral N-donor ligands, these MOFs have not progressed sufficiently owing to lack of stability as a direct consequence of weaker coordination bond. To address this issue, different approaches have been proposed in the literature, which include strengthening of the coordination bond or protection of the metal-ligand bond by imparting hydrophobicity by linker backbone.<sup>11</sup> MOFs having hard cations such as Zr(IV), Cr(III) have found to have probability of forming hydrolytically stable MOFs. Typically MOFs built from larger cations such as are prone to dissociation as the metal node is accessible to attack from foreign species. Recently, the efficacy of using Ni(II) to afford stable MOFs has been presented in multiple reports owing its favorable binding with both N- and O-donor ligands and the higher CFSE (Crystal Field Splitting Energy) relative to other transition metal cations.<sup>12</sup> Thus, much attention has been devoted to the understanding and consequently directing the appropriate choice of the metal ion for a given function and with regard to stability aspects. We sought to screen the aspects of stability and the consequent application features in MOFs constructed from neutral N-donor linkers. Herein we report the systematic evaluation of structural diversity with respect to stability and functional studies by fixing a neutral tridentate N-donor linker and Cd(II) metal ion and varying the nature of the counter anion. The choice of anion was selected from a weakly coordinating anion to strongly coordinating anion to form a series of MOFs having diverse structural features. The compound having a cationic framework could function as a fast probe for the capture of radioactive pertechnetate anions via surrogate permanganate and perhenate anions. Another compound having polar sites aligned along the pore walls could function as a selective sorbent of  $CO_2$ .

## 2.2 Experimental

### 2.2.1 Materials:

All solvents and reagents were commercially available and used without further purification.

### 2.2.2 Synthesis:

**Synthesis of Ligand {tris(4-(1H-imidazol-1-yl)phenyl)amine}**: The ligand was synthesized according to a reported protocol.<sup>13</sup> A mixture of tris(4-bromophenyl)amine (500 mg, 1.04 mmol), imidazole (423 mg, 6.22 mmol), K<sub>2</sub>CO<sub>3</sub> (573 mg, 4.15 mmol) and CuSO<sub>4</sub> (6.5 mg, 0.041 mmol) was heated at 150 °C under inert atmosphere for 60 hours. After cooling to ambient temperature, the mixture was dissolved in CH<sub>2</sub>Cl<sub>2</sub> (50 ml) and washed with water several times. The organic layer was brought to dryness to give a pale coloured powder. The ligand was recrystallized from a mixture of MeOH:CH<sub>2</sub>Cl<sub>2</sub> (1:1) in yield of 68%.

**Synthesis of Compound IPM-206**: A DCM solution of ligand (8.86 mg, 0.02 mmol) was taken in a glass tube. Over this solution, 1-butanol (1ml) was carefully added and methanolic solution of Cd(ClO<sub>4</sub>)<sub>2</sub> (6.22 mg, 0.02 mmol) was carefully layered over it. Single crystals of IPM-206 viz. {[Cd(L)<sub>2</sub>](ClO<sub>4</sub>)<sub>2</sub>·xG}<sub>n</sub> (G - guest solvent molecules), suitable for X-ray diffraction were formed after 10-12 days and were isolated in 40% yield. These crystals were dipped in MeOH solution to exchange the occluded solvents and heated under vacuum at 75°C to obtain the guest free phase. We could not estimate the uncoordinated anion and solvent molecules in the structure crystallographically due to high disorder. The formula for the guest-free phase was estimated to be {[Cd(L)<sub>2</sub>](ClO<sub>4</sub>)<sub>2</sub>]<sub>n</sub>.

**Synthesis of Compound IPM-310**: A DCM solution of ligand (8.86 mg, 0.02 mmol) was taken in a glass tube. Over this solution, benzene (1ml) was carefully added and methanolic solution of Cd(NO<sub>3</sub>)<sub>2</sub> (6.16 mg, 0.02 mmol) was carefully layered over it. Single crystals of IPM-310 viz. {[Cd(L)(NO<sub>3</sub>)<sub>2</sub>](xG)<sub>n</sub>, suitable for X-ray diffraction were formed after 8-9 days and were isolated in 35% yield. We could not estimate the solvent molecules and free anions in the structure crystallographically due to high disorder. The formula for the guest-free phase was estimated to be {[Cd(L)(NO<sub>3</sub>)<sub>2</sub>]<sub>n</sub>.

**Synthesis of Compound IPM-312**: A methanolic solution of ligand (8.86 mg, 0.02 mmol) was taken in a glass tube. Over this solution, ethanol (1ml) was carefully added and aqueous solution of Cd(SO<sub>4</sub>) (6.22 mg, 0.02 mmol) was carefully layered over it. Single crystals of IPM-312 viz. {[Cd<sub>2</sub>(SO<sub>4</sub>)<sub>2</sub>(L)<sub>2</sub>](xG)<sub>n</sub>, were formed after 2 weeks and were isolated in 30% yield. We could not estimate the solvent molecules in the structure crystallographically due to high disorder. The formula for the guest-free phase was estimated to be {[Cd<sub>2</sub>(SO<sub>4</sub>)<sub>2</sub>(L)<sub>2</sub>]<sub>n</sub>.

**Synthesis of Compound IPM-315**: A mixture of ligand (8.86 mg, 0.02 mmol), Cd(NO<sub>3</sub>)<sub>2</sub> (6.16 mg, 0.02 mmol) and sulfanilic acid (5.22 mg, 0.02 mmol), DMF (2 ml) and 1-butanol (1 ml) was placed in a glass vial and heated at 120°C for 48 hours followed by slow cooling to room temperature. The compound IPM-315 viz. {[Cd(L)(NO<sub>3</sub>)(SA)](DMF)<sub>n</sub>, was filtered and washed with methanol several times. The compound was isolated in 50% yield.



**Synthesis of Compound IPM-311:** A mixture of ligand (8.86 mg, 0.02 mmol),  $\text{Cd}(\text{NO}_3)_2$  (6.16 mg, 0.02 mmol) and sulfanilic acid (5.22 mg, 0.02 mmol), DMF (2 ml) and water (1 ml) was placed in a glass vial and heated at  $120^\circ\text{C}$  for 48 hours followed by slow cooling to room temperature. The compound IPM-311 viz.  $\{[\text{Cd}(\text{L})(\text{HCOO})_2] \cdot x\text{G}\}_n$ , was filtered and washed with methanol several times. The compound was isolated in 60% yield.

### 2.2.3 Water stability Studies

~20 mg of the activated compound was dipped in 5 ml of deionised water and kept at room temperature. Subsequently, the compound was filtered off and dried in air for further characterization.

### 2.2.4 Anion exchange Studies

2 mg activated phase of IPM-206 was dispersed in an aqueous solution of  $\text{KMnO}_4$  (1mM, 0.2 ml in 2 ml D.I.  $\text{H}_2\text{O}$ ) and the UV-vis spectra of the supernatant was monitored in periodic time intervals. Similar studies were carried out for  $\text{ReO}_4^-$ . To monitor the sensing features, 1 mg activated phase of IPM-206 was dispersed in an aqueous solution and  $\text{KMnO}_4$  (1 mM stock, 20-200  $\mu\text{l}$ ) was added stepwise and the corresponding fluorescence spectra were monitored. Similar studies were carried out with  $\text{ReO}_4^-$ . For capture studies in presence of competing anions, stepwise addition of competing anion and  $\text{KMnO}_4$  were carried out and corresponding emission spectra were recorded.

### 2.2.5 Physical Measurements:

Powder X-ray diffraction patterns were recorded on Bruker D8 Advanced X-Ray diffractometer using  $\text{Cu K}\alpha$  radiation ( $\lambda = 1.5406 \text{ \AA}$ ) in  $5^\circ$  to  $40^\circ$   $2\theta$  range with a scan speed of  $1.2^\circ\text{min}^{-1}$ . The IR Spectra were acquired by using NICOLET 6700 FT-IR spectrophotometer using KBr pellet in  $400\text{-}4000 \text{ cm}^{-1}$  range. UV spectra were recorded on Shimadzu UV 2600 Spectrophotometer having stirring attachment. The SEM images & EDX data were obtained using FEI Quanta 3D dual beam FESEM. Thermogravimetric analysis profiles were recorded on Perkin-Elmer STA6000, TGA analyser under  $\text{N}_2$  atmosphere with heating rate of  $10^\circ\text{C}/\text{min}$ . Gas adsorption measurements were performed using BelSorp-Max instrument (Bel Japan). Prior to adsorption measurements, the activated samples were heated at  $105^\circ\text{C}$  under vacuum for 4 hours using BelPrepvacII.

### 2.2.6 X-ray Structural Studies:

Single-crystal X-ray data of compounds were collected at 100 K on a Bruker D8 Venture Duo X-ray diffractometer equipped with Microfocus X-ray source (operated at 50W; 50kV/1mA), graded multilayer optics for monochromatic  $\text{Mo K}\alpha$  radiation ( $\lambda = 0.71073 \text{ \AA}$ ) focused X-ray beam and Photon 100 CMOS

chip based detector system. Crystal was mounted on nylon CryoLoops (Hampton Research) with Paratone-N (Hampton Research). The data integration and reduction were processed with SAINT software.<sup>14</sup> A multi-scan absorption correction was applied to the collected reflections.<sup>15</sup> The structure was solved by the direct method using SHELXTL<sup>16</sup> and was refined on  $F^2$  by full-matrix least-squares technique using the SHELXL-2014/7<sup>17</sup> program package within the WINGX<sup>18</sup> programme. All non-hydrogen atoms were refined anisotropically. All hydrogen atoms were located in successive difference Fourier maps and they were treated as riding atoms using SHELXL default parameters. The structures were examined using the *Adsym* subroutine of PLATON to assure that no additional symmetry could be applied to the models. The SQUEEZE option<sup>19</sup> was used to eliminate the contribution of disordered guest molecules. CCDC 1846341, 1846342, 1846344, 1846346, 1846347 for IPM-206, IPM-310, IPM-311, IPM-312, IPM-315 respectively, contains the supplementary crystallographic data for this paper. These data can be obtained free of charge from The Cambridge Crystallographic Data Centre via [www.ccdc.cam.ac.uk/data\\_request/cif](http://www.ccdc.cam.ac.uk/data_request/cif).

### 2.3 Results and discussion

Based on our target of evaluating structural diversity and functional properties of MOFs based on neutral N-donor ligands, we chose a tridentate linker having smaller imidazole donor sites and a flexible core viz. tris(4-imidazolylphenyl)amine (TIPA). By keeping the ligand and metal ion same, we varied the anions in the reaction medium to obtain a series of compounds viz. IPM-206, IPM-310, IPM-311, IPM-312 and IPM-315 (IPM stands for IISER Pune Materials) (Figure 2.1). The choice of the metal ion was based on the higher size of the cation which can bind well with different donor groups and accommodate the variations in the building blocks. The anions were varied from weakly coordinating perchlorate anions ( $\text{ClO}_4^-$ ) to strongly coordinating sulfate ( $\text{SO}_4^{2-}$ ) anions.

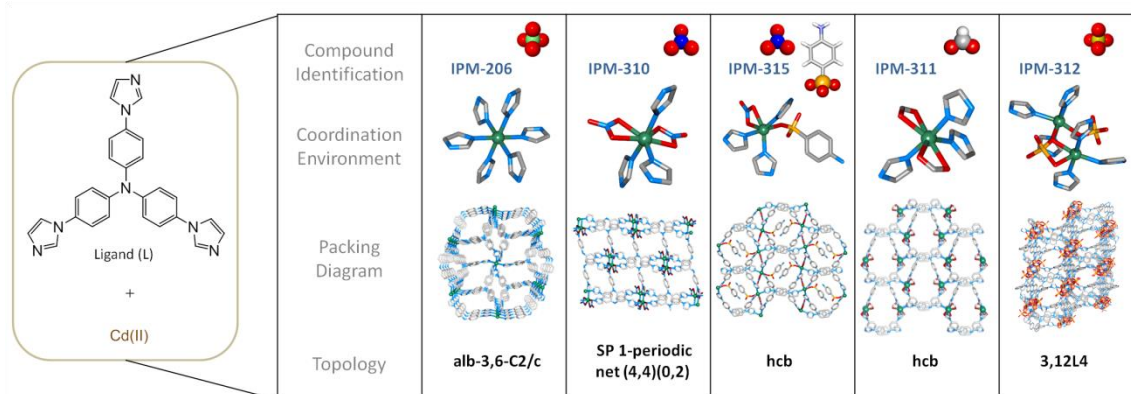


Figure 2.1 Representation of the basic features of the different structures synthesized in this work.

Crystals of IPM-206 were prepared at room temperature in a solvent mixture of DCM, methanol and *n*-butanol as the blank template. Information collected from single-crystal X-ray diffraction (SCXRD) studies suggested that the compound crystallized in monoclinic space group of C2/c. One Cd(II) metal unit, one linker unit constitute the asymmetric unit, with the disordered anions unassigned crystallographically (Appendix 2.4). The formula of the MOF was calculated to be  $\{[\text{Cd}(\text{L})_2] \cdot (\text{ClO}_4)_2 \cdot x\text{G}\}_n$ . *Adsym* subroutine of PLATON was applied to check the possibility of any higher symmetry, but no further symmetry was suggested. The metal node of Cd(II) has octahedral geometry with coordination from six independent linkers (Appendix 2.5). One Cd(II) metal cation is ligated to six independent linkers which link to further 10 Cd(II) metal cations, which extends the framework to 3-dimensions. FESEM images suggested the formation of neat crystalline morphologies (Appendix 2.6). Topological analysis using TOPOS, suggested that the compound had a rare topology of alb-3,6-C2/c. The distance between adjacent linkers, as calculated by the distance between central N-atom, was calculated to be 8.94 Å. The angles between the donor N-atoms and the central core N-atom of the ligand were found to be 115.6°, 113.4° and 130.6° (Appendix 2.17). PLATON analysis suggested that the compound had 3645 Å<sup>3</sup> void volume, considering only the cationic network. The packing features suggest that compound has a porous channel along *b*-axis. Basic characterization was done for the compound where we found that the bulk phase of the compound was pure and the thermogravimetric analysis suggested loss of solvent molecules upto 350°C (Appendix 2.22-Appendix 2.23).

From perchorate, we then chose a moderately coordinating nitrate anion (NO<sub>3</sub><sup>-</sup>). Crystals of IPM-310 were obtained at room temperature by layering technique. SCXRD studies revealed that the framework crystallized in P-1 space group. The asymmetric unit comprises of one Cd(II) unit, one ligand unit, two nitrate anions (Appendix 2.7) and formula for the compound was  $\{[\text{Cd}(\text{L})(\text{NO}_3)_2] \cdot x\text{G}\}_n$ . The coordination environment for Cd(II) has pentagonal bipyramidal geometry with N3O4 donor set and the coordination polymer extended only in one dimension (Appendix 2.8-Appendix 2.9). The distance between adjacent linkers was found to be 11.98 Å (distance between central N-atoms) and the angles between the different N-atoms were found to be 127.1°, 117.2° and 115.6° (Appendix 2.18). PLATON analysis revealed that the void volume in the compound was 779 Å<sup>3</sup>. Powder X-ray diffraction (PXRD) studies were checked to confirm the bulk phase formation of the product (Appendix 2.24) and TGA profile suggested that the compound had reasonable thermal stability (Appendix 2.25).

Another moderately coordinating anion formate (HCOO<sup>-</sup>) was used to obtain a neutral MOF IPM-311. The crystals were obtained in a solvothermal reaction in solvent mixture of DMF:H<sub>2</sub>O (2:1) at 120°C. SCXRD analysis revealed that the compound crystallized in C2 space group. The asymmetric unit of the compound had one Cd(II) unit, one ligand molecule and two formate anions coordinated to the metal centres (Appendix

2.1). The compound has only one kind of Cd(II) metal centres having pentagonal bipyramidal geometry from N3O4 donor groups (Appendix 2.1) and the formula was found to be  $\{[\text{Cd}(\text{L})(\text{HCOO})_2] \cdot x\text{G}\}_n$ . The compound was found to have **hcb** topology as calculated using TOPOS. The distance between adjacent ligands was found to be 8.87 Å. The angles for the ligands were found to be 120.5°, 112.8°, 125.6° (Appendix 2.19). The compound was found to have 1D porous channel along c-axis and PLATON analysis revealed that the void volume in the system was 1015 Å<sup>3</sup> (Appendix 2.2). PXRD patterns validated the bulk phase purity of the compound (Appendix 2.29). Upon heating we found that the compound underwent slight structural, which can be attributed to slight structural changes associated for 2-dimensional compounds.

To extend the coordinating strength of the anions, we employed a monodentate sulfanilic acid in addition to nitrate anions to yield compound IPM-315. The compound was synthesized under solvothermal conditions in solvent system of DMF: n-butanol (2:1) at 120°C. The compound crystallized in P2<sub>1</sub>2<sub>1</sub>2<sub>1</sub> space group. One Cd(II) unit, one ligand, one unit of sulfanilic acid, one nitrate anion and one full DMF molecule constitute the asymmetric unit (Appendix 2.15). The coordination environment of the metal centre is octahedral with N3O3 donor groups and the overall coordination network is 2-dimensional (Appendix 2.20). The topology of the framework was calculated to be hcb. The structural analysis revealed that the distance between adjacent linkers was 8.92 Å and the angles between the N-atoms of the ligand were 122.7°, 118.6°, 116.4° (Appendix 2.16). The solvent molecules (DMF) occupy the pores along a-axis. The presence of the bulky anion (sulfanilic acid) blocks the pore. PXRD patterns ascertained the bulk phase purity of the compound (Appendix 2.27). TGA profiles exhibited a loss of solvent molecules and the decomposition was found after 320°C (Appendix 2.28). FT-IR spectra exhibited peaks corresponding to the presence of both the anions (Appendix 2.31).

Further we employed the strongly coordinating sulphate anions to examine the influence on structural packing. Single crystals of IPM-312 were obtained by slow diffusion process. SCXRD studies yielded that the compound crystallized in triclinic P-1 space group. The asymmetric unit consists of two Cd(II) metal ions, two ligands and two full sulphate anions (Appendix 2.11), and the formula of the compound was estimated to be  $\{[\text{Cd}_2(\text{SO}_4)_2(\text{L})_2] \cdot x\text{G}\}_n$ . Cd(II) was found to be octahedral with coordination from N3O3 donor groups (Appendix 2.11). One metal node binds to 3 independent linkers and two adjacent metal nodes are bridged by sulphate anions and the coordination network extended in two dimensions (Appendix 2.12-Appendix 2.13). TOPOS analysis suggested that the compound a rare topology of 3,12L4. The distance between central N-atoms of adjacent linkers was calculated to be 7.11 Å, while the angles between the N-atoms of the individual linkers were found to be 118.7°, 113.8°, 127.2° (Appendix 2.24). PLATON analysis revealed that the compound had void volume of 1038 Å<sup>3</sup>. Importantly from the perspective of application, the compound had oxygen atoms of sulphate pointing towards the pore (Appendix 2.13), making the pore

surface polar and providing recognition sites for interacting with guest molecules. PXRD patterns validated the purity of the bulk phase (Appendix 2.44).

The choice of building blocks renders luminescence character to the framework. The emission and absorption characteristics for all the MOFs were recorded by dispersing the compounds in acetonitrile. Excitation spectra had peak at 310nm for all cases (Appendix 2.32). We observed almost similar emission character for all the compounds, with slight shifts in case of IPM-206. As observed previously, ligand-ligand interactions and ligand-to-metal-charge transfer (LMCT) processes could be primarily ascribed to the observed luminescence character. These observations suggest that despite the different anions, the absorption and emission character is determined by the ligand and metal, although the structural characteristics are different.

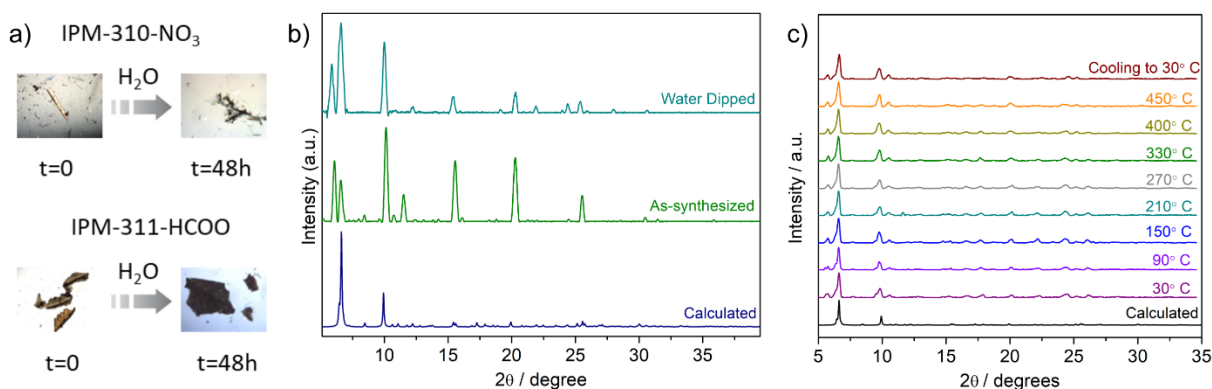


Figure 2.2 a) Optical microscopic images of IPM-310 and IPM-311 after dipping in deionised water for 1 day. PXRD patterns for IPM-312 for b) water dipped phase (1 day) and c) variable temperature heating.

As outlined above, one of the objectives of this work was to evaluate the role of counter ions in influencing the stability of the systems. Based on the series of synthesized compounds, the coordinating tendencies varied from weakly coordinating ClO<sub>4</sub><sup>-</sup> to strongly coordinating SO<sub>4</sub><sup>2-</sup>; thus we anticipated that the stability could be directly proportional to the coordinating strength of the anions. To examine this hypothesis, initially crystals of all the compounds were initially dipped in deionised water and monitored under optical microscope for 24 hours. Barring IPM-206 and IPM-312, the crystals in other cases became opaque and broke down (Figure 2.2a). The water stability of the two stable crystals was then tested on the bulk scale, where powders of the compounds were dispersed in water and the PXRD patterns were checked after 24 hours (Figure 2.2b). The observation sheds important insights into the binding ability driven stability in

neutral N-donor systems. In the case of IPM-206, the high density of the ligands provides steric crowding and local hydrophobicity which shields the metal ion from the influence of external species, as observed for N-donor ligand based MOFs. In case of IPM-312, the strongly coordinating anions provide high stability to the framework and make it resistant to the hydrolysis. While in all other cases, the lewis basicity of other anions was not sufficient to protect the metal ion from the influence of water. To characterize the hydrolytic stability of IPM-312, the FESEM images were recorded which should no change to the morphology. In addition to hydrolytic stability, the compound IPM-312 was found to present high thermal stability (upto 450°C) which is uncommonly observed for neutral N-donor linker based MOFs (Figure 2.2c). This observation too can be ascribed to the strong binding ability of the sulfate anions to the metal centres.

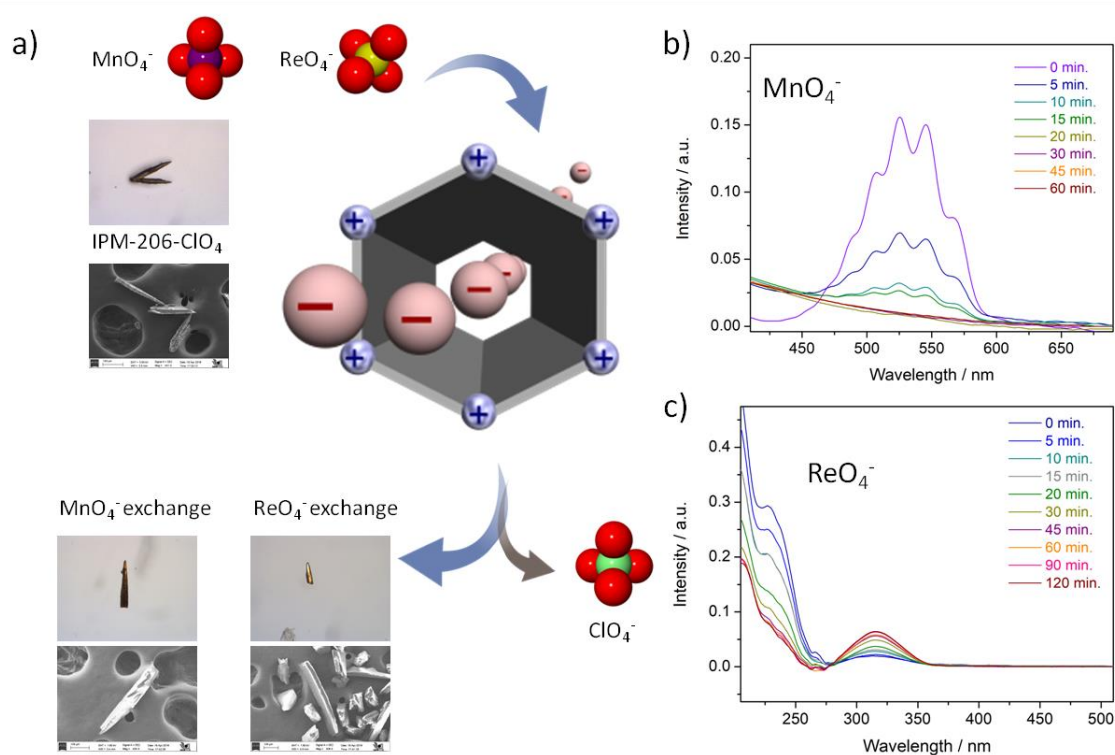


Figure 2.3 a) Schematic illustration of the ion-exchange process in IPM-206 along the corresponding microscopic and FESEM images. Time dependent UV-vis spectra of the supernatant for b) MnO<sub>4</sub><sup>-</sup> and c) ReO<sub>4</sub><sup>-</sup>.

Encouraged from these observations, we sought to study the applications of the compounds which were hydrolytically stable. As IPM-206 bears dual features of being a cationic MOF and having luminescent properties, we sought to test its ability to sense and capture of environmentally hazardous anionic pollutants.<sup>3,4</sup> The rise of alternate fuels sources has paved way for the expansion of nuclear power stations

across the globe. These lead to contamination of water streams by radioactive pollutants such as pertechnetate ( $\text{TcO}_4^-$ ) which have a long half life of  $2 \times 10^6$  years and have high water solubility. As  $\text{TcO}_4^-$  is not used in routine laboratory conditions, researchers have employed  $\text{MnO}_4^-/\text{ReO}_4^-$ , which have similar physical characteristics as model ions to study the performance towards  $\text{TcO}_4^-$ . Although few reports have shown potential of MOFs for the capture of such oxo-anions, there remains potential for improvement in terms of signalling mechanism and kinetics.<sup>3</sup> To evaluate the ability of IPM-206 for these functions, we initially monitored the fate of single crystals after dipping in aqueous solutions of  $\text{MnO}_4^-$  and  $\text{ReO}_4^-$  (Figure 2.3a, Appendix 2.33). Both under the optical microscope and in FESEM analysis, the crystal morphology remained unchanged and the colour became dark. Simultaneously the colour of the supernatant decoloured rapidly. Time dependent UV-vis spectra were recorded for the supernatant solutions and the peaks corresponding to the absorption by  $\text{MnO}_4^-$  (540 nm) and  $\text{ReO}_4^-$  (208 nm) were found to decrease gradually (Figure 2.3b-2.3c, Appendix 2.34-Appendix 2.35). The exchanged compounds were characterized using EDX, which confirmed the exchange process. As the MOF had luminescence character, we sought to examine the ability to sense the inclusion of the oxoanions. Stepwise addition of  $\text{MnO}_4^-$  and  $\text{ReO}_4^-$  was carried in separately dispersed IPM-206 powders (Appendix 2.36-Appendix 2.37). We observed rapid quenching of the luminescence and the response was linear with increasing concentration (Appendix 2.42-Appendix 2.43). The reason for the quenching could be ascribed to the differential interactions of the incoming anions with the framework. Apart from sensing of the targeted anions, detection in presence of competing anions is important. To check this, the emission profiles were recorded in concurrent presence of common anions such as  $\text{PF}_6^-$  and  $\text{CF}_3\text{SO}_3^-$ . The response of  $\text{MnO}_4^-$  and  $\text{ReO}_4^-$  in presence of such common anions was not perturbed significantly suggesting the selective interaction based sensory process (Appendix 2.38-2.41). The results suggest that IPM-206 could present dual function of capture and recognition of radioactive  $\text{TcO}_4^-$  anions, as examined via its surrogate anions.

The emergence of carbon capture and sequestration (CCS) has propelled the development of MOFs for this application. In particular the low energy costs associated with capture and release of  $\text{CO}_2$  by MOFs has put them as frontrunners in the synthesis of new materials.<sup>3b</sup> The ability to tune the pore size, character and subsequently impart selectivity features are certain features for MOFs which score over other porous materials. Among this, the presence of specific polar groups has found to bestow highly selective capture of  $\text{CO}_2$ . In this regard other inorganic anions studied include  $\text{SiF}_6^{2-}$ ,  $\text{Cr}_2\text{O}_7^{2-}$ ,  $\text{MoO}_4^{2-}$ ,  $\text{CrO}_4^{2-}$  and more recently the utility of sulfonate donor groups has been shown. As the compound IPM-312 bears the presence of polar sulphate anions aligned along the pore walls, we sought to investigate the ability to capture  $\text{CO}_2$ . The adsorption isotherms yielded an uptake amount of 1.17 mmol/g and 0.76 mmol/g at 273K and 298K respectively (Appendix 2.46). Importantly, the compound had negligible uptake for  $\text{N}_2$ . The observed

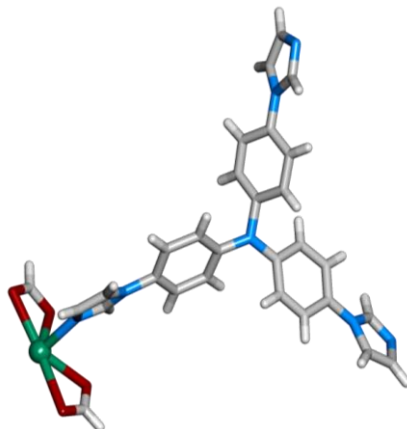
selectivity could be ascribed the ultramicroporous nature of the compound having highly polar groups along the pore walls. As discussed in the previous section, we checked the water stability of the compound in the bulk phase and found that the structure was not affected (Appendix 2.44). After recovering the compound, we checked whether the pore character was altered but found almost same uptake at 298K. The findings suggest that sulphate coordinated frameworks could simultaneously offer the features of stability and polar sites in an ultramicroporous system.

## **2.4 Conclusions**

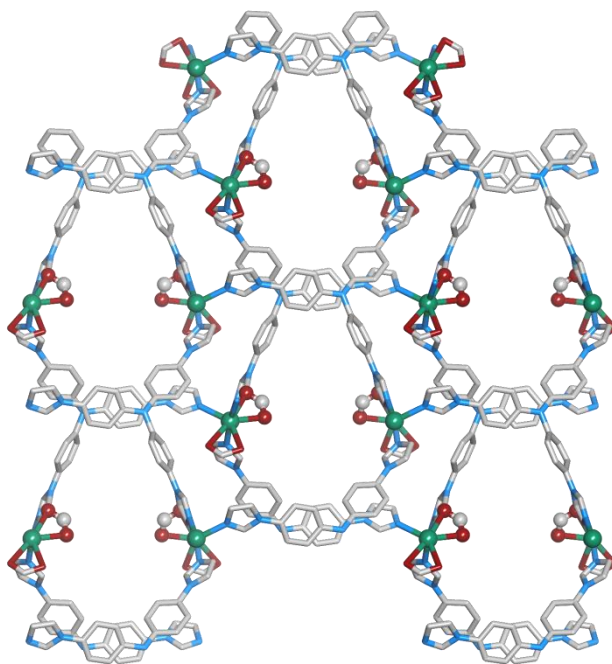
In summary, we have synthesized a series of MOFs based on a neutral N-donor linker and varying the anions in the structure. Structural diversity was based on the coordinating ability of the anions which could be accommodated by the using a metal ion with high coordination sphere and a linker having a flexible core. The stability of the compounds was thoroughly investigated which could be directly correlated to the binding ability of the anions in case of the neutral MOFs. The functional character afforded in case of the hydrolytically stable MOFs was evaluated for the capture of radioactive pollutant pertechnetate anion via its surrogate anions permanganate and perrhenate and the ability of a MOF bearing polar sites for the capture of greenhouse gas CO<sub>2</sub>.



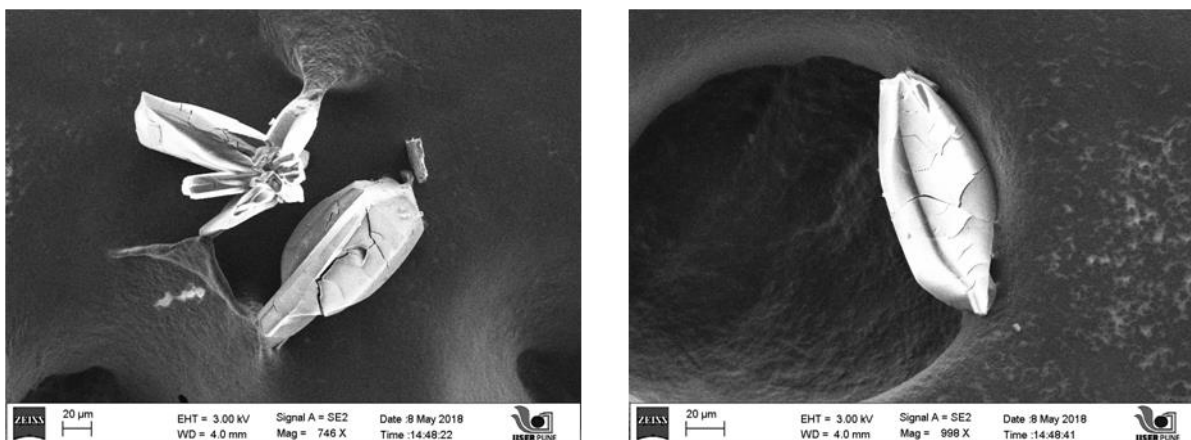
## 2.5 Appendix Section



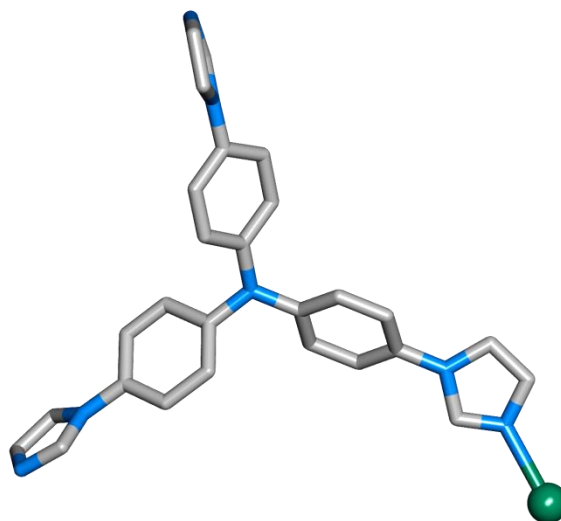
**Appendix 2.1:** Asymmetric unit of IPM-311. (Colour code: C, grey; N, blue; Cd, green; O, dark red; H, white)



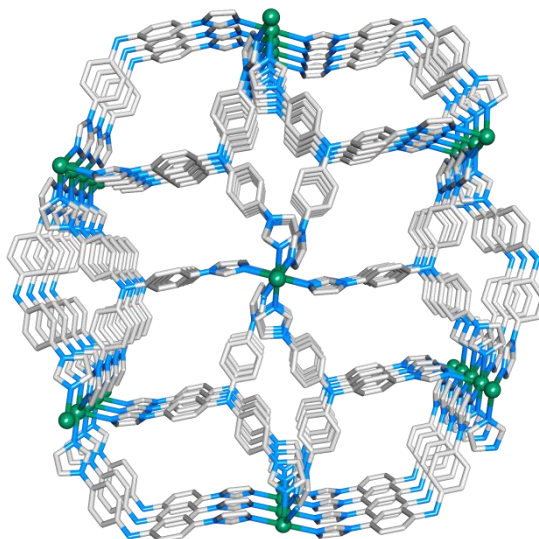
**Appendix 2.2:** Figure showing packing of IPM-311 along crystallographic *b*-axis, (Hydrogen atoms have been omitted for clarity (Colour code: C, grey; N, blue; Cd, green; O, dark red)



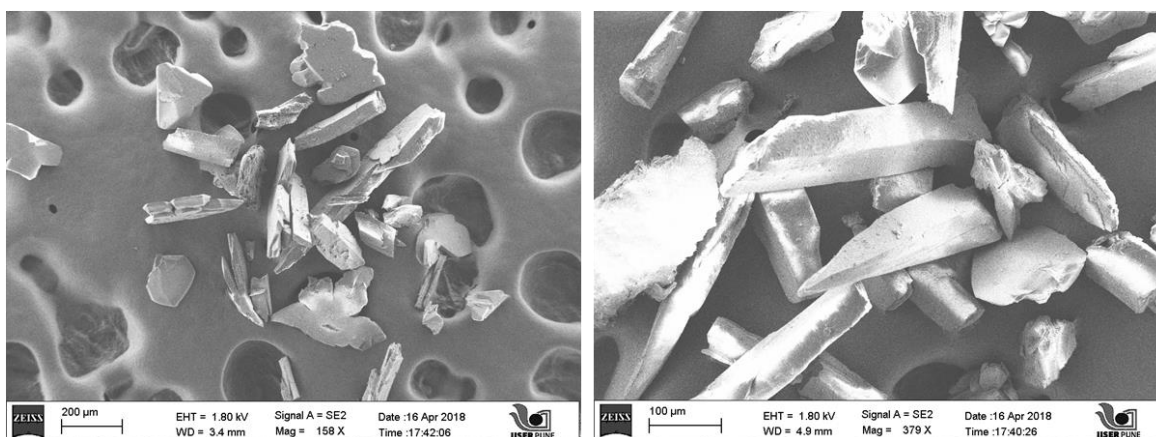
**Appendix 2.3:** FESEM images for compound IPM-311. The images were recorded for the solid sample on carbon tape.



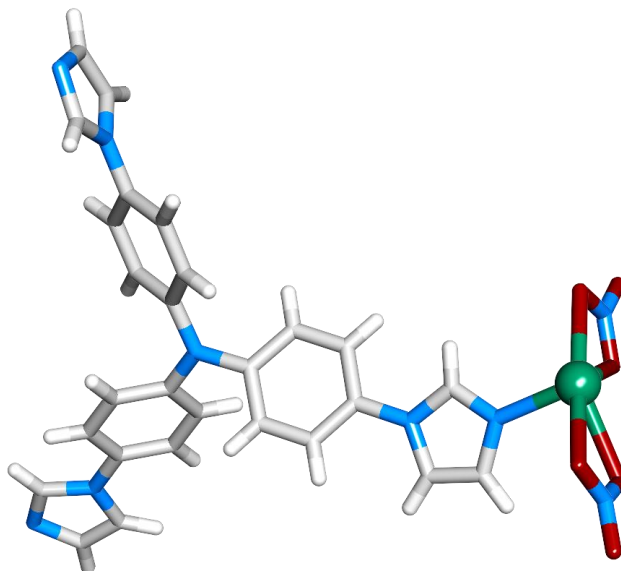
**Appendix 2.4:** Asymmetric unit of IPM-206. (Colour code: C, grey; N, blue; Cd, green; O, dark red. H-atoms and disordered anions have been omitted for clarity)



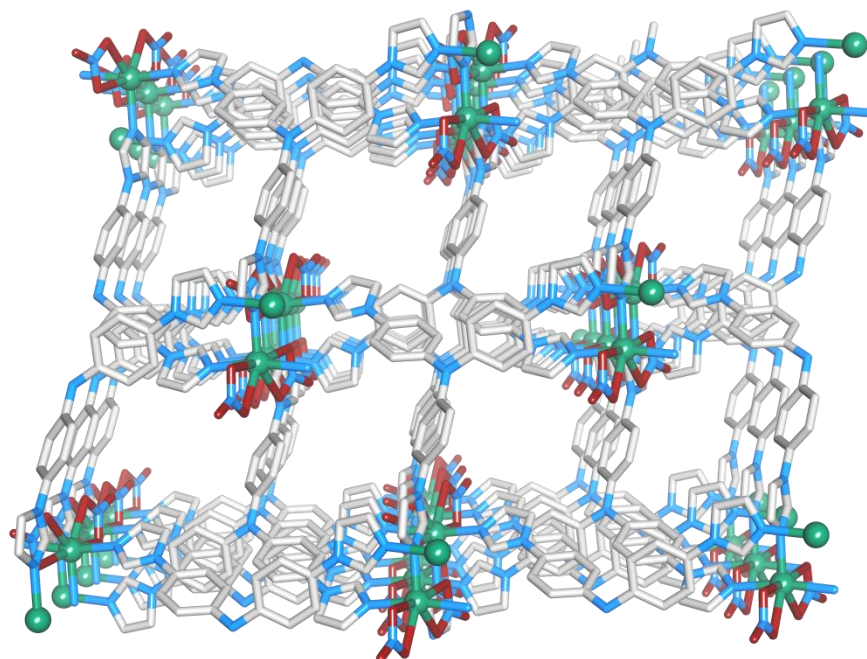
**Appendix 2.5:** Figure showing packing of IPM-206 along crystallographic *b*-axis, (Hydrogen atoms have been omitted for clarity (Colour code: C, grey; N, blue; Cd, green))



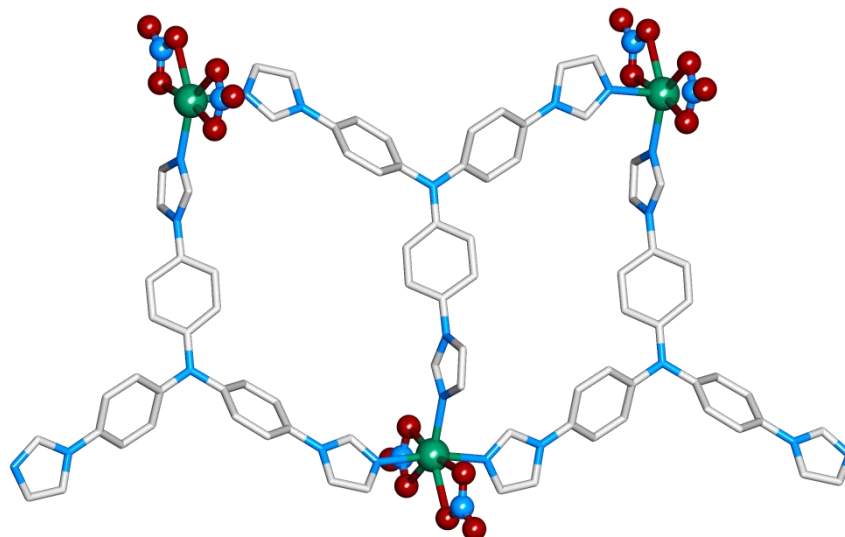
**Appendix 2.6:** FESEM images for compound IPM-206. The images were recorded for the solid sample on carbon tape.



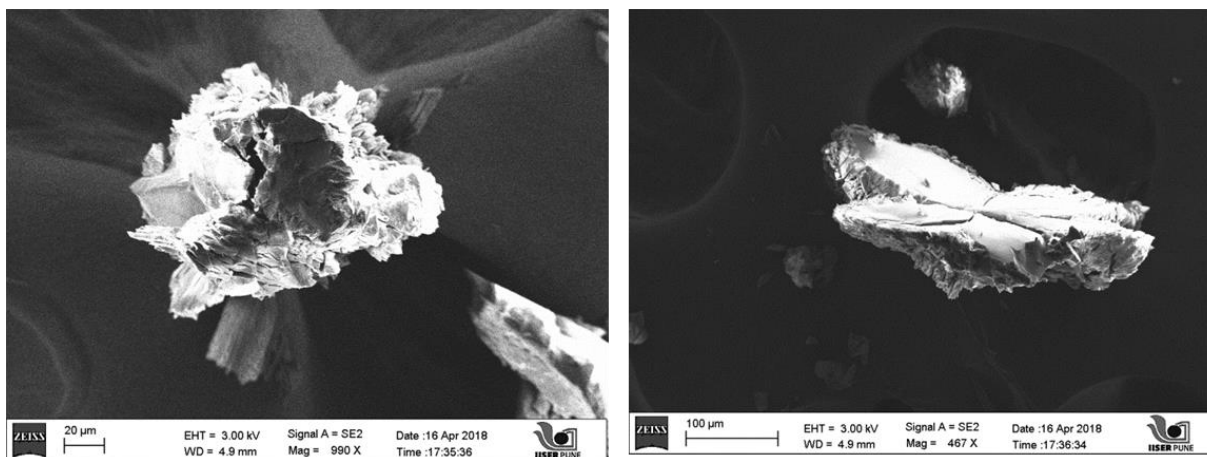
**Appendix 2.7:** Asymmetric unit of IPM-310. (Colour code: C, grey; N, blue; Cd, green; O, dark red; H, white)



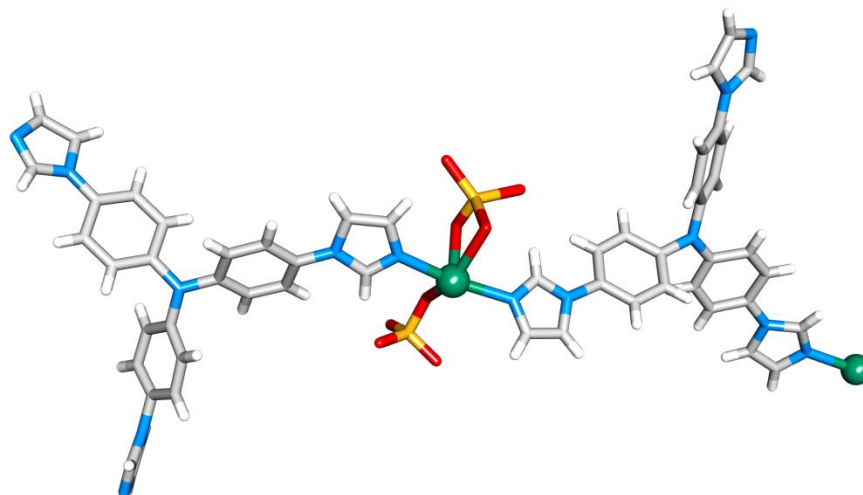
**Appendix 2.8:** Figure showing packing of IPM-310 along crystallographic *b*-axis, (Hydrogen atoms have been omitted for clarity (Colour code: C, grey; N, blue; Cd, green))



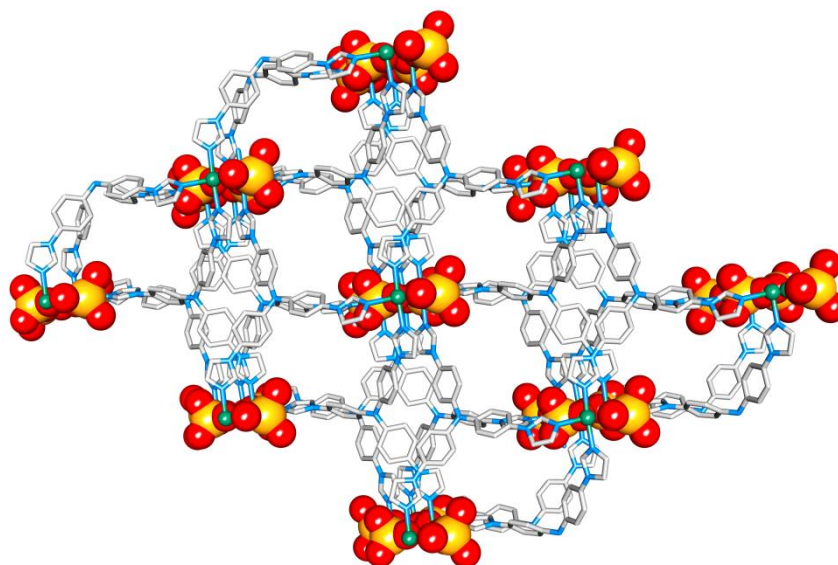
**Appendix 2.9:** Figure showing packing of IPM-310 along crystallographic showing coordinated nitrate anions along *b*-axis, (Hydrogen atoms have been omitted for clarity (Colour code: C, grey; N, blue; Cd, green))



**Appendix 2.10:** FESEM images for compound IPM-310. The images were recorded for the solid sample on carbon tape.

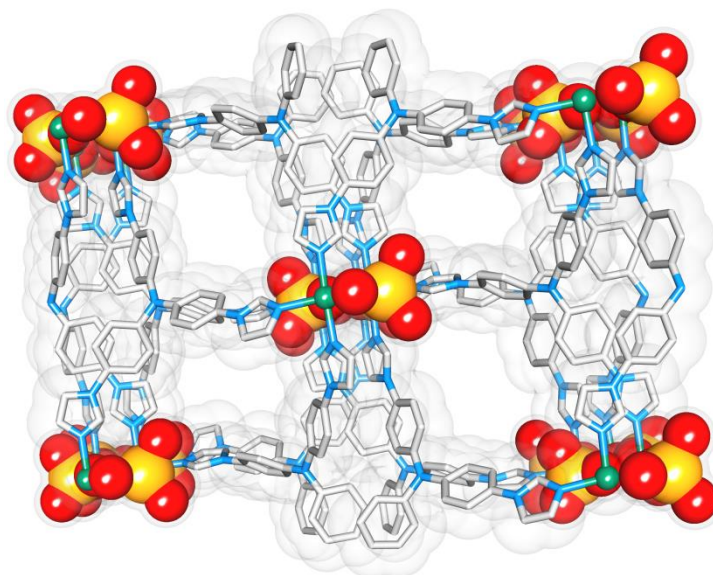


**Appendix 2.11:** Asymmetric unit of IPM-312. (Colour code: C, grey; N, blue; Cd, green; O, dark red; H, white; S, yellow)

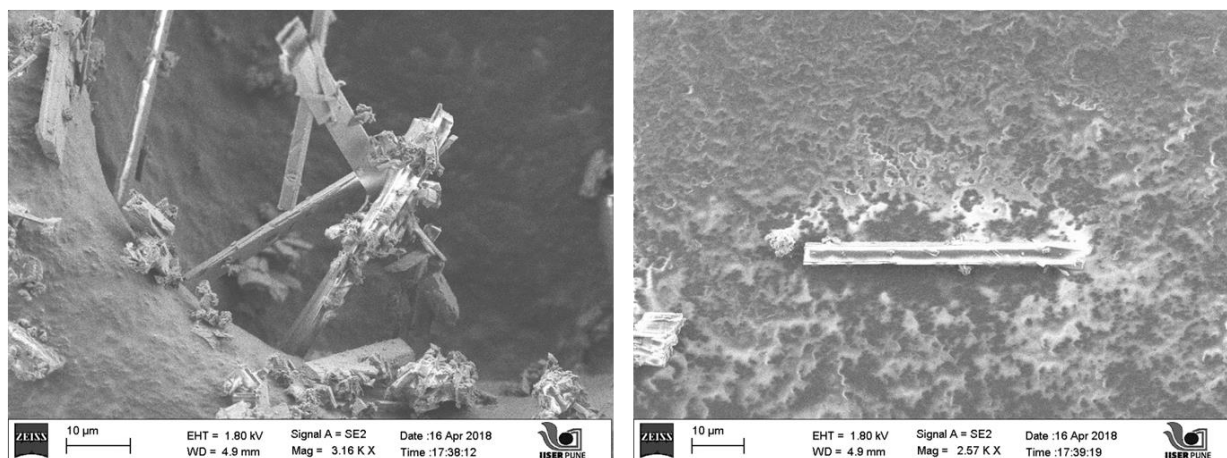


**Appendix 2.12:** Figure showing packing of IPM-312 along crystallographic *b*-axis, (Hydrogen atoms have been omitted for clarity (Colour code: C, grey; N, blue; Cd, green; S, yellow)).

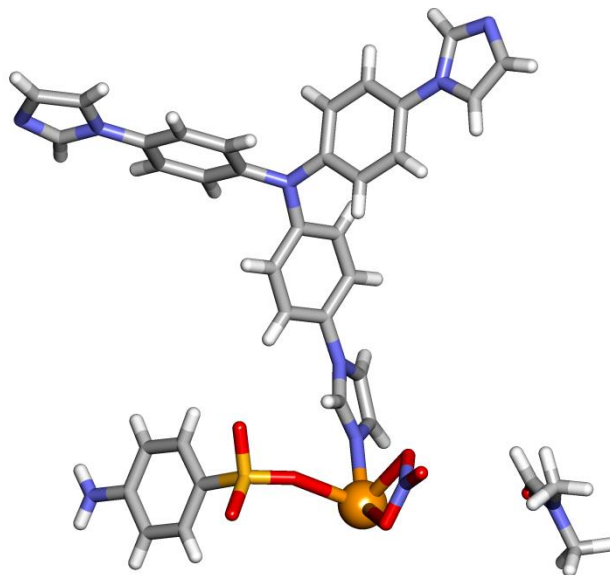




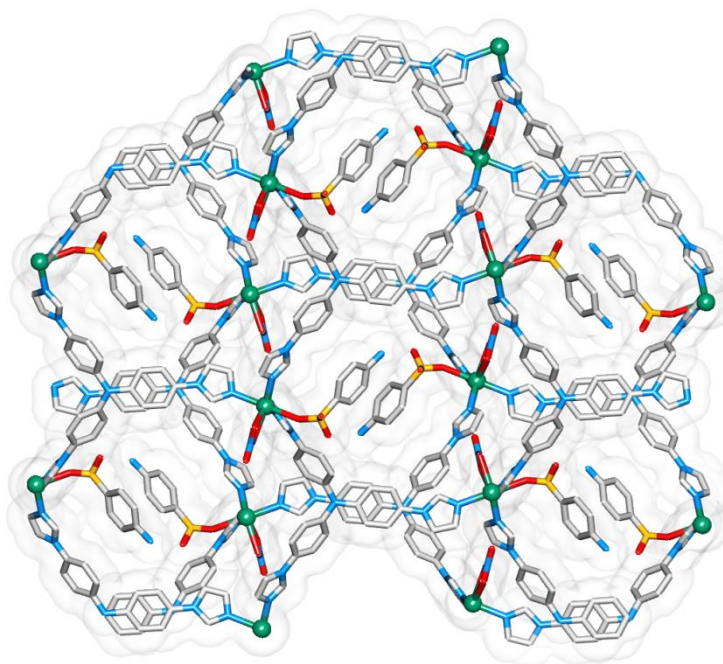
**Appendix 2.13:** Figure showing packing of IPM-312 along crystallographic *b*-axis, (Hydrogen atoms have been omitted for clarity (Colour code: C, grey; N, blue; Cd, green; S, yellow))



**Appendix 2.14:** FESEM images for compound IPM-312. The images were recorded for the solid sample on carbon tape.

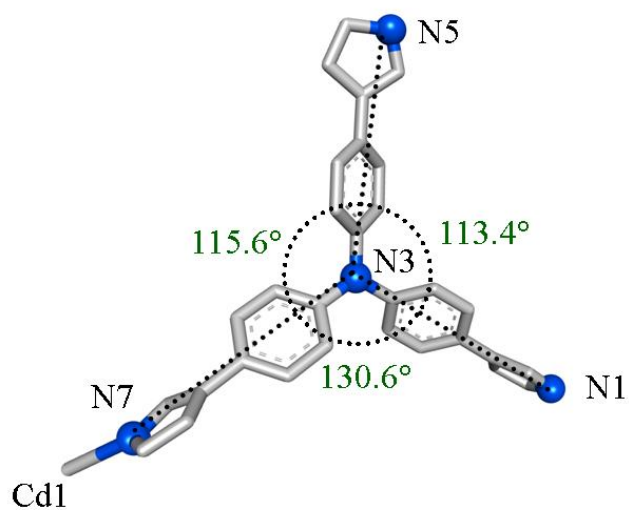


**Appendix 2.15:** Asymmetric unit of IPM-315. (Colour code: C, grey; N, blue; Cd, green; O, dark red; S, yellow)

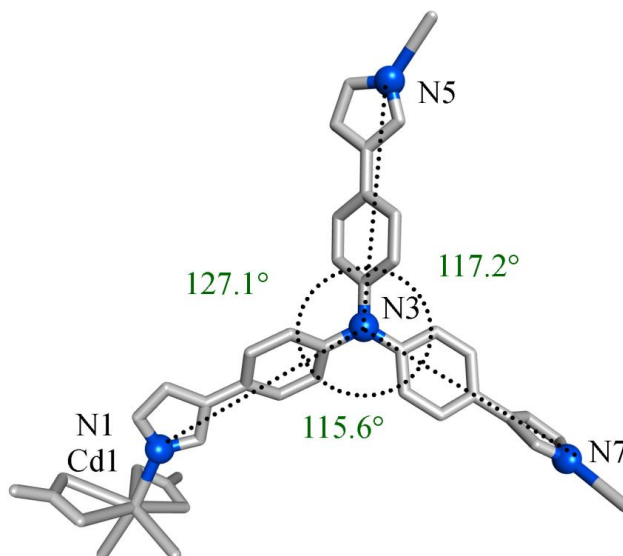


**Appendix 2.16:** Figure showing packing of IPM-315 along crystallographic *b*-axis, (Hydrogen atoms have been omitted for clarity (Colour code: C, grey; N, blue; Cd, green; S, yellow)).

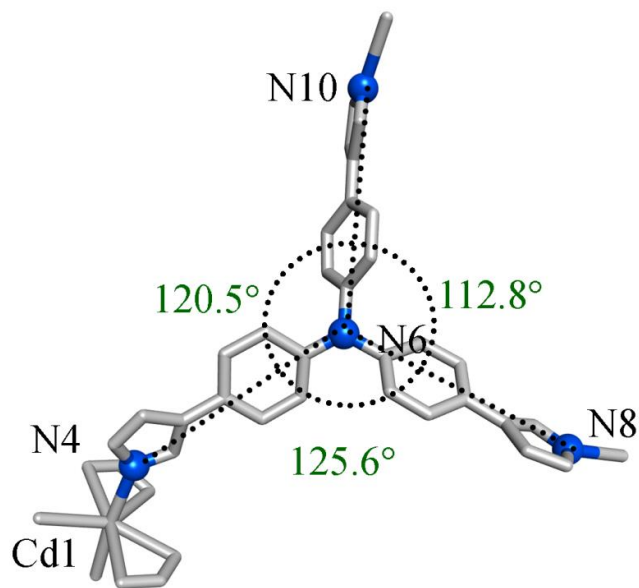




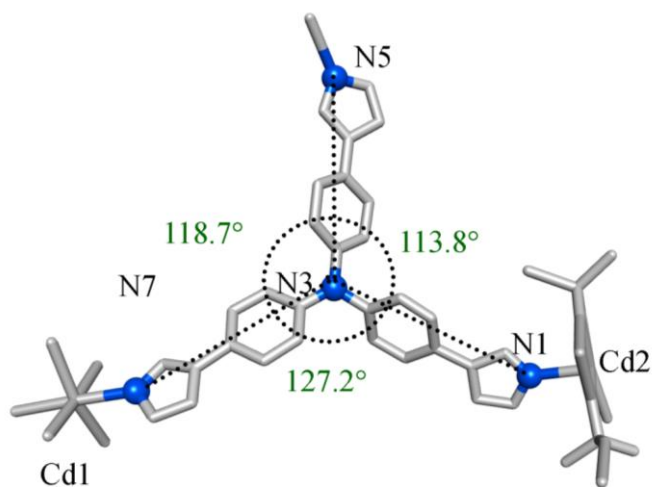
**Appendix 2.17:** Figure showing angles in IPM-206 (Hydrogen atoms have been omitted for clarity).



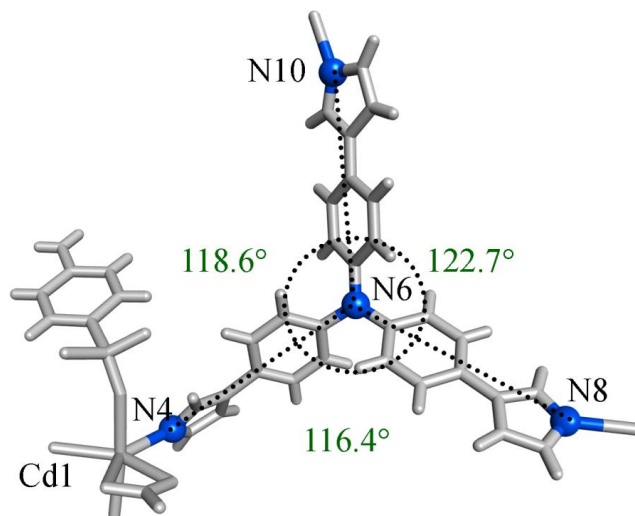
**Appendix 2.18:** Figure showing angles of IPM-310 (Hydrogen atoms have been omitted for clarity).



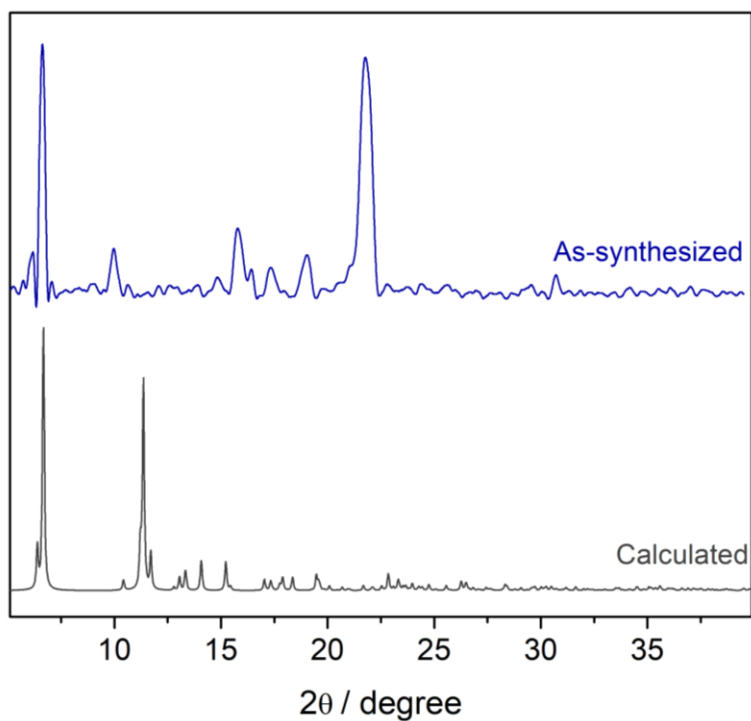
**Appendix 2.19:** Figure showing angles of IPM-311 (Hydrogen atoms have been omitted for clarity).



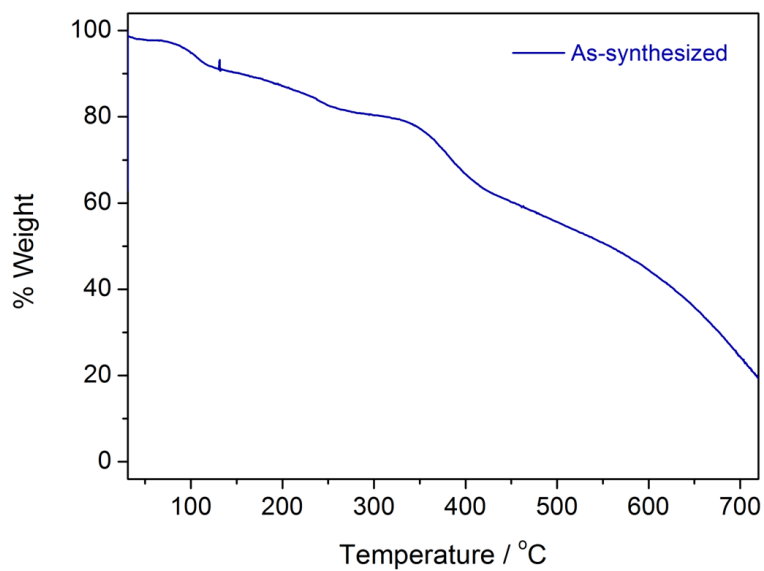
**Appendix 2.20:** Figure showing packing of IPM-312 (Hydrogen atoms have been omitted for clarity).



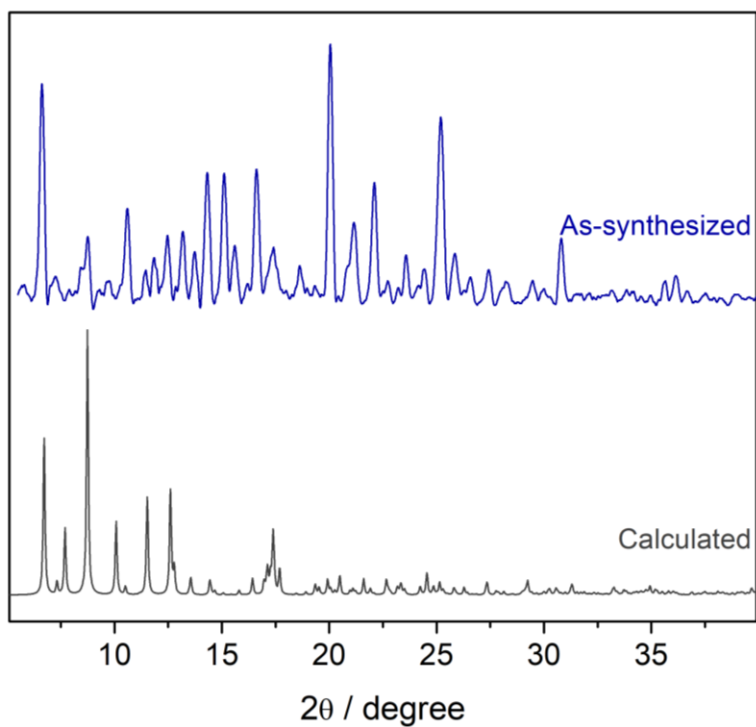
**Appendix 2.21:** Figure showing packing of IPM-315 (Hydrogen atoms have been omitted for clarity).



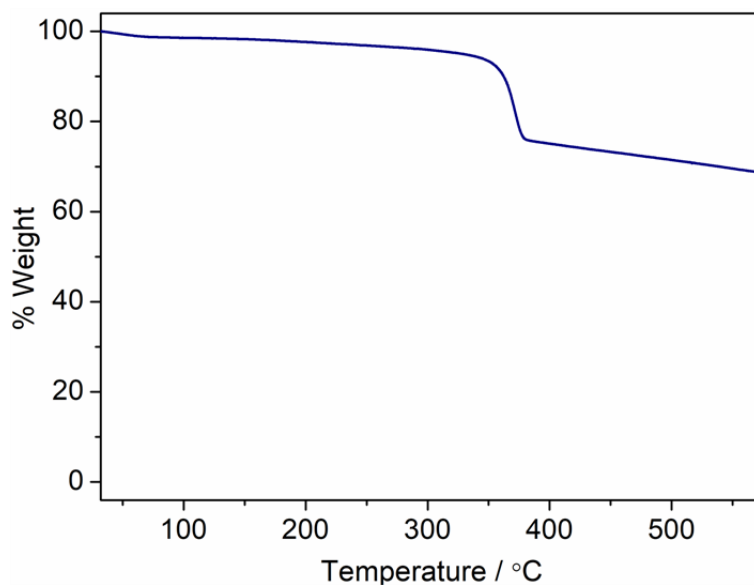
**Appendix 2.22:** Powder X-ray diffraction patterns of IPM-206. Calculated (gray), as-synthesized (blue).



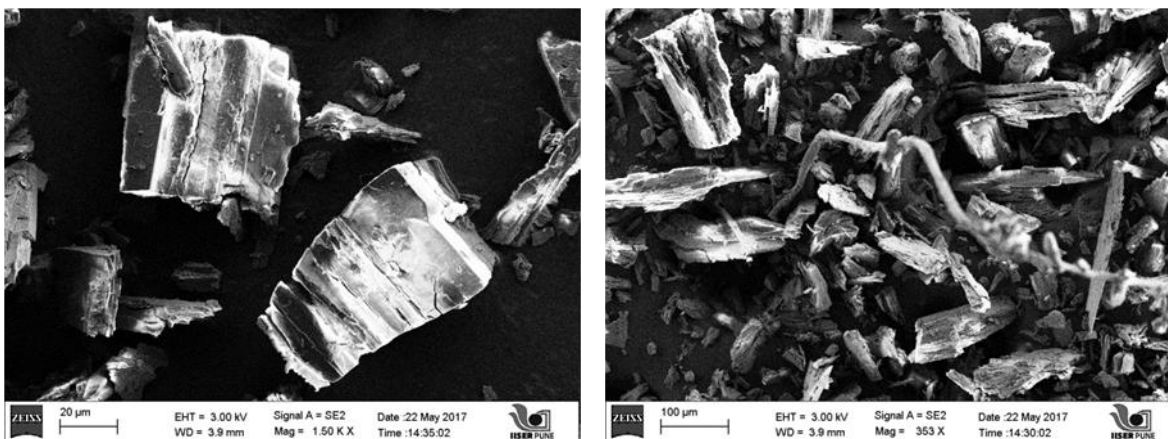
**Appendix 2.23:** TGA profile for compound IPM-206.



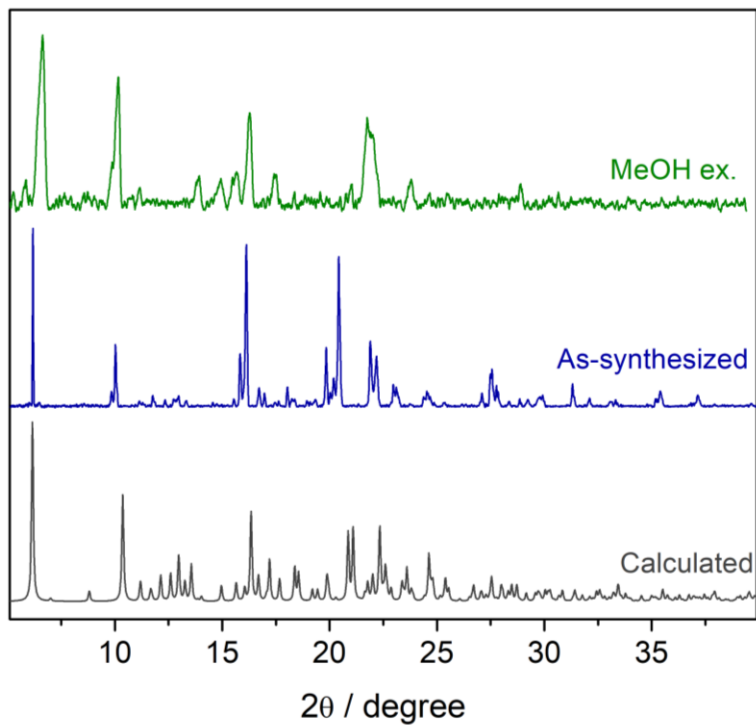
**Appendix 2.24:** Powder X-ray diffraction patterns of IPM-310. Calculated (gray), as-synthesized (blue).



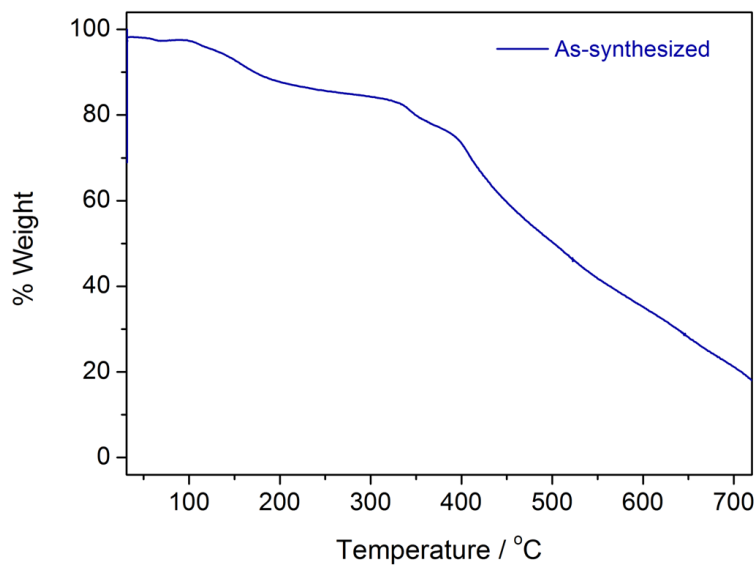
**Appendix 2.25:** TGA profiles for compound IPM-310.



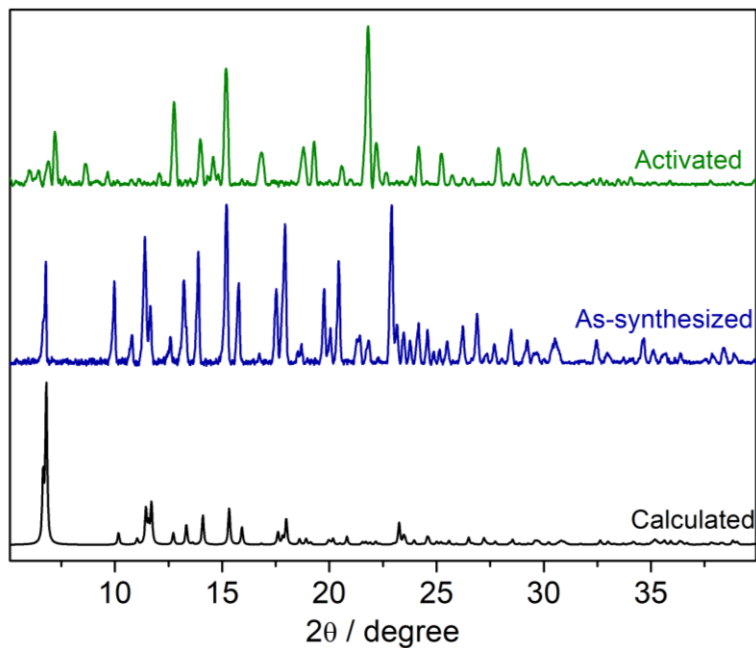
**Appendix 2.26:** FESEM images for compound IPM-310. The images were recorded for the solid sample on carbon tape.



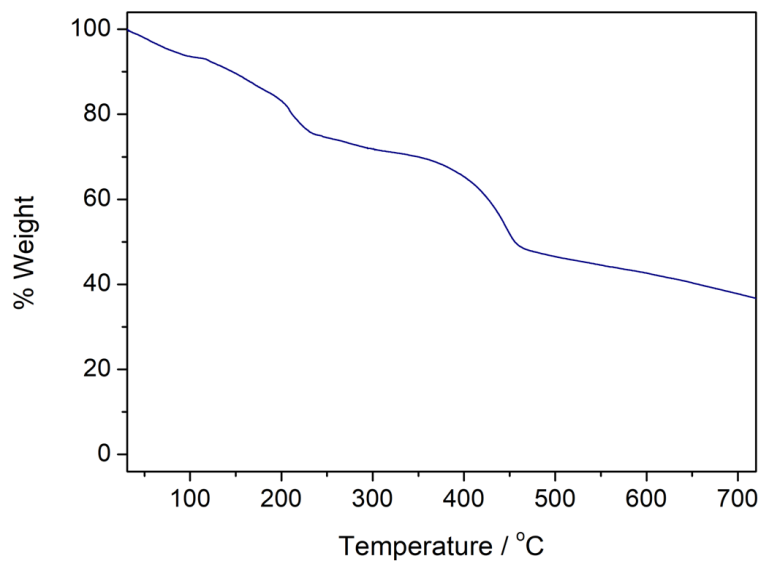
**Appendix 2.27:** Powder X-ray diffraction patterns of IPM-315 Calculated (gray), as-synthesized (blue), MeOH exchanged (green).



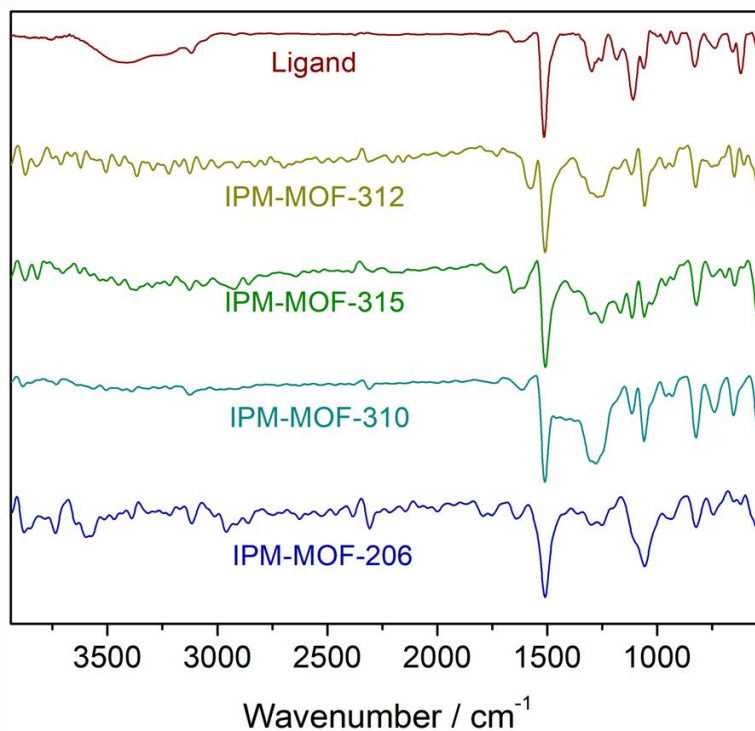
**Appendix 2.28:** TGA profiles for compound IPM-315.



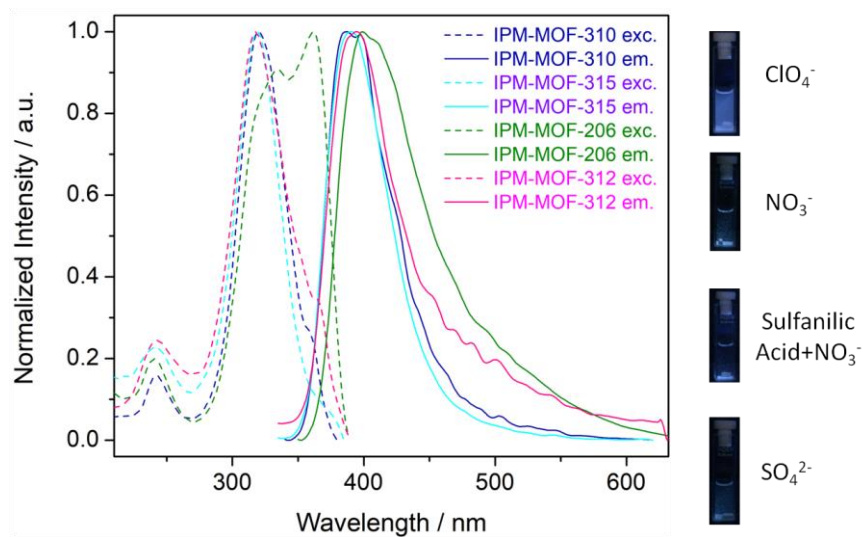
**Appendix 2.29:** Powder X-ray diffraction patterns of IPM-311 Calculated (gray), as-synthesized (blue), Activated (green).



**Appendix 2.30:** TGA profiles for compound IPM-311.

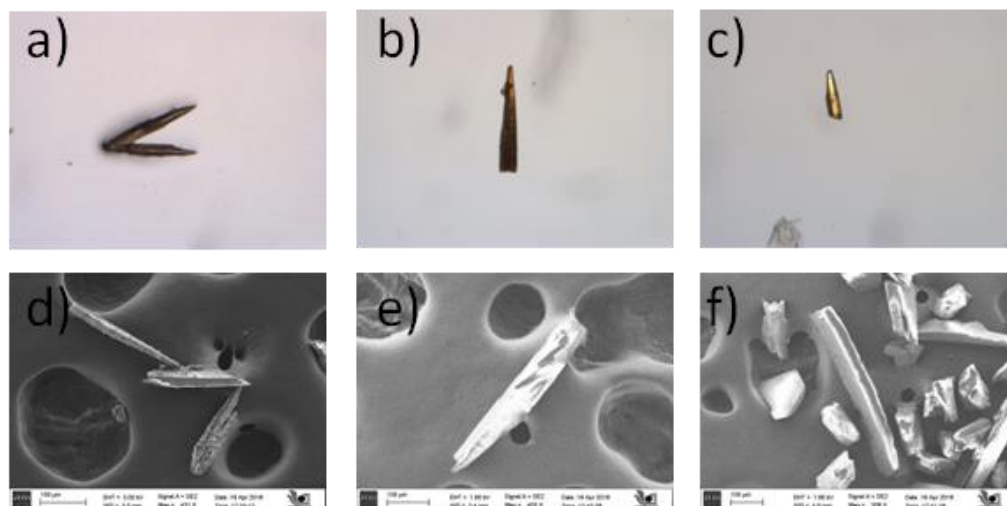


**Appendix 2.31:** FT-IR profiles for various compound.

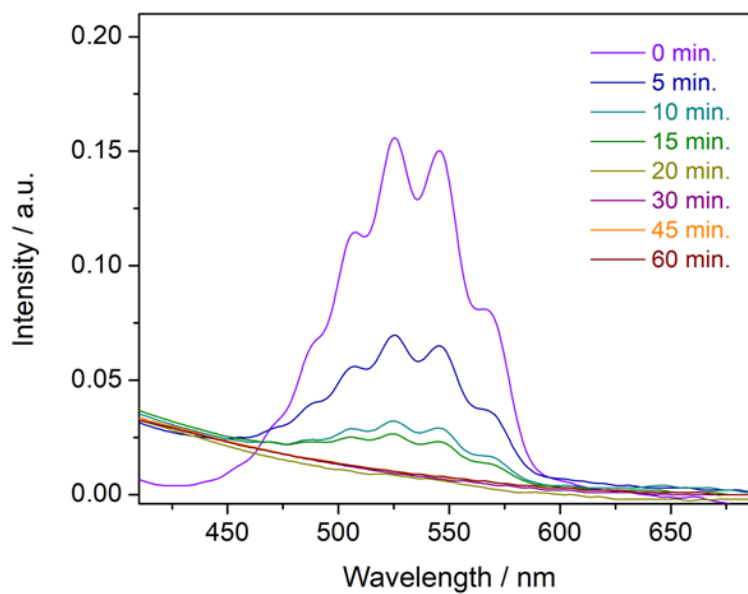


**Appendix 2.32:** Excitation and emission profiles for various profile

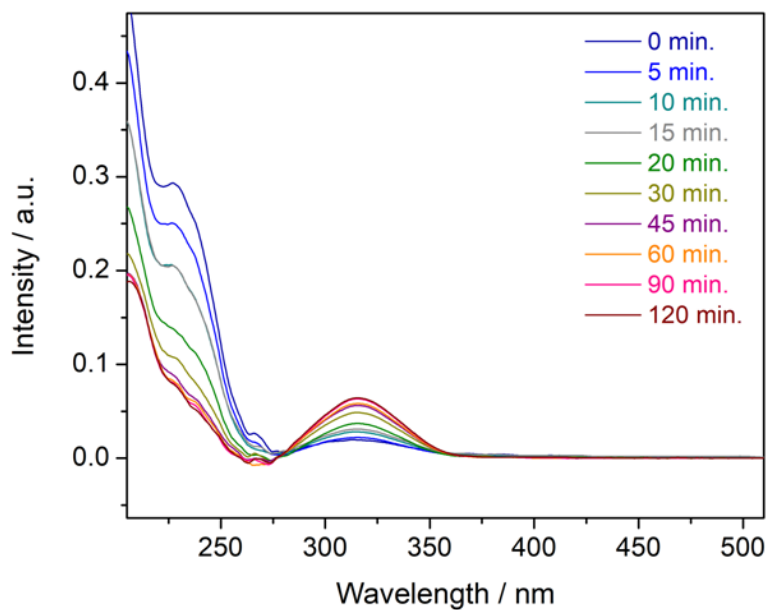




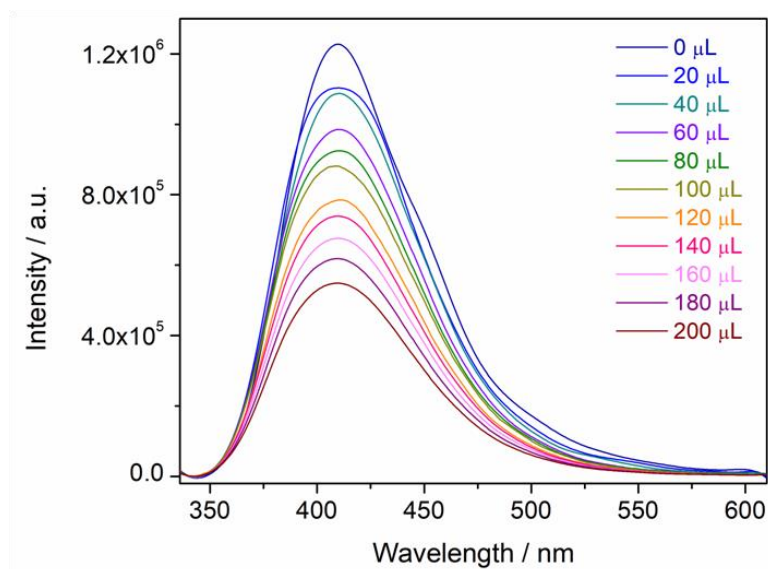
**Appendix 2.33:** Naked eye images of IPM-206; a) As-synthesized, b) MnO<sub>4</sub><sup>-</sup> exchanged, c) ReO<sub>4</sub><sup>-</sup> exchanged. & SEM image of d) As-synthesized, e) MnO<sub>4</sub><sup>-</sup> exchanged, f) ReO<sub>4</sub><sup>-</sup> exchanged.



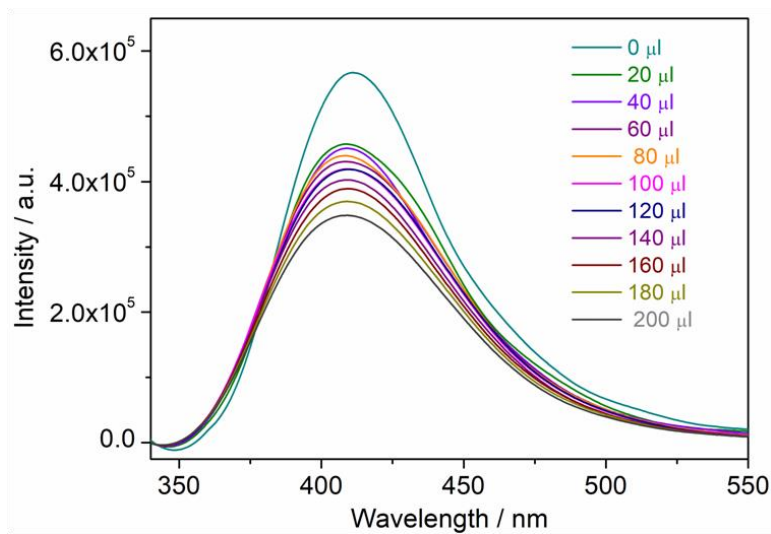
**Appendix 2.34:** UV-Vis absorption spectra of MnO<sub>4</sub><sup>-</sup> after addition of IPM-206 after different intervals.



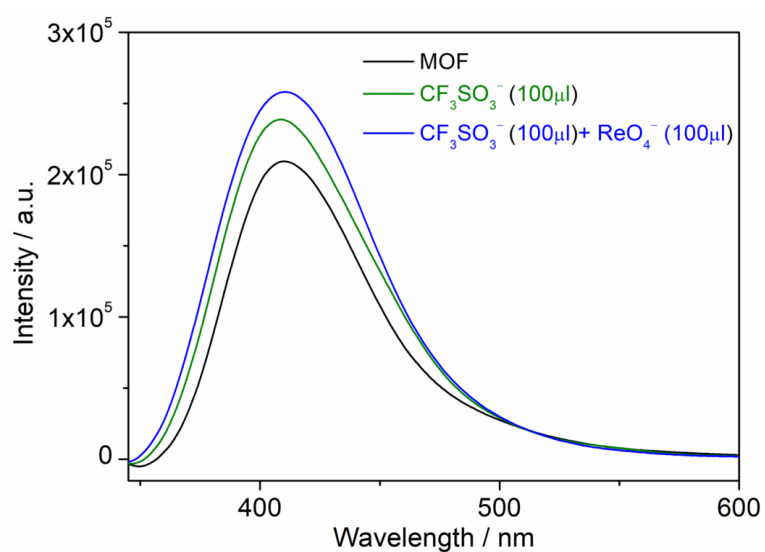
**Appendix 2.35:** UV-Vis absorption spectra of  $\text{ReO}_4^-$  after addition of IPM-206 after different intervals.



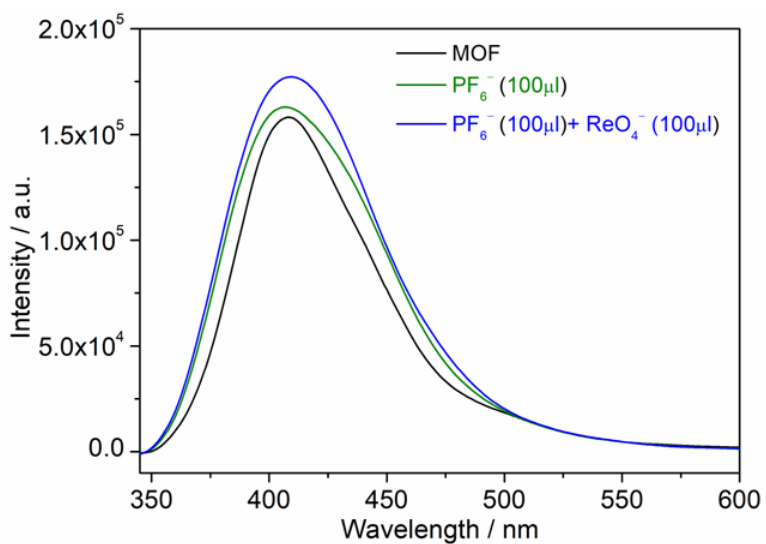
**Appendix 2.36:** Photoluminescence spectra of  $\text{MnO}_4^-$  after addition of IPM-206 after different intervals.



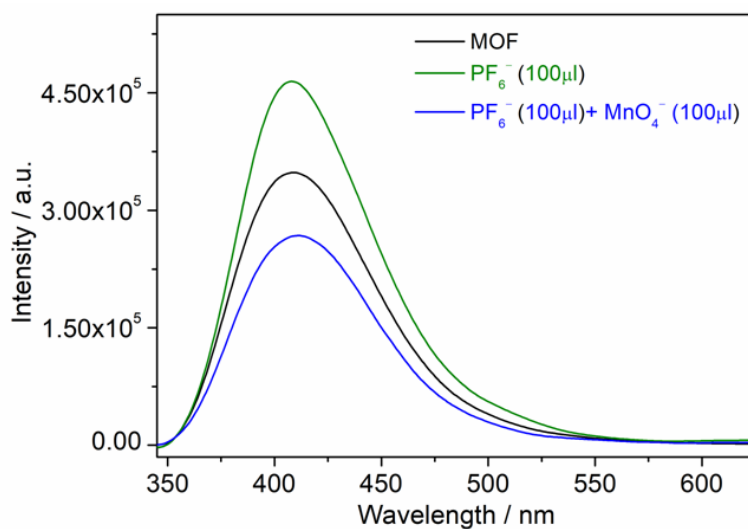
**Appendix 2.37:** Photoluminescence spectra of  $\text{ReO}_4^-$  after addition of IPM-206 after different intervals.



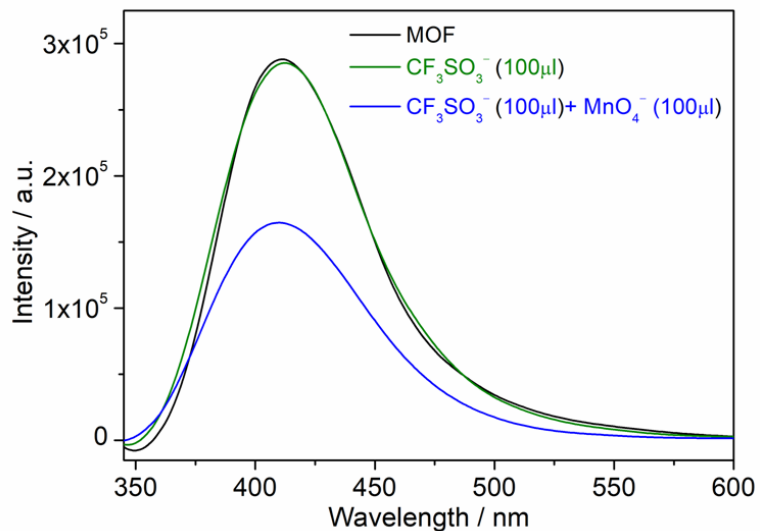
**Appendix 2.38:** Photoluminescence spectra of IPM-206 after addition of different analytes.



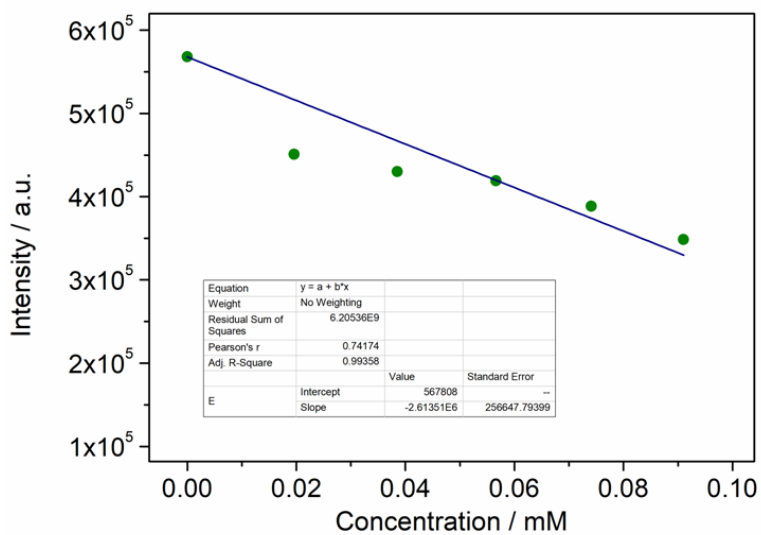
**Appendix 2.39:** Photoluminescence spectra of IPM-206 after addition of different analytes.



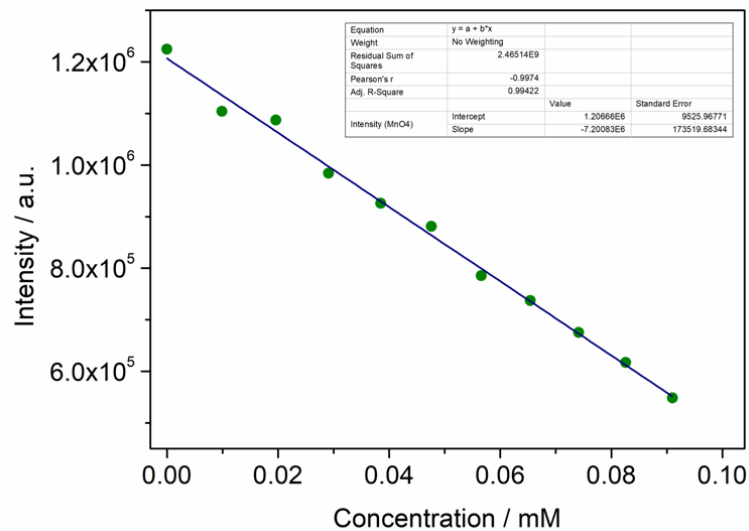
**Appendix 2.40:** Photoluminescence spectra of IPM-206 after addition of different analytes.



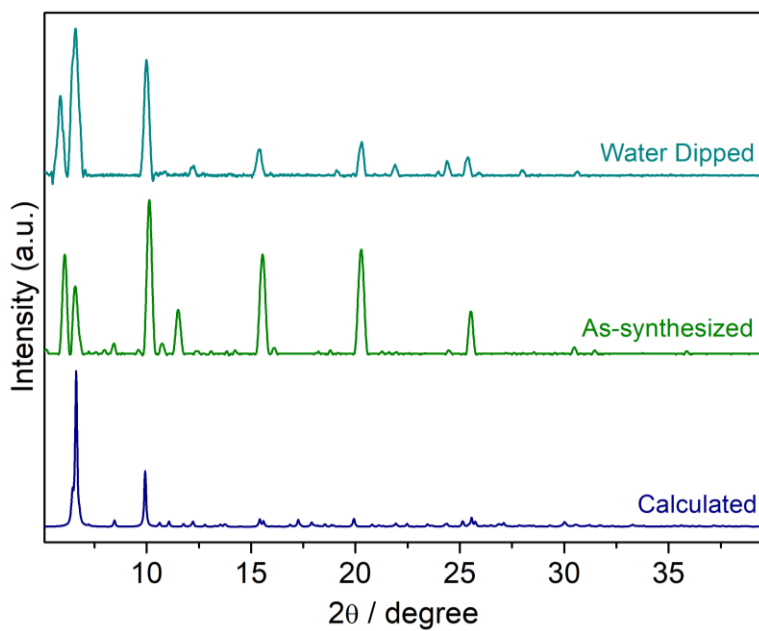
**Appendix 2.41:** Photoluminescence spectra of IPM-206 after addition of different analytes.



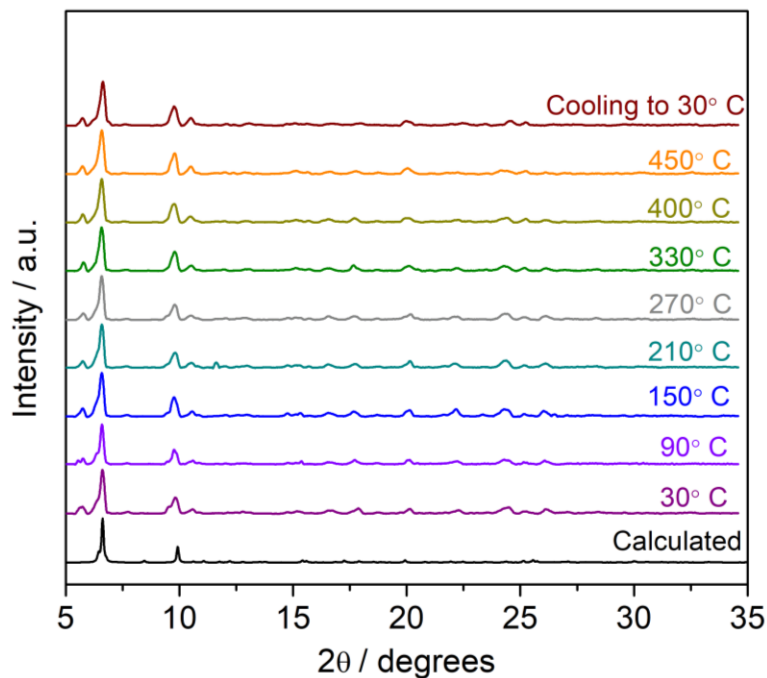
**Appendix 2.42:** Linear region in the photoluminescence spectra after addition of  $\text{ReO}_4^-$  to IPM-206 at  $\lambda_{\text{em}} = 410\text{nm}$  ( $\lambda_{\text{exc.}} = 325\text{nm}$ ) ( $R^2 = 99.35\%$ ).



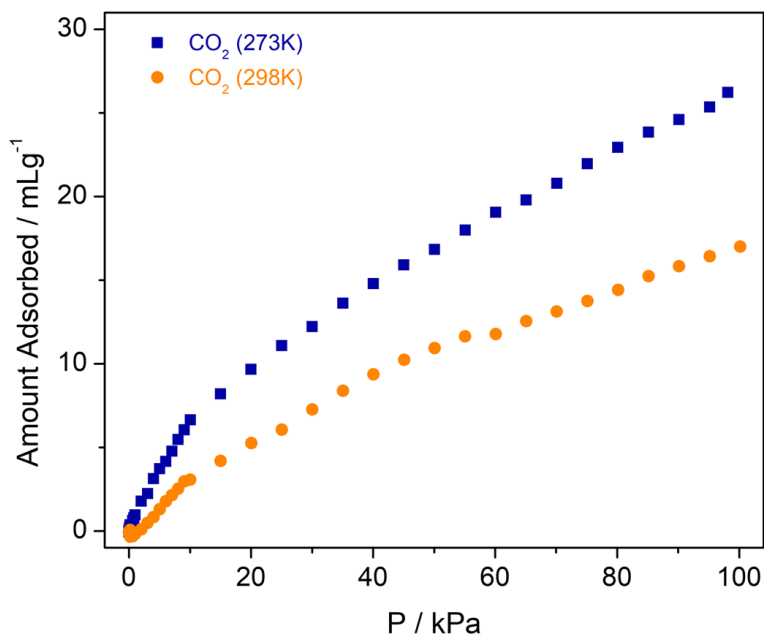
**Appendix 2.43:** Linear region in the photoluminescence spectra after addition of  $\text{MnO}_4^-$  to IPM-206 at  $\lambda_{\text{em}} = 410\text{nm}$  ( $\lambda_{\text{exc.}} = 325\text{nm}$ ) ( $R^2 = 99.42\%$ ).



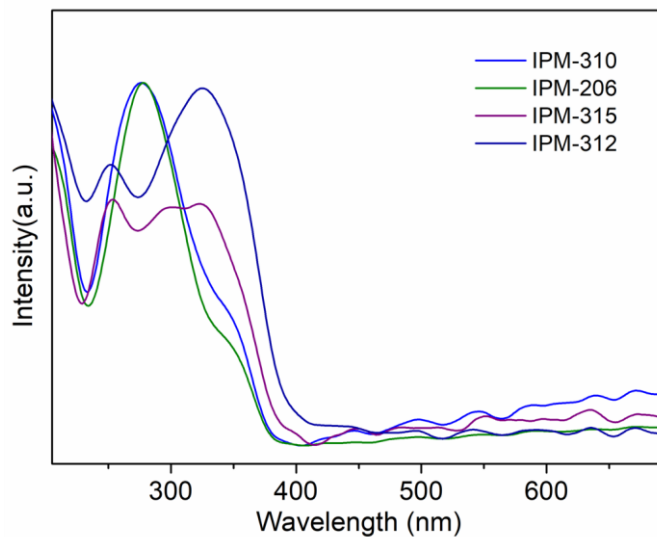
**Appendix 2.44:** Powder X-Ray diffraction pattern for IPM-312 after dipping in water (12h).



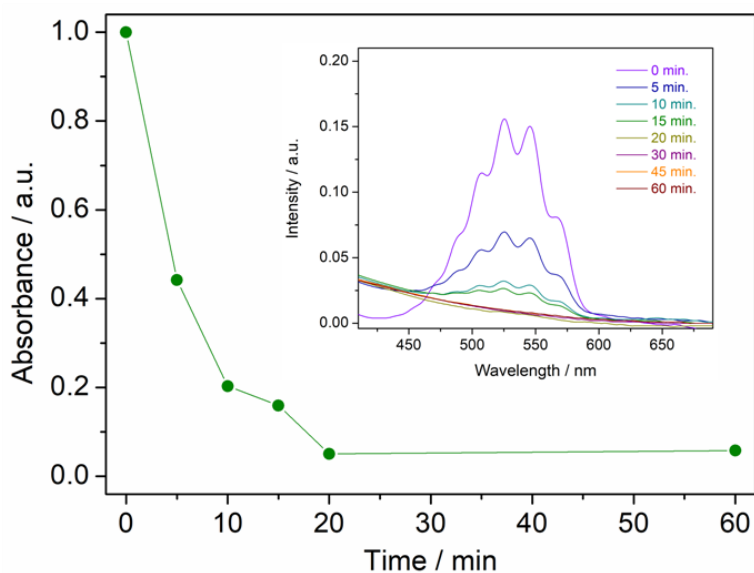
**Appendix 2.45:** Variable temperature Powder X-Ray diffraction pattern for IPM-312.



**Appendix 2.46:** Comparative CO<sub>2</sub> adsorption profile for IPM-312 at 273K (Blue) and 298K (Orange).

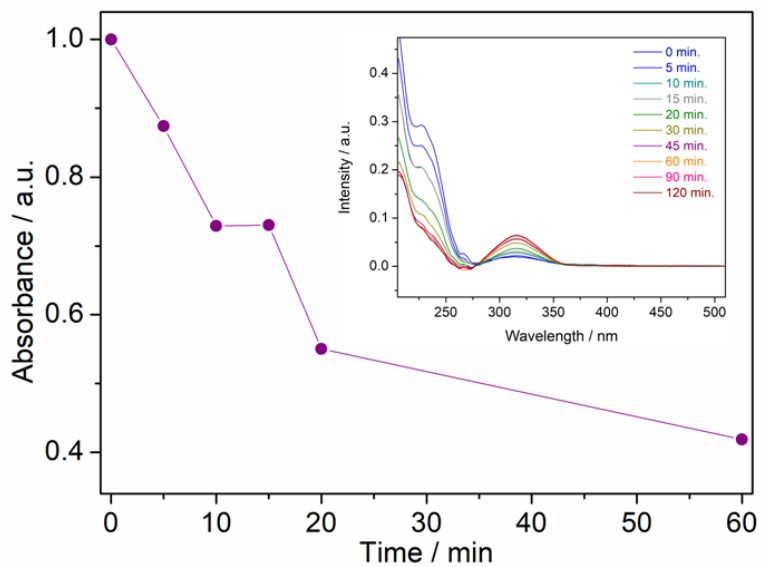


**Appendix 2.47:** Solid State UV-Vis absorption profiles for IPM-310 (Blue), IPM-206 (green), IPM-315 (violet), IPM-312 (Navy Blue).



**Appendix 2.48:** UV-Vis absorption studies of capture of  $\text{MnO}_4^-$  after addition of IPM-206 at different intervals of time. (Inset depicting time dependent decay in the absorption profile.)





**Appendix 2.49:** UV-Vis absorption studies of capture of  $\text{ReO}_4^-$  after addition of IPM-206 at different intervals of time. (Inset depicting time dependent decay in the absorption profile.)

**Appendix Table 2.1.** Crystal data and structure refinement for IPM-206.

Identification code	IPM-206 (CCDC 1846341)	
Empirical formula	C <sub>54</sub> H <sub>42</sub> Cd N <sub>14</sub>	
Formula weight	999.41	
Temperature	150(2) K	
Wavelength	0.71073 Å	
Crystal system	Monoclinic	
Space group	C2/c	
Unit cell dimensions	a = 30.2102(19) Å	α = 90°
	b = 8.9486(6) Å	β = 118.440(2)°
	c = 31.4489(17) Å	γ = 90°
Volume	7475.8(8) Å <sup>3</sup>	
Z	4	
Density (calculated)	0.888 Mg/m <sup>3</sup>	
Absorption coefficient	0.326 mm <sup>-1</sup>	
F(000)	2048	
Crystal size	0.14 x 0.12 x 0.10 mm <sup>3</sup>	
Theta range for data collection	2.402 to 28.344°.	
Index ranges	-40 ≤ h ≤ 40, -11 ≤ k ≤ 11, -41 ≤ l ≤ 38	
Reflections collected	113594	
Independent reflections	9296 [R(int) = 0.0974]	
Completeness to theta = 28.42°	100.0 %	
Refinement method	Full-matrix least-squares on F <sup>2</sup>	
Data / restraints / parameters	9296 / 0 / 313	
Goodness-of-fit on F <sup>2</sup>	1.100	
Final R indices [I > 2σ(I)]	R <sub>I</sub> = 0.0482, wR <sub>2</sub> = 0.1128	
R indices (all data)	R <sub>I</sub> = 0.0885, wR <sub>2</sub> = 0.1307	
Largest diff. peak and hole	0.450 and -0.392 e.Å <sup>-3</sup>	

**Appendix Table 2.2.** Crystal data and structure refinement for IPM-310.

Identification code	IPM-310 (CCDC 1846342)	
Empirical formula	C <sub>27</sub> H <sub>21</sub> N <sub>9</sub> Cd O <sub>6</sub>	
Formula weight	679.93	
Temperature	150(2) K	
Wavelength	0.71073 Å	
Crystal system	Triclinic	
Space group	<i>P</i> -1	
Unit cell dimensions	a = 11.984(4) Å	α = 73.727(10)°
	b = 12.573(4) Å	β = 73.273 (10)°
	c = 14.220(5) Å	γ = 84.150 (12)°
Volume	1969.1(11) Å <sup>3</sup>	
Z	2	
Density (calculated)	1.147 Mg/m <sup>3</sup>	
Absorption coefficient	0.597 mm <sup>-1</sup>	
F(000)	684	
Crystal size	0.12 x 0.11 x 0.10 mm <sup>3</sup>	
Theta range for data collection	2.421 to 28.396°.	
Index ranges	-15 ≤ h ≤ 14, -16 ≤ k ≤ 16, -18 ≤ l ≤ 18	
Reflections collected	39207	
Independent reflections	9768 [R(int) = 0.0540]	
Completeness to theta = 28.42°	99.9 %	
Refinement method	Full-matrix least-squares on F <sup>2</sup>	
Data / restraints / parameters	9768 / 0 / 388	
Goodness-of-fit on F <sup>2</sup>	1.035	
Final R indices [I > 2σ(I)]	R <sub>I</sub> = 0.0430, wR <sub>2</sub> = 0.1054	
R indices (all data)	R <sub>I</sub> = 0.0642, wR <sub>2</sub> = 0.1160	
Largest diff. peak and hole	1.922 and -0.636 e.Å <sup>-3</sup>	

**Appendix Table 2.3.** Crystal data and structure refinement for IPM-315.

Identification code	IPM-315 (CCDC 1846347)	
Empirical formula	C <sub>36</sub> H <sub>34</sub> N <sub>10</sub> Cd O <sub>7</sub> S	
Formula weight	863.19	
Temperature	100(2) K	
Wavelength	0.71073 Å	
Crystal system	Orthorhombic	
Space group	P2 <sub>1</sub> 2 <sub>1</sub> 2 <sub>1</sub>	
Unit cell dimensions	a = 8.9284(4) Å	α = 90°.
	b = 14.0416(7) Å	β = 90°.
	c = 28.6683(14) Å	γ = 90°.
Volume	3594.1(3) Å <sup>3</sup>	
Z	4	
Density (calculated)	1.595 Mg/m <sup>3</sup>	
Absorption coefficient	0.731 mm <sup>-1</sup>	
F(000)	1760	
Crystal size	0.12 x 0.10 x 0.08 mm <sup>3</sup>	
Theta range for data collection	2.389 to 28.362°.	
Index ranges	-11 ≤ h ≤ 11, -18 ≤ k ≤ 18, -38 ≤ l ≤ 38	
Reflections collected	89134	
Independent reflections	8957 [R(int) = 0.1167]	
Completeness to theta = 28.42°	99.9 %	
Refinement method	Full-matrix least-squares on F <sup>2</sup>	
Data / restraints / parameters	8957 / 6 / 498	
Goodness-of-fit on F <sup>2</sup>	1.035	
Final R indices [I > 2σ(I)]	R <sub>I</sub> = 0.0616, wR <sub>2</sub> = 0.1437	
R indices (all data)	R <sub>I</sub> = 0.1019, wR <sub>2</sub> = 0.1608	
Largest diff. peak and hole	1.713 and -1.366 e.Å <sup>-3</sup>	

**Appendix Table 2.4.** Crystal data and structure refinement for IPM-311.

Identification code	IPM-311 (CCDC 1846344)	
Empirical formula	C <sub>29</sub> H <sub>23</sub> N <sub>7</sub> Cd O <sub>4</sub>	
Formula weight	645.94	
Temperature	150(2) K	
Wavelength	0.71073 Å	
Crystal system	Monoclinic	
Space group	C2	
Unit cell dimensions	a = 26.535(2) Å	α = 90°
	b = 15.453(2) Å	β = 101.627(4)°
	c = 8.8765(9) Å	γ = 90°
Volume	3565(7) Å <sup>3</sup>	
Z	4	
Density (calculated)	1.203 Mg/m <sup>3</sup>	
Absorption coefficient	0.650 mm <sup>-1</sup>	
F(000)	1304	
Crystal size	0.18 x 0.16 x 0.14 mm <sup>3</sup>	
Theta range for data collection	2.343 to 28.280°.	
Index ranges	-34 ≤ h ≤ 35, -20 ≤ k ≤ 20, -10 ≤ l ≤ 11	
Reflections collected	43878	
Independent reflections	8814 [R(int) = 0.1057]	
Completeness to theta = 28.42°	99.9 %	
Refinement method	Full-matrix least-squares on F <sup>2</sup>	
Data / restraints / parameters	8814 / 7 / 371	
Goodness-of-fit on F <sup>2</sup>	0.981	
Final R indices [I > 2σ(I)]	R <sub>I</sub> = 0.0504, wR <sub>2</sub> = 0.0968	
R indices (all data)	R <sub>I</sub> = 0.1214, wR <sub>2</sub> = 0.1167	
Largest diff. peak and hole	0.546 and -0.448 e.Å <sup>-3</sup>	

**Appendix Table 2.5.** Crystal data and structure refinement for IPM-312.

Identification code	IPM-312 (CCDC 1846346)	
Empirical formula	C <sub>54</sub> H <sub>42</sub> N <sub>14</sub> Cd <sub>2</sub> O <sub>8</sub> S <sub>2</sub>	
Formula weight	1303.93	
Temperature	150(2) K	
Wavelength	1.54178 Å	
Crystal system	Triclinic	
Space group	<i>P</i> -1	
Unit cell dimensions	a = 15.9617(11) Å	α = 113.108(4)°
	b = 16.1208(11) Å	β = 113.283(4)°
	c = 16.3842(11) Å	γ = 99.327(5)°
Volume	3301.3(4) Å <sup>3</sup>	
Z	2	
Density (calculated)	1.312 Mg/m <sup>3</sup>	
Absorption coefficient	6.220 mm <sup>-1</sup>	
F(000)	1312	
Crystal size	0.15 x 0.12 x 0.10 mm <sup>3</sup>	
Theta range for data collection	3.216 to 67.393°.	
Index ranges	-18 ≤ h ≤ 19, -19 ≤ k ≤ 19, -16 ≤ l ≤ 19	
Reflections collected	24186	
Independent reflections	11522 [R(int) = 0.0704]	
Completeness to theta = 28.42°	97.0 %	
Refinement method	Full-matrix least-squares on F <sup>2</sup>	
Data / restraints / parameters	11522 / 36 / 721	
Goodness-of-fit on F <sup>2</sup>	0.936	
Final R indices [I > 2σ(I)]	R <sub>I</sub> = 0.0800, wR <sub>2</sub> = 0.2361	
R indices (all data)	R <sub>I</sub> = 0.1170, wR <sub>2</sub> = 0.2652	
Largest diff. peak and hole	3.778 and -2.110 e.Å <sup>-3</sup>	

## 2.6 References

1. (a) Zhou, H.-C.; Long, J.-R.; Yaghi, O. M., *Chem. Rev.* **2012**, *112*, 673-674. (b) Zhou, H.-C.; Kitagawa, S., *Chem. Soc. Rev.* **2014**, *43*, 5415-5418.
2. (a) Han, L.; Zhang, S.; Wang, Y.; Yan, X.; Lu, X., *Inorg. Chem.* **2009**, *48*, 786-788. (b) Karmakar, A.; Desai, A. V.; Ghosh, S. K., *Coord. Chem. Rev.* **2016**, *307*, 313-341.
3. (a) Kumar, P.; Pournara, A.; Kim, K.-H.; Bansal, V.; Rapti, S.; Manos, M. J., *Prog. Mater. Sci.* **2017**, *86*, 25-74. (b) Lin, Y.; Kong, C.; Zhang, Q.; Chen, L., *Adv. Energy Mater.* **2017**, *7*, 1601296.
4. Banerjee, D.; Kim, D.; Schweiger, M. J.; Kruger, A. A.; Thallapally, P. K., *Chem. Soc. Rev.* **2016**, *45*, 2724-2739.
5. (a) Manna, B.; Desai, A. V.; Ghosh, S. K., *Dalton Trans.* **2016**, *45*, 4060-4072. (b) Sheng, D.; Zhu, L.; Xu, C.; Xiao, C.; Wang, Y.; Wang, Y.; Chen, L.; Diwu, J.; Chen, J.; Chai, Z.; Albrecht-Schmitt, T. E.; Wang, S., *Environ. Sci. Technol.* **2017**, *51*, 3471-3479. (c) Chen, Y.-Q.; Li, G.-R.; Chang, Z.; Qu, Y.-K.; Zhang, Y.-H.; Bu, X.-H., *Chem. Sci.* **2013**, *4*, 3678-3682.
6. (a) Burtch, N. C.; Jasuja, H.; Walton, K. S., *Chem. Rev.* **2014**, *114*, 10575-10612. (b) Wang, C.; Liu, X.; Demir, N. K.; Chen, J. P.; Li, K., *Chem. Soc. Rev.* **2016**, *45*, 5107-5134.
7. (a) Chen, S. S., *CrystEngComm* **2016**, *18*, 6543-6565. (b) Yuan, S.; Feng, L.; Wang, K.; Pang, J.; Bosch, M.; Lollar, C.; Sun, Y.; Qin, J.; Yang, P.; Wang, Q.; Zou, L.; Zhang, Y.; Zhang, L.; Fang, Y.; Li, J.; Zhou, H.-C., *Adv. Mater.* **2018**, 1704303.
8. Zhang, J.-P.; Zhang, Y.-B.; Lin, J.-B.; Chen, X.-M., *Chem. Rev.* **2012**, *112*, 1001-1033.
9. Wang, K.; Lv, X.-L.; Feng, D.; Li, J.; Chen, S.; Sun, J.; Song, L.; Xie, Y.; Li, J.-R.; Zhou, H.-C., *J. Am. Chem. Soc.* **2016**, *138*, 914-919.
10. (a) Allendorf, M. D.; Bauer, C. A.; Bhakta, R. K.; Houk, R. J. T., *Chem. Soc. Rev.* **2009**, *38*, 1330-1352. (b) Hu, Z.; Deibert, B. J.; Li, J., *Chem. Soc. Rev.* **2014**, *43*, 5815-5840.
11. (a) Duan, J.; Jin, W.; Kitagawa, S., *Coord. Chem. Rev.* **2017**, *332*, 48-74. (b) Huang, N.; Wang, K.; Drake, H.; Cai, P.; Pang, J.; Li, J.; Che, S.; Huang, L.; Wang, Q.; Zhou, H.-C., *J. Am. Chem. Soc.* **2018**, *140*, 6383-6390.
12. Howarth, A. J.; Liu, Y.; Li, P.; Li, Z.; Wang, T. C.; Hupp, J. T.; Farha, O. K., *Nat. Rev. Mater.* **2016**, *1*, 15018.

13. Maity, R.; Koppetz, H.; Hepp, A.; Hahn, F. E., *J. Am. Chem. Soc.* **2013**, *135*, 4966-4969.
14. *SAINT Plus*, Bruker AXS Inc.: Madison, WI, **2004**.
15. Krause, L.; Herbst-Irmer, R.; Sheldrick, G. M.; Stalke, D., *J. Appl. Cryst.* **2015**, *48*, 3-10.
16. (a) Sheldrick, G. M.; *SHELXTL*, Reference Manual, version 5.1; Bruker AXS Inc.: Madison, WI, **1997**. (b) Sheldrick, G. M., *Acta. Cryst.*, **2008**, *A64*, 112-122.
17. Sheldrick, G. M., *Acta. Cryst.*, **2015**, *C71*, 3-8.
18. Farrugia, L., *WinGX*, University of Glasgow: Glasgow, Scotland.
19. Spek, A. L., *Acta. Cryst.*, **2015**, *C71*, 9-18.



---

## *Chapter 3*

---

# **Water Stable Cationic MOF for Heavy Metal Oxoanion Pollutant Capture**

### 3.1 Introduction

Water pollution has become a pressing global concern and is commanding significant research attention with regards to sequestration of toxic contaminants present in water streams. Especially, with the widespread growth of modern industry, heavy metal-contaminant segregation from industrial effluents has become a pertinent problem.<sup>1</sup> Few inorganic pollutants, present in the form of oxo-anions, feature prominently in the list of the Environment Protection Agency (EPA) priority pollutants.<sup>2</sup> The capture and removal of these species from water streams has been pursued by developing materials and/or methods for selective entrapment. In particular, separation of Cr(VI), generated from chromium plating, pigment synthesis, leather tanning etc. has been focused owing to the severe health hazards posed by its prevailing ionic species.<sup>3</sup> Likewise the presence of pertechnetate ( $\text{TcO}_4^-$ ) ions in radioactive waste vitrification poses serious disposal issues on account of long half-life and facile mobility.<sup>4</sup> Although several techniques like ion exchange, adsorption, photocatalytic reduction have been trialled for this purpose in general,<sup>5</sup> the preferred routes have applied ion-exchange pathways owing to cost, sensitivity, simplicity and selectivity considerations.<sup>6</sup> The limitations of the currently employed ion-exchangers like slow process kinetics and poor selectivity actuates the development of newer materials or optimization of the performance in the currently studied adsorbents.

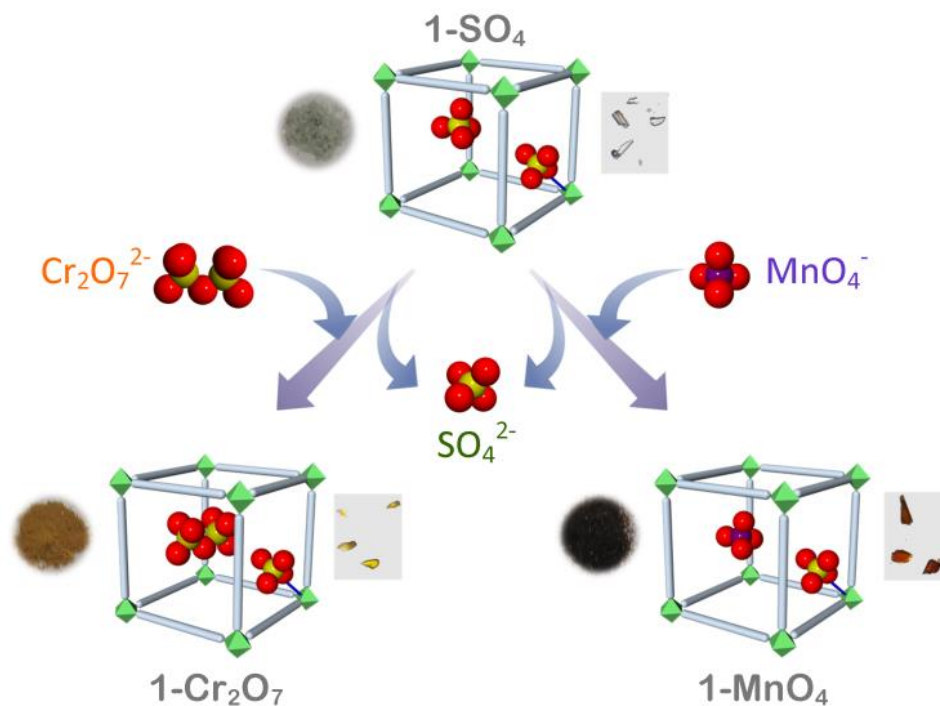


Figure 3.1 Schematic illustration of naked-eye heavy metal oxo-anion capture by  $1\text{-SO}_4$ . The optical pictographs of the different phases along-with the respective crystal images are shown alongside each representation.

Metal-organic frameworks (MOFs), built from organic linkers and metal ions, have evolved as a distinctly notable class of porous materials.<sup>7</sup> The feasible control over tuning the pore size and surface bestows MOFs as suitable receptors for selective sorption and separation applications.<sup>8</sup> As a sub-class, cationic MOFs are seeking significant attention as anion receptors/separators due to the desired confinement of substitutable uncoordinated anionic species.<sup>9</sup> Broadly, such frameworks are fabricated from neutral N-donor ligands wherein the residual charge-balancing ions reside in the void spaces.<sup>10</sup> Although porous cationic materials, including MOFs, have been explored for several applications as anion-exchange hosts, the development of MOFs as adsorbents for toxic oxo-anion capture is still in the nascent stages, both in terms of design strategies and loading capacities.<sup>11</sup> We sought to develop an efficient route to construct cationic MOFs for the trapping of oxo-anions encountered in wastewater streams by employing aquatic compatible building blocks of metal-salts (e.g. metal-sulfates, metal-phosphates), to overcome the common drawback of poor hydrolytic stability in systems built from neutral ligands. Further we hypothesized that the tetrahedral geometry of the exchangeable uncoordinated anion (like  $\text{SO}_4^{2-}$ ,  $\text{PO}_4^{3-}$ ) would facilitate its substitution with the targeted anions, both monovalent and multivalent heavy metal oxo-anions having tetrahedral geometry. Also utilizing a multi-dentate neutral ligand would cooperate in keeping such anions free within the porous network and lead to the formation of higher dimensional coordination polymers.

Combining all these aspects and experimenting the hypothesis, herein we report a water stable, 3D cationic MOF  $1' \cdot \text{SO}_4$  viz.  $[\{\text{Ni}_2(\text{L})_3(\text{SO}_4)(\text{H}_2\text{O})_3\} \cdot (\text{SO}_4) \cdot x(\text{G})]_n$  (L = tris(4-(1H-imidazol-1-yl)phenyl)amine, G = DMF,  $\text{H}_2\text{O}$ ) built from a tripodal neutral ligand and bearing free sulfate ions as a fast, selective and naked-eye adsorbent for the capture of both monovalent and divalent tetrahedral oxo-anions viz. pertechnetate modelled permanganate and dichromate anions (Figure 3.1).

## 3.2 Experimental

### 3.2.1 Materials:

All solvents and reagents were commercially available and used without further purification.

### 3.2.2 Synthesis:

**Synthesis of Ligand {tris(4-(1H-imidazol-1-yl)phenyl)amine}:** The ligand was synthesized according to a reported protocol.<sup>12</sup> A mixture of tris(4-bromophenyl)amine (500 mg, 1.04 mmol), imidazole (423 mg, 6.22 mmol),  $\text{K}_2\text{CO}_3$  (573 mg, 4.15 mmol) and  $\text{CuSO}_4$  (6.5 mg, 0.041 mmol) was heated at 150 °C under inert atmosphere for 60 hours. After cooling to ambient temperature, the mixture was dissolved in  $\text{CH}_2\text{Cl}_2$  (50 ml) and washed with water several times. The organic layer was brought to dryness to give a pale coloured powder. The ligand was recrystallized from a mixture of  $\text{MeOH}:\text{CH}_2\text{Cl}_2$  (1:1) in yield of 68%.

**Synthesis of 1-SO<sub>4</sub>:** A mixture of ligand (8.86 mg, 0.02 mmol), NiSO<sub>4</sub>•xH<sub>2</sub>O (5.60 mg, 0.02 mmol), N,N-dimethylformamide (1.5 ml) and water (1.5 ml), was placed in a teflon capped glass vial, and heated at 90 °C for 48 hours followed by cooling to room temperature. The compound was filtered and washed with water and methanol several times. Pale green colour crystals of compound 1'-SO<sub>4</sub> were obtained in ~48% yield. These crystals were dipped in MeOH solution for 2 days prior to heating it under vacuum at 75 °C to obtain the guest free phase 1-SO<sub>4</sub>. We were unable to locate the highly disordered guest molecules in the structure crystallographically. From the SQUEEZE function of PLATON the formula of the compound 1-SO<sub>4</sub> was determined to be  $[\{Ni_2(L)_3(SO_4)(H_2O)_3\} \cdot SO_4]_n$ . Anal Calcd for 1-SO<sub>4</sub>: C/N, 3.31; C/S, 15.19. Found: C/N, 3.37; C/S, 15.43. CCDC 1422306 (1-SO<sub>4</sub>) contains the supplementary crystallographic data for this paper. These data can be obtained free of charge from The Cambridge Crystallographic Data Centre via [www.ccdc.cam.ac.uk/data\\_request/cif](http://www.ccdc.cam.ac.uk/data_request/cif).

### 3.2.3 Ion-exchange Studies

**Anion Exchange:** Single crystals of 1-SO<sub>4</sub> were dipped in aqueous solutions (1 μM/2 ml) of K<sub>2</sub>Cr<sub>2</sub>O<sub>7</sub> and KMnO<sub>4</sub> separately for 4 days at r.t. to yield the respective anion-exchanged products viz. 1-Cr<sub>2</sub>O<sub>7</sub> and 1-MnO<sub>4</sub>. After anion exchange the compounds were washed with deionized water several times and air-dried. The air-dried compounds were characterized by FT-IR spectroscopy, UV-Vis spectroscopy, PXRD and EDX. ICP-AES analysis was performed on the compound after 7 days of exchange.

**Anion Selectivity Studies:** Single crystals of 1-SO<sub>4</sub> were dipped in aqueous mixture of (1 μM/1 ml) of K<sub>2</sub>Cr<sub>2</sub>O<sub>7</sub> and (5 μM/1 ml) KNO<sub>3</sub> for 3 days at r.t. to yield the anion-exchanged products. After anion exchange the compounds were washed with deionized water several times and air-dried. The compounds were characterized by FT-IR spectroscopy and PXRD. The same procedure was followed for Cr<sub>2</sub>O<sub>7</sub><sup>2-</sup>/BF<sub>4</sub><sup>-</sup>, Cr<sub>2</sub>O<sub>7</sub><sup>2-</sup>/CF<sub>3</sub>SO<sub>3</sub><sup>-</sup> and Cr<sub>2</sub>O<sub>7</sub><sup>2-</sup>/ClO<sub>4</sub><sup>-</sup> mixtures. Similarly anion selectivity experiments were performed for MnO<sub>4</sub><sup>-</sup> exchange as well.

**Reversibility Studies:** Crystals of 1-Cr<sub>2</sub>O<sub>7</sub> were dipped in separate aqueous solutions of Na<sub>2</sub>SO<sub>4</sub> (10 μM/2 ml) for 5 days at r.t. Upon completion the compound was collected by filtration and washed with water several times. FT-IR spectroscopy and PXRD were used to characterize these experiments. The same protocol was followed for 1-MnO<sub>4</sub> as well. For ICP-AES analysis, fresh batch of 1-Cr<sub>2</sub>O<sub>7</sub> was dipped in an aqueous solution of Na<sub>2</sub>SO<sub>4</sub> (45 μM/5 ml) for 3 days at room temperature. For checking the adsorption features for the 2nd time, the desorbed phase was dipped in an aqueous K<sub>2</sub>Cr<sub>2</sub>O<sub>7</sub> solution (0.5 μM/5 ml) for 2 days at room temperature.

**Anion Competing Studies:** Compound 1-MnO<sub>4</sub> was dipped in an aqueous solution of K<sub>2</sub>Cr<sub>2</sub>O<sub>7</sub> (5 μM/2 ml) for 3 days at r.t. The compound was filtered off and washed with water several times and air-dried for

further characterization. The obtained compound was characterized using FT-IR spectroscopy and PXRD. Likewise compound 1-Cr<sub>2</sub>O<sub>7</sub> was dipped in an aqueous solution of KMnO<sub>4</sub> (5 μM/2 ml) and a similar protocol as above was followed.

**Anion Affinity Studies:** Compound 1-SO<sub>4</sub> was dipped in an aqueous mixture NaNO<sub>3</sub> (0.05 mmol) and NaClO<sub>4</sub> (0.05 mmol) in 4 ml water for 2 days at r.t. The compound was filtered off and washed with water several times and air-dried for further characterization. The obtained compound was characterized using FT-IR spectroscopy. The same procedure was followed for NO<sub>3</sub><sup>-</sup>/BF<sub>4</sub><sup>-</sup>, NO<sub>3</sub><sup>-</sup>/CF<sub>3</sub>SO<sub>3</sub><sup>-</sup>, BF<sub>4</sub><sup>-</sup>/CF<sub>3</sub>SO<sub>3</sub><sup>-</sup>, ClO<sub>4</sub><sup>-</sup>/CF<sub>3</sub>SO<sub>3</sub><sup>-</sup> and BF<sub>4</sub><sup>-</sup>/ClO<sub>4</sub><sup>-</sup> mixtures.

### 3.2.4 Physical Measurements:

Powder X-ray diffraction patterns were recorded on Bruker D8 Advanced X-Ray diffractometer using Cu K $\alpha$  radiation ( $\lambda = 1.5406 \text{ \AA}$ ) in 5° to 40° 2 $\theta$  range with a scan speed of 0.6°min<sup>-1</sup>. The IR Spectra were acquired by using NICOLET 6700 FT-IR spectrophotometer using KBr pellet in 400-4000 cm<sup>-1</sup> range. UV spectra were recorded on Shimadzu UV 2600 Spectrophotometer having stirring attachment. The EDX data were obtained using FEI Quanta 3D dual beam ESEM at 30KV.

### 3.2.5 X-ray Structural Studies:

Single-crystal X-ray data of compound 1-SO<sub>4</sub> was collected at 100 K on a Bruker KAPPA APEX II CCD Duo diffractometer (operated at 1500 W power: 50 kV, 30 mA) using graphite-monochromated Mo K $\alpha$  radiation ( $\lambda = 0.71073 \text{ \AA}$ ). Crystal was on nylon CryoLoops (Hampton Research) with Paratone-N (Hampton Research). The data integration and reduction were processed with SAINT<sup>13</sup> software. A multi-scan absorption correction was applied to the collected reflections. The structure was solved by the direct method using SHELXTL<sup>14</sup> and was refined on F<sup>2</sup> by full-matrix least-squares technique using the SHELXL-97<sup>15</sup> program package within the WINGX<sup>16</sup> programme. All non-hydrogen atoms were refined anisotropically. All hydrogen atoms were located in successive difference Fourier maps and they were treated as riding atoms using SHELXL default parameters. The structures were examined using the Adsym subroutine of PLATON<sup>17</sup> to assure that no additional symmetry could be applied to the models. The SQUEEZE option was used to eliminate the contribution of disordered guest molecules.

## 3.3 Results and discussion

The compound 1'-SO<sub>4</sub> was synthesized solvothermally by heating a mixture of ligand (L) and NiSO<sub>4</sub>·xH<sub>2</sub>O at 90°C for 48 h. Single-crystal X-ray diffraction (SC-XRD) studies revealed that 1'-SO<sub>4</sub> crystallized in C2/c space group. The asymmetric unit comprises of two half and one full Ni<sup>2+</sup> ions, three L units, one coordinated sulfate (SO<sub>4</sub><sup>2-</sup>) anion, three water (H<sub>2</sub>O) molecules and one uncoordinated SO<sub>4</sub><sup>2-</sup> anion (Figure

3.2a, Appendix 3.1-3.2). The *Adsym* subroutine confirmed that no additional symmetry could be applied to the model. Although all Ni<sup>2+</sup> ions are octahedral, there are two different coordination modes (Appendix 3.3). Ni1 centre is coordinated by four nitrogen atoms from four independent L units, one H<sub>2</sub>O molecule and one SO<sub>4</sub><sup>2-</sup> anion via oxygen atom. Four independent ligands coordinate to Ni2 and Ni3 along with two water molecules.

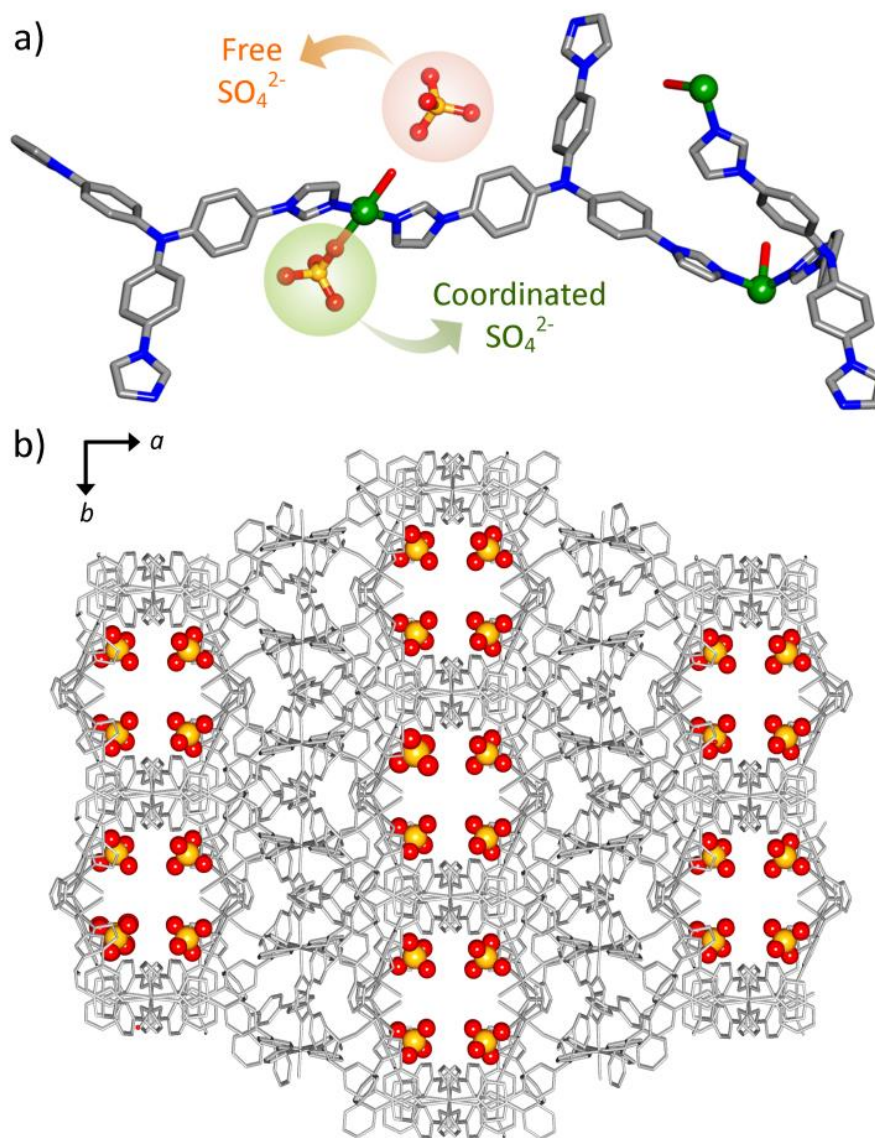


Figure 3.2 (a) Asymmetric unit of 1-SO<sub>4</sub>. (colour - C: grey, N: blue, Ni: green, O: red, S: yellow, H atoms have been omitted for clarity) (b) Overall packing in 1-SO<sub>4</sub> along c-axis highlighting alignment of free SO<sub>4</sub><sup>2-</sup> ions. (colour - 1-SO<sub>4</sub> framework: grey, O: red, S: yellow, H atoms have been omitted for clarity)

The free sulfate anions are held inside the porous cavities by weak non-covalent interactions with the framework components (Appendix 3.4). PLATON calculations revealed that the total empty volume of the compound is  $4592.8 \text{ \AA}^3$ , which corresponds to 24.6% of the total volume. The compound bears aligned arrangement of the uncoordinated  $\text{SO}_4^{2-}$  anions along the c-axis (Figure 3.2b, Appendix 3.5-3.8). It is noteworthy that although metal-sulfate based open frameworks are well known in the literature,<sup>18a-18e</sup> coordination polymers having free sulfate ions are uncommon<sup>18f-18h</sup> and structures with presence of both free and ligated  $\text{SO}_4^{2-}$  anions, like in the present case, are even rarer.<sup>18i-18j</sup> Powder x-ray diffraction (PXRD) patterns (Appendix 3.9) and elemental analysis confirmed the bulk phase purity of the compound. Thermogravimetric analysis (TGA) revealed that there is loss of free guest molecules within the framework and coordinated water molecules upto  $\sim 250 \text{ }^\circ\text{C}$  (Appendix 3.10). PXRD patterns recorded upon heating the compound at higher temperatures validated the structural integrity of the compound (Appendix 3.11). At higher temperatures subtle variation in the PXRD patterns were observed probably on account of slight structural changes accompanied by the loss of coordinated water molecules.

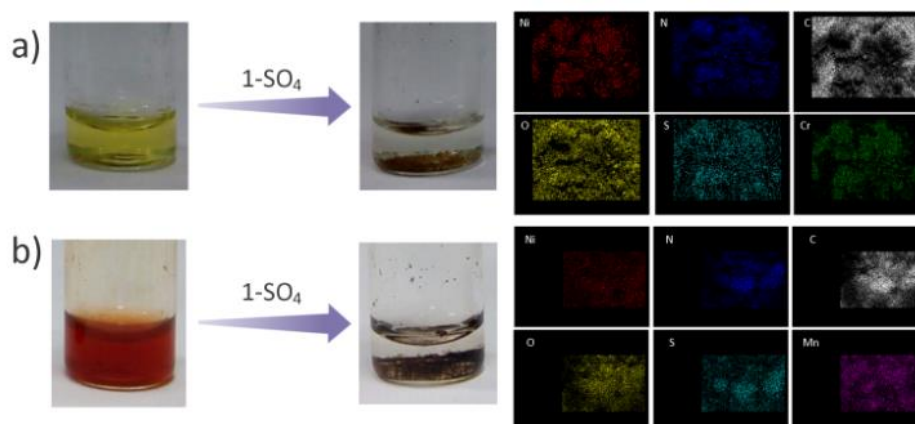


Figure 3.3 Visual decolouration of a)  $\text{K}_2\text{Cr}_2\text{O}_7$  and b)  $\text{KMnO}_4$  solutions by  $1\text{-SO}_4$  and corresponding EDX mapping profiles of  $1\text{-Cr}_2\text{O}_7$  &  $1\text{-MnO}_4$ .

We sought to harness the ionic functionality imparted by the cationic framework to investigate the anion exchange and loading properties of  $1\text{-SO}_4$ . Owing to the hydrolytic stability, robust 3D architecture and channelized alignment of the free  $\text{SO}_4^{2-}$  ions, the efficacy of  $1\text{-SO}_4$  for trapping dichromate anions was examined initially. Crystals of  $1\text{-SO}_4$  were dipped in an aqueous solution of  $\text{K}_2\text{Cr}_2\text{O}_7$  and the exchange process was monitored by PXRD, FT-IR and UV-Vis spectroscopy techniques. The partial decolouration of the solution and change in colour of the crystals were visibly noticed (Figure 3.3a) within 6 hours upon commencement of the exchange process, and almost complete decolouration of the solution was observed after 72 hours to yield the exchanged phase of  $1\text{-Cr}_2\text{O}_7$  (Appendix 3.12-3.13). PXRD patterns suggested



the retention of crystallinity and integrity of the framework after the exchange process (Appendix 3.14). Due to weak diffraction, SC-XRD studies could not be performed despite repeated attempts. FT-IR spectroscopy and energy-dispersive X-ray (EDX) spectra confirmed the inclusion of dichromate ions with a new peak corresponding to Cr-O stretching appearing at  $\sim 950$  &  $770$   $\text{cm}^{-1}$  in the former spectrum (Appendix 3.15) and holistic distribution of chromium in the elemental mapping profiles (Appendix 3.16-3.17).

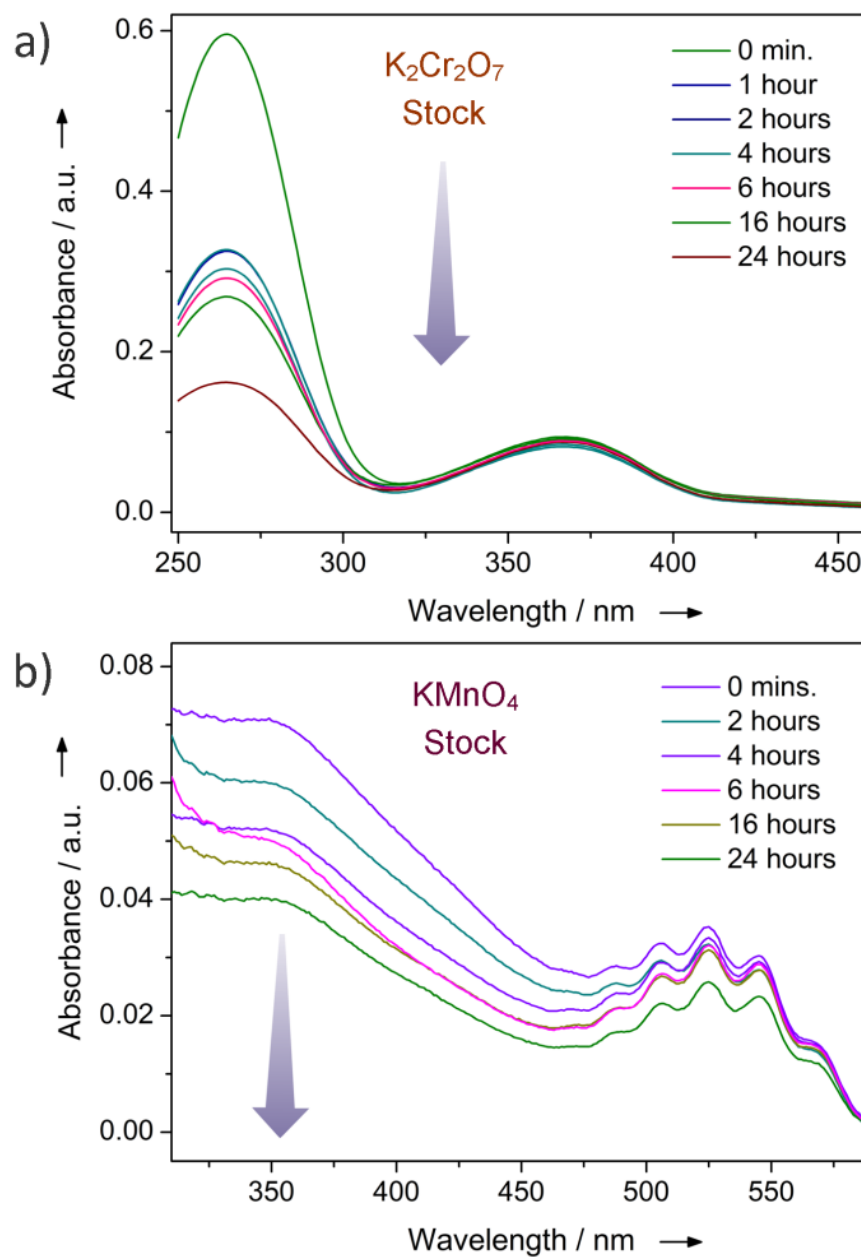


Figure 3.4 UV-Vis spectra of solution at various time intervals of a)  $\text{Cr}_2\text{O}_7^{2-}$  exchange, b)  $\text{MnO}_4^-$  exchange.



UV-Vis spectrum for 1-Cr<sub>2</sub>O<sub>7</sub> dispersed in deionized water overlapped well with that for K<sub>2</sub>Cr<sub>2</sub>O<sub>7</sub> solution (Appendix 3.18), thereby endorsing the inclusion of the dichromate ions within the framework. Time dependent UV-Vis spectra of the supernatant solution during the exchange process accorded well with the visual changes in the colour of 1-SO<sub>4</sub> (Figure 3.4a, Appendix 3.19). The presence of sulphur in the EDX analysis and incomplete disappearance of the peak corresponding to SO<sub>4</sub><sup>2-</sup> in the FT-IR spectrum implied the exchange of only the free SO<sub>4</sub><sup>2-</sup> ions in the framework. We believe that on account of the free SO<sub>4</sub><sup>2-</sup> anions aligned in the porous channels, the Cr<sub>2</sub>O<sub>7</sub><sup>2-</sup> anions occupy the position of sulfate anions by virtue of one-half of the dichromate ion resembling tetrahedral geometry, even though the entire anion is not tetrahedral in shape. The other half could then reorganize itself in the free space as the anion position is directed towards the pore. Inductively coupled plasma (ICP-AES) measurements yielded the loading capacity of the MOF for dichromate ions to be ~166 mg·g<sup>-1</sup>, which is among the best known values in the MOF regime.<sup>11t</sup>

Although anion exchange is important, selective inclusion of the targeted anion has greater relevance and is more challenging. To test the selectivity aspect of dichromate capture, 1-SO<sub>4</sub> was dipped in an aqueous mixture comprising of K<sub>2</sub>Cr<sub>2</sub>O<sub>7</sub> and salts of ClO<sub>4</sub><sup>-</sup>, NO<sub>3</sub><sup>-</sup>, BF<sub>4</sub><sup>-</sup> and CF<sub>3</sub>SO<sub>3</sub><sup>-</sup> separately. FT-IR spectroscopic tool was employed to study the preferential anion uptake. Careful analysis revealed that in all the cases Cr<sub>2</sub>O<sub>7</sub><sup>2-</sup> was selectively incorporated inside the porous matrix over other competing anions (Appendix 3.20). The peaks corresponding to the competing anions were absent in the FT-IR spectra, while the characteristics peaks for Cr<sub>2</sub>O<sub>7</sub><sup>2-</sup> were present for all mixtures. This validated the hypothesis of employing tetrahedral exchangeable anion for targeted capture of oxo-anions of heavy metals. In addition the affinity order of the anions examined in this work was studied using FT-IR (Appendix 3.21).

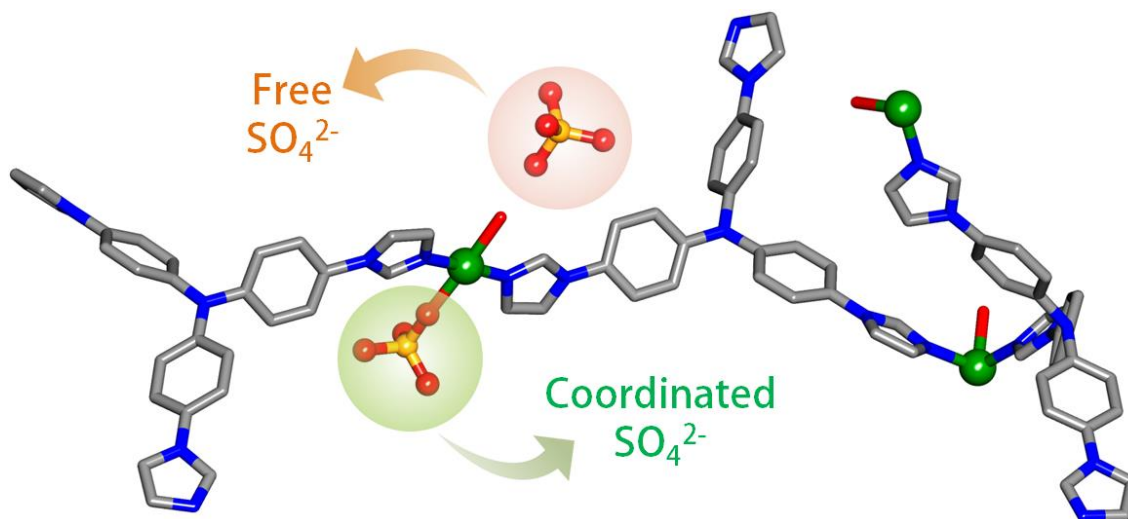
A qualitative order of uptake was estimated to be as follows: Cr<sub>2</sub>O<sub>7</sub><sup>2-</sup> > NO<sub>3</sub><sup>-</sup> ≈ ClO<sub>4</sub><sup>-</sup> > BF<sub>4</sub><sup>-</sup> > CF<sub>3</sub>SO<sub>3</sub><sup>-</sup>. Although ClO<sub>4</sub><sup>-</sup> and BF<sub>4</sub><sup>-</sup> have the similar tetrahedral geometry, their weakly interacting tendencies can be attributed to the comparatively lower uptake for these anions.<sup>11n,19</sup> The desorption of the loaded Cr<sub>2</sub>O<sub>7</sub><sup>2-</sup> ions by SO<sub>4</sub><sup>2-</sup> anions was checked for 1-SO<sub>4</sub> to function as reversible adsorbent. Although desorption was visibly noticed in the change of the colour of the supernatant and that of the solid (Appendix 3.22), FT-IR spectra suggested that for SO<sub>4</sub><sup>2-</sup> anions, desorption was partial (Appendix 3.23). ICP-AES analysis were performed to quantify these observations and the desorption corresponding to 45 μM of Na<sub>2</sub>SO<sub>4</sub> was found to be ~94 mg·g<sup>-1</sup>. The framework was found to be stable in the desorbed phase as well (Appendix 3.22). Further the desorbed phase of 1-Cr<sub>2</sub>O<sub>7</sub> could be used as a Cr<sub>2</sub>O<sub>7</sub><sup>2-</sup> adsorbent with complete regenerative capacity corresponding to the desorbed amount in the first cycle.

Similarly, 1-SO<sub>4</sub> was probed as an adsorbent for pertechnetate ion trapping by studying the response towards its congener permanganate anion. Crystals of 1-SO<sub>4</sub> were dipped in an aqueous solution of KMnO<sub>4</sub> and rapid decolouration of the solution with simultaneous change in colour of the crystals from pale green to dark red was observed (Figure 3.3b, Appendix 3.12). Like the previous case, almost complete decolouration was noted after 72 hours giving rise to the exchanged phase of 1-MnO<sub>4</sub>. Single crystal X-ray diffraction (SC-XRD) studies were attempted several times, but weak diffraction precluded investigation of the exchange process with crystallographic evidence. PXRD patterns substantiated the retention in the integrity of the framework (Appendix 3.14). EDX mapping corroborated with the inclusion of the permanganate ions and presence of sulphur confirmed the exchange of only the free anions (Appendix 3.24-3.25). Time dependent UV-Vis spectra of the supernatant solution during the exchange process corresponded with the changes in the visual chroma with gradual decrement of the absorption peak at 540 nm (Figure 3.4b, Appendix 3.19). The selective entrapment of MnO<sub>4</sub><sup>-</sup> was explored by dipping 1-SO<sub>4</sub> in an aqueous solution of KMnO<sub>4</sub> and salts of ClO<sub>4</sub><sup>-</sup>, NO<sub>3</sub><sup>-</sup>, BF<sub>4</sub><sup>-</sup> and CF<sub>3</sub>SO<sub>3</sub><sup>-</sup> separately. FT-IR spectra confirmed the non-inclusion of competing anions and suggested the selective uptake of permanganate ions (Appendix 3.26). These observations further establish the presence of a tetrahedral substitutable anion as a facilitator for toxic metal oxo-anion capture. An experiment to understand the preferential uptake between MnO<sub>4</sub><sup>-</sup> and Cr<sub>2</sub>O<sub>7</sub><sup>2-</sup> was undertaken by dipping 1-Cr<sub>2</sub>O<sub>7</sub> in an aqueous solution of KMnO<sub>4</sub> and vice versa. This process was monitored by FT-IR which suggested higher affinity of the framework towards MnO<sub>4</sub><sup>-</sup> ions (Appendix 3.27). PXRD patterns suggested the retention of crystallinity even after the second exchange process, reiterating the stability of the framework (Appendix 3.28).

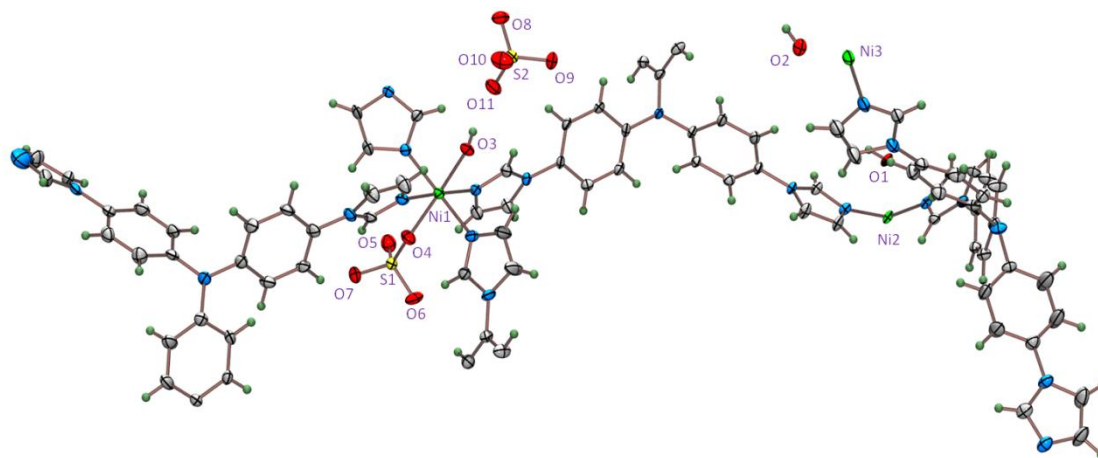
### 3.4 Conclusions

In conclusion, we have synthesized a rigid water stable 3D cationic MOF bearing free sulfate (SO<sub>4</sub><sup>2-</sup>) anions. The compound serves as uncommon example of a MOF-based dual adsorbent for environmental pollutant dichromate (Cr<sub>2</sub>O<sub>7</sub><sup>2-</sup>) anions and radioactive-contaminant pertechnetate (TcO<sub>4</sub><sup>-</sup>) modelled permanganate (MnO<sub>4</sub><sup>-</sup>) anions. The anion exchange features are individually rapid and selective, and a visual colorimetric change in both the cases renders the compound as a potential real-time sensor. The compound exhibits a moderately high uptake capacity for the MOF regime with ~166 mg·g<sup>-1</sup> for Cr<sub>2</sub>O<sub>7</sub><sup>2-</sup> ions. We believe that these results afford significant strategic simplicity for construction of heavy metal ion adsorbents and can contribute affirmatively in the development of MOF based aqueous phase sorbents.

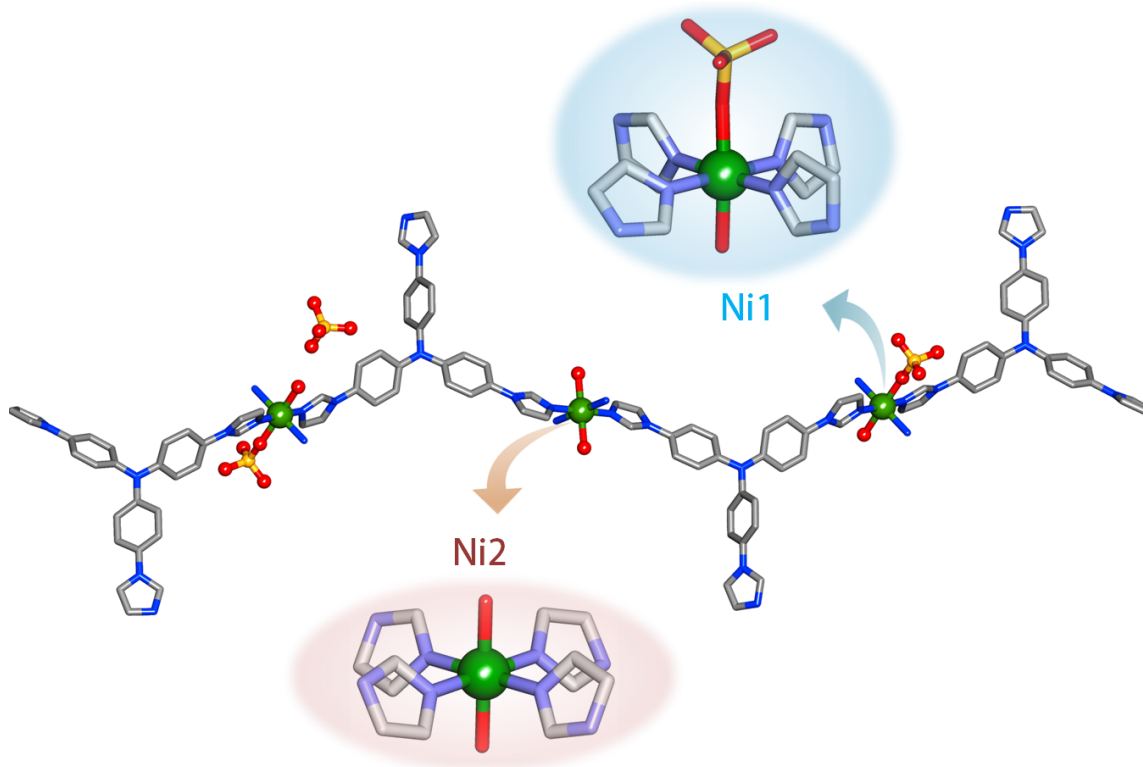
## 3.5 Appendix Section



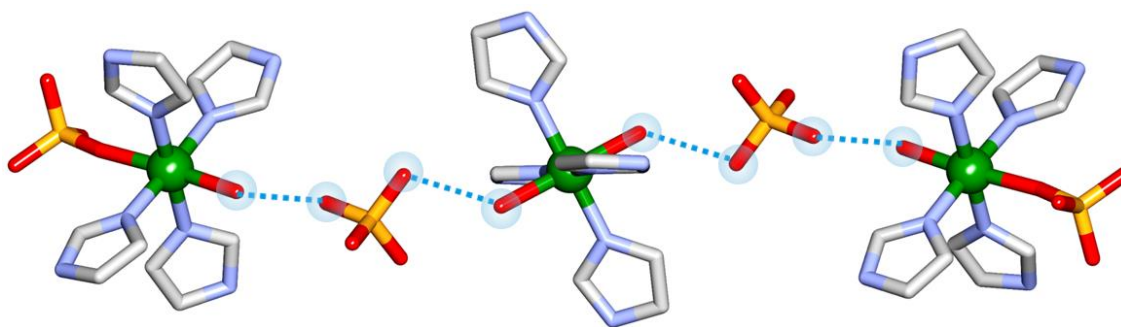
**Appendix 3.1:** Asymmetric unit of **1-SO<sub>4</sub>** (Hydrogen atoms have been omitted for clarity, colour: Gray - C, Blue - N, Green - Ni, Red - Oxygen, Yellow - S).



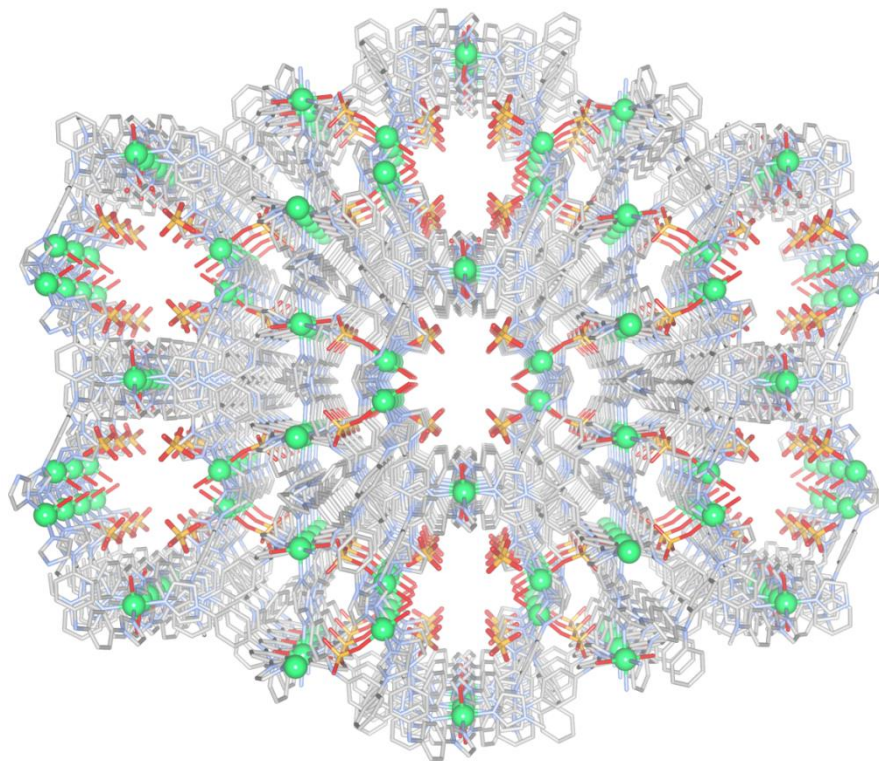
**Appendix 3.2:** ORTEP diagram of asymmetric unit of **1-SO<sub>4</sub>** in thermal ellipsoids (50% probability).



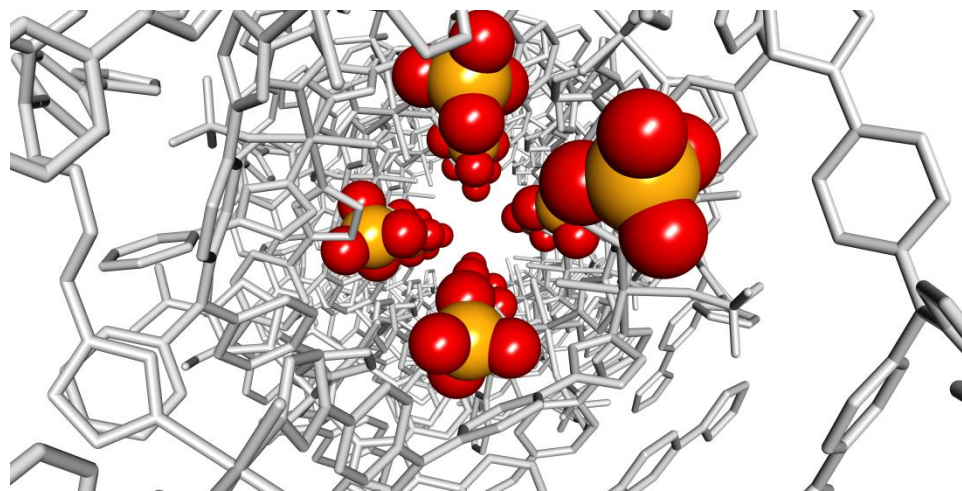
**Appendix 3.3:** Coordination environment in **1-SO<sub>4</sub>** (Hydrogen atoms have been omitted for clarity, colour: Gray - C, Blue - N, Green - Ni, Red - Oxygen, Yellow - S).



**Appendix 3.4:** Non-covalent interactions between the free sulphate anions and framework components (Hydrogen atoms have been omitted for clarity, colour: Gray - C, Blue - N, Green - Ni, Red - Oxygen, Yellow - S).

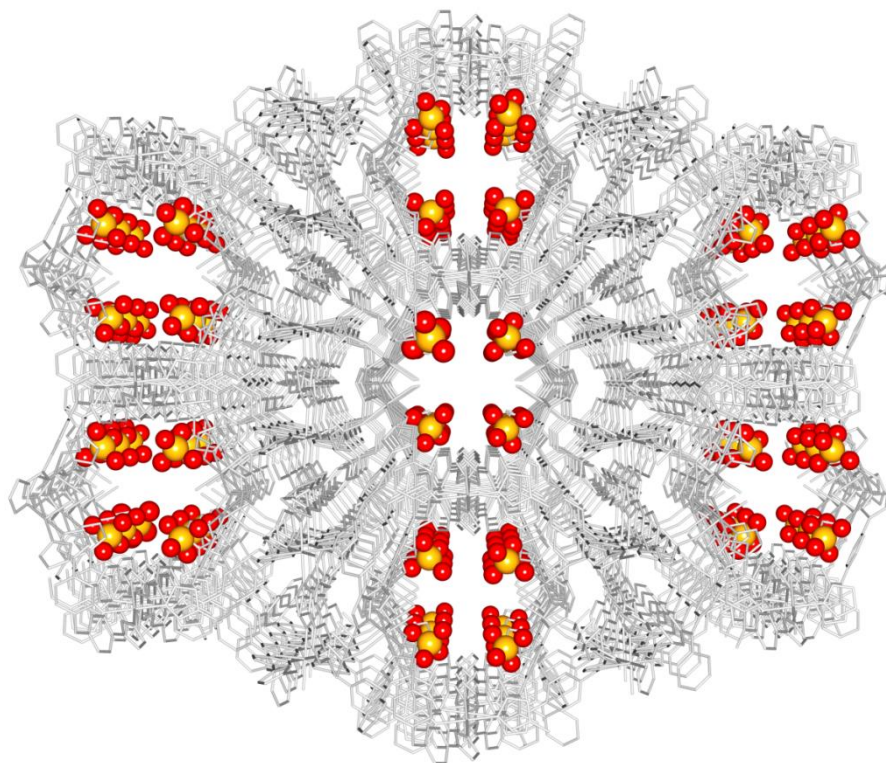


**Appendix 3.5:** Perspective view of packing in compound 1-SO<sub>4</sub> along *c*-axis (Hydrogen atoms have been omitted for clarity, colour: Gray - C, Blue - N, Green - Ni, Red - Oxygen, Yellow - S).

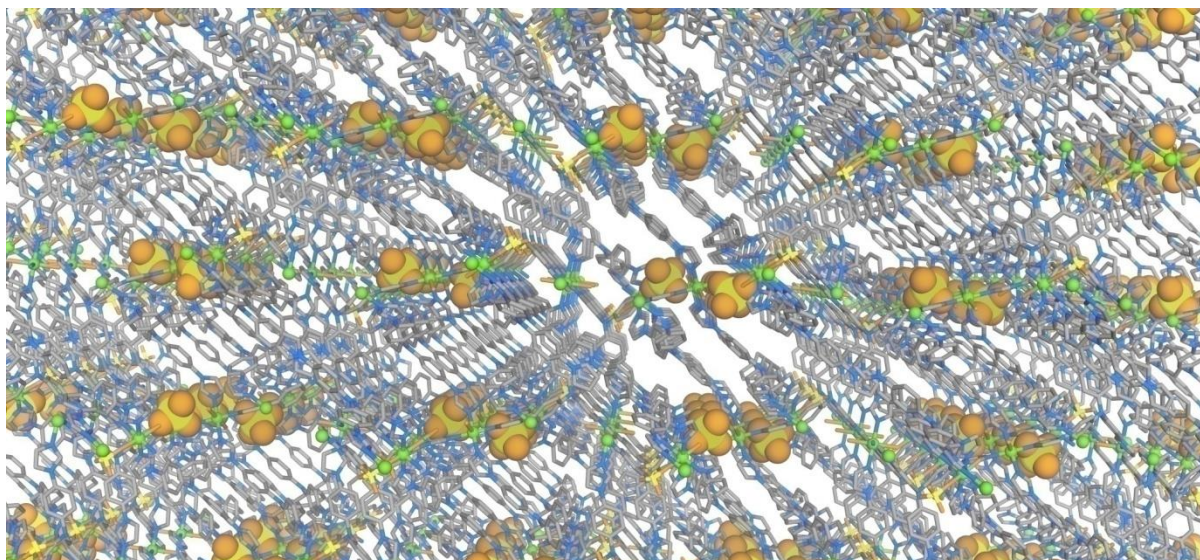


**Appendix 3.6:** Perspective view of single pore showing the alignment of free SO<sub>4</sub><sup>2-</sup> anions along the *c*-axis (Hydrogen atoms have been omitted for clarity, colour: Gray - 1-SO<sub>4</sub> framework, Red - Oxygen, Yellow - S).

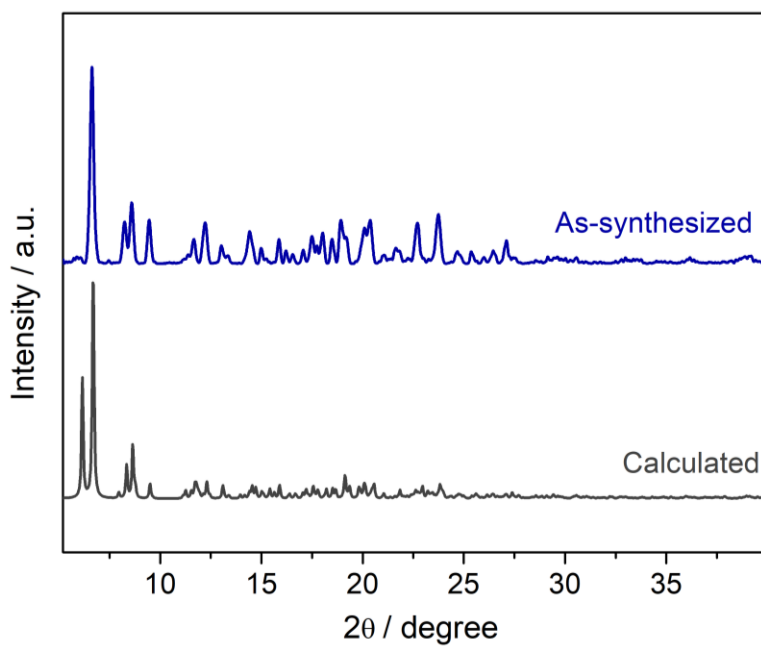




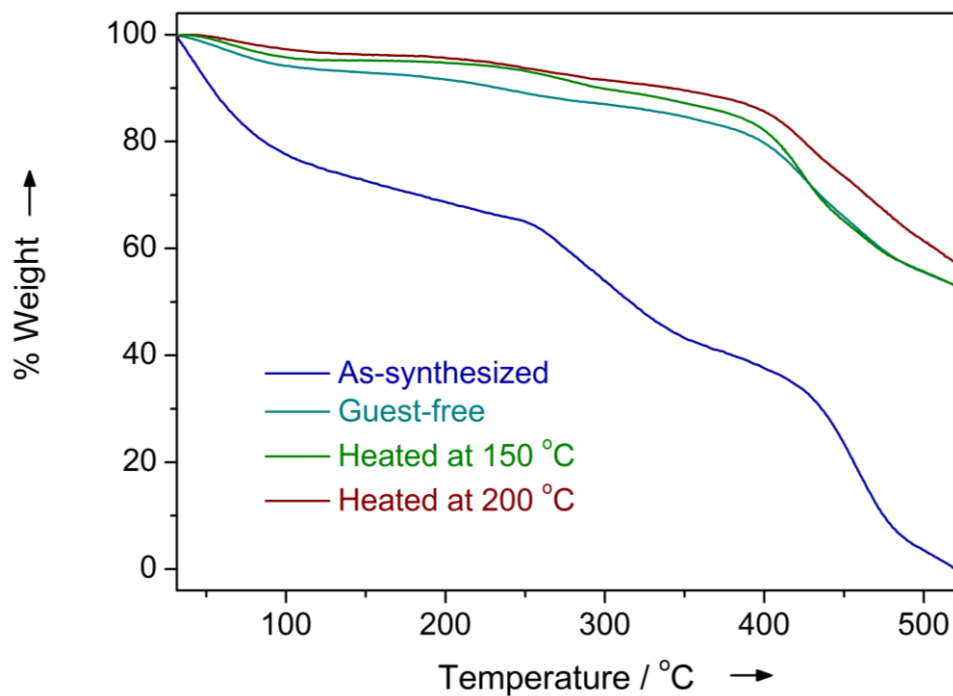
**Appendix 3.7:** Perspective view of packing showing the alignment of free  $\text{SO}_4^{2-}$  anions along the  $c$ -axis (Hydrogen atoms have been omitted for clarity, colour: Gray - 1- $\text{SO}_4$  framework, Red - Oxygen, Yellow - S).



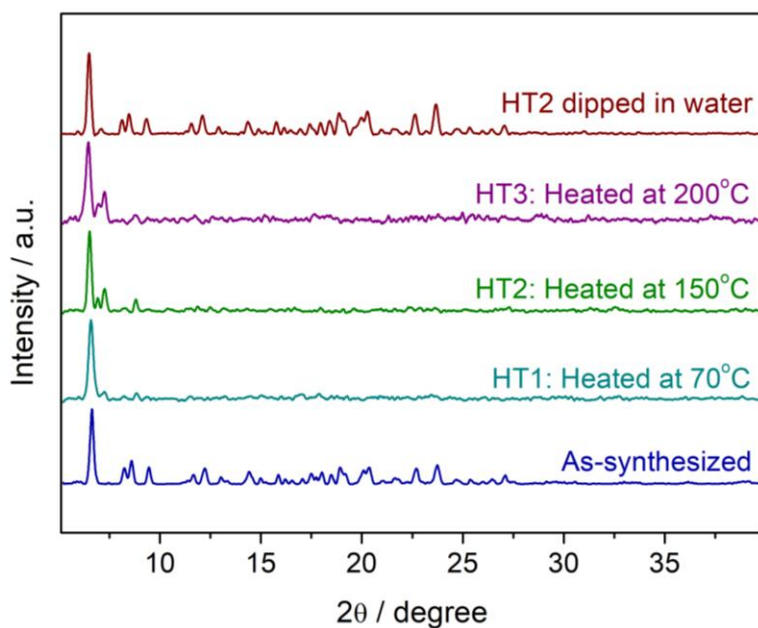
**Appendix 3.8:** Perspective view of packing in compound 1- $\text{SO}_4$  along  $b$ -axis (Hydrogen atoms have been omitted for clarity, colour: Gray - C, Blue - N, Green - Ni, Red - Oxygen, Yellow - S).



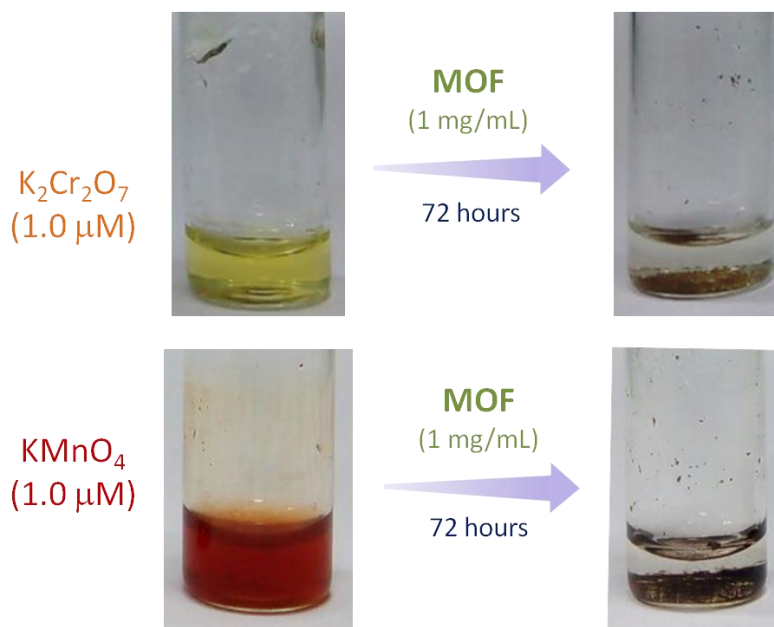
**Appendix 3.9:** Powder X-ray diffraction patterns of 1-SO<sub>4</sub> calculated (gray), as-synthesized (blue).



**Appendix 3.10:** Thermogravimetric analysis (TGA) plot of 1-SO<sub>4</sub> as-synthesized (blue), guest free phase (light blue), sample heated at 150 °C for 12 hours (green) and sample heated at 200 °C for 12 hours (wine).

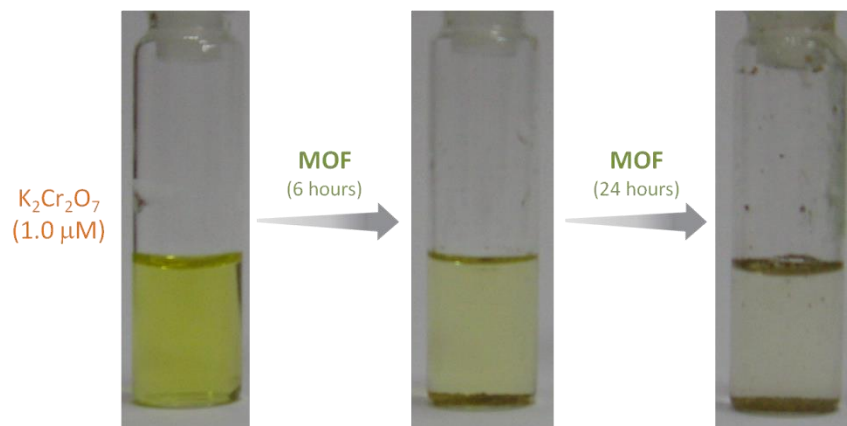


**Appendix 3.11:** Powder X-ray diffraction (PXRD) patterns of 1-SO<sub>4</sub> upon heating in 3 steps for 12 hours at each temperature. PXRD pattern (wine) of the sample H2 dipped in water for 4 hours.

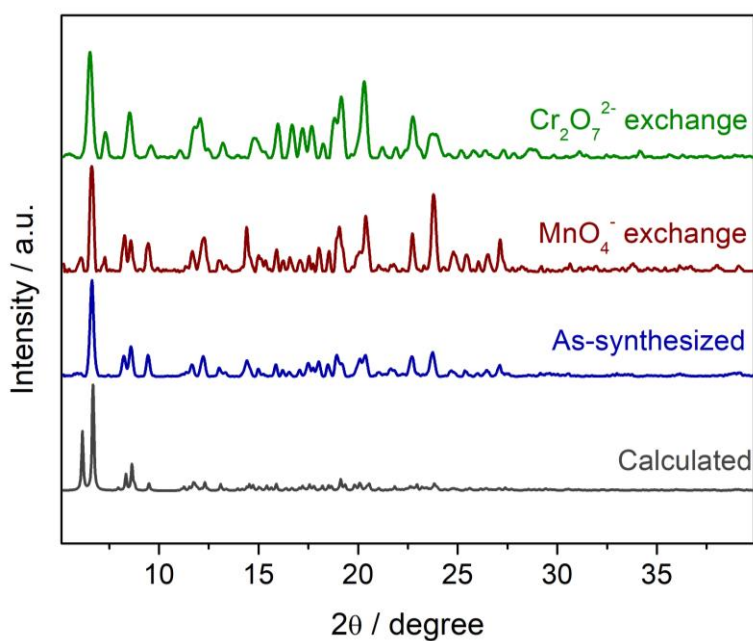


**Appendix 3.12:** Photographs of Cr<sub>2</sub>O<sub>7</sub><sup>2-</sup> & MnO<sub>4</sub><sup>-</sup> trapping by addition of compound 1-SO<sub>4</sub> to K<sub>2</sub>Cr<sub>2</sub>O<sub>7</sub> (top) & KMnO<sub>4</sub> (below) solutions respectively.

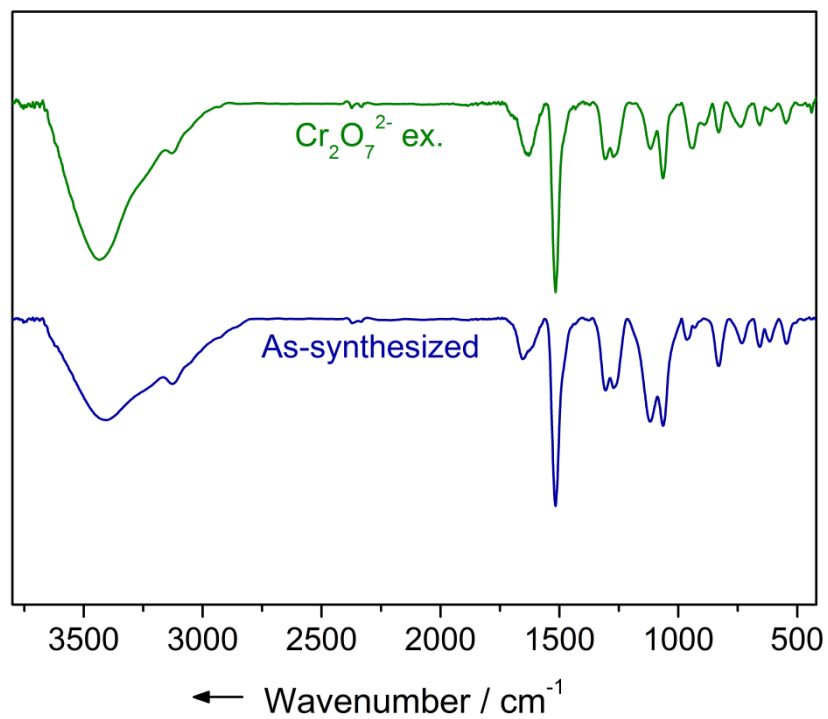




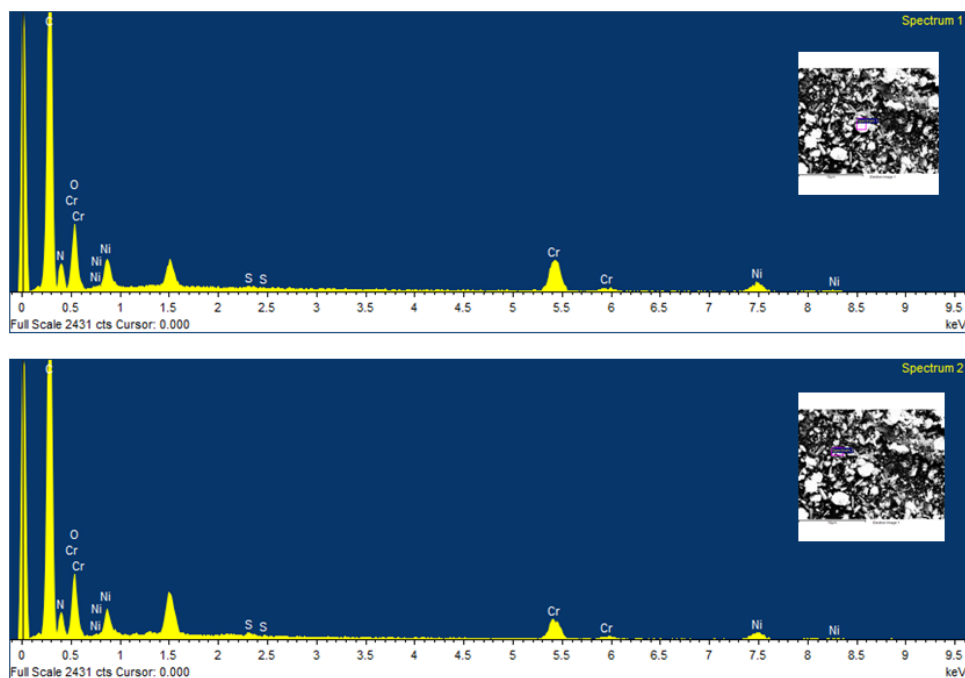
**Appendix 3.13:** Photographs of time-dependent uptake of  $\text{Cr}_2\text{O}_7^{2-}$  by 1- $\text{SO}_4$ .



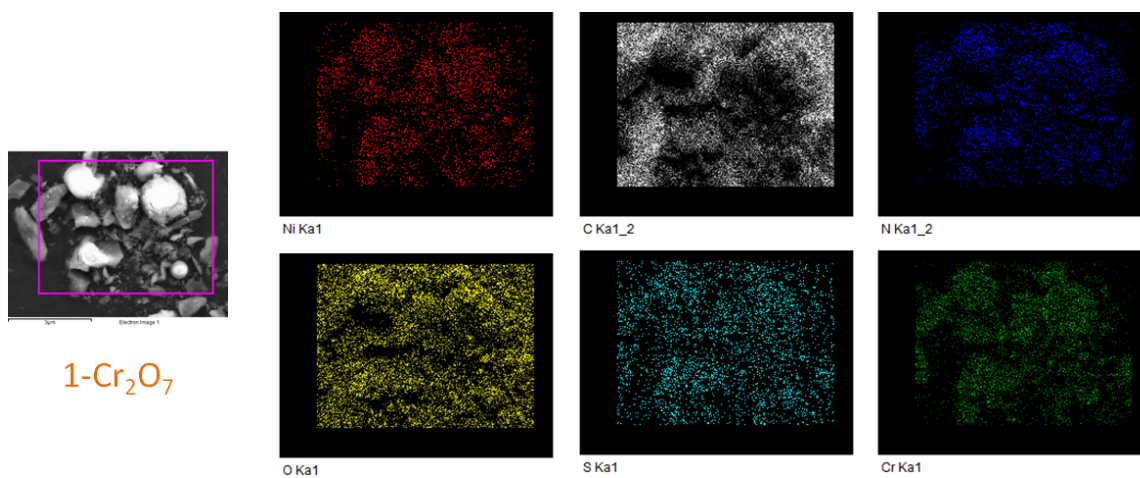
**Appendix 3.14:** Powder X-ray diffraction patterns of 1- $\text{SO}_4$  calculated (gray), as-synthesized (blue),  $\text{MnO}_4^-$  exchange (wine),  $\text{Cr}_2\text{O}_7^{2-}$  exchange (green).



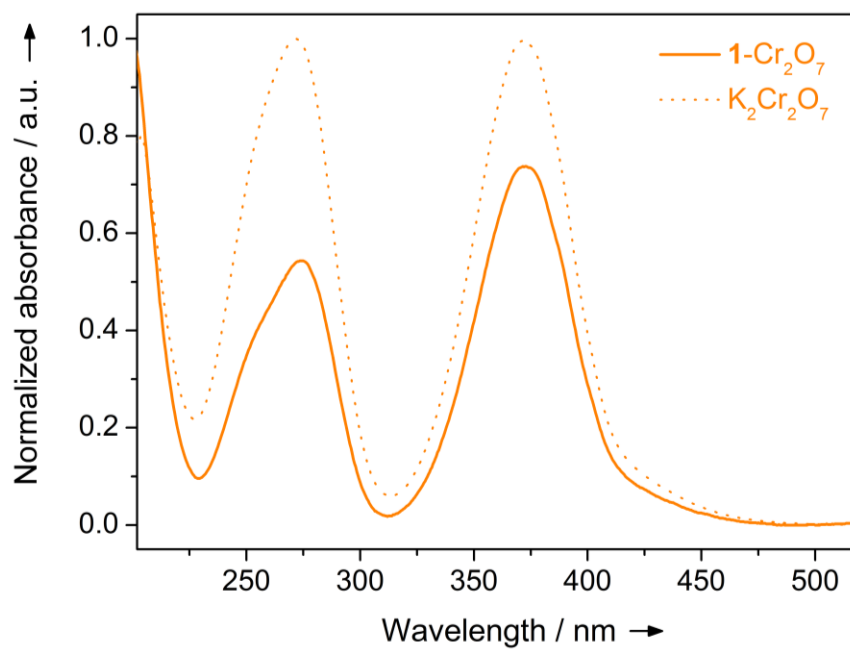
**Appendix 3.15:** FT-IR spectra for as-synthesized compound (blue) and Cr<sub>2</sub>O<sub>7</sub><sup>2-</sup> exchange (green).



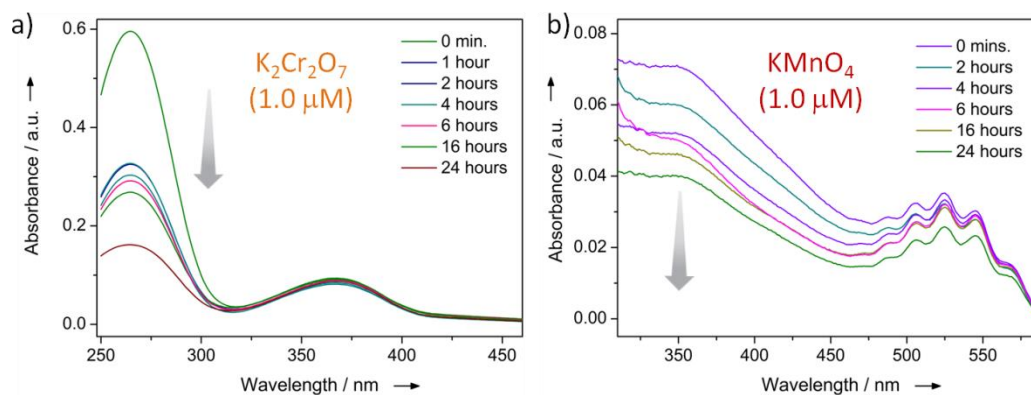
**Appendix 3.16:** EDX spectra of 1-Cr<sub>2</sub>O<sub>7</sub>.



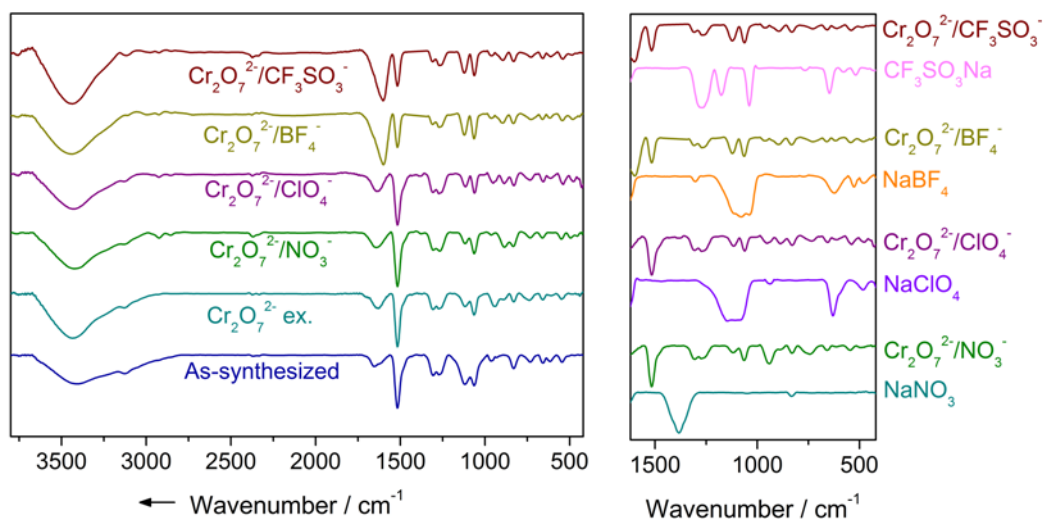
**Appendix 3.17:** Elemental mapping for 1-Cr<sub>2</sub>O<sub>7</sub>.



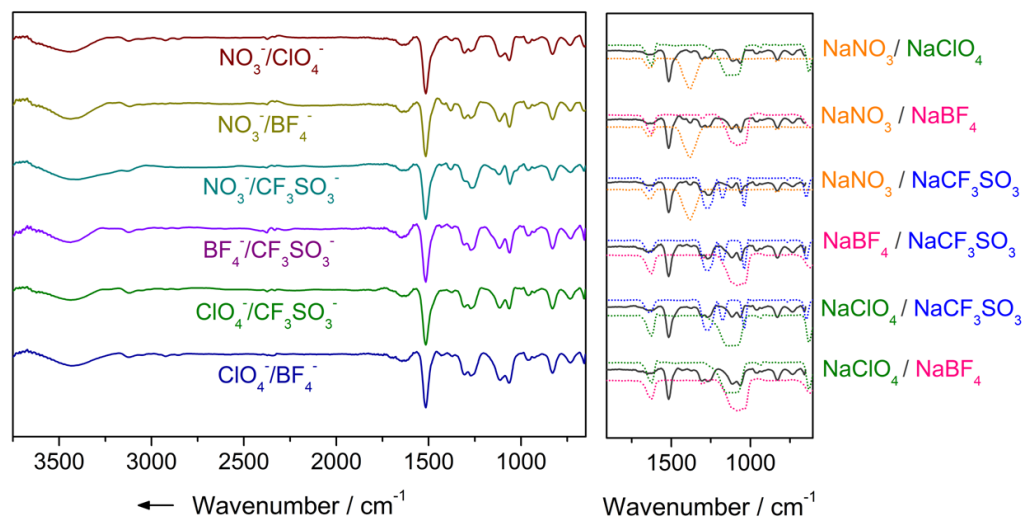
**Appendix 3.18:** Normalized UV-Vis spectra for K<sub>2</sub>Cr<sub>2</sub>O<sub>7</sub> and 1-Cr<sub>2</sub>O<sub>7</sub> dispersed in water.



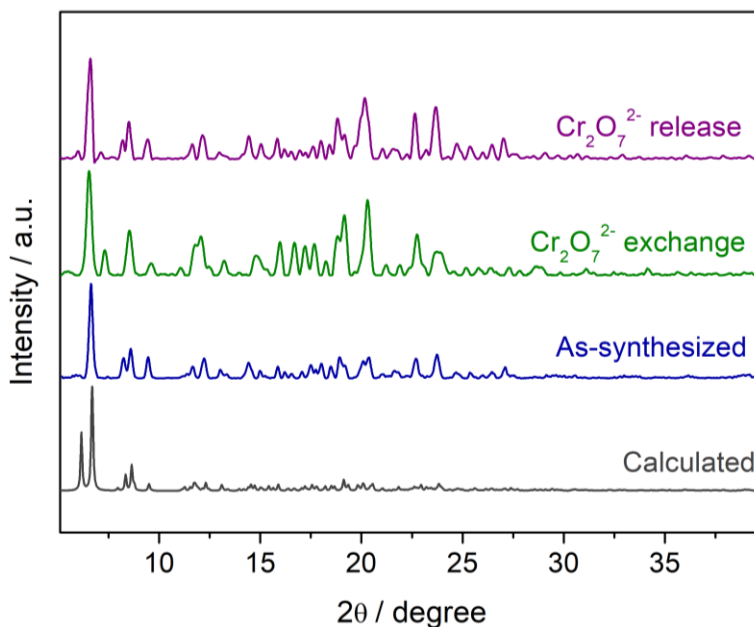
**Appendix 3.19:** UV-Vis spectra of solution at various time intervals of a)  $Cr_2O_7^{2-}$  exchange, b)  $MnO_4^-$  exchange.



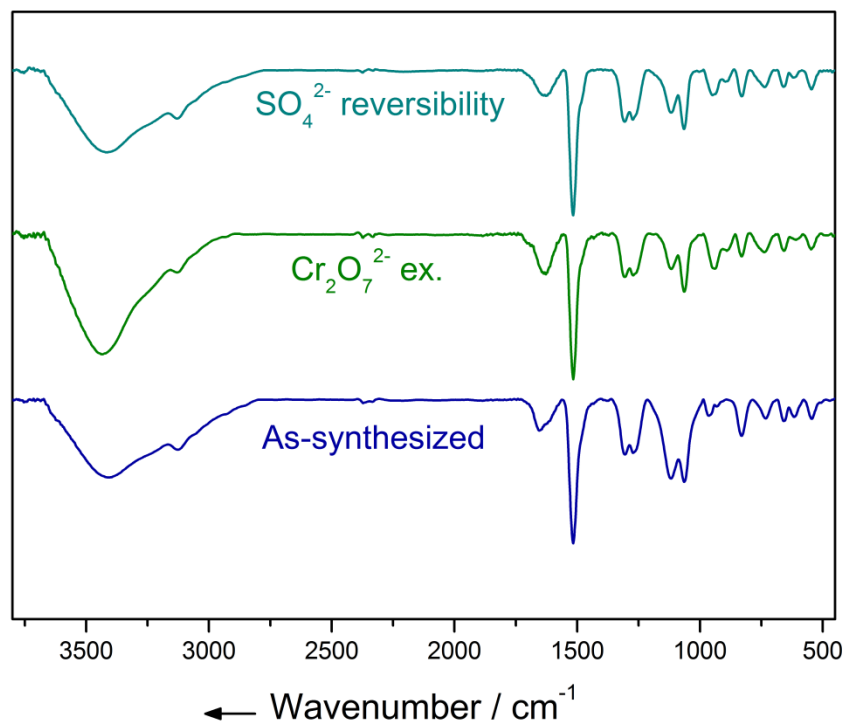
**Appendix 3.20:** FT-IR spectra for selective anion exchange studies. Concise view of the fingerprint region comparing spectra of blank anions with those in the mixture upon addition to 1-SO<sub>4</sub>.



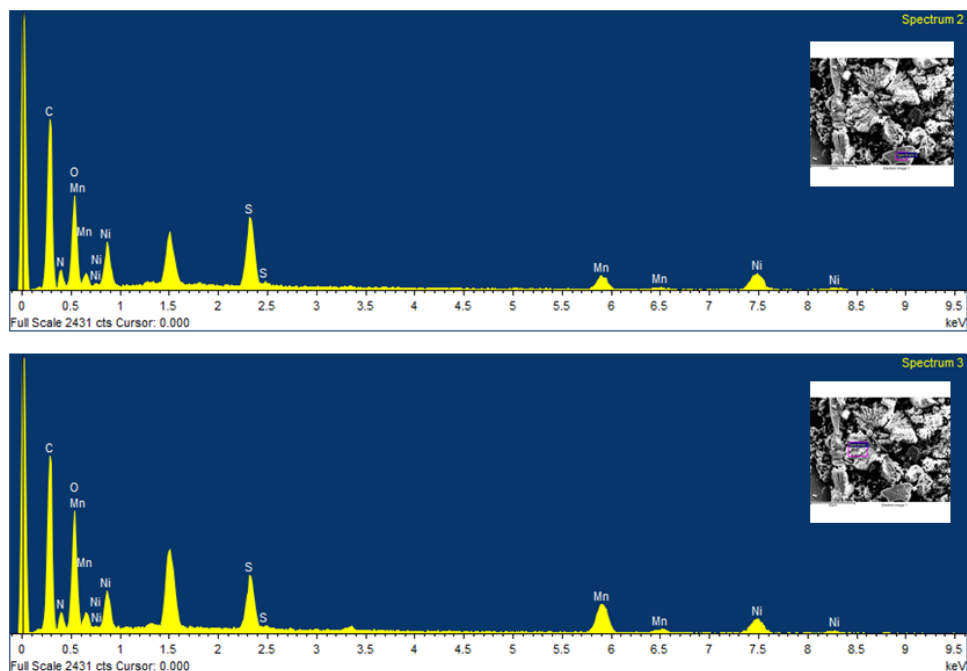
**Appendix 3.21:** (Left) FT-IR spectra for anion affinity studies in 1-SO<sub>4</sub>. (Right) concise view of the fingerprint region, comparing spectra of blank anions (dotted lines and matching line colours) with those in the mixture upon addition to 1-SO<sub>4</sub> (dark gray).



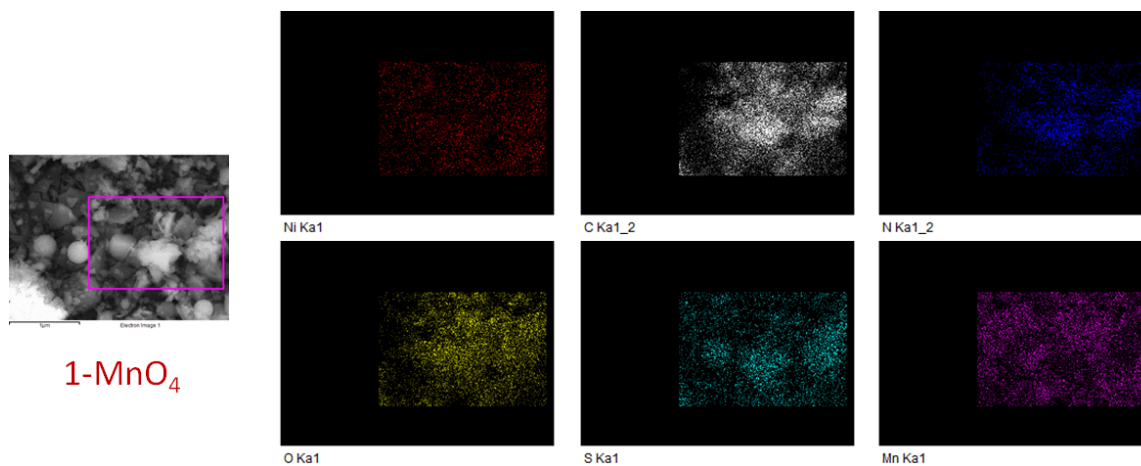
**Appendix 3.22:** PXRD patterns of calculated (gray), as-synthesized (blue), dichromate exchange (green) and dichromate desorption (purple). The corresponding optical pictographs are shown alongside.



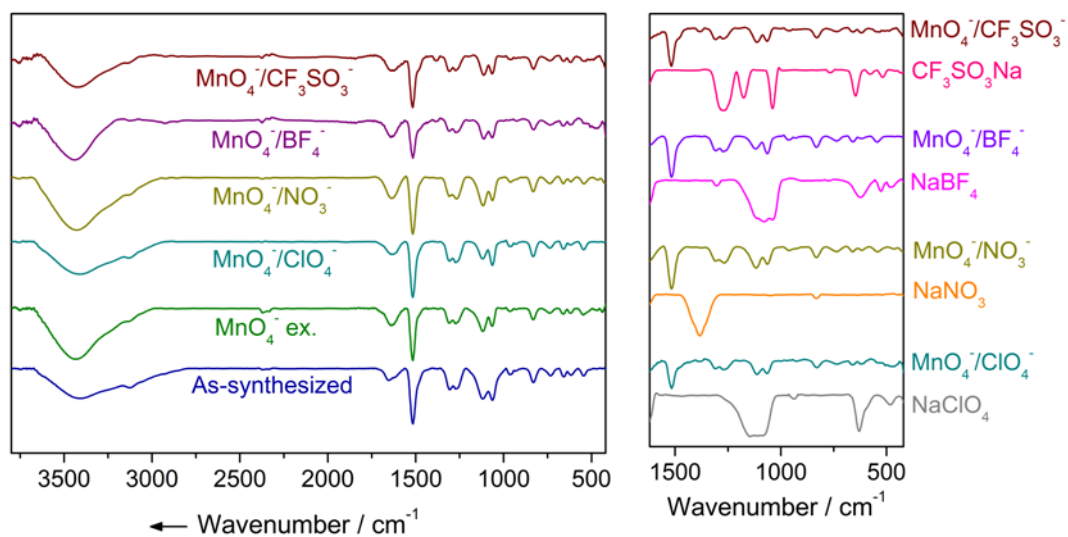
**Appendix 3.23:** FT-IR spectra for reversible anion exchange studies for 1-Cr<sub>2</sub>O<sub>7</sub>.



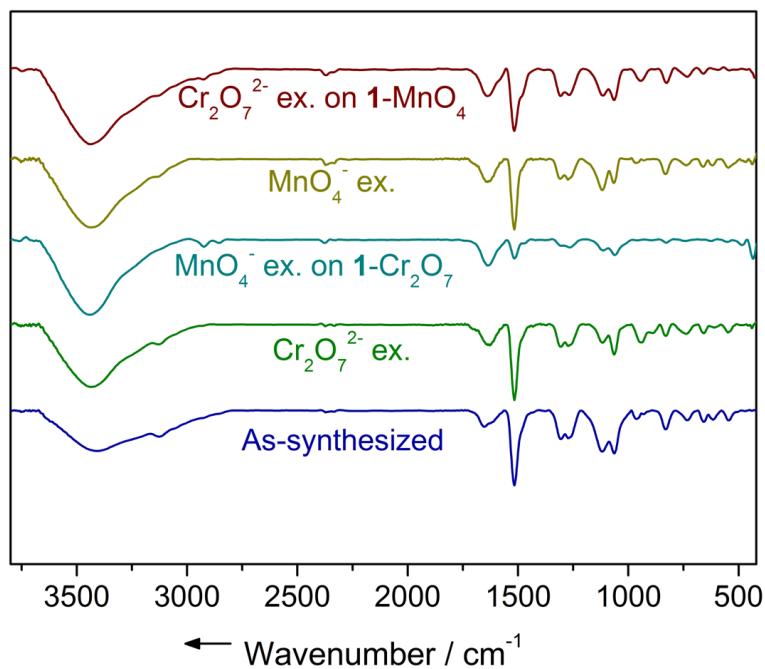
**Appendix 3.24:** EDX spectra of 1-MnO<sub>4</sub>.



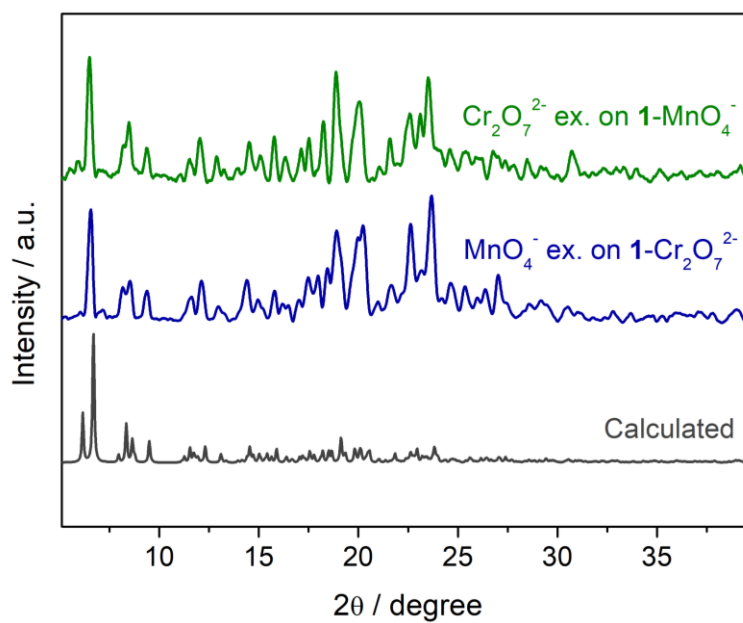
**Appendix 3.25:** Elemental mapping for 1-MnO<sub>4</sub>.



**Appendix 3.26:** FT-IR spectra for selective anion exchange studies. Concise view of the fingerprint region comparing spectra of blank anions with those in the mixture upon addition to 1-SO<sub>4</sub>.



**Appendix 3.27:** FT-IR spectra for competing anion exchange studies.



**Appendix 3.28:** PXRD patterns of calculated (gray),  $\text{MnO}_4^-$  exchange by 1- $\text{Cr}_2\text{O}_7^{2-}$  (blue) and  $\text{Cr}_2\text{O}_7^{2-}$  exchange by 1- $\text{MnO}_4^-$  (green).



**Appendix Table 1.** Crystal data and structure refinement for 1SO4.

Identification code	1SO4 (CCDC 1422306)	
Empirical formula	C <sub>81</sub> H <sub>69</sub> N <sub>21</sub> Ni <sub>2</sub> O <sub>11</sub> S <sub>2</sub>	
Formula weight	1694.09	
Temperature	100(2) K	
Wavelength	0.71073 Å	
Crystal system	Monoclinic	
Space group	C2/c	
Unit cell dimensions	a = 46.618(8) Å	α = 90°
	b = 15.159(2) Å	β = 107.721(5)°
	c = 27.704(4) Å	γ = 90°
Volume	18649(5) Å <sup>3</sup>	
Z	8	
Density (calculated)	1.205 Mg/m <sup>3</sup>	
Absorption coefficient	0.512 mm <sup>-1</sup>	
F(000)	7000	
Crystal size	0.17 x 0.12 x 0.10 mm <sup>3</sup>	
Theta range for data collection	0.92 to 28.42°.	
Index ranges	-62 ≤ h ≤ 62, -20 ≤ k ≤ 19, -36 ≤ l ≤ 36	
Reflections collected	169189	
Independent reflections	23293 [R(int) = 0.1794]	
Completeness to theta = 28.42°	99.3 %	
Absorption correction	Semi-empirical from equivalents	
Max. and min. transmission	0.9505 and 0.9179	
Refinement method	Full-matrix least-squares on F <sup>2</sup>	
Data / restraints / parameters	23293 / 0 / 1060	
Goodness-of-fit on F <sup>2</sup>	1.366	
Final R indices [I > 2σ(I)]	R <sub>I</sub> = 0.0705, wR <sub>2</sub> = 0.1128	
R indices (all data)	R <sub>I</sub> = 0.1614, wR <sub>2</sub> = 0.1201	
Largest diff. peak and hole	0.700 and -0.589 e.Å <sup>-3</sup>	

### 3.6 References

1. Fu, F.; Wang, Q., *J. Environ. Manage.* **2011**, *92*, 407-418.
2. Keith, L. H.; Teillard, W. A., *Environ. Sci. Technol.* **1979**, *13*, 416-423.
3. (a) Costa, M.; Klein, C. B., *Crit. Rev. Toxicol.* **2006**, *36*, 155-163. (b) Khemazi, L.; Capart, R., *J. Hazard. Mater.* **2005**, *123*, 223-231. (c) Zhitkovich, A. *Chem. Res. Toxicol.* **2005**, *18*, 3-11.
4. (a) Darab, J. G.; Smith, P. A., *Chem. Mater.* **1996**, *8*, 1004-1021. (b) Katayev, E. A.; Kolesnikov, G. V.; Sessler, J. L., *Chem. Soc. Rev.* **2009**, *38*, 1572-1586.
5. (a) Boyer, T. H.; Singer, P. C., *Environ. Sci. Technol.* **2008**, *42*, 608-613. (b) Parasuraman, D.; Sarker, A. K.; Serpe, M. J., *ChemPhysChem* **2012**, *13*, 2507-2515.
6. (a) Bhatnagar, A.; Sillanpaa, M., *Chem. Eng. J.* **2010**, *157*, 277-296. (b) Blaney, L. M.; Cinar, S.; Sengupta, A. K., *Water Res.* **2007**, *41*, 1603.
7. (a) Eddaoudi, M.; Kim, J.; Rosi, N.; Vodak, D.; Watcher, J.; O’Keeffe, M.; Yaghi, O. M., *Science* **2002**, *295*, 469-472. (b) Long, J. R.; Yaghi, O. M., *Chem. Soc. Rev.* **2009**, *38*, 1213-1214. (c) Horike, S.; Shimomura, S.; Kitagawa, S., *Nat. Chem.* **2009**, *1*, 695-704. (d) Ramaswamy, P.; Wong, N. E.; Shimizu, G. K. H., *Chem. Soc. Rev.* **2014**, *43*, 5913-5932. (e) Hu, Z.; Deibert, B. J.; Li, J., *Chem. Soc. Rev.* **2014**, *43*, 5815-5840. (f) Nagarkar, S. S.; Desai, A. V.; Ghosh, S. K., *Chem. Asian J.* **2014**, *9*, 2358-2376. (g) Bradshaw, D.; El-Hankari, S.; Lupica-Spagnolo, L., *Chem. Soc. Rev.* **2014**, *43*, 5431-5443.
8. (a) Mulfort, K. L.; Farha, O. K.; Stern, C. L.; Sarjeant, A. A.; Hupp, J. T., *J. Am. Chem. Soc.* **2009**, *131*, 3866-3868. (b) Demessence, A.; D’Alessandro, D. M.; Foo, M. L.; Long, J. R., *J. Am. Chem. Soc.* **2009**, *131*, 8784-8786. (c) Zhang, Z.; Gao, W. Y.; Wojtas, L.; Ma, S.; Eddaoudi, M.; Zaworotko, M. J., *Angew. Chem. Int. Ed.* **2012**, *51*, 9330-9334. (d) Joarder, B.; Mukherjee, S.; Chaudhari, A. K.; Desai, A. V.; Manna, B.; Ghosh, S. K., *Chem. Eur. J.* **2014**, *20*, 15303-15308. (e) Duan, J.; Higuchi, M.; Krishna, R.; Kiyonaga, R.; Tsutsumi, Y.; Sato, Y.; Kubota, Y.; Takata, M.; Kitagawa, S., *Chem. Sci.* **2014**, *5*, 660-666. (f) Xuan, Z.-H.; Zhang, D.-S.; Chang, Z.; Hu, T.-L.; Bu, X.-H., *Inorg. Chem.* **2014**, *53*, 8985-8990. (g) Li, B.; Wen, H.-M.; Wang, H.; Wu, H.; Yildirim, T.; Zhou, W.; Chen, B., *Energy Environ. Sci.* **2015**, *8*, 2504-2511. (h) Chang, G.; Huang, M.; Su, Y.; Xing, H.; Su, B.; Zhang, Z.; Yang, Q.; Yang, Y.; Ren, Q.; Bao, Z.; Chen, B., *Chem. Commun.* **2015**, *51*, 2859-2862.
9. (a) Fei, H.; Rogow, D. L.; Oliver, S. R. J., *J. Am. Chem. Soc.* **2010**, *132*, 7202-7209. (b) Schoedel, A.; Wojtas, L.; Kelley, S. P.; Rogers, R. D.; Eddaoudi, M.; Zaworotko, M. J., *Angew. Chem. Int. Ed.* **2011**, *50*, 11421-11424. (c) Ma, J.-P.; Yu, Y.; Dong, Y.-B., *Chem. Commun.* **2012**, *48*, 2946-2948. (d) Chen, Y.-

Q.; Li, G.-R.; Chang, Z.; Qu, Y.-K.; Zhang, Y.-H.; Bu, X.-H., *Chem. Sci.* **2013**, *4*, 3678-3682. (e) Hou, S.; Liu, Q.-K.; Ma, J.-P.; Dong, Y.-B., *Inorg. Chem.* **2013**, *52*, 3225-3235. (f) Manna, B.; Joarder, B.; Desai, A. V.; Karmakar, A.; Ghosh, S. K., *Chem. Eur. J.* **2014**, *20*, 12399-12404. (g) Chen, D.-m.; Shi, W.; Cheng, P., *Chem. Commun.* **2015**, *51*, 370-372. (h) Karmakar, A.; Desai, A. V.; Manna, B.; Joarder, B.; Ghosh, S. K., *Chem. Eur. J.* **2015**, *21*, 7071-7076. (i) Song, B.-Q.; Wang, X.-L.; Zhang, Y.-T.; Wu, X.-S.; Liu, H.-S.; Shao, K.-Z.; Su, Z.-M., *Chem. Commun.* **2015**, *51*, 9515-9518.

10. (a) Karmakar, A.; Desai, A. V.; Ghosh, S. K., *Coord. Chem. Rev.* **2016**, *307*, 313-341. (b) Muthu, S.; Yip, J. H. K.; Vittal, J. J., *J. Chem. Soc., Dalton Trans.* **2001**, 3577-3584. (c) Wang, J. H.; Li, M.; Li, D., *Chem. Sci.* **2013**, *4*, 1793-1801. (d) Cheng, J.-Y.; Wang, P.; Ma, J.-P.; Liu, Q.-K.; Dong, Y.-B., *Chem. Commun.* **2014**, *50*, 13672-13675. (e) Aijaz, A.; Lama, P.; Bharadwaj, P. K., *Inorg. Chem.* **2010**, *49*, 5883-5889. (f) Manna, B.; Desai, A. V.; Ghosh, S. K., *Dalton Trans.* **2016**, *45*, 4060-4072.

11. (a) Min, K. S.; Suh, M. P., *J. Am. Chem. Soc.* **2000**, *122*, 6834-6840. (b) Noro, S.-i.; Kitaura, R.; Kondo, M.; Kitagawa, S.; Ishii, T.; Matsuzaka, H.; Yamashita, M., *J. Am. Chem. Soc.* **2002**, *124*, 2568-2583. (c) Tran, D. T.; Zavalij, P. Y.; Oliver, S. R. J., *J. Am. Chem. Soc.* **2002**, *124*, 3966-3968. (d) Hamilton, B. H.; Wagler, T. A.; Espe, M. P.; Ziegler, C. J., *Inorg. Chem.* **2005**, *44*, 4891-4893. (e) Du, M.; Zhao, X.-J.; Guo, J.-H.; Batten, S. R., *Chem. Commun.* **2005**, 4836-4838. (f) Maji, T. K.; Matsuda, R.; Kitagawa, S., *Nat. Mater.* **2007**, *6*, 142-148. (g) Oliver, S. R. J., *Chem. Soc. Rev.* **2009**, *38*, 1868-1881. (h) Fei, H.; Oliver, S. R. J., *Angew. Chem. Int. Ed.* **2011**, *50*, 9066-9070. (i) Kolesnikov, G. V.; German, K. E.; Kirakosyan, G.; Tananaev, I. G.; Ustynyuk, Y. A.; Khrustalev, V. N.; Katayev, E. A., *Org. Biomol. Chem.* **2011**, *9*, 7358-7364. (j) Fei, H.; Bresler, M. R.; Oliver, S. R. J., *J. Am. Chem. Soc.* **2011**, *133*, 11110-11113. (k) Cao, R.; McCarthy, B. D.; Lippard, S. J., *Inorg. Chem.* **2011**, *50*, 9499-9507. (l) Custelcean, R.; Bonnesen, P. V.; Duncan, N. C.; Zhang, X.; Watson, L. A.; Berkel, G. V.; Parson, W. B.; Hay, B. P., *J. Am. Chem. Soc.* **2012**, *134*, 8525-8534. (m) Fang, C.; Liu, Q.-K.; Ma, J.-P.; Dong, Y.-B., **2012**, *51*, 3923-3925. (n) Wang, S.; Yu, P.; Purse, B. A.; Orta, M. J.; Diwu, J.; Casey, W. H.; Phillips, B. L.; Alekseev, E. V.; Depmeier, W.; Hobbs, D. T.; Albrecht-Schmitt, T. E., *Adv. Funct. Mater.* **2012**, *22*, 2241-2250. (o) Shi, P.-F.; Zhao, B.; Xiong, G.; Hou, Y.-L.; Cheng, P., *Chem. Commun.* **2012**, *48*, 8231-8233. (p) Fei, H.; Hen, C. S.; Robins, J. C.; Oliver, S. R. J., *Chem. Mater.* **2013**, *25*, 647-652. (q) Li, X.; Xu, H.; Kong, F.; Wang, R., *Angew. Chem. Int. Ed.* **2013**, *52*, 13769-13773. (r) Manna, B.; Chaudhari, A. K.; Joarder, B.; Karmakar, A.; Ghosh, S. K., *Angew. Chem. Int. Ed.* **2013**, *52*, 998-1002. (s) Fu, H.-R.; Xu, Z.-X.; Zhang, J., *Chem. Mater.* **2015**, *27*, 205-210. (t) Zhang, Q.; Yu, J.; Cai, J.; Zhang, L.; Cui, Y.; Yang, Y.; Chen, B.; Qian, G., *Chem. Commun.* **2015**, *51*, 14732-14734. (u) Howarth, A. J.; Liu, Y.; Hupp, J. T.; Farha, O. K., *CrystEngComm* **2015**, *17*, 7245-7253.

12. Maity, R.; Koppetz, H.; Hepp, A.; Hahn, F. E., *J. Am. Chem. Soc.* **2013**, *135*, 4966-4969.
13. *SAINT Plus*, version 7.03; Bruker AXS Inc.: Madison, WI, **2004**.
14. Sheldrick, G. M., *SHELXTL*, Reference Manual, version 5.1; Bruker AXS Inc.: Madison, WI, **1997**.
15. Sheldrick, G. M., *Acta. Crystallogr., Sect. A* **2008**, *64*, 112-122.
16. Farrugia, L., *WinGX*, version 1.80.05; University of Glasgow: Glasgow, Scotland, **2009**.
17. Spek, A. L., *PLATON*, a Multipurpose Crystallographic Tool; Utrecht University: Utrecht, The Netherlands, **2005**.
18. (a) Choudhary, A.; Krishnamoorthy, J.; Rao, C. N. R., *Chem. Commun.* **2001**, 2610-2611. (b) Behra, J. N.; Gopalkrishnan, K. V.; Rao, C. N. R., *Inorg. Chem.* **2004**, *43*, 2636-2642. (c) Sudik, A. C.; Millward, A. R.; Ockwig, N. W.; Cote, A. P.; Kim, J.; Yaghi, O. M., *J. Am. Chem. Soc.* **2005**, *127*, 7110-7118. (d) Ramaswamy, P.; Hegde, N. N.; Prabhu, R.; Vidya, V. M.; Datta, A.; Natarajan, S., *Inorg. Chem.* **2009**, *48*, 11697-11711. (e) Zhang, D.; Lu, Y.; Zhu, D.; Xu, Y., *Inorg. Chem.* **2013**, *52*, 3253-3258. (f) Carlucci, L.; Ciani, G.; Proserpio, D. M., *Chem. Commun.* **2004**, 380-381. (g) Wu, B.; Liang, J.; Zhao, Y.; Li, M.; Li, S.; Liu, Y.; Zhang, Y.; Yang, X.-J., *CrystEngComm* **2010**, *12*, 2129-2134. (h) Murdock, C. R.; Jenkins, D. M.; *J. Am. Chem. Soc.* **2014**, *136*, 10983-10988. (i) Habib, H. A.; Hoffmann, A.; Hoppe, H. A.; Steinfeld, G.; Janaik, C., *Inorg. Chem.* **2009**, *48*, 2166-2180. (j) Seeber, G.; Cooper, G. J. T.; Newton, G. N.; Rosnes, M. H.; Long, D.-L.; Kariuki, B. M.; Kogerler, P.; Cronin, L., *Chem. Sci.* **2010**, *1*, 62-67.
19. (a) Krossing, I.; Raabe, I., *Angew. Chem. Int. Ed.* **2004**, *43*, 2066-2090. (b) Ravikumar, I.; Ghosh, P., *Chem. Soc. Rev.* **2012**, *41*, 3077-3098.

---

## *Chapter 4*

---

# **Multifunctional Sulfonate-based Isostructural MOFs for CO<sub>2</sub> Capture**

## 4.1 Introduction

The field of metal-organic frameworks has witnessed a steady rise over the last couple of decades,<sup>1</sup> owing to the plethora of applications presented by these systems.<sup>2</sup> Although several seminal advances have been made, work on design strategies continues to command significant research attention on account of unresolved issues of hydrolytic and chemical stabilities in majority of the compounds.<sup>3</sup> Several approaches have been proposed to address these core drawbacks from the outlines derived by knowledge guiding the stability of benchmark compounds.<sup>4</sup> Typically the emphasis has been laid on protecting the metal-ligand bond or by imparting hydrophobic character to the coordination polymer, by virtue of employing the advantage of reticular chemistry in MOFs.<sup>5</sup> Among these lines, stability can also be improved by strengthening the metal-ligand bond, as seen for strongly coordinating anions, but hitherto less attention has been devoted for the exploration in this regard. Carboxylates have been the most popular choice of linker donor groups for the preparation of MOFs.<sup>6</sup> Compared to such ligands, phosphonates or sulfonates which offer similar binding moieties can offer similar properties or in some superior character.<sup>7</sup> In particular, the distinguishable features include diversity in binding geometries, versatile structural packing and higher resistance to dissociation of the metal-ligand bond.<sup>7i</sup> Despite sulfonates offering superior characteristics, they have not been investigated sufficiently as they have weak binding ability with transition metals and generally MOFs constructed from these linkers result in systems which cannot sustain porosity permanently. Shimizu and co-workers had proposed the feasibility of formation of extended networks using sulfonate linkers<sup>8</sup> but since then very few compounds have been reported in the literature. In the same period, carboxylate based MOFs were studied in detail both in terms of design strategies and application studies but sulfonate/phosphonate based MOFs were very few in number. Thus the design principles guiding the synthesis of sulfonate/phosphonate based systems is of high topical demand.

Alike stability, another feature of MOFs which has sought attention is the ability to create multiple functions in the same system.<sup>9</sup> Broadly, the approach of having mixed-ligand systems has been proposed as the efficient approach to attain such multifunctional compounds. In general, neutral N-donor linkers have been deployed for the function of enhancing the dimensionality of carboxylate-based MOFs and afford access to the functions appended to the framework backbone. Another important function of neutral N-donor ligands has been to yield cationic MOFs and to prepare dynamic MOFs as the metal-ligand bond strength is not rigid owing to the softness of the coordination bond.<sup>10</sup> Among the different donor groups, 5-membered molecules such as imidazole, pyrazole or triazole have found higher preference owing to steric advantage and on account of stronger binding tendencies over 6-membered groups such as pyridine.<sup>10c,10e,10f</sup> As mentioned earlier, generally sulfonate-based MOFs are not able to withstand permanent porosity and hence

use of strongly coordinating neutral N-donor linkers as a support to such frameworks can lead to formation of stable systems and assist in realizing the true potential of strongly coordinating groups.

To experiment this approach we synthesized a uncommon example of a robust, permanently porous MOF having Cd(II) metal nodes viz. IPM-301  $\{[\text{Cd}_2(1,5\text{-NDS})(\text{L})_2(\text{SO}_4)] \cdot x\text{G}\}_n$  where IPM, 1,5-NDS and L represent IISER Pune Materials, 1,5-naphthalene disulfonate and N-donor ligand respectively. The compound was found to have aligned polar groups in the porous channels which resulted in high affinity for  $\text{CO}_2$  and the uptake capacities were found to be among the highest reported in the domain of organosulfonate-MOFs. The ability to access reticular chemistry in such frameworks was demonstrated by synthesizing an isostructural MOF with pendant amine groups. In addition to the stability of the frameworks, the additional benefits bestowed by the choice of the building blocks resulted in multifunctional character for  $\text{C}_6$ -cyclic hydrocarbon separation and selective recognition of neurotransmitter gas nitric oxide (NO). Remarkably, both the functions have not been proposed for frameworks built from sulfonate/phosphonate based ligands.

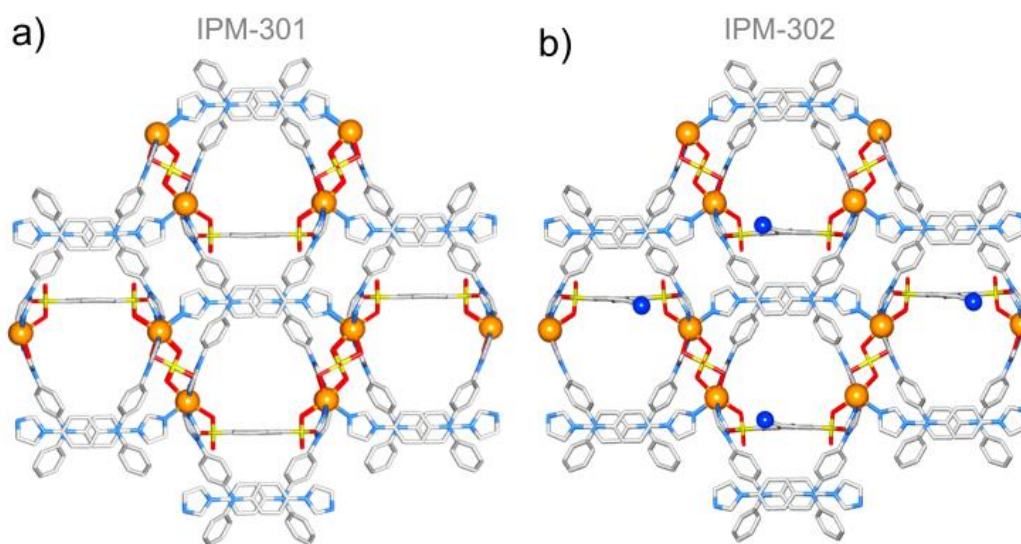


Figure 4.1 a) Packing diagram of IPM-301 and b) IPM-302 along crystallographic  $a$ -axis (Colour code: C, grey; N, blue; S, yellow; O, red; Cd, orange. H-atoms have been omitted for clarity and pendant N-atoms of  $-\text{NH}_2$  in IPM-302 have been highlighted in Fig. 4.1b).

## 4.2 Experimental

### 4.2.1 Materials:

The reagents and solvents used in this work were available from commercial sources and were used directly. Commercial grade pH buffer solutions (pH = 4.01, 10.01) were bought from Eutech Instruments. The neutral N-donor ligand [L - tris(4-(1H-imidazol-1-yl)phenyl)amine] was prepared according to a previously reported procedure.<sup>10c</sup>

### 4.2.2 Synthesis:

**Synthesis of Compound IPM-301:** A mixture of ligand (8.86 mg, 0.02 mmol),  $3\text{CdSO}_4 \cdot 8\text{H}_2\text{O}$  (15.4 mg, 0.02 mmol), 1,5-naphthalenedisulfonic acid tetrahydrate (9.00 mg, 0.025 mmol), N,N-dimethylformamide (1 ml) and water (2 ml), was placed in a glass vial, and heated at  $90^\circ\text{C}$  for 48 hours followed by slow cooling to room temperature. The compound was filtered and washed with water and methanol several times. Single crystals of compound IPM-301 viz.  $[\{\text{Cd}_2(1,5\text{-NDS})(\text{L})_2(\text{SO}_4)\} \cdot x\text{G}]_n$  were isolated in ~45% yield. These crystals were dipped in MeOH solution for exchange, and heated under vacuum at  $75^\circ\text{C}$  to obtain the guest free phase. We were unable to locate the highly disordered guest solvent molecules in the structure crystallographically. The formula for the guest-free phase was estimated to be  $[\{\text{Cd}_2(1,5\text{-NDS})(\text{L})_2(\text{SO}_4)\}]_n$  (1,5-NDS refers to 1,5-naphthalene disulfonate). Anal. Calcd. (guest free phase): C/N, 3.92; N/S, 2.04; C/S, 7.99. Found: C/N, 3.98; N/S, 2.06; C/S, 8.24.

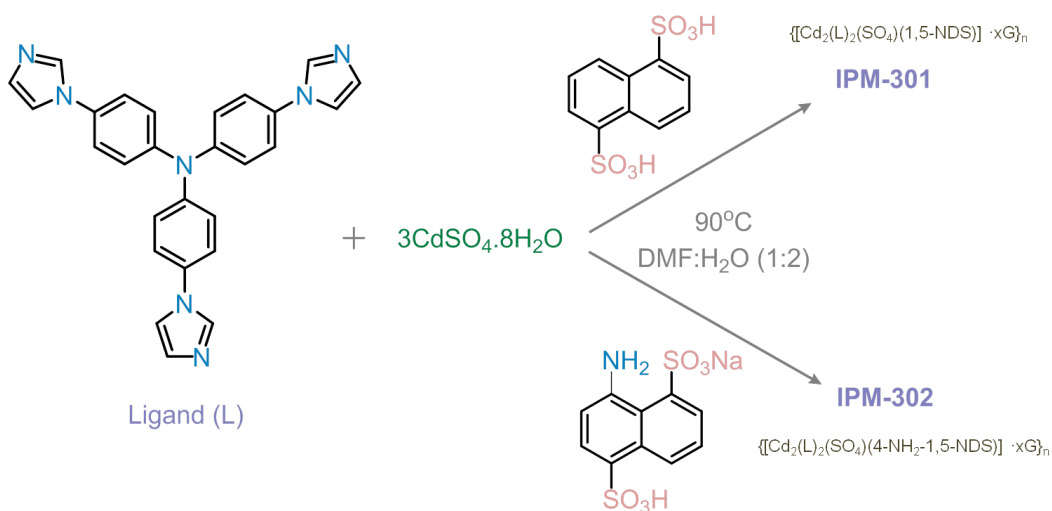


Figure 4.2 Representation of the protocol employed for the synthesis of IPM-301 and IPM-302.



**Synthesis of Compound IPM-302:** This compound was synthesized similarly as above, except using sodium 4-amino-1,5-naphthalenedisulfonate (9.75 mg) instead of 1,5-naphthalenedisulfonic acid tetrahydrate. The formula for the guest-free phase was estimated to be  $[\{Cd_2(NH_2-1,5-NDS)(L)_2(SO_4)\}]_n$  (NH<sub>2</sub>-1,5-NDS refers to 4-amino-1,5-naphthalene disulfonate). Anal. Calcd. (guest free phase): C/N, 3.66; N/S, 2.18; C/S, 7.99. Found: C/N, 3.70; N/S, 2.23; C/S, 8.28.

**4.2.3 Water Stability Test:** ~55 mg of the activated compound IPM-301 and IPM-302 was dipped in 5 ml of deionised water and kept at room temperature. Subsequently, the compound was filtered off and dried in air for further characterization. The supernatant was collected and its ICP-AES analysis was recorded.

**4.2.4 pH Stability Test:** ~20 mg of the activated compound IPM-301 and IPM-302 was dipped in 5 ml of separate pH solution (pH = 4, 10.01) and stirred at room temperature for 24 hours. The respective supernatant solutions were collected and the residue was washed with deionised water multiple times, followed by washing with methanol. The recovered solid phases were then degassed by heating under reduced pressure for further characterization. For gas adsorption studies, the compounds were pre-treated at 110°C under vacuum before measurement.

**4.2.5 Fluorescence measurements:** To a dispersed aqueous solution of IPM-302, nitric oxide (NO) was bubbled for 15 minutes. The crystals were recovered and washed with deionised water and dried under vacuum for further characterization. Other analytes were prepared according to reported protocol.<sup>24b</sup> The respective solutions (200 µl) were added to 2ml aqueous solution of IPM-302 and equilibrated for 2 minutes before recording the emission spectra.

**4.2.6 Physical Measurements:** Powder X-ray diffraction patterns were recorded on Bruker D8 Advanced X-Ray diffractometer using Cu K $\alpha$  radiation ( $\lambda = 1.5406 \text{ \AA}$ ) in 5° to 40° 2 $\theta$  range with a scan speed of 1.2°min<sup>-1</sup>. The IR Spectra were acquired by using NICOLET 6700 FT-IR spectrophotometer using KBr pellet in 400-4000 cm<sup>-1</sup> range. UV spectra were recorded on Shimadzu UV 2600 Spectrophotometer having stirring attachment. The SEM images & EDX data were obtained using FEI Quanta 3D dual beam ESEM. Thermogravimetric analysis profiles were recorded on Perkin-Elmer STA6000, TGA analyser under N<sub>2</sub> atmosphere with heating rate of 10°C/min. Gas adsorption measurements were performed using BelSorp-Max instrument (Bel Japan). Solvent adsorption measurements were performed on Bel-Aqua instrument (Bel Japan). Prior to adsorption measurements, the activated samples were heated at 110°C under vacuum for 6 hours using BelPrepvacII. <sup>1</sup>H & <sup>13</sup>C NMR spectra were recorded on a JEOL 400 MHz or Bruker 400 MHz spectrometer.

**4.2.7 X-ray Structural Studies:** Single-crystal X-ray data of compound IPM-301 and IPM-302 was collected at 100 K on a Bruker D8 Venture Duo X-ray diffractometer equipped with Microfocus X-ray

source (operated at 50W; 50kV/1mA), graded multilayer optics for monochromatic Mo K $\alpha$  radiation ( $\lambda = 0.71073\text{\AA}$ ) focused X-ray beam and Photon 100 CMOS chip based detector system. Crystal was mounted on nylon CryoLoops (Hampton Research) with Paraton-N (Hampton Research). The data integration and reduction were processed with SAINT software.<sup>11</sup> A multi-scan absorption correction was applied to the collected reflections.<sup>12</sup> The structure was solved by the direct method using SHELXTL<sup>13</sup> and was refined on F2 by full-matrix least-squares technique using the SHELXL-2014/7<sup>14</sup> program package within the WINGX<sup>15</sup> programme. All non-hydrogen atoms were refined anisotropically. All hydrogen atoms were located in successive difference Fourier maps and they were treated as riding atoms using SHELXL default parameters. The structures were examined using the Adsym subroutine of PLATON to assure that no additional symmetry could be applied to the models. The SQUEEZE option<sup>16</sup> was used to eliminate the contribution of disordered guest molecules. The bridging SO<sub>4</sub><sup>2-</sup> anions in both the compounds are having two O-atoms disordered. In case of IPM-302, the pendant -NH<sub>2</sub> group is disordered over two positions. CCDC 1831060-1831061, for IPM-301 and IPM-302 respectively, contains the supplementary crystallographic data for this paper. These data can be obtained free of charge from The Cambridge Crystallographic Data Centre via [www.ccdc.cam.ac.uk/data\\_request/cif](http://www.ccdc.cam.ac.uk/data_request/cif).

**4.2.8 Binding Energy Calculations** (*In collaboration with Dr. Ravichandar Babarao, RMIT University, Australia*): Static binding energies for CO<sub>2</sub> in IPM-301 and IPM-302 were calculated using density functional theory (DFT) as implemented in the software package VASP.<sup>17</sup> It is well-known that standard DFT methods based on generalized gradient approximation do not fully account for the long-range dispersion interactions between the framework and the weakly bound gaseous adsorbates. To accurately estimate static binding energies for weakly bound guest molecules with IPM-301 and IPM-302 framework, we implemented dispersion corrections using DFT-D3 method.<sup>18</sup> Electron exchange and correlation were described using the generalized gradient approximation Perdew, Burke, and Ernzerhof (PBE)<sup>19</sup> form and the projector-augmented wave potentials were used to treat core and valence electrons.<sup>20</sup> In all cases, we used a plane-wave kinetic energy cutoff of 600 eV and a Gamma-point mesh for sampling the Brillouin zone. The ionic coordinates were relaxed until the Hellman-Feynman ionic forces were less than 0.01 eV/Å. The initial location of the guest molecule in the primitive cell of IPM-301 and IPM-302 was obtained from the classical simulated annealing technique using classical force field as implemented in sorption module in Materials Studio.<sup>21</sup> In the simulated annealing method, the temperature was lowered stepwise, allowing the gas molecule to reach a desirable configuration based on different moves such as rotation, translation and re-positioning with preset probabilities of occurrence. This process of heating and cooling the system was repeated in several heating cycles to find the local minima. Forty heating cycles were performed where the maximum temperature and the final temperature were 105 K and 100 K, respectively. Static binding

energies ( $\Delta E$ ) at 0K were calculated using the following expression;  

$$\Delta E = E_{MOF+gas} - E_{MOF} - E_{gas}$$

where  $E_x$  refers, respectively, to the total energies of the MOF + gas complex, the MOF alone, and gas molecule.

### 4.3 Results and discussion

Compound IPM-301 was synthesized as a neat single crystalline product in a reaction of CdSO<sub>4</sub>, 1,5-NDS and neutral N-donor linker under solvothermal conditions (Figure 4.2). Single crystal x-ray diffraction studies revealed the compound had space group of P222<sub>1</sub>. One unit of Cd(II) cation, one full ligand, half units of both NDS and SO<sub>4</sub><sup>2-</sup> anions constituted the asymmetric unit of the crystal structure (Appendix 4.1). The coordination geometry of Cd(II) was octahedral with 3 coordination from 3 distinct ligands, one coordination from NDS and two adjacent Cd(II) cations were bridged via sulfate anion (Figure 4.1a, Appendix 4.2). As observed in previous chapters and reported in the literature,<sup>22</sup> the sulfate anions can afford strong coordination bonds and afford stability. Interestingly, we found that the crystal structure of IPM-301 was unique in terms of binding of both sulfate and organosulfonate groups to the same metal node, which has not been previously reported as per Cambridge structural database (CSD) screening approach. The efficacy of using higher dimensional linkers was emphasized in the resulting 3D packing of the structure (Appendix 4.2-4.4).<sup>4c</sup> In addition to the alignment of polar groups in the 1D channel, the compound bears the presence of naphthalene groups facing towards the pore (Figure 4.1a). TOPOS software was used to estimate the topology of the compound, which yielded the formation of a new topology having (4.6<sup>2</sup>)(4<sup>3</sup>.6<sup>6</sup>.8) point symbol. The isostructural MOF viz. IPM-302, having free amine group was also synthesized (Figure 4.2).

Both the compounds were first examined for their basic properties where the powder x-ray diffraction (PXRD) profiles substantiated the bulk-phase purity (Appendix 4.7, 4.25). The gradual loss of guest solvent occupying the free voids was displayed by the thermogravimetric analysis (TGA) profiles (Appendix 4.8, 4.26). Variable temperature PXRD (VT-PXRD) patterns were recorded to confirm the thermal stability of the compounds (Appendix 4.9). The formation of neat crystalline product was further endorsed by the morphological analysis using field emission scanning electron microscopy (FESEM) images (Appendix 4.10, 4.27). The retention of sulfate groups in the bulk phase was further validated by fourier-transform infra-red spectroscopy (FT-IR) spectrum (Appendix 4.11). Routine activation protocol was employed to obtain the guest-free phases and we found the MOFs retained bulk-phase crystallinity, which makes it a rare example of MOFs based on sulfonate-based linker having the feature of permanent porosity. The presence of accessible polar sites propelled us to test the ability of the MOFs for capture of greenhouse gas

CO<sub>2</sub>.<sup>2a,2b,2j</sup> Initially low temperature adsorption behavior of CO<sub>2</sub> (195K) was checked which resulted in an uptake of 106mLg<sup>-1</sup> for IPM-301 (Appendix 4.12). The corresponding low temperature adsorption isotherm for N<sub>2</sub> (77K) did not register noticeable uptake (Appendix 4.15). Encouraged from these observations, CO<sub>2</sub> uptakes were checked at 273K, 298K and 310K where we found substantial uptake at 1 bar (Figure 4.3a, Appendix 4.12, 4.13). Importantly, these values are among the highest registered by MOFs based on sulfonate-ligands.<sup>7d,7h</sup>

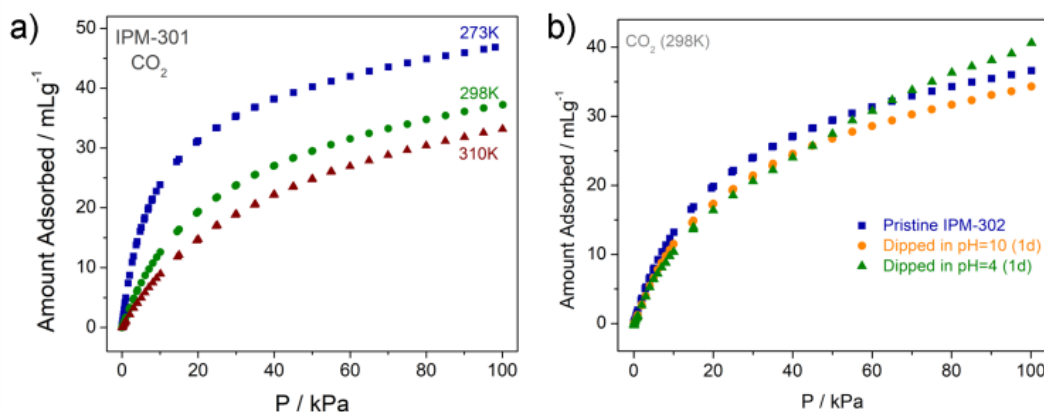


Figure 4.3 a) Temperature dependent CO<sub>2</sub> adsorption isotherms of IPM-301 and; b) CO<sub>2</sub> adsorption isotherms for IPM-302 under different pH conditions.

The variable temperature CO<sub>2</sub> adsorption isotherms were used to estimate the heat of adsorption which was calculated to be 31.1kJmol<sup>-1</sup>, which corroborated with the high affinity of CO<sub>2</sub> (Appendix 4.14). Apart from high uptake, selectivity is of prime importance and hence uptakes for related gas molecules [kinetic diameters: N<sub>2</sub> - 3.64Å and O<sub>2</sub> - 3.46Å] were checked, where we found negligible uptake amounts (Appendix 4.16). The bulk phase purity of the compound was found to be retained even after the adsorption cycles (Appendix 4.17). Ideal adsorbed solution theory (IAST) was employed to estimate the selectivity of adsorption by simulating flue gas composition (CO<sub>2</sub>/N<sub>2</sub> ratio of 15:85 at 1bar and 298K) (Appendix 4.45-4.46). The selectivity under the given parameters was calculated to be 38.2, which is highly competitive with some of the benchmark MOF compounds.<sup>2j</sup> Apart from high uptake capacities, the estimation of selectivity in sulfonate MOFs opens a new frontier as such calculations have not been reported previously. The choice of the building blocks was made with the primary motive of attaining stability. To test this aspect, we dipped crystals of IPM-301 in water and recorded the PXRD patterns and CO<sub>2</sub> isotherms after 7 days. Remarkably, both the bulk phase purity and pore character were found to be retained even after treatment with water for 7 days (Appendix 4.18-4.19). In addition we carried out cycling water adsorption experiments and found no effect on the nature of the isotherm and the uptake capacities (Appendix 4.20).

For a MOF built with higher coordination sphere, such high stability in hydrolytic conditions is not commonly observed. Encouraged from these observations, we further checked the stability of the MOF under varying pH conditions. The bulk phase purity was found to be retained even after dipping the compound at pH=4.01 and pH=10.01 after 1 day and the porosity of the compound was unaltered (Appendix 4.21-4.22). The morphology of the MOF too was unaffected by the treated under different pH conditions (Appendix 4.23-4.24).

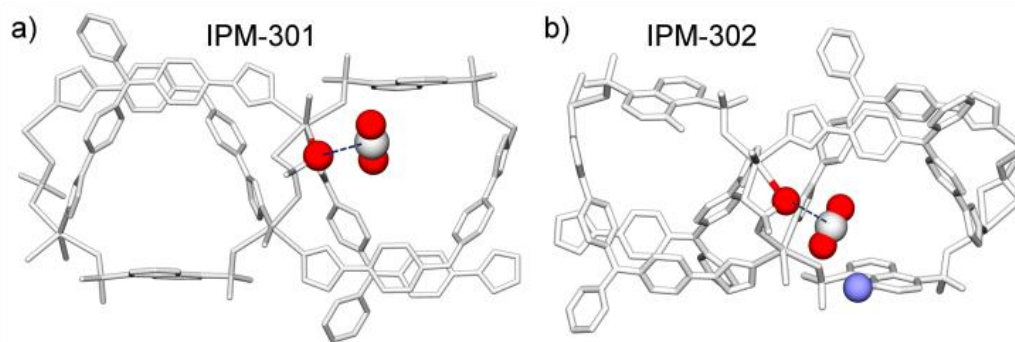


Figure 4.4 DFT optimized locations of CO<sub>2</sub> for a) IPM-301 and b) IPM-302 (the framework is shown in greyscale and the atoms of interest shown in colour. Colour code: O, red; C, dark grey; N, blue).

IPM-302 was tested for its adsorption capacity by similar studies. Alike previous MOF, IPM-302 registered high uptakes for CO<sub>2</sub> at different temperatures (Appendix 4.28-4.29, 4.31-4.32). The heat of adsorption was calculated as 28.7 kJmol<sup>-1</sup> (Appendix 4.30). The selectivity of CO<sub>2</sub> over N<sub>2</sub> as estimated from IAST was found to be 51.7 (Appendix 4.45-4.46). Similar to previous case, IPM-302 presented high stability in water and even over wide pH range (Figure 4.3b, Appendix 4.33-4.37). Comparing the adsorption isotherms, the two MOFs displayed similar adsorption tendencies even though IPM-302 had the presence of pendant amine moiety (Appendix 4.38-4.40). This was necessary as amine groups have been found to provide robust binding sites for CO<sub>2</sub>.<sup>2b,2j</sup> To explain this trend, theoretical calculations based on DFT-D3 were examined to find the binding tendencies in the two compounds for CO<sub>2</sub>. From the DFT measurements at 0K, the binding energies were estimated to be 44 kJ/mol (IPM-301) and 36 kJ/mol (IPM-302) for the two MOFs. Apart from that, we found that in both the cases the preferential interaction site for CO<sub>2</sub> was with the O-atom of the bridging sulfate anion, even though IPM-302 has the presence of pendant amine groups (Figure 4.4).

Owing to the choice of the building blocks, the compounds were found to present additional features. The presence of d<sup>10</sup> metal ion and luminescent linkers led to emissive nature to the compounds (Appendix 4.42). The fluorescence emission spectra suggested that the emissive character of the MOFs was directly linked to the emissive nature of the linkers (Appendix 4.41). Among the different strategies proposed for MOFs

to function as selective probes, presence of secondary recognition sites has been identified as an efficient approach.<sup>2g</sup> Detection of neurotransmitters by artificial probes has emerged as an important research interest owing to the necessity for understanding the mechanism of such molecules in biological systems.<sup>2g,24</sup> In the domain of MOFs, sensing of nitric oxide (NO) has recently emerged and in the limited reports, the MOFs have been based carboxylate based linkers.<sup>13</sup> Thus there is sufficient scope and premise for evaluating sensory functions of MOFs based on other kinds of ligands. IPM-302 which has a pendant amine group was tested for the detection of nitric oxide, on the basis of knowledge gained from previous reports of deamination reaction.<sup>24b</sup> Upon treatment with nitric oxide, there was decrement in the peak corresponding to the amine linker and this response was found to be selective (Figure 4.5a, Appendix 4.43). The bulk-phase crystallinity was found to be retained even after the NO treatment (Appendix 4.44). The sensory features provide a new platform for development of luminescent MOFs.

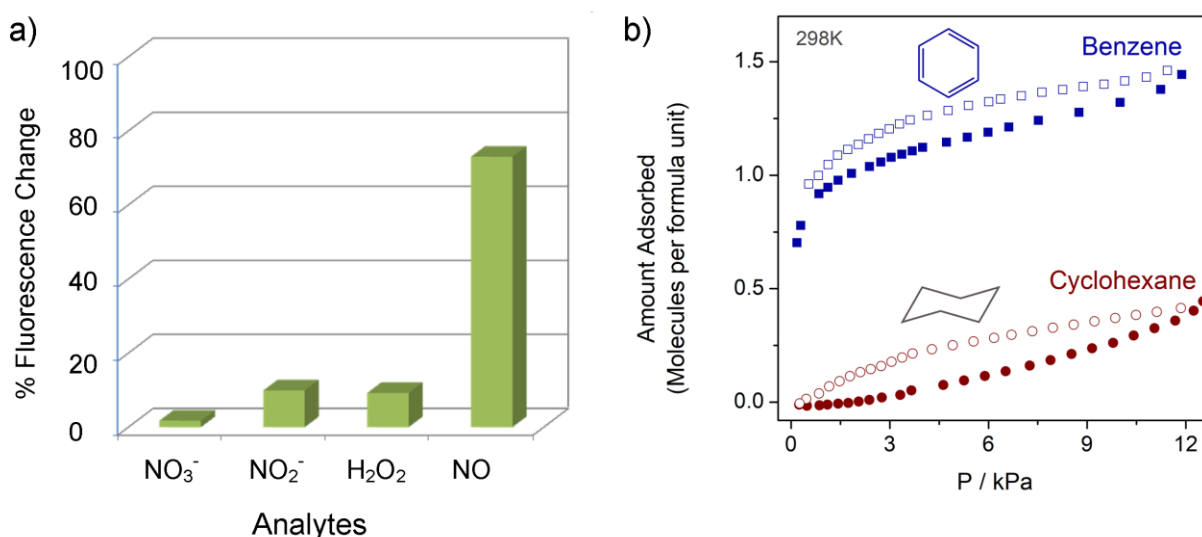


Figure 4.5 a) Change in fluorescence spectra upon addition of nitric oxide to IPM-302 relative to competing reactive species; b) adsorption isotherms of benzene and cyclohexane at 298K for IPM-301 (open and closed symbols represent adsorption and desorption respectively).

Apart from sensing, the presence of naphthalene groups and 1D porous channel was tapped for the adsorptive separation of  $\text{C}_6$ -liquid hydrocarbons viz. benzene and cyclohexane, which is an important industrial challenge.<sup>2f</sup> Room temperature single-component adsorption isotherms were recorded which presented clear uptake for benzene (around 1.5 molecules per NDS unit), whereas negligible adsorption for

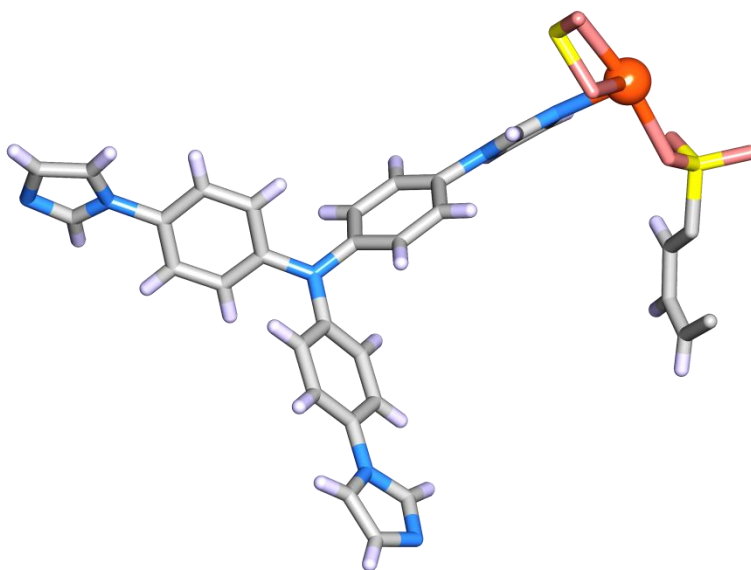
cyclohexane (Figure 4.5b). This selectivity could be ascribed to the possibility of strong  $\pi$ - $\pi$  interactions with the framework backbone of IPM-301.<sup>2f</sup> This happens to be the first example where a sulfonate based MOF has been sought for the function of benzene-cyclohexane separation.

#### **4.4 Conclusions**

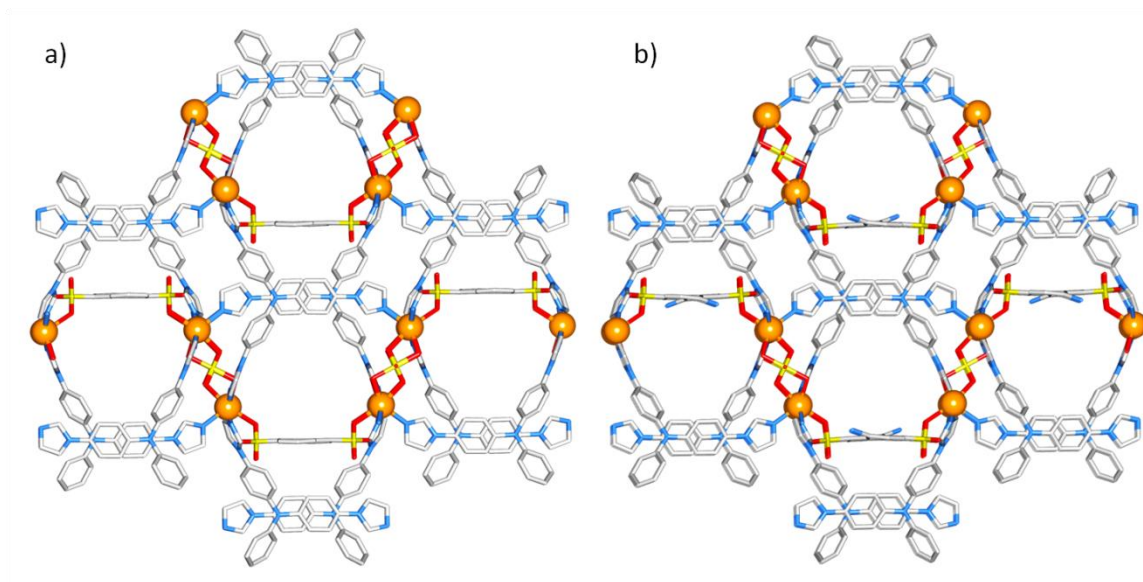
In conclusion, an unusual pair of isostructural MOFs based on sulfonate-based linkers has been synthesized which has a permanent porous character and exhibits multifunctional behavior. The compounds present high hydrolytic stability and resistance over wide pH range. The structures represent a new topology and the binding modes are unprecedented in the domain of coordination polymers. The MOF bearing pendant amine groups is found to be a selective sensory probe for neurotransmitter gas nitric oxide. IPM-301 functions as an efficient adsorbent for the separation of C<sub>6</sub>-cyclic liquid hydrocarbons which is an important industrial challenge. The results provide a new pathway for developing multifunctional MOFs and open up new frontiers for the development of sulfonate-based MOFs having the possibility of reticular chemistry alike carboxylate-based counterparts.



#### 4.5 Appendix Section

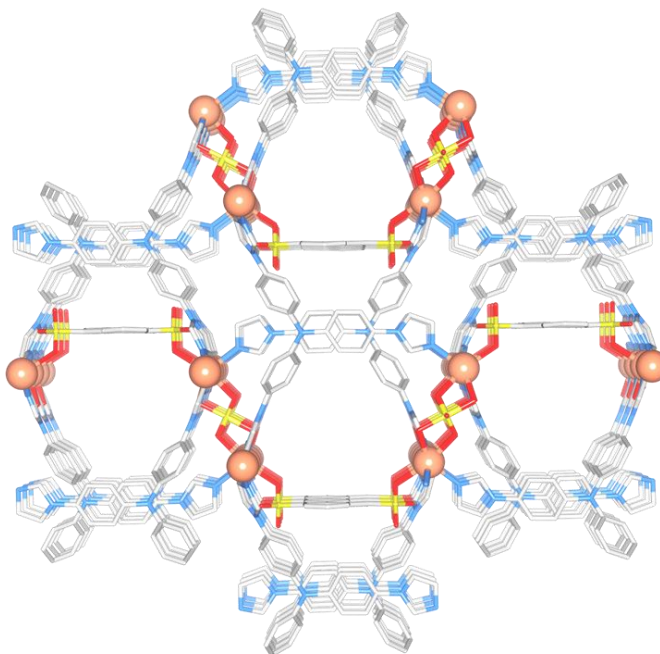


**Appendix 4.1:** Asymmetric unit of **IPM-301**. (Colour code: C, grey; N, blue; Cd, orange; S, yellow; O, pale red; H, pale violet)

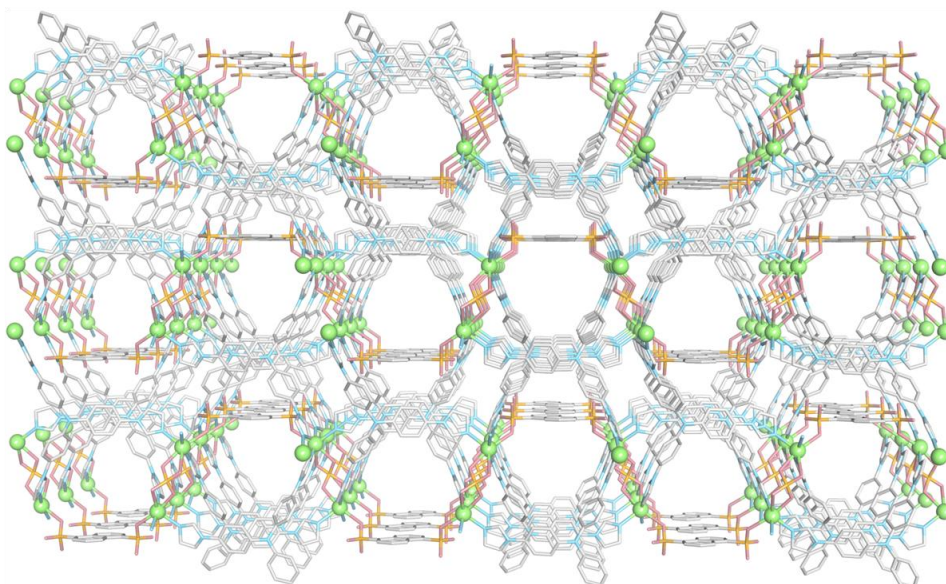


**Appendix 4.2:** Figure showing packing of a) **IPM-301** & b) **IPM-302** along crystallographic *c*-axis, (Hydrogen atoms have been omitted for clarity, colour: Gray - C, Blue - N, Orange - Cd, Yellow - S, Red - O).

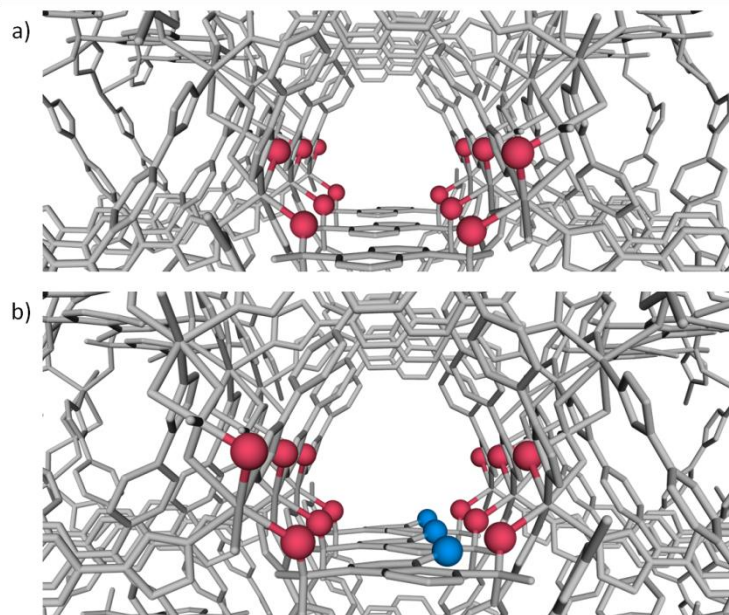




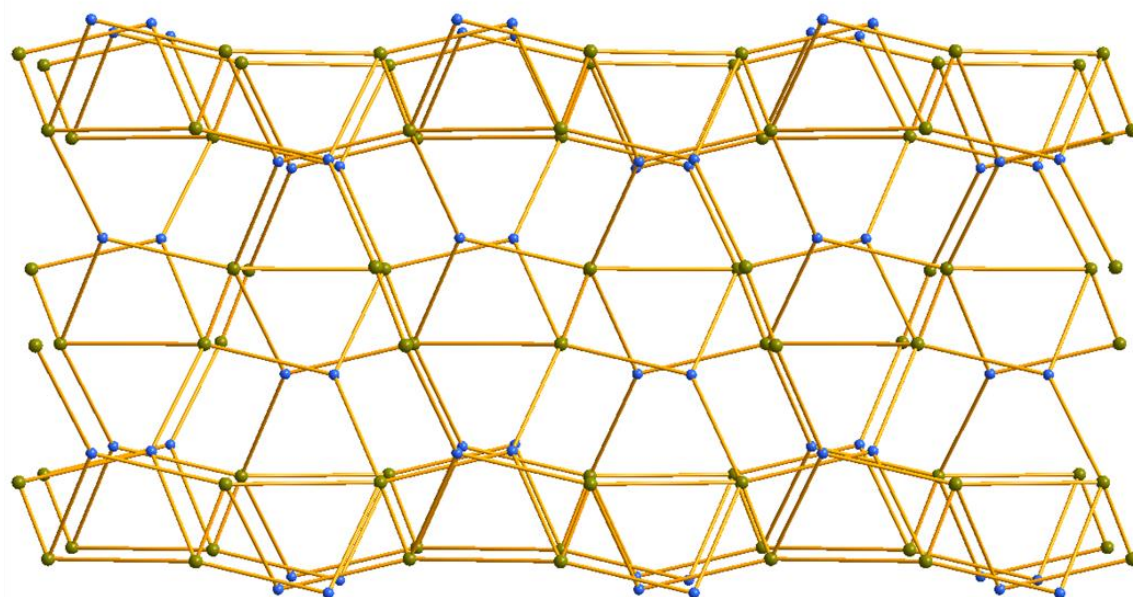
**Appendix 4.3:** Perspective view of **IPM-301** showing porous channel. (Hydrogen atoms have been omitted for clarity, colour: Gray - C, Blue - N, Orange - Cd, Yellow - S, Red - O).



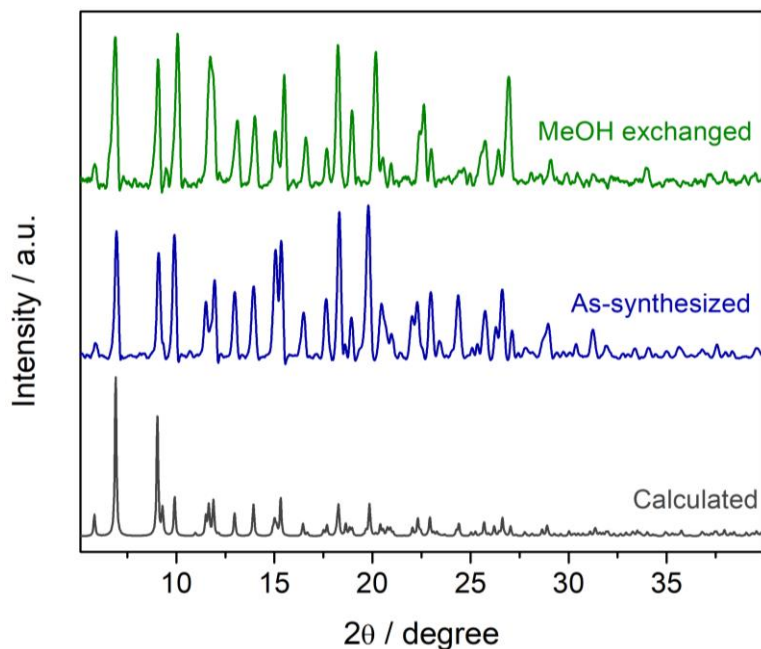
**Appendix 4.4:** Packing diagram of **IPM-301** showing porous channel. (Hydrogen atoms have been omitted for clarity, colour: Gray - C, Blue - N, Green - Cd, Yellow - S, Red - O).



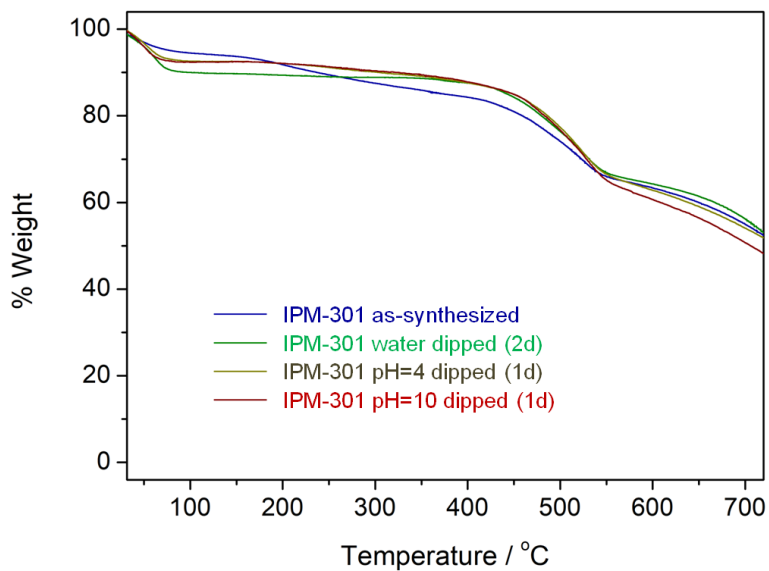
**Appendix 4.5:** Perspective view of the packing showing 1D porous channel in a) **IPM-301** and b) **IPM-302**. (H-atoms have been omitted for clarity, colour: Light Gray - framework, Red - O atoms lining the pore, Blue - N atoms lining the pore).



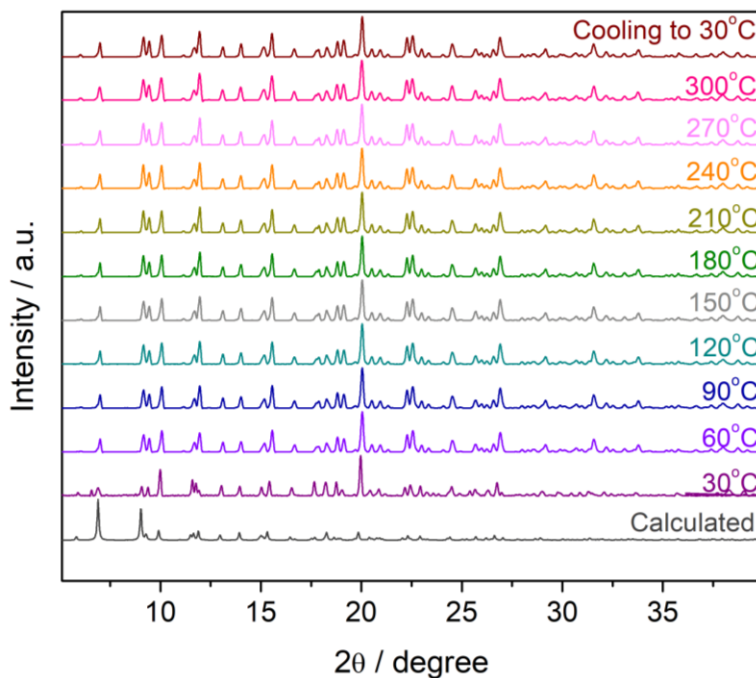
**Appendix 4.6:** Simplified topological representation of **IPM-301**.



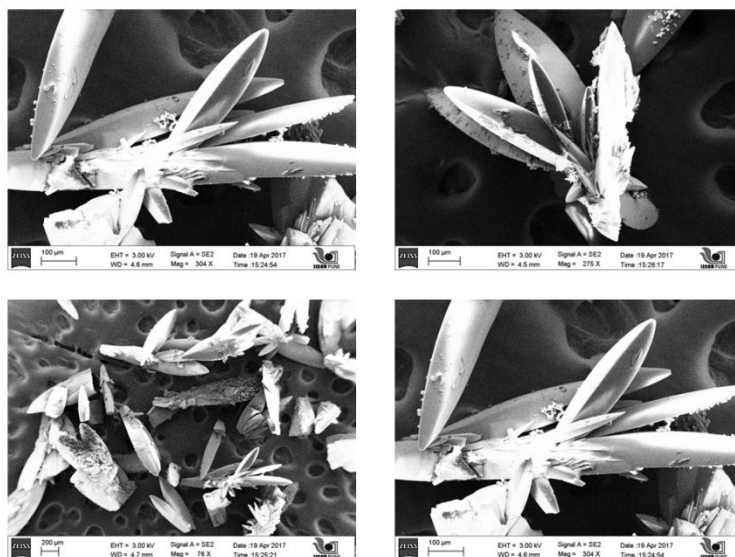
**Appendix 4.7:** Powder X-ray diffraction patterns of **IPM-301** - calculated (gray), as-synthesized (blue), MeOH exchange (green).



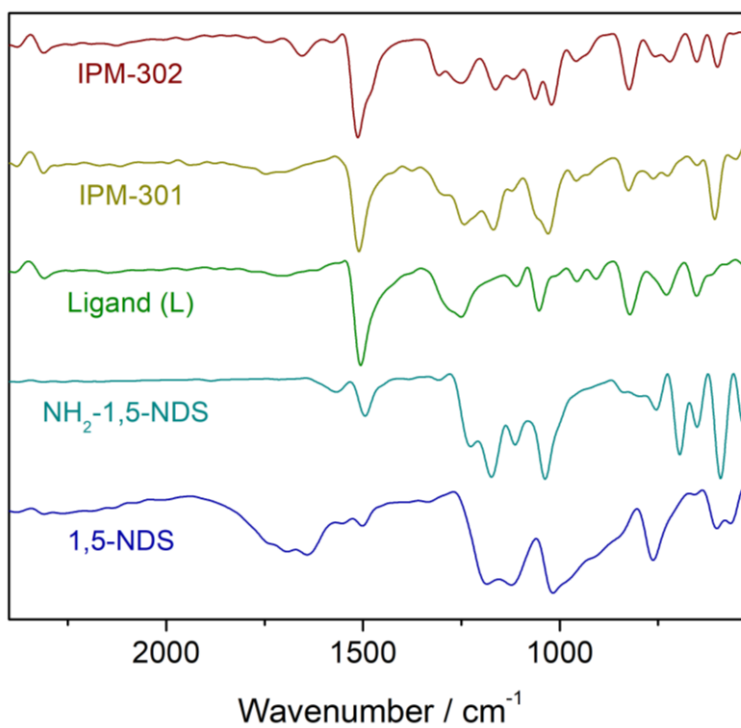
**Appendix 4.8:** TGA profiles for compound **IPM-301**.



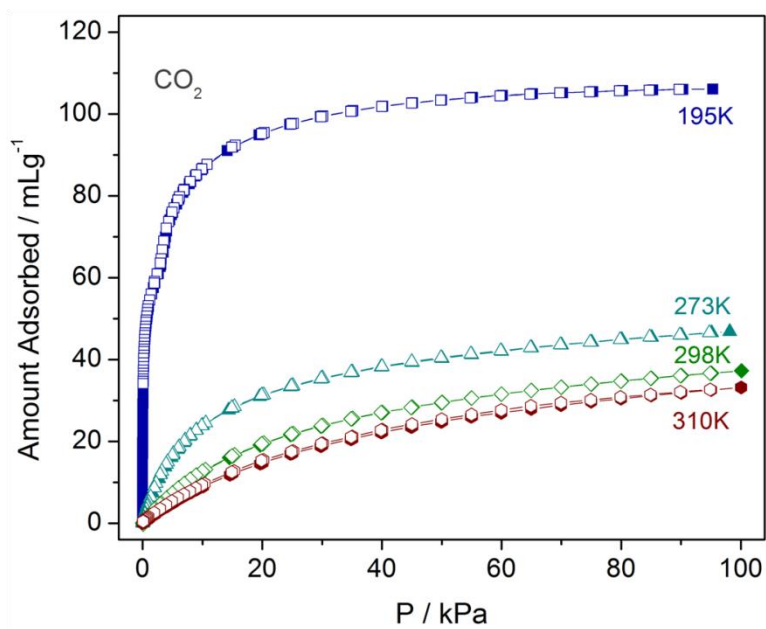
**Appendix 4.9:** Variable temperature PXRD profiles for compound **IPM-301**.



**Appendix 4.10:** FESEM images for compound **IPM-301**. The images were recorded for the solid samples on carbon tape.

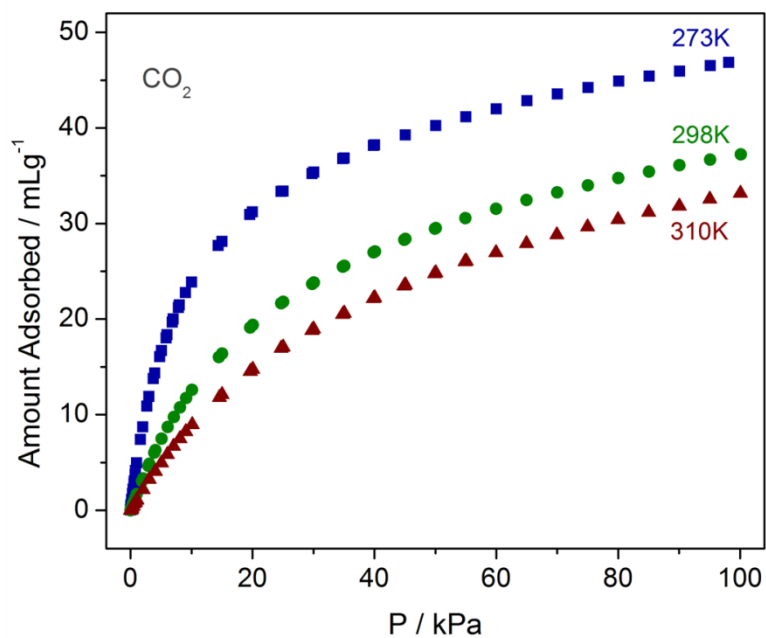


**Appendix 4.11:** FT-IR spectra for the precursors and compounds **IPM-301**, **IPM-302**.

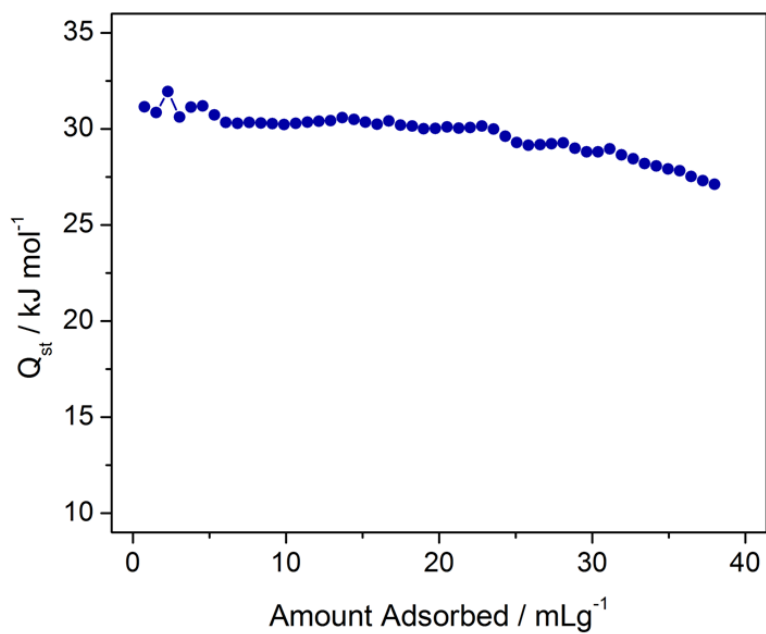


**Appendix 4.12:** CO<sub>2</sub> adsorption isotherms for **IPM-301**. Closed and open symbols denote adsorption and desorption respectively.

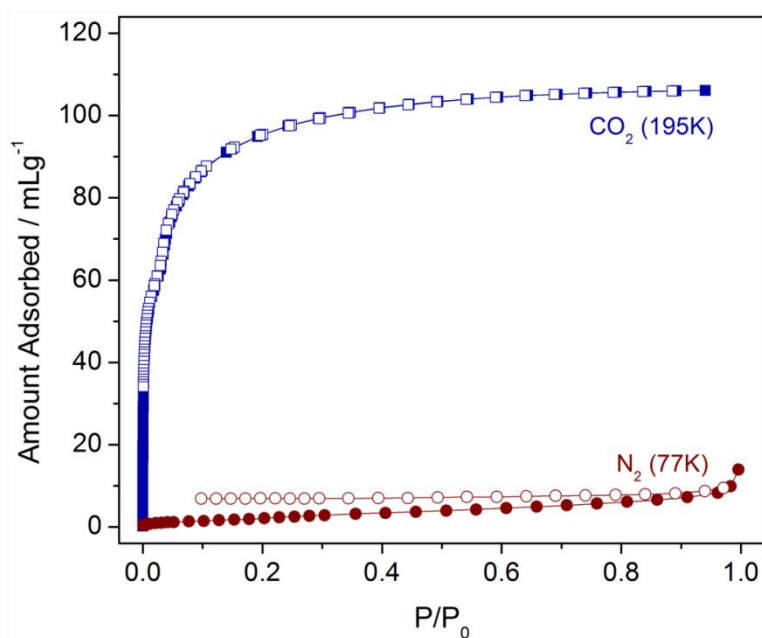




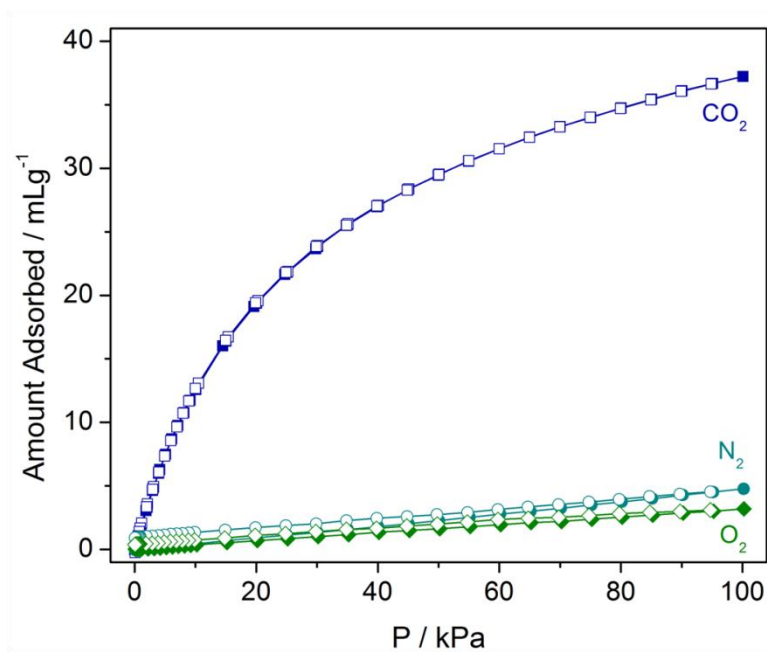
**Appendix 4.13:** Comparative plots of CO<sub>2</sub> adsorption isotherms for **IPM-301** at 273K (blue), 298K (green) and 310K (wine red).



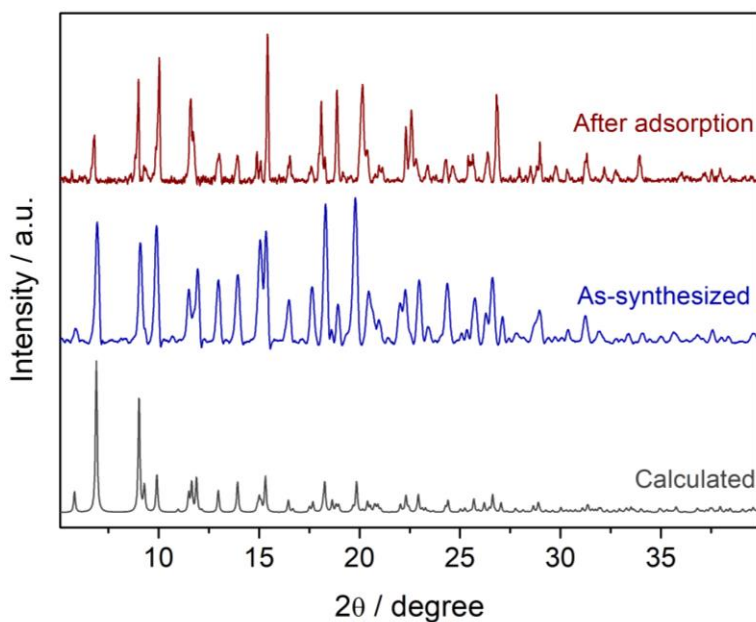
**Appendix 4.14:** Isosteric heat of adsorption ( $Q_{st}$ ) plot for compound **IPM-301**, obtained from data recorded at 273K and 298K.



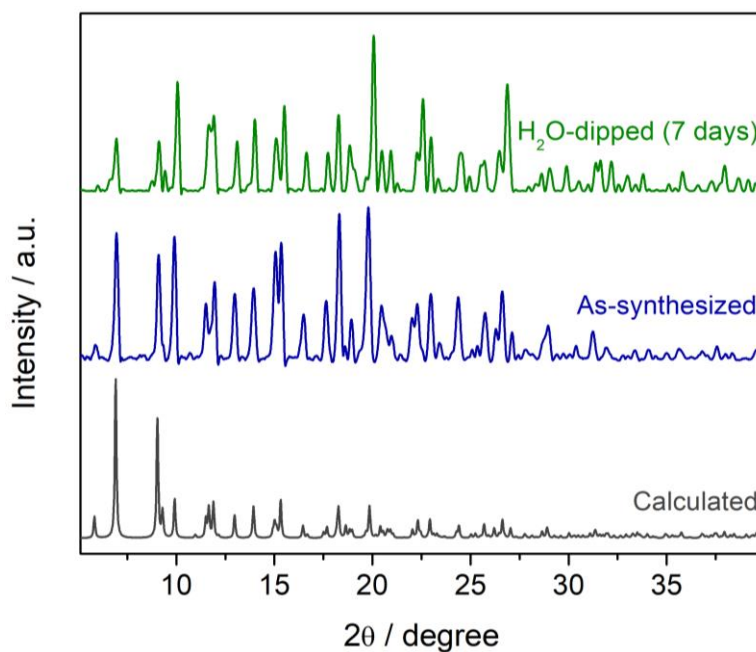
**Appendix 4.15:** Low temperature gas adsorption isotherms for **IPM-301**. Closed and open symbols denote adsorption and desorption respectively.



**Appendix 4.16:** Gas adsorption isotherms at 298K for **IPM-301**. Closed and open symbols denote adsorption and desorption respectively.

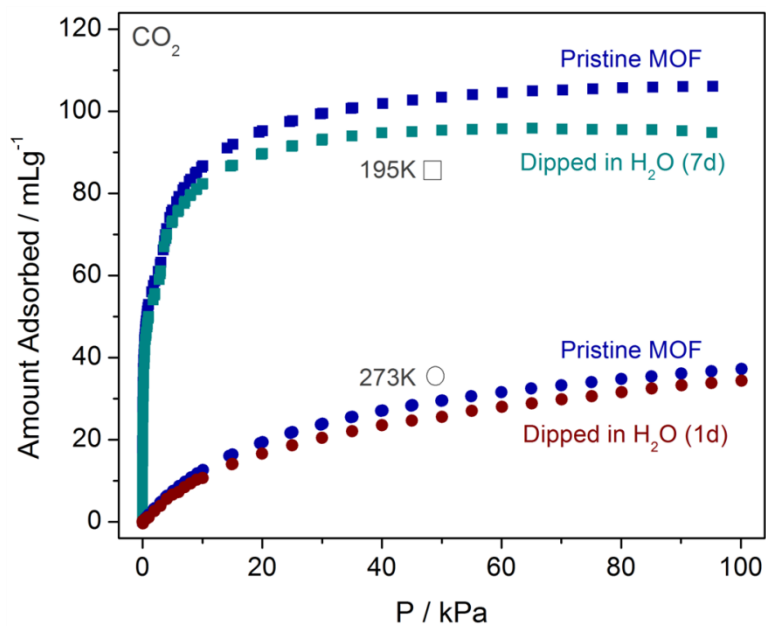


**Appendix 4.17:** Powder x-ray diffraction patterns for **IPM-301** recovered after adsorption measurements (wine red), relative to the calculated (grey) and as-synthesized (blue).

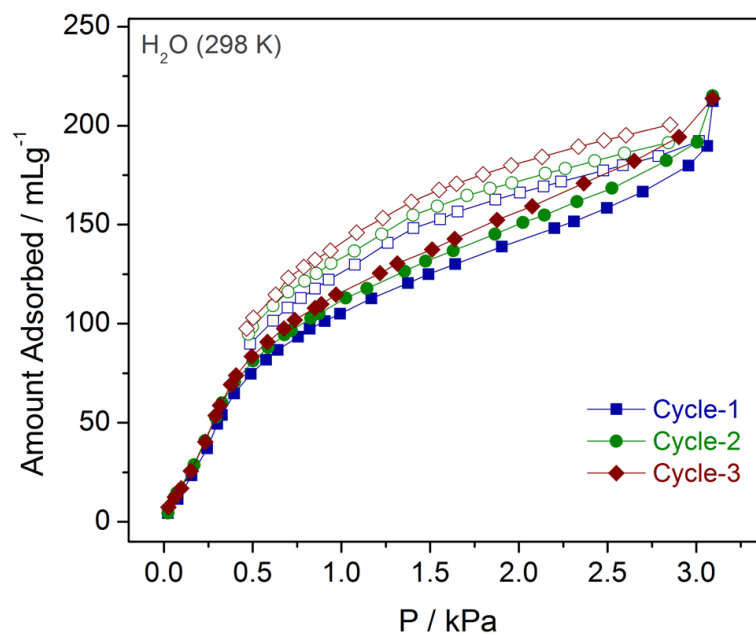


**Appendix 4.18:** Powder X-ray diffraction patterns of **IPM-301** - calculated (grey), as-synthesized (blue), water dipped phase (green).

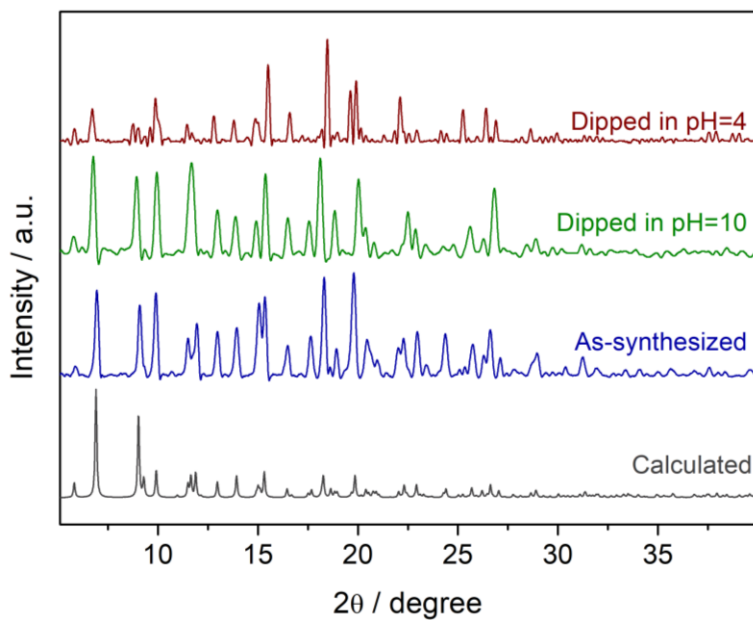




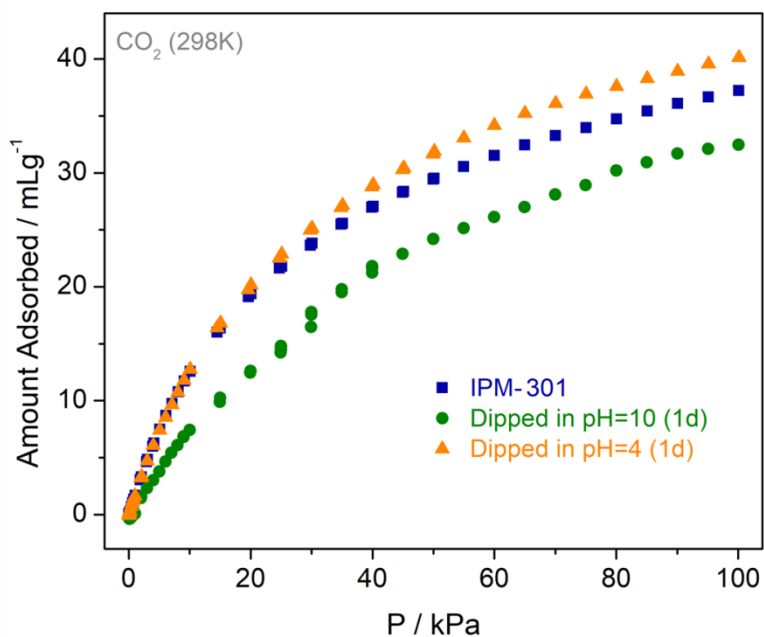
**Appendix 4.19:** CO<sub>2</sub> adsorption isotherms for **IPM-301**.



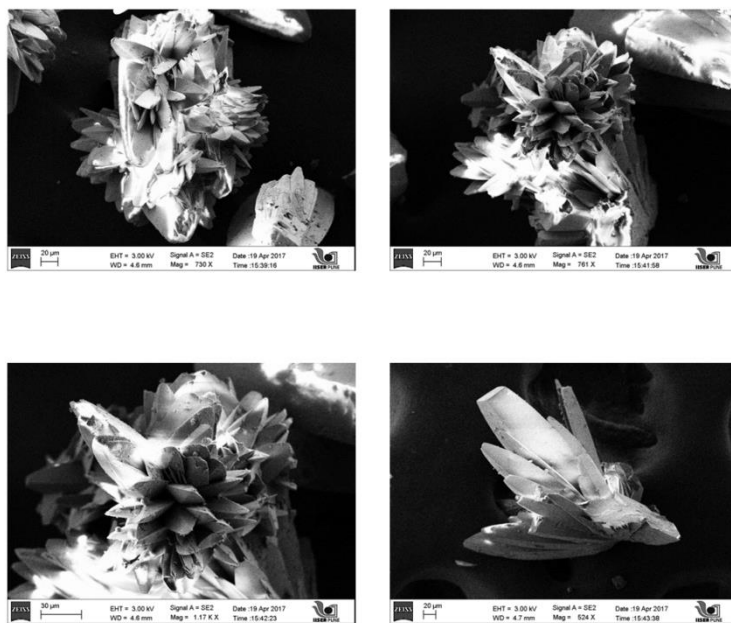
**Appendix 4.20:** Water adsorption isotherm over 3 cycles of adsorption-desorption for **IPM-301**. Closed and open symbols denote adsorption and desorption respectively.



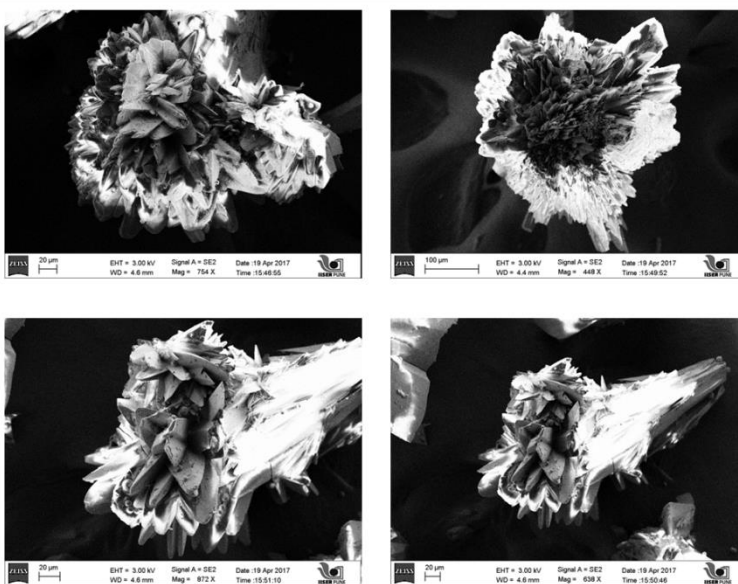
**Appendix 4.21:** Powder X-ray diffraction patterns of **IPM-301** - calculated (gray), as-synthesized (blue), pH=10 dipped phase (green) and pH=4 dipped phase (wine red).



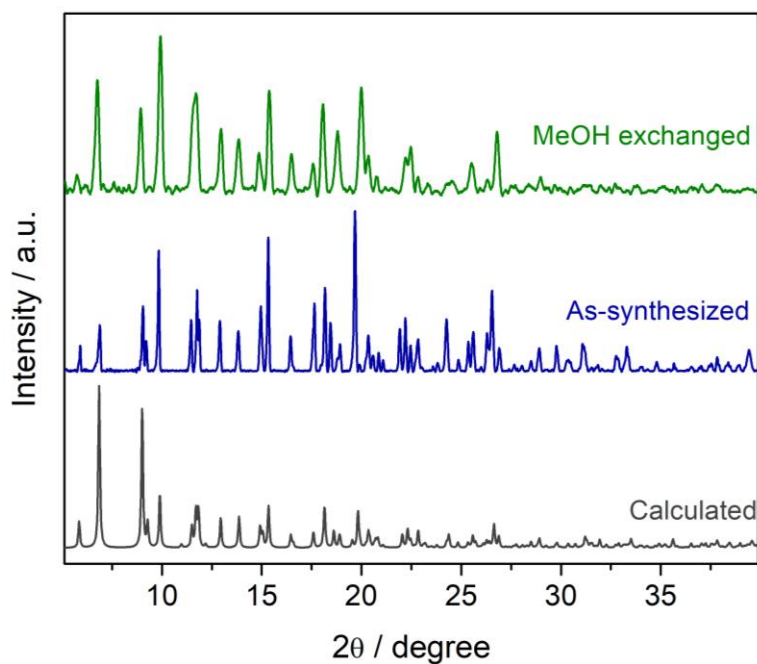
**Appendix 4.22:** CO<sub>2</sub> adsorption isotherms for different pH dipped phases of **IPM-301**.



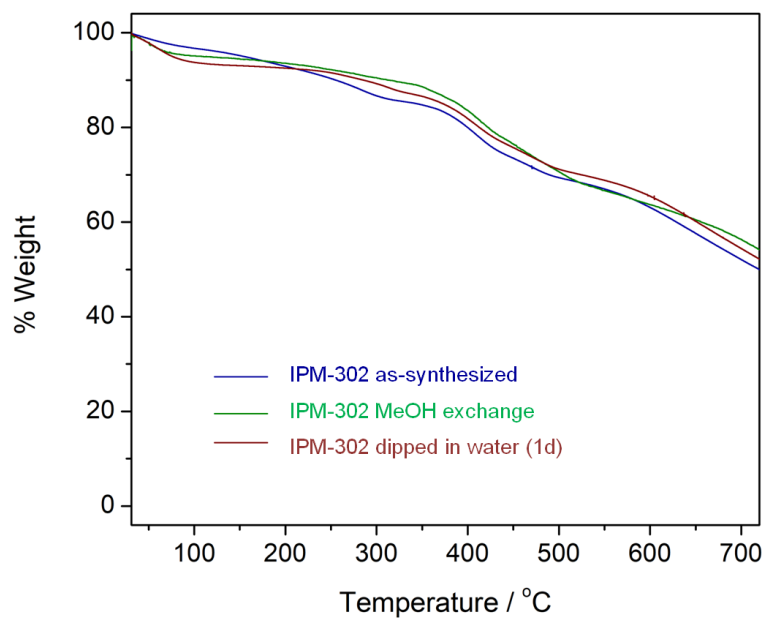
**Appendix 4.23:** FESEM images for pH=10 dipped phase of **IPM-301**.



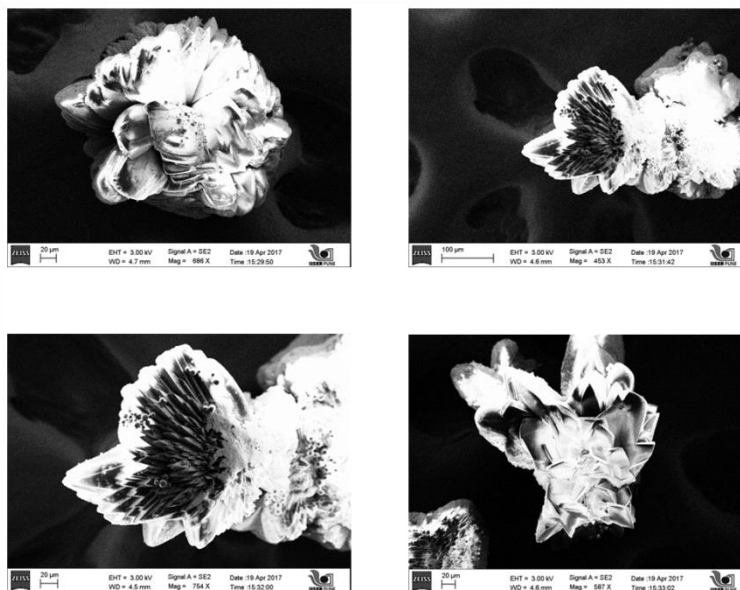
**Appendix 4.24:** FESEM images for pH=4 dipped phase of **IPM-301**.



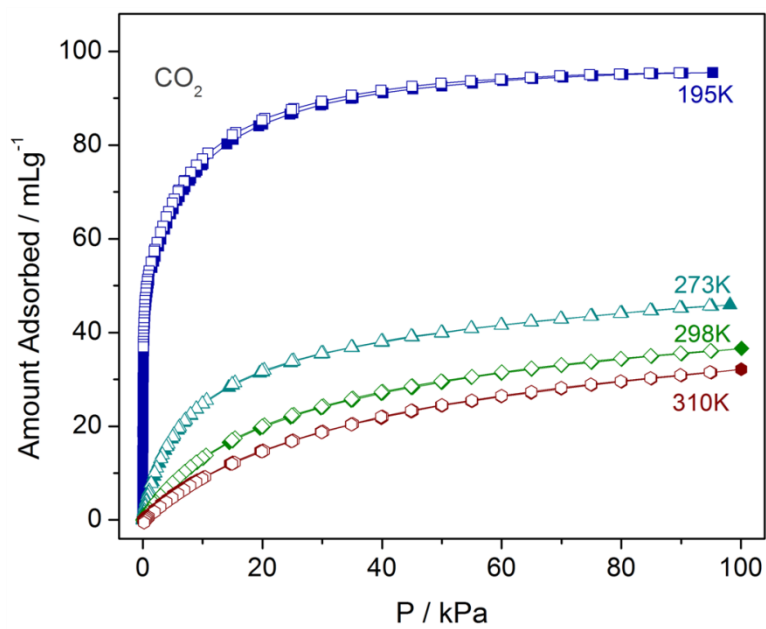
**Appendix 4.25:** Powder X-ray diffraction patterns of **IPM-302** - calculated (gray), as-synthesized (blue), MeOH exchange (green).



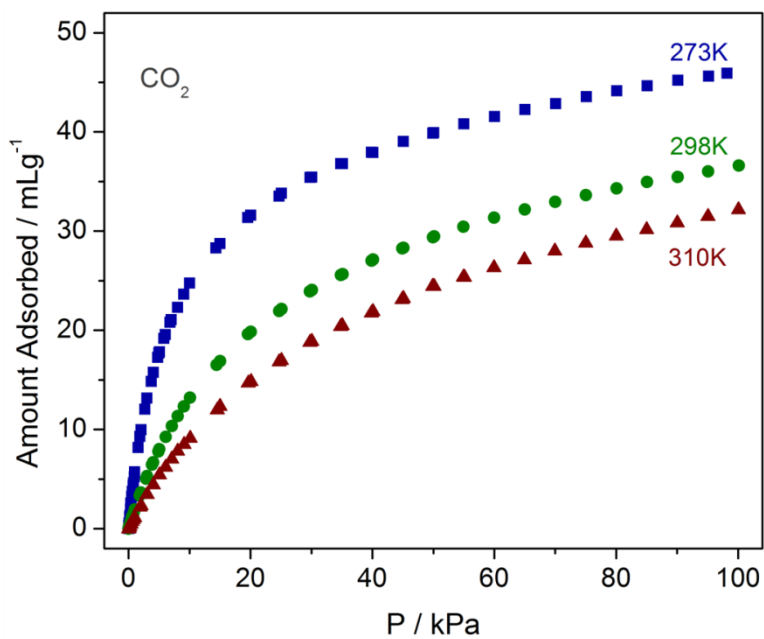
**Appendix 4.26:** TGA profiles for compound **IPM-302**.



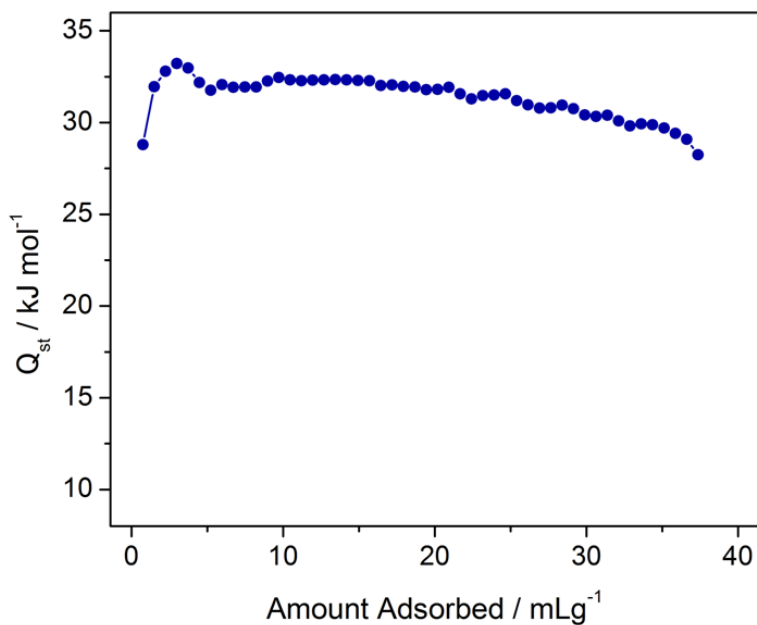
**Appendix 4.27:** FESEM images for compound **IPM-302**.



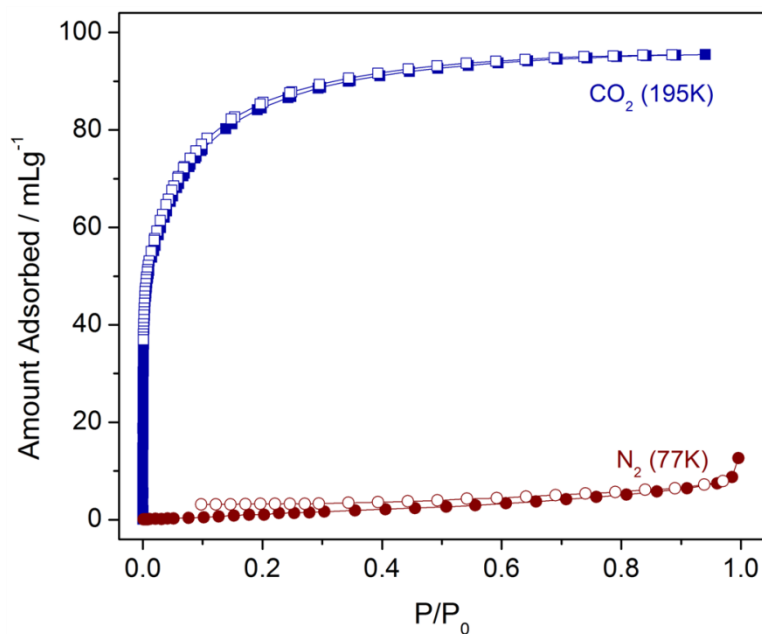
**Appendix 4.28:** CO<sub>2</sub> adsorption isotherms for **IPM-302**. Closed and open symbols denote adsorption and desorption respectively.



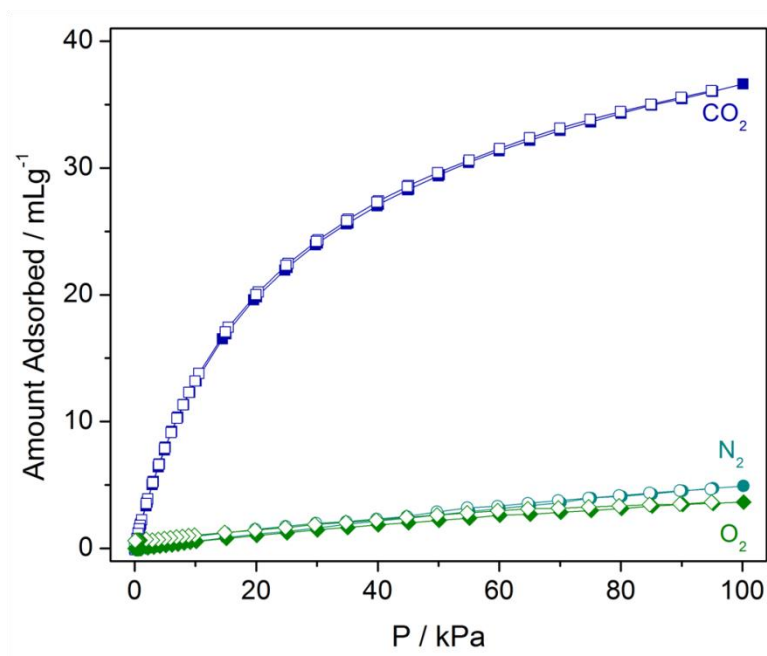
**Appendix 4.29:** Comparative plots of CO<sub>2</sub> adsorption isotherms for **IPM-302** at 273K (blue), 298K (green) and 310K (wine red).



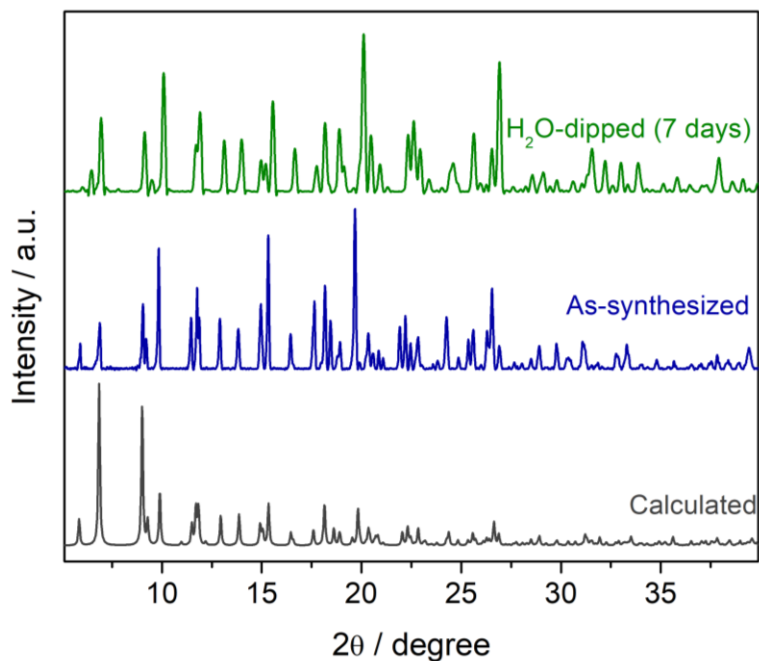
**Appendix 4.30:** Isosteric heat of adsorption (Q<sub>st</sub>) plot for compound **IPM-302**, obtained from data recorded at 273K and 298K.



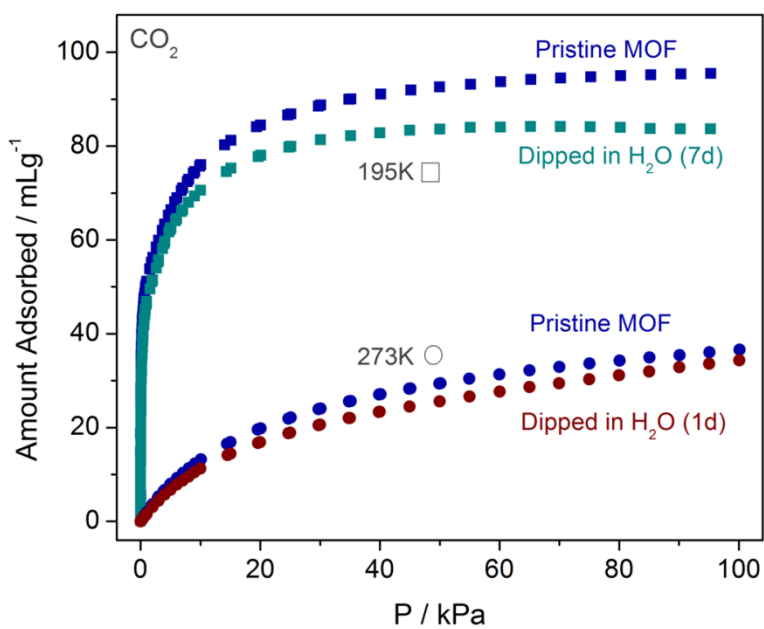
**Appendix 4.31:** Low temperature gas adsorption isotherms for **IPM-302**. Closed and open symbols denote adsorption and desorption respectively.



**Appendix 4.32:** Gas adsorption isotherms at 298K for **IPM-302**. Closed and open symbols denote adsorption and desorption respectively.

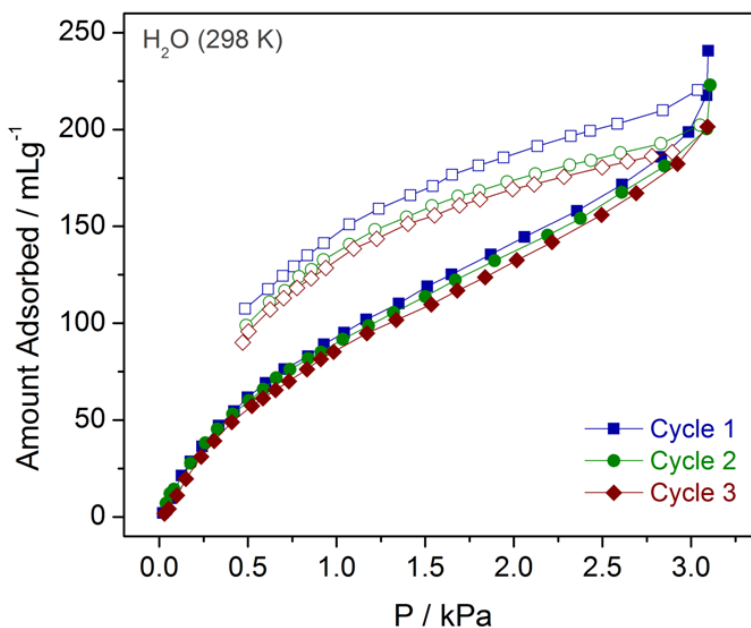


**Appendix 4.33:** Powder X-ray diffraction patterns of **IPM-302** - calculated (gray), as-synthesized (blue), water dipped phase (green).

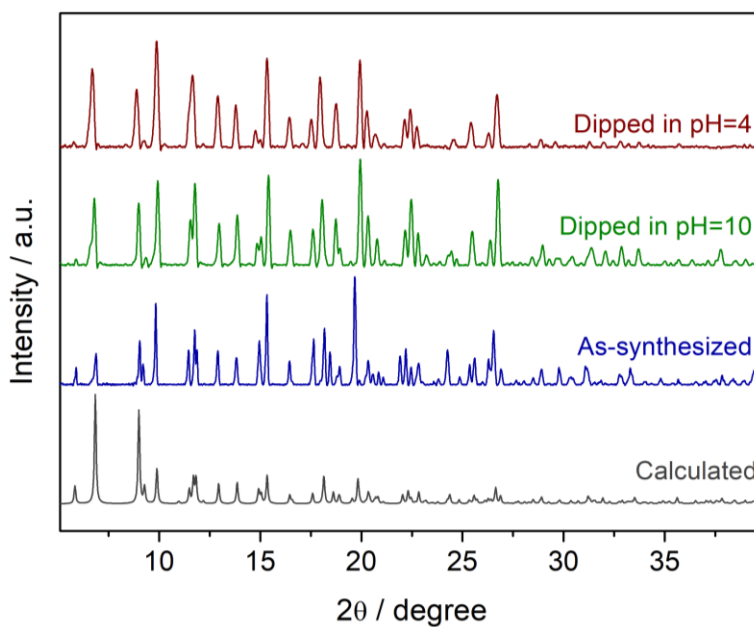


**Appendix 4.34:** CO<sub>2</sub> adsorption isotherms for **IPM-302**.

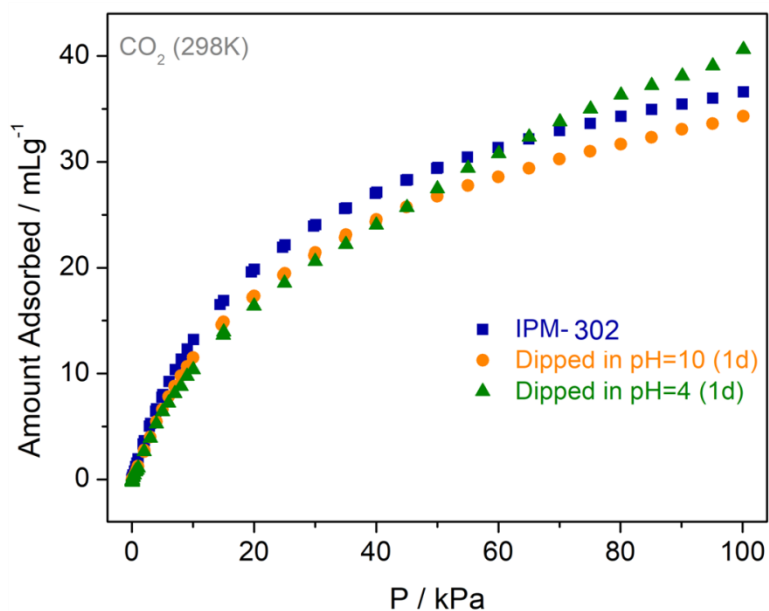




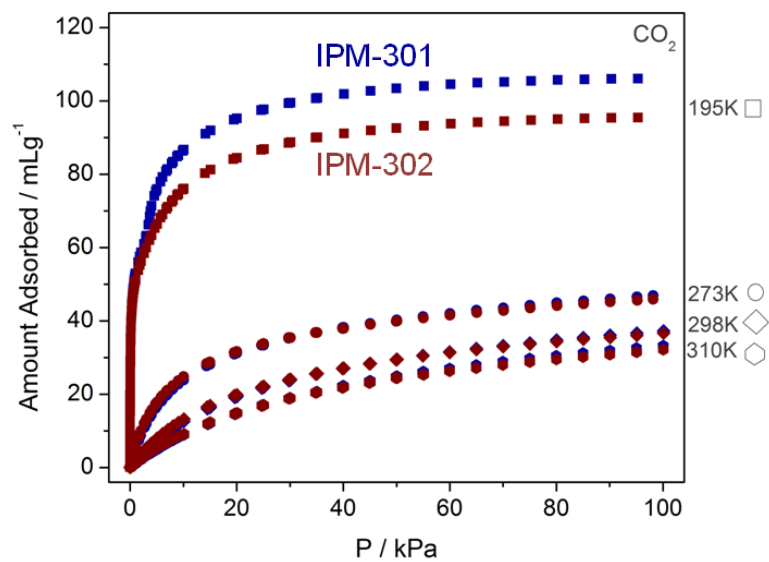
**Appendix 4.35:** Water adsorption isotherm over 3 cycles of adsorption-desorption for **IPM-302**. Closed and open symbols denote adsorption and desorption respectively.



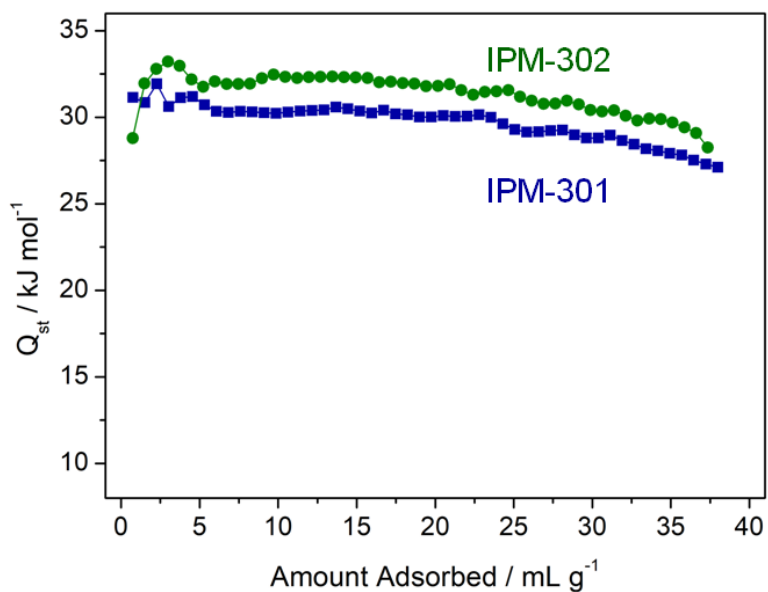
**Appendix 4.36:** Powder X-ray diffraction patterns of **IPM-302** - calculated (gray), as-synthesized (blue), pH=10 dipped phase (green) and pH=4 dipped phase (wine red).



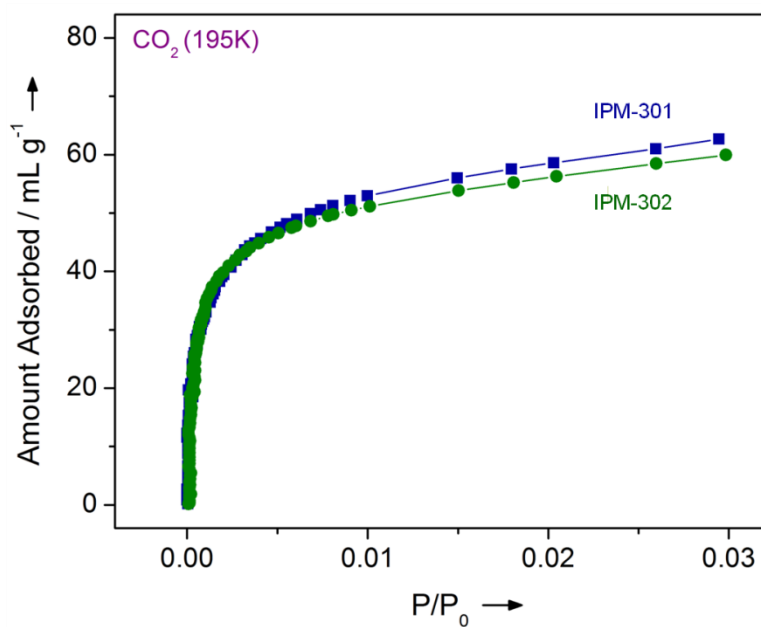
**Appendix 4.37:** CO<sub>2</sub> adsorption isotherms for different pH dipped phases of **IPM-302**.



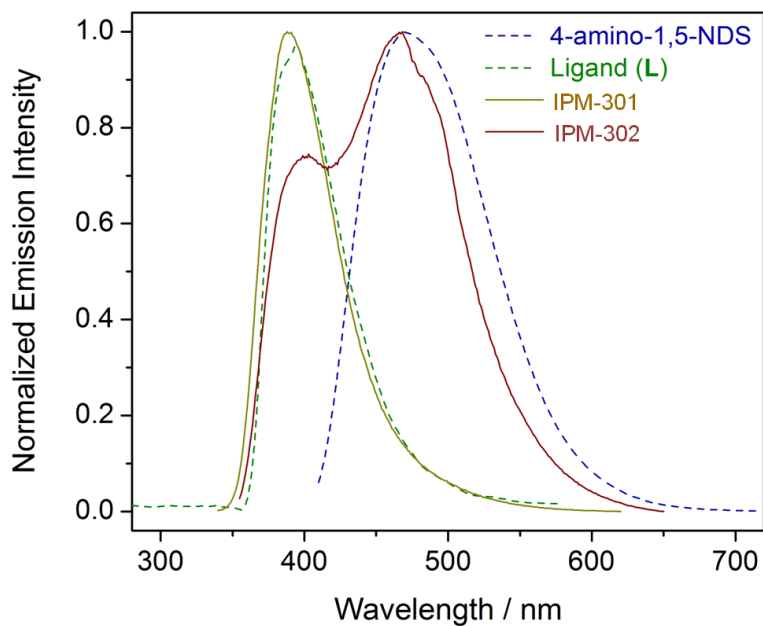
**Appendix 4.38:** Comparative CO<sub>2</sub> adsorption isotherms for **IPM-301** (blue) and **IPM-302** (wine red).



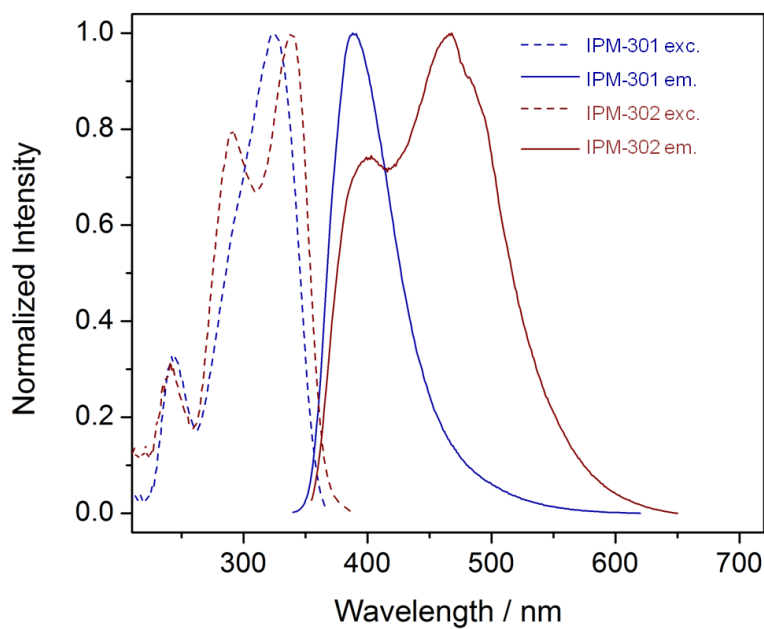
**Appendix 4.39:** Comparative isosteric heat of adsorption plots for **IPM-301** (blue) and **IPM-302** (green), calculated from  $\text{CO}_2$  adsorption isotherms at 273K and 298K.



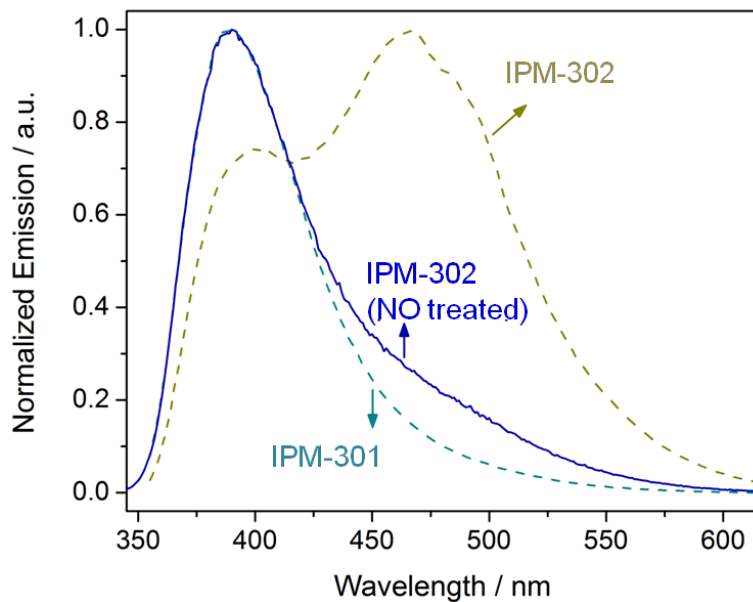
**Appendix 4.40:** Comparative  $\text{CO}_2$  adsorption isotherms at low pressure for **IPM-301** (blue) and **IPM-302** (green).



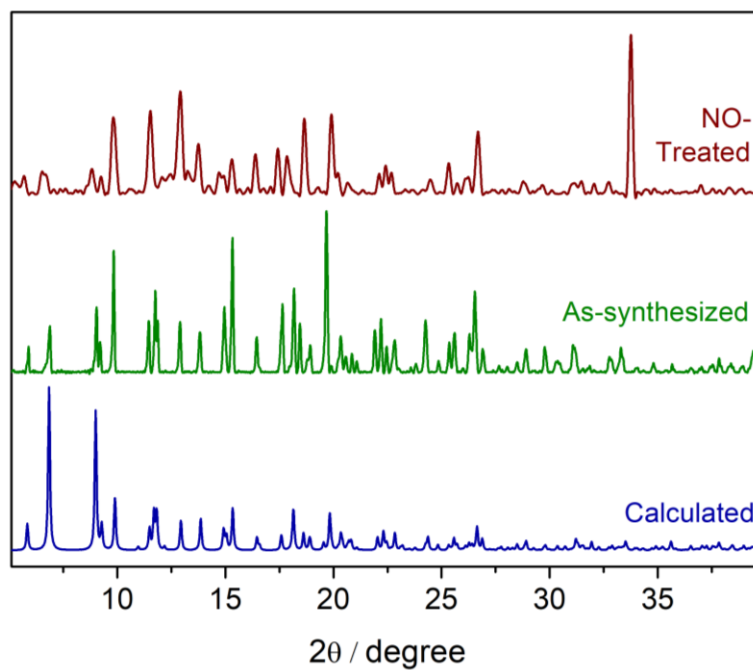
**Appendix 4.41:** Fluorescence emission spectra recorded in MeOH:H<sub>2</sub>O (1:1) solvent system.



**Appendix 4.42:** Excitation and emission spectra recorded for IPM-301 and IPM-302. (For emission spectra,  $\lambda_{\text{exc}}$ =325nm and 340nm respectively; for excitation spectra,  $\lambda_{\text{em}}$  = 390nm and 405nm respectively).



**Appendix 4.43:** Emission spectra recorded for IPM-302 after treatment with nitric oxide (NO). Emission spectrum of IPM-301 is shown (dotted blue line) for comparison.



**Appendix 4.44:** Powder x-ray diffraction (PXRD) pattern for IPM-302 after treatment with nitric oxide (NO).

**Appendix Table 4.1:** Content of Cd (in ppm) in the supernatant solution (for water stability test) recorded using ICP-AES.

<b>Phase</b>	<b>Cd(ppm)</b>
IPM-301	1.015
IPM-302	0.866

**Appendix Table 4.2** Crystal data and structure refinement for **IPM-301**.

Identification code	IPM-301 (CCDC 1831060)	
Empirical formula	$C_{64} H_{48} Cd_2 N_{14} O_{10} S_3$	
Formula weight	1494.14	
Temperature	150(2) K	
Wavelength	0.71073 Å	
Crystal system	Orthorhombic	
Space group	$P 2 2 2_1$	
Unit cell dimensions	$a = 9.513(5) \text{ \AA}$	$\alpha = 90^\circ$
	$b = 15.181(8) \text{ \AA}$	$\beta = 90^\circ$
	$c = 25.601(14) \text{ \AA}$	$\gamma = 90^\circ$
Volume	$3697(3) \text{ \AA}^3$	
Z	2	
Density (calculated)	1.342 Mg/m <sup>3</sup>	
Absorption coefficient	0.721 mm <sup>-1</sup>	
F(000)	1508	
Crystal size	0.180 x 0.160 x 0.140 mm <sup>3</sup>	
Theta range for data collection	2.284 to 26.000°.	
Index ranges	-11 ≤ h ≤ 11, -18 ≤ k ≤ 18, -31 ≤ l ≤ 31	
Reflections collected	50483	
Independent reflections	7292 [R(int) = 0.1308]	
Completeness to theta = 25.242°	99.9 %	
Absorption correction	Semi-empirical from equivalents	
Max. and min. transmission	0.904 and 0.878	
Refinement method	Full-matrix least-squares on F <sup>2</sup>	
Data / restraints / parameters	7292 / 6 / 425	
Goodness-of-fit on F <sup>2</sup>	1.136	
Final R indices [I > 2σ(I)]	$R_I = 0.0717$ , $wR_2 = 0.1659$	
R indices (all data)	$R_I = 0.1129$ , $wR_2 = 0.1841$	
Absolute structure parameter	0.023(16)	
Largest diff. peak and hole	1.263 and -1.558 e.Å <sup>-3</sup>	

**Appendix Table 4.3** Crystal data and structure refinement for **IPM-302**.

Identification code	IPM-302 (CCDC 1831061)	
Empirical formula	$C_{64} H_{46} Cd_2 N_{15} O_{10} S_3$	
Formula weight	1506.14	
Temperature	150(2) K	
Wavelength	0.71073 Å	
Crystal system	Orthorhombic	
Space group	$P 2 2 2_1$	
Unit cell dimensions	$a = 9.5251(6) \text{ \AA}$	$\alpha = 90^\circ$
	$b = 15.1178(8) \text{ \AA}$	$\beta = 90^\circ$
	$c = 25.8099(14) \text{ \AA}$	$\gamma = 90^\circ$
Volume	$3716.6(4) \text{ \AA}^3$	
Z	2	
Density (calculated)	1.346 Mg/m <sup>3</sup>	
Absorption coefficient	0.718 mm <sup>-1</sup>	
F(000)	1518	
Crystal size	0.180 x 0.150 x 0.110 mm <sup>3</sup>	
Theta range for data collection	2.279 to 28.370°.	
Index ranges	-12 ≤ h ≤ 12, -19 ≤ k ≤ 20, -34 ≤ l ≤ 33	
Reflections collected	70970	
Independent reflections	9286 [R(int) = 0.0792]	
Completeness to theta = 25.242°	99.9 %	
Absorption correction	Semi-empirical from equivalents	
Max. and min. transmission	0.924 and 0.879	
Refinement method	Full-matrix least-squares on F <sup>2</sup>	
Data / restraints / parameters	9286 / 16 / 434	
Goodness-of-fit on F <sup>2</sup>	0.854	
Final R indices [I > 2σ(I)]	$R_1 = 0.0550$ , $wR_2 = 0.1416$	
R indices (all data)	$R_1 = 0.0789$ , $wR_2 = 0.1588$	
Absolute structure parameter	0.000(9)	
Largest diff. peak and hole	2.416 and -1.803 e.Å <sup>-3</sup>	



**Appendix Table 4.4: Topology Analysis for IPM-301**

Structure consists of molecules (ZD1). The composition of molecule is N

Structure consists of molecules (ZE1). The composition of molecule is Cd

Topology for ZD1

-----

Atom ZD1 links by bridge ligands and has

Common vertex with	R(A-A)				f	Total SA
ZE 1 0.7118 0.6783 0.4593 (0 0 0)	9.597A	1	33.51			
ZE 1 -0.2882 -0.3217 0.4593 (-1-1 0)	9.611A	1	33.35			
ZE 1 0.2882 0.3217 -0.0407 (1 1-1)	9.616A	1	33.14			

Topology for ZE1

-----

Atom ZE1 links by bridge ligands and has

Common vertex with	R(A-A)				f	Total SA
ZE 1 0.7118 0.3217 0.5407 (0 1 1)	5.802A	1	15.97			
ZD 1 0.2164 0.1771 0.3240 (0 0 0)	9.597A	1	22.36			
ZD 1 1.2164 1.1771 0.3240 (1 1 0)	9.611A	1	20.74			
ZD 1 0.7836 0.8229 0.8240 (1 1 0)	9.616A	1	21.36			
ZE 1 0.2882 0.6783 0.0407 (1 0 0)	11.449A	1	19.57			

-----

Structural group analysis

-----

-----

Structural group No 1

-----

Structure consists of 3D framework with ZEZD

There are 2 interpenetrating nets

FIV: Full interpenetration vectors

-----

[1,0,0] (9.51A)

-----

PIC: [2,0,0][1,1,0][0,0,1] (PICVR=2)

Zt=2; Zn=1

Class Ia Z=2

Coordination sequences

-----

ZD1: 1 2 3 4 5 6 7 8 9 10

Num 3 11 21 37 72 110 158 211 269 336

Cum 4 15 36 73 145 255 413 624 893 1229

-----

ZE1: 1 2 3 4 5 6 7 8 9 10

Num 5 11 23 45 75 116 161 213 272 340

Cum 6 17 40 85 160 276 437 650 922 1262

-----

TD10=1246

Vertex symbols for selected sublattice

-----  
 ZD1 Point symbol: {4.6^2}

Extended point symbol:[4.6(2).6(2)]  
 -----

ZE1 Point symbol: {4^3.6^6.8}

Extended point symbol:[4.4.4.6.6.6.6(2).6(2).8(3)]  
 -----

Point symbol for net: {4.6^2}{4^3.6^6.8}

3,5-c net with stoichiometry (3-c)(5-c); 2-nodal net

New topology, please, contact the authors (17461 types in 3 databases)

Elapsed time: 1.83 sec.

### Calculation of CO<sub>2</sub>/N<sub>2</sub> selectivity:

#### IAST selectivity:

The selectivity of IPM-301 and IPM-302 for CO<sub>2</sub>/N<sub>2</sub> (15:85) mixture at 298K and 1bar was based on the ideal adsorbed solution theory (IAST) given by Myers and Prausnitz.<sup>25</sup> The parameters were fitted from single-component adsorption isotherms based on single-site Langmuir-Freundlich model and were calculated using the equation<sup>26</sup> given below:

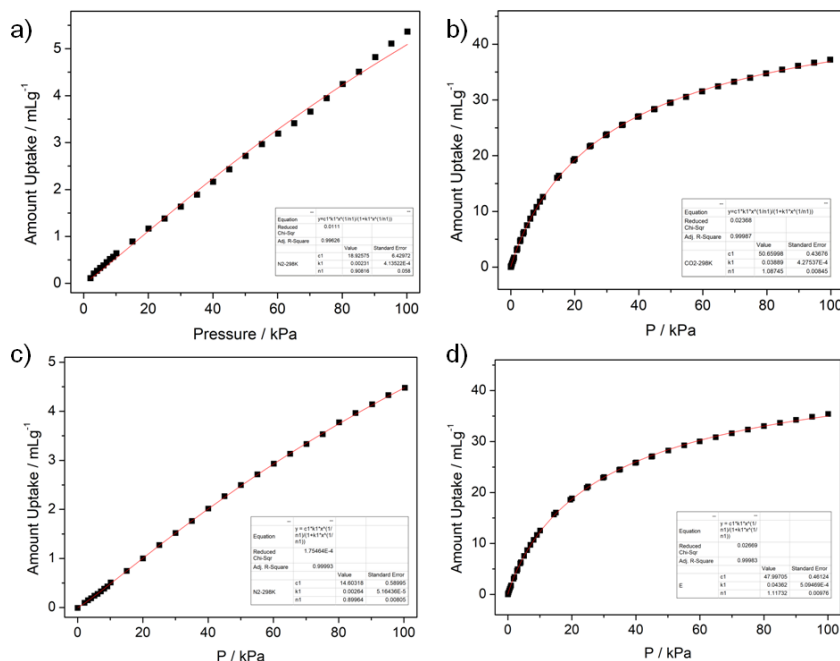
$$y = \frac{q_m b x^{1/n}}{1 + b x^{1/n}}$$

where,  $y$  is the adsorbed amount (mmol/g),  $q_m$  is the saturation capacity (mmol/g),  $x$  is the equilibrium pressure (kPa) and  $b$  and  $n$  are the Langmuir and Freundlich constants.

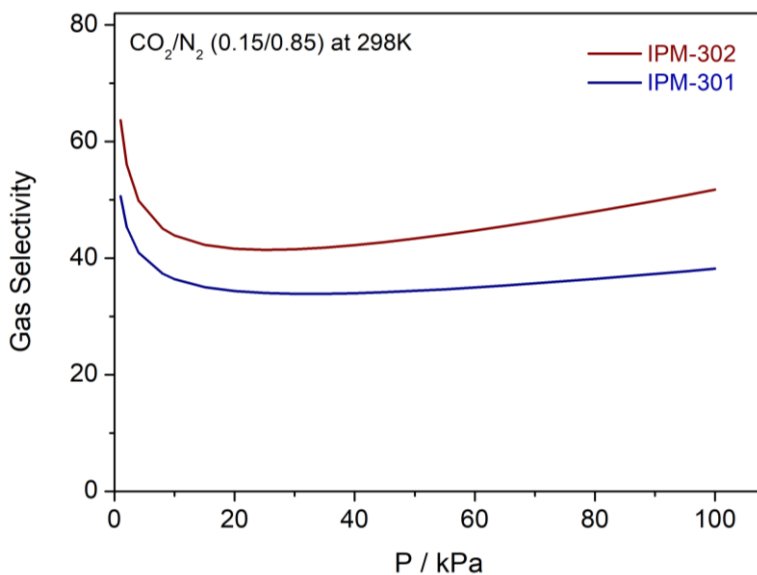
The predicted selectivity is given by:

$$S = \frac{x_1/y_1}{x_2/y_2}$$

where,  $x_i$  and  $y_i$  are mole fractions of component  $i$  ( $i=1,2$ ) in the adsorbed and bulk phase, respectively. The IAST calculations were performed on a mixture containing 15% CO<sub>2</sub> ( $y_1$ ) and 85% N<sub>2</sub> ( $y_2$ ), which is typical composition of the flue gas.



**Appendix 4.45:** Langmuir-Freundlich fitting (red line) for **IPM-301** - a)  $N_2$  (298K) and b)  $CO_2$  (298K). Corresponding fitting for **IPM-302** - c)  $N_2$  (298K) and d)  $CO_2$  (298K).



**Appendix 4.46:** Separation selectivity at 298K predicted by IAST for  $CO_2/N_2$  (15/85) for **IPM-301** (blue) and **IPM-302** (wine red).

## 4.6 References

- (a) Horike, S.; Shimomura, S.; Kitagawa, S., *Nat. Chem.* **2009**, *1*, 695-704. (b) Furukawa, H.; Cordova, K. E.; O’Keeffe, M.; Yaghi, O. M., *Science* **2013**, *341*, 1230444.
- (a) Kuppler, R. J.; Timmons, D. J.; Fang, Q.-R.; Li, J.-R.; Makal, T. A.; Young, M. D.; Yuan, D.; Zhao, D.; Zhuang, W.; Zhou, H.-C., *Coord. Chem. Rev.* **2009**, *253*, 3042-3066. (b) Vaidhyanathan, R.; Iremonger, S. S.; Shimizu, G. K. H.; Boyd, P. G.; Alavi, S.; Woo, T. K., *Science* **2010**, *330*, 650-653. (c) Horcajada, P.; Gref, R.; Baati, T.; Allan, P. K.; Maurin, G.; Couvreur, P.; Ferey, G.; Morris, R. E.; Serre, C., *Chem. Rev.* **2012**, *112*, 1232-1268. (d) Li, S. L.; Xu, Q., *Energy Environ. Sci.* **2013**, *6*, 1656-1683. (e) Van de Voorde, B.; Bueken, B.; Denayer, J.; De Vos, D., *Chem. Soc. Rev.* **2014**, *43*, 5766-5788. (f) Bao, Z.; Chang, G.; Xing, H.; Krishna, R.; Ren, Q.; Chen, B., *Energy Environ. Sci.* **2016**, *9*, 3612-3641. (g) Lustig, W. P.; Mukherjee, S.; Rudd, N. D.; Desai, A. V.; Li, J.; Ghosh, S. K., *Chem. Soc. Rev.* **2017**, *46*, 3242-3285. (h) Scott Bobbitt, N.; Mendonca, M. L.; Howarth, A. J.; Islamoglu, T.; Hupp, J. T.; Farha, O. K.; Snurr, R. Q., *Chem. Soc. Rev.* **2017**, *46*, 3357-3385. (i) Zhu, L.; Liu, X.-Q.; Jiang, H.-L.; Sun, L.-B., *Chem. Rev.* **2017**, *117*, 8129-8176. (j) Lin, Y.; Kong, C.; Zhang, Q.; Chen, L., *Adv. Energy Mater.* **2017**, *7*, 1601296. (k) Doonan, C.; Ricco, R.; Liang, K.; Bradshaw, D.; Falcaro, P., *Acc. Chem. Res.* **2017**, *50*, 1423-1432.
- (a) Qadir, N.; Said, S. A. M.; Bahaidarah, H. M., *Microporous Mesoporous Mater.* **2015**, *201*, 61-90. (b) Gelfand, B. S.; Shimizu, G. K. H., *Dalton Trans.* **2016**, *45*, 3668-3678. (c) Duan, J.; Jin, W.; Kitagawa, S., *Coord. Chem. Rev.* **2017**, *332*, 48-74.
- (a) Howarth, A. J.; Liu, Y.; Li, P.; Li, Z.; Wang, T. C.; Hupp, J. T.; Farha, O. K., *Nat. Rev. Mater.* **2016**, DOI: 10.1038/natrevmats.2015.18. (b) Yuan, S.; Feng, L.; Wang, K.; Pang, J.; Bosch, M.; Lollar, C.; Sun, Y.; Qin, J.; Yang, X.; Zhang, P.; Wang, Q.; Zou, L.; Zhang, Y.; Zhang, L.; Fang, Y.; Li, J.; Zhou, H.-C., *Adv. Mater.* **2018**, DOI: 10.1002/adma.201704303. (c) Wang, K.; Lv, X.-L.; Feng, D.; Li, J.; Chen, S.; Sun, J.; Song, L.; Xie, Y.; Li, J.-R.; Zhou, H.-C., *J. Am. Chem. Soc.* **2016**, *138*, 914-919. (d) Mouchaham, G.; Wang, S.; Serre, C., *The Stability of Metal-Organic Frameworks* (Metal-Organic Frameworks: Applications in Separations and Catalysis, Eds.: H. Garcia, S. Navalon), *Wiley-VCH*, Weinheim, **2018**, DOI: 10.1002/9783527809097.
- (a) Cordova, K. E.; Yaghi, O. M., *Mater. Chem. Front.* **2017**, *1*, 1304-1309. (b) Alezi, D.; Spanopoulos, I.; Tsangarakis, C.; Shkurenko, A.; Adil, K.; Belmabkhout, Y.; O’Keeffe, M.; Eddaoudi, M.; Trikalitis, P. N., *J. Am. Chem. Soc.* **2016**, *138*, 12767-12770.

6. (a) Tranchemontagne, D. J.; Mendoza-Cortes, J. L.; O’Keeffe, M.; Yaghi, O. M., *Chem. Soc. Rev.* **2009**, *38*, 1257-1283. (b) Li, M.; Li, D.; O’Keeffe, M.; Yaghi, O. M., *Chem. Rev.* **2014**, *114*, 1343-1370.
7. (a) Cote, A. P.; Shimizu, G. K. H., *Coord. Chem. Rev.* **2003**, *245*, 49-64. (b) Shimizu, G. K. H.; Vaidhyanathan, R.; Taylor, J. M., *Chem. Soc. Rev.* **2009**, *38*, 1430-1449. (c) Gagnon, K. J.; Perry, H. P.; Clearfield, A., *Chem. Rev.* **2012**, *112*, 1034-1054. (d) Zhang, G.; Wei, G.; Liu, Z.; Oliver, S. R. J.; Fei, H.; *Chem. Mater.* **2016**, *28*, 6276-6281. (e) Bao, S.-S.; Shimizu, G. K. H.; Zheng, L.-M., *Coord. Chem. Rev.* **2017**, DOI: 10.1016/j.ccr.2017.11.029. (f) Zheng, T.; Yang, Z.; Gui, D.; Liu, Z.; Wang, X.; Dai, X.; Liu, S.; Zhang, L.; Gao, Y.; Chen, L.; Sheng, D.; Wang, Y.; Diwu, J.; Wang, J.; Zhou, R.; Chai, Z.; Albrecht-Schmitt, T. E.; Wang, S., *Nat. Commun.* **2017**, *8*, 15369. (g) Zhang, G.; Fei, H., *Chem. Commun.* **2017**, *53*, 4156-4159. (h) Zhang, G.; Yang, H.; Fei, H., *ACS Catal.* **2018**, *8*, 2519-2525. (i) Reynolds, J. E.; Dunning, S. G.; McCulley, C. M.; Humphrey, S. M., *A Survey of Metal-Organic Frameworks Based on Phosphorus- and Sulfur-Containing Building Blocks*. (Vol. 2. Elaboration and Applications of Metal-Organic Frameworks; Eds.: S. Ma, J. A. Perman), *World Scientific Publishing Co Pte Ltd*, **2018**, 37-141, DOI: 10.1142/9789813226739\_0002.
8. (a) Cote, A. P.; Shimizu, G. K. H., *Chem. Commun.* **2001**, 251-252. (b) Chandler, B. D.; Cramb, D. T.; Shimizu, G. K. H., *J. Am. Chem. Soc.* **2006**, *128*, 10403-10412.
9. (a) Li, B.; Wen, H.-M.; Cui, Y.; Zhou, W.; Qian, G.; Chen, B., *Adv. Mater.* **2016**, *28*, 8819-8860. (b) Qin, J.-S.; Yuan, S.; Wang, Q.; Alsalme, A.; Zhou, H.-C., *J. Mater. Chem. A* **2017**, *5*, 4280-4291.
10. (a) Chen, Y.-Q.; Li, G.-R.; Chang, Z.; Qu, Y.-K.; Zhang, Y.-H.; Bu, X.-H., *Chem. Sci.* **2013**, *4*, 3678-3682. (b) Manna, B.; Desai, A. V.; Ghosh, S. K., *Dalton Trans.* **2016**, *45*, 4060-4072. (c) Desai, A. V.; Manna, B.; Karmakar, A.; Sahu, A.; Ghosh, S. K., *Angew. Chem. Int. Ed.* **2016**, *55*, 7811-7815. (d) Colinas, I. R.; Silva, R. C.; Oliver, S. R. J., *Environ. Sci. Technol.* **2016**, *50*, 1949-1954. (e) Chen, S.-S., *CrystEngComm* **2016**, *18*, 6543-6565. (f) Sheng, D.; Zhu, L.; Xu, C.; Xiao, C.; Wang, Y.; Wang, Y.; Chen, L.; Diwu, J.; Chen, J.; Chai, Z.; Albrecht-Schmitt, T. E.; Wang, S., *Environ. Sci. Technol.* **2017**, *51*, 3471-3479.
11. *SAINT Plus*, Bruker AXS Inc.: Madison, WI, **2004**.
12. Krause, L.; Herbst-Irmer, R.; Sheldrick, G. M.; Stalke, D., *J. Appl. Cryst.* **2015**, *48*, 3-10.
13. (a) Sheldrick, G. M.; *SHELXTL*, Reference Manual, version 5.1; Bruker AXS Inc.: Madison, WI, **1997**. (b) Sheldrick, G. M., *Acta. Cryst.*, **2008**, *A64*, 112-122.
14. Sheldrick, G. M., *Acta. Cryst.*, **2015**, *C71*, 3-8.

15. Farrugia, L., *WinGX*, University of Glasgow: Glasgow, Scotland.
16. Spek, A. L., *Acta. Cryst.*, **2015**, *C71*, 9-18.
17. Kresse, G.; Hafner, J., *Phys. Rev. B* **1993**, *48*, 13115-13118.
18. Grimme, S.; Ehrlich, S.; Goerigk, L., *J. Comp. Chem.* **2011**, *32*, 1456-1465.
19. Perdew, J. P.; Burke, K.; Ernzerhof, M., *Phys. Rev. Lett.* **1996**, *77*, 3865-3868.
20. Kresse, G.; Joubert, D., *Phys. Rev. B* **1999**, *59*, 1758-1775.
21. *Materials Studio*, 8.0 Ed.; Accelrys, San Diego, **2015**.
22. (a) Scott, H. S.; Bajpai, A.; Chen, K.-J.; Pham, T.; Space, B.; Perry IV, J. J.; Zaworotko, M., *Chem. Commun.* **2015**, *51*, 14832-14835. (b) Scott, H. S.; Ogiwara, N.; Chen, K.-J.; Madden, D. G.; Pham, T.; Forrest, K.; Space, B.; Horike, S.; Perry IV, J. J.; Kitagawa, S.; Zaworotko, M. J., *Chem. Sci.* **2016**, *7*, 5470-5476.
23. Blatov, V. A., *TOPOS*. Samara State University, Russia, **2004**.
24. (a) Wu, P.; Wang, J.; He, C.; Zhang, X.; Wang, Y.; Liu, T.; Duan, C., *Adv. Funct. Mater.* **2012**, *22*, 1698-1703. (b) Desai, A. V.; Samanta, P.; Manna, B.; Ghosh, S. K., *Chem. Commun.* **2015**, *51*, 6111-6114.
25. Myers, A. L.; Prausnitz, J. M., *AIChE J.* **1965**, *11*, 121-127.
26. Li, B.; Zhang, Y.; Krishna, R.; Yao, K.; Han, Y.; Wu, Z.; Ma, D.; Shi, Z.; Pham, T.; Space, B.; Liu, J.; Thallapally, P. K.; Liu, J.; Chrzanowski, M.; Ma, S., *J. Am. Chem. Soc.* **2014**, *136*, 8654-8660.

---

## *Chapter 5*

---

# **Base-resistant Cationic MOF as Ion-exchanger of Organic Dyes over Wide pH Range**

## 5.1 Introduction

Metal-organic frameworks (MOFs) or porous coordination polymers (PCPs) have rapidly evolved as an important subset of porous materials.<sup>1</sup> The interest in this domain has expanded in recent years owing to wide range of applicability exhibited by these materials.<sup>2</sup> MOFs can be broadly be segregated into two classes, based on the charge of the coordination network viz. neutral and ionic-MOFs (i-MOFs); ionic MOFs are further classified into cationic and anionic.<sup>3</sup> MOFs afford significant advancement over congener polymeric materials owing to crystalline nature which furnishes precise structure-property correlation. Despite several advantages, there remain a few core issues such as hydrolytic and chemical stability which have stalled the progress of MOFs for real-time applications.<sup>4</sup> Although few benchmark MOF compounds having hydrolytic or chemical stability are known, majority of them are found to be stable predominantly in acidic pH.<sup>5</sup> The infrequent MOFs exhibiting base resistance, they are typically neutral frameworks built from azolate-based ligands.<sup>5d</sup> Development of ionic-MOFs is seeking greater relevance owing to them being potentially viable alternatives to conventional ion-exchangers for various applications.<sup>3a,6</sup> The challenges of stability assume greater relevance for cationic MOFs which generally are vulnerable to disintegration in aqueous medium or mild acid/basic conditions. To overcome the limitations of weak hydrolytic or chemical stability, design strategies which can provide robust compounds offering resistance are highly sought after.

Surveying the literature, some reviews have chalked out broad principles guiding the design of water and chemically stable, porous MOFs. These include strengthening the metal-ligand bond and shielding this bond from influence of foreign species.<sup>4c,5h</sup> The proper choice of the metal ions or the suitable kind of the organic ligand have also been found to play a crucial role in bestowing stability to a compound. This formal outline has generally been derived from stable benchmark compounds which in most cases are neutral MOFs. The systematic design and development of stable cationic-MOFs from the insights gained in literature reports is extremely uncommon.<sup>3a</sup>

With this background we sought to focus on the development of approaches for designing stable cationic MOFs. Typically, cationic MOFs are fabricated from neutral N-donor ligands which render cationic frameworks and afford the presence of uncoordinated, substitutable anions.<sup>7</sup> For affording stability, ligands with higher pKa have found greater preference,<sup>8</sup> and hence ligands with imidazole/triazole donating units can be more effective as neutral donor ligands.<sup>9</sup> Further the smaller size of 5-membered donating moieties can render greater density of the ligands around the metal nodes by feasibility of hexa-coordination, which may shield the metal nodes from the influence of external species. In general, higher dentate ligands are better suited for generating higher dimensional frameworks. In the present discourse, the additional benefit of such linkers is in affording superior kinetic stability.<sup>5i</sup> Likewise the appropriate selection of metal centre



is vital while fabricating stable systems. The choice of the metal node is directed by its ability to bind to the donor groups of the ligands, and the resistance to dissociation of the resulting bonds. Among transition metals which bind equally well with N- & O-donor ligands, Ni(II)-based MOFs have been found to offer remarkable hydrolytic stability and in certain cases resistance to varying chemical environments.<sup>5d,5i,8a,10</sup> In case of cationic MOFs, although the uncoordinated anions are not a direct part of the framework backbone, their choice can be significant in the preparation. From the existing literature it is observed that organic sulfonates, which are bulky molecules, are known to bind to metal centres typically at higher temperatures only.<sup>11</sup> In the current context, such compounds can adapt the function of template anions for creation of voids and being an integral part of the framework.

Combining the above-mentioned facets, herein we report the synthesis of a two-dimensional Ni(II)-centred cationic MOF viz  $[\{Ni(L)_2\} \cdot (BPSA) \cdot xG]_n$  (L - Ligand; BPSA - 4,4'-biphenyldisulfonic acid; G - guest; hereafter referred to as IPM-MOF-201, where IPM stands for IISER Pune Materials). The compound is built from a tridentate ligand having terminal imidazole rings and bears the presence of free organosulfonate anions. The compound was found to exhibit extraordinary base resistance, which is uncommonly observed in porous MOFs and even more infrequently among ionic-MOFs. The stability over wide pH range has been tapped for the function of trapping of small organic dye molecules across different pH conditions.

## 5.2 Experimental

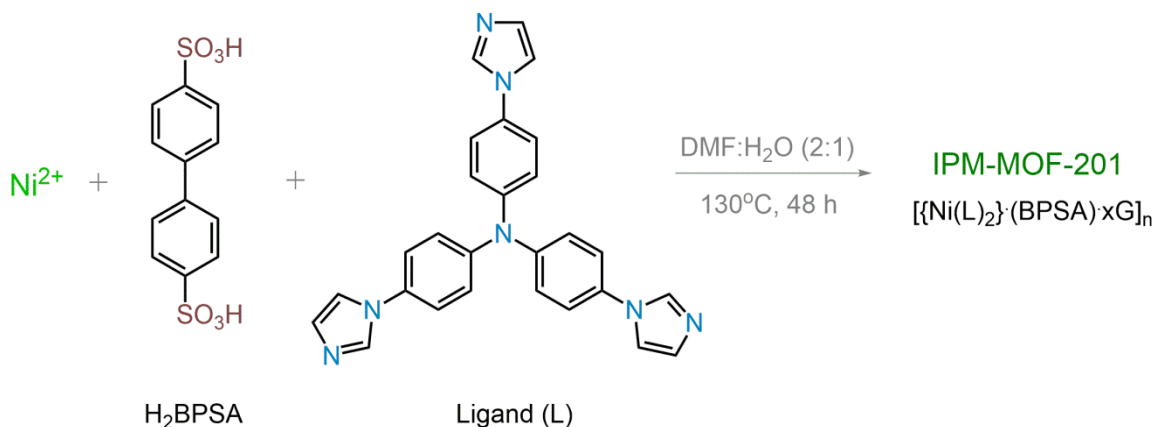
### 5.2.1 Materials:

All solvents and reagents were commercially available and used without further purification. Standard pH buffers (pH = 4.01, 10.01, 12.45) were procured from Eutech Instruments. The other pH conditions were prepared using concentrated HCl and NaOH flakes. The ligand was synthesized according to reported protocol.<sup>10a</sup>

### 5.2.2 Synthesis:

**Synthesis of Compound IPM-MOF-201:** A mixture of ligand (8.86 mg, 0.02 mmol), NiSO<sub>4</sub>·xH<sub>2</sub>O (5.60 mg, 0.02 mmol), 4,4'-biphenyldisulfonic acid [H<sub>2</sub>BPSA] (9.45 mg, 0.03 mmol), N,N-dimethylformamide (2 ml) and water (1 ml), was placed in a teflon capped pyrex tube, and heated at 130°C for 48 hours followed by slow cooling to room temperature. The compound was filtered and washed with water and methanol several times. Pale green colour crystals of compound IPM-MOF-201 viz.  $[\{Ni(L)_2\} \cdot (BPSA) \cdot xG]_n$  were isolated in ~40% yield. These crystals were dipped in MeOH solution for 2 days prior to heating it under vacuum at 75°C to obtain the guest free phase. We were unable to locate the highly disordered guest solvent molecules and uncoordinated anion in the structure crystallographically. From the SQUEEZE function of

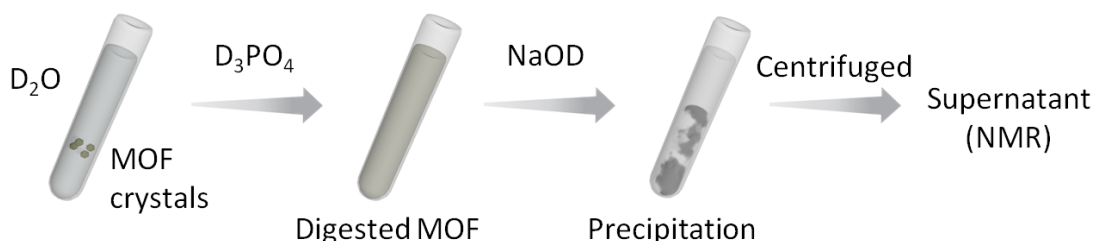
PLATON the formula for the guest-free phase was estimated to be  $[\{\text{Ni}(\text{L})_2\} \cdot (\text{BPSA})]_n$ . Anal. Calcd.: C/N, 4.04; N/S, 3.06; C/S, 12.35. Found: C/N, 3.98; N/S, 3.15; C/S, 12.57. CCDC 1561299 contains the supplementary crystallographic data for this paper. These data can be obtained free of charge from The Cambridge Crystallographic Data Centre via [www.ccdc.cam.ac.uk/data\\_request/cif](http://www.ccdc.cam.ac.uk/data_request/cif).



**Scheme 5.1:** Representation of the protocol employed for the synthesis of IPM-MOF-201.

**Synthesis of analogous Ni-MOFs:** Metal salts of  $\text{Ni}^{2+}$  ( $\text{NO}_3^-$ ,  $\text{Cl}^-$ ,  $\text{SiF}_6^{2-}$ ,  $\text{Br}^-$ ,  $\text{OTf}^-$ ; 0.02 mmol each) were added separately to the mixture of ligand (8.86 mg, 0.02 mmol), 4,4'-biphenyldisulfonic acid [BPSA] (9.45 mg, 0.03 mmol) in *N,N'*-dimethylformamide (DMF; 2 ml) and water (1 ml). The mixture was heated at 130°C for 48 hours in a Pyrex tube. Upon cooling the compounds were washed with water and methanol and dried in air for further characterization.

**5.2.3 Characterization of the free anion:** The presence of the free anion ( $\text{BPSA}^{2-}$ ) was characterized by digesting the MOF. To minimize the content of the transition metal ion Ni(II) in the NMR sample, a 2-step protocol was employed for validating the presence of the free anion (Scheme 5.2). To 20 mg of the activated phase of IPM-MOF-201 in 0.5 ml  $\text{D}_2\text{O}$ , 0.2 ml  $\text{D}_3\text{PO}_4$  (85% in  $\text{D}_2\text{O}$ ) was added.

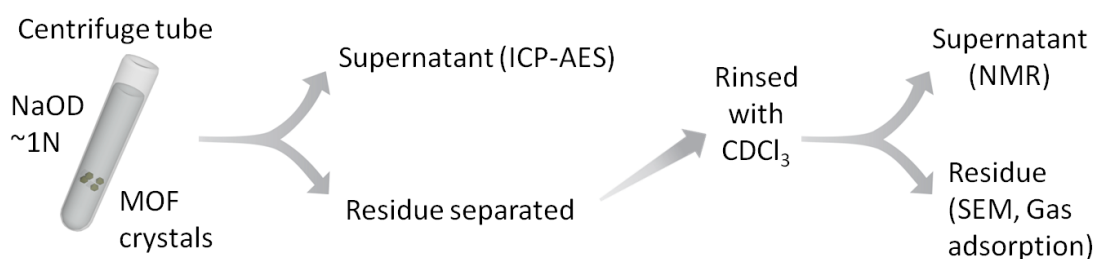


**Scheme 5.2:** Schematic illustration of the protocol employed for digesting IPM-MOF-201.

To this solution NaOD (40 wt%) was added dropwise till the pH became neutral. As the pH reached neutral heavy precipitation was observed. This was separated by centrifugation and the supernatant was used to record the  $^1\text{H-NMR}$  spectrum.

**5.2.4 Water Stability Test:** 20 mg of activated compound IPM-MOF-201 was dipped in 5 ml of deionised water and kept at room temperature for 7 days. Subsequently, the compound was filtered off and dried in air for further characterization. For FESEM images, the compound was kept in deionised water for 30 days.

**5.2.5 pH Stability Test:** ~50 mg of the activated compound IPM-MOF-201 was dipped in 5 ml of separate pH solution (pH = 4, 10.01, 12.45, 14) and stirred at room temperature for 24 hours. The respective solutions were filtered off (the supernatant was collected and submitted for ICP-AES analyses) and the residue was washed with deionised water multiple times, followed by washing with methanol. All the phases were then degassed by heating under reduced pressure for further characterization. For gas adsorption studies, the compounds were pre-treated at  $120^\circ\text{C}$  under vacuum before measurement.



**Scheme S3:** Schematic illustration of the protocol employed for the ascertaining the base stability of IPM-MOF-201.

To validate the base resistance of the compound, 20 mg of the activated phase of IPM-MOF-201 was added to a solution of ~1N NaOD (0.5 ml, 40 wt%; Sigma Aldrich) in  $\text{D}_2\text{O}$  (4.5 ml; Sigma Aldrich) and kept at room temperature for 24 hours. This mixture was centrifuged and ICP-AES analysis was performed on the supernatant. The residue was then treated with  $\text{CDCl}_3$  (3.0 ml; Sigma Aldrich) and the NMR spectra for this supernatant was also recorded. The residue obtained after the second step was used for further characterization (Scheme S3).

**5.2.6 Dye Exchange Studies:** ~10 mg of activated crystalline powder of IPM-MOF-201 was dipped in aqueous solution of methyl orange [MO] (1 mM, 2 ml) for 2 days at room temperature to yield the dye-encapsulated product. After anion exchange the compound was washed with deionised water and methanol several times to remove any dye adsorbed on the surface of the compound. The air-dried compounds were then used for further characterization. The same protocol was followed for other dyes viz. indigo carmine

[IC], alizarin red S [ARS], methyl red [MR], 4-phenylazophenol [PAP]. Similarly, the dye exchange experiments were carried out at other pH conditions (pH = 4, 10.01, 12.45, 14). For the UV-vis measurements, the standard deviation was calculated from five blank measurements of the dye solutions. The standard deviations for MO, IC, ARS, MR, PAP dyes were calculated to be 0.00589, 0.00728, 0.00187, 0.00083, 0.0013 respectively.

**5.2.7 Control Experiment:** Compound IPM-MOF-201(Co) was synthesized following above protocol, replacing  $\text{NiSO}_4 \cdot x\text{H}_2\text{O}$  with  $\text{CoSO}_4 \cdot 7\text{H}_2\text{O}$  (5.62 mg, 0.02 mmol). The crystalline powder thus obtained was filtered off and washed with water and methanol. It was activated under reduced pressure at  $75^\circ\text{C}$  and used for further characterization. For checking the pH stability, 10 mg of the crystalline powder was dipped in pH=12.45 buffer and pH=14 solution for 24 hours at room temperature. Subsequently it was washed with deionised water and acetonitrile, and dried in air for further characterization. The Co-MOF & Cd-MOF used for comparison were synthesized according to reported protocols.<sup>19b,19e</sup>

**5.2.8 Dye Content Calculation:** The dye content in the solution was calculated using a reported protocol.<sup>25d</sup> Time dependent UV-vis absorbance of the supernatant were recorded. The absorbance maxima corresponding to each dye in different pH was chosen to compute the dye content using the formula:

$$D = (A_t/A_o) \times 100\%$$

where D is the dye content in the corresponding pH solution,  $A_o$  characteristic absorbance of the solution before addition of the MOF,  $A_t$  is the absorbance of the solution at different time intervals.

**Blank Dye Solution Experiment:** The UV-vis spectra of blank aqueous dye solutions [ $\sim 0.05\text{mM}$ ] (without addition of MOF) was recorded at two time intervals ( $t=0$  and  $t=24\text{h}$ ) to validate the ion-exchange experiments in the presence of MOF.

**5.2.9 Recycling Experiment:** To an aqueous solution of MO (0.09 mM)  $\sim 10$  mg of the activated phase of IPM-MOF-201 was added. After keeping it for 24 hours, the supernatant was collected and its UV-vis spectrum was recorded. The filtrate was air-dried and added to an aqueous solution of tetrabutylammonium chloride (50wt%, 2 ml). The supernatant was collected after 24 hours and its UV-vis spectrum was monitored. The filtrate was air-dried and this cycle was repeated further.

**5.2.10 MOF-loaded Column Experiment:** A glass tube with narrow opening was used for this experiment which was plugged by thick cotton at the bottom.  $\sim 20$  mg of the activated phase of IPM-MOF-201 was filled followed by addition of a uniform layer of white sand. This set-up was rinsed with deionised water 2-3 times before further use. A mixture of MO and MB (0.05 mM, 5 ml each) in deionised water was added to this column. The eluted MB solution was collected and then deionised water was purged until no further

dye eluted out. Following this tetrabutyl ammonium chloride aqueous solution (50wt%) was passed to elute the trapped MO dye. This was passed until no further MO dye passed out.

**5.2.11 Physical Measurements:** Powder X-ray diffraction patterns were recorded on Bruker D8 Advanced X-Ray diffractometer using Cu K $\alpha$  radiation ( $\lambda = 1.5406 \text{ \AA}$ ) in  $5^\circ$  to  $40^\circ$   $2\theta$  range with a scan speed of  $0.6^\circ\text{min}^{-1}$ . The IR Spectra were acquired by using NICOLET 6700 FT-IR spectrophotometer using KBr pellet in 400-4000  $\text{cm}^{-1}$  range. UV spectra were recorded on Shimadzu UV 2600 Spectrophotometer having stirring attachment. The SEM images & EDX data were obtained using FEI Quanta 3D dual beam ESEM. Thermogravimetric analysis profiles were recorded on Perkin-Elmer STA6000, TGA analyser under  $\text{N}_2$  atmosphere with heating rate of  $10^\circ\text{C}/\text{min}$ . Gas adsorption measurements were performed using BelSorp-Max instrument (Bel Japan). Solvent adsorption measurements were performed on Bel-Aqua instrument (Bel Japan).  $^1\text{H}$  &  $^{13}\text{C}$  NMR spectra were recorded on a JEOL 400 MHz or Bruker 400 MHz spectrometer.

**5.2.12 X-ray Structural Studies:** Single-crystal X-ray data of compound IPM-MOF-201 was collected at 100 K on a Bruker D8 Venture Duo X-ray diffractometer equipped with Microfocus X-ray source (operated at 50W; 50kV/1mA), graded multilayer optics for monochromatic Mo K $\alpha$  radiation ( $\lambda = 0.71073 \text{ \AA}$ ) focused X-ray beam and Photon 100 CMOS chip based detector system. Crystal was mounted on nylon CryoLoops (Hampton Research) with Paraton-N (Hampton Research). The data integration and reduction were processed with SAINT<sup>12</sup> software. A multi-scan absorption correction was applied to the collected reflections.<sup>13</sup> The structure was solved by the direct method using SHELXTL<sup>14</sup> and was refined on  $F^2$  by full-matrix least-squares technique using the SHELXL-2014/7<sup>15</sup> program package within the WINGX<sup>16</sup> programme. All non-hydrogen atoms were refined anisotropically. All hydrogen atoms were located in successive difference Fourier maps and they were treated as riding atoms using SHELXL default parameters. The structures were examined using the Adsym subroutine of PLATON<sup>17</sup> to assure that no additional symmetry could be applied to the models. High disorder was observed for the guest solvent molecules and the anion (BPSA). The SQUEEZE option was used to eliminate the contribution of disordered guest molecules and anion. The number of the anions required to maintain the electrical neutrality was estimated and the molecular formula was calculated accordingly.

### 5.3 Results and discussion

Hexagonal-shaped single crystals of compound IPM-MOF-201 were obtained in a solvothermal reaction at  $130^\circ\text{C}$  from a mixture of  $\text{NiSO}_4 \cdot x\text{H}_2\text{O}$ , 4,4'-biphenyldisulfonic acid (BPSA) and ligand (L) (1:1.5:1), in a solvent system of N,N'-dimethylformamide (DMF) and water (2:1) (Scheme 5.1). Compound IPM-MOF-201 was found to crystallize in R-3 space group, as revealed by single-crystal X-ray diffraction (SC-XRD) studies.

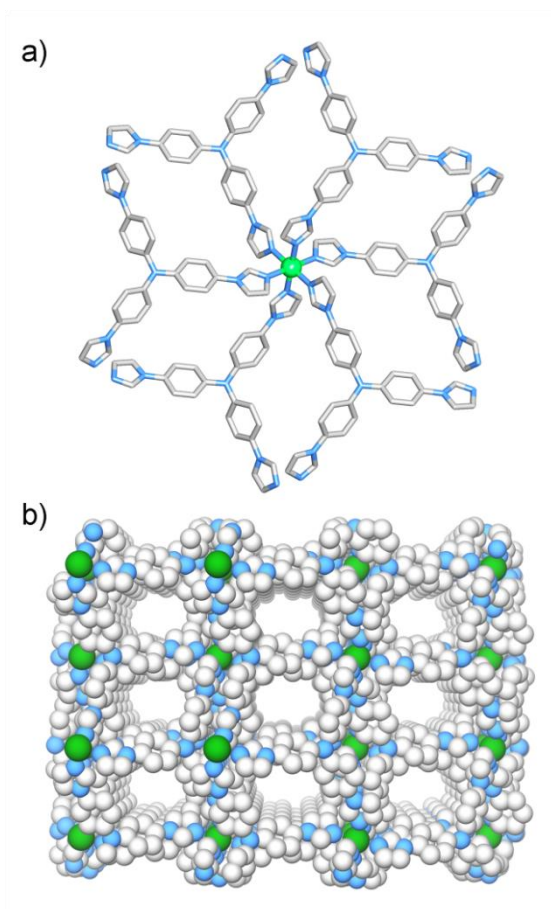


Figure 5.1 a) Coordination environment in IPM-MOF-201; b) Perspective view of packing in IPM-MOF-201 showing porous channels. (Hydrogen atoms and disordered anions have been omitted for clarity. Color code: Ni, green; C, grey, N, blue).

The asymmetric unit comprises of one Ni(II) cation with 1/6 occupancy, one ligand (L) with 1/3 occupancy and disordered solvent and organic anions (Appendix 5.1). The presence of the organic anion (BPSA) was validated in the  $^1\text{H-NMR}$  obtained after digesting the MOF in  $\text{D}_3\text{PO}_4/\text{D}_2\text{O}$ , followed by neutralization by NaOD (Appendix 5.11; Scheme 5.2). The metal centre is octahedral with coordination from six nitrogen atoms of six independent ligand units (Figure 5.1a). We determined the topology of the cationic framework to understand the structure further.<sup>18</sup> The analysis revealed that compound has a (3,6)-connected binodal **kgd** topology (Appendix 5.8). Notably, this topology is not commonly found in the domain of MOFs.<sup>19</sup> The rational choice of building units for obtaining compounds with such topology would be tris-monodentate trigonal ligands. In the context of the present work, the selection of the ligands would be limited to neutral N-donor linkers. CSD (Cambridge Structural Database) screening approach suggests that MOFs having tridentate 5-membered ligands having neutral donating sites with Ni(II) nodes and crystallizing in such packing modes have not been profoundly explored yet, which can lead to realization of chemically stable

frameworks. The important feature of this topology is in the creation of intrinsic porosity<sup>19a</sup> (Figure 1b, Appendix 5.2-5.5), as the resulting 2D sheets are non-planar. In the context of the present study, the non-planarity of the ligands is well-suited as it keeps the metal nodes sterically crowded and enclosed within the 2D layers (Appendix 5.6-5.7). The networks crystallizing in kgd topology disfavour interpenetration which furnishes large voids in the overall packing.<sup>19a</sup> Based on the PLATON calculations, the solvent accessible void in IPM-MOF-201 is estimated to be 2754 Å<sup>3</sup> (49%), considering only the cationic network.

Basic characterization of the compound was carefully performed before all subsequent studies. The purity of the bulk phase was validated using powder x-ray diffraction (PXRD) patterns (Appendix 5.9). The peaks corresponding to the ligand were found to be retained in the FT-IR spectrum for IPM-MOF-201, along with the peak corresponding to S-O stretching frequency (Appendix 5.10).<sup>20</sup> FE-SEM images of IPM-MOF-201 confirmed the hexagonal morphology of the crystallites and EDX spectra supported the purity of the crystallites (Appendix 5.12-5.13). Thermogravimetric analysis (TGA) profile suggested initial loss of guest molecules, water and DMF (Appendix 5.14). To substantiate the formation of the compound as the favourable product, the synthesis was carried out using different Ni<sup>2+</sup> salts keeping the molar ratios same. In all the cases we observed purity of the product from PXRD patterns, FT-IR spectra, EDX profiles and morphological analysis using SEM images (Appendix 5.15-5.17). The formation of the compound in different batches validated the favourable formation of IPM-MOF-201.

Low temperature gas adsorption measurements were performed to substantiate the porosity of the compound. While we observed almost no uptake for N<sub>2</sub> (77 K) (Appendix 5.18), there was considerable uptake for CO<sub>2</sub> (195 K) with strong hysteresis (Appendix 5.18), which suggested strong interactions with the uncoordinated anions. CO<sub>2</sub> adsorption isotherms were also recorded at 273 K and 298 K which exhibited uptake of ~31 mLg<sup>-1</sup> and ~20 mLg<sup>-1</sup> respectively (Appendix 5.19). The water adsorption isotherm (298 K) revealed that the voids present in the compound permitted the entry of water molecules (Figure 5.2a, Appendix 5.20). To check hydrolytic stability of the compound over a period of time, single crystals of IPM-MOF-201 were dipped in water for 30 days and we found that the morphology of crystals remained unaffected (Appendix 5.21). The hydrolytic stability was further substantiated by the retention of the bulk-phase purity (Appendix 5.22) and CO<sub>2</sub> adsorption (Appendix 5.31).

Enthused from these basic characterizations and the robust nature of the compound in aqueous medium, we then set out to investigate the stability of the compound across varying pH. Initially single crystals of IPM-MOF-201 were dipped in pH solutions of 4, 10, 12.45 and the retention of the crystallinity was monitored under optical microscope at different time intervals (Figure 5.2d, Appendix 5.23). In all the three cases we found that the crystals remained intact with no significant loss to crystallinity. To extrapolate this



observation even further, single crystals were dipped in 1N NaOH (pH = 14) solution and observed at different time intervals, and even in this case the crystals appeared to remain unaffected (Figure 5.2d, Appendix 5.23).

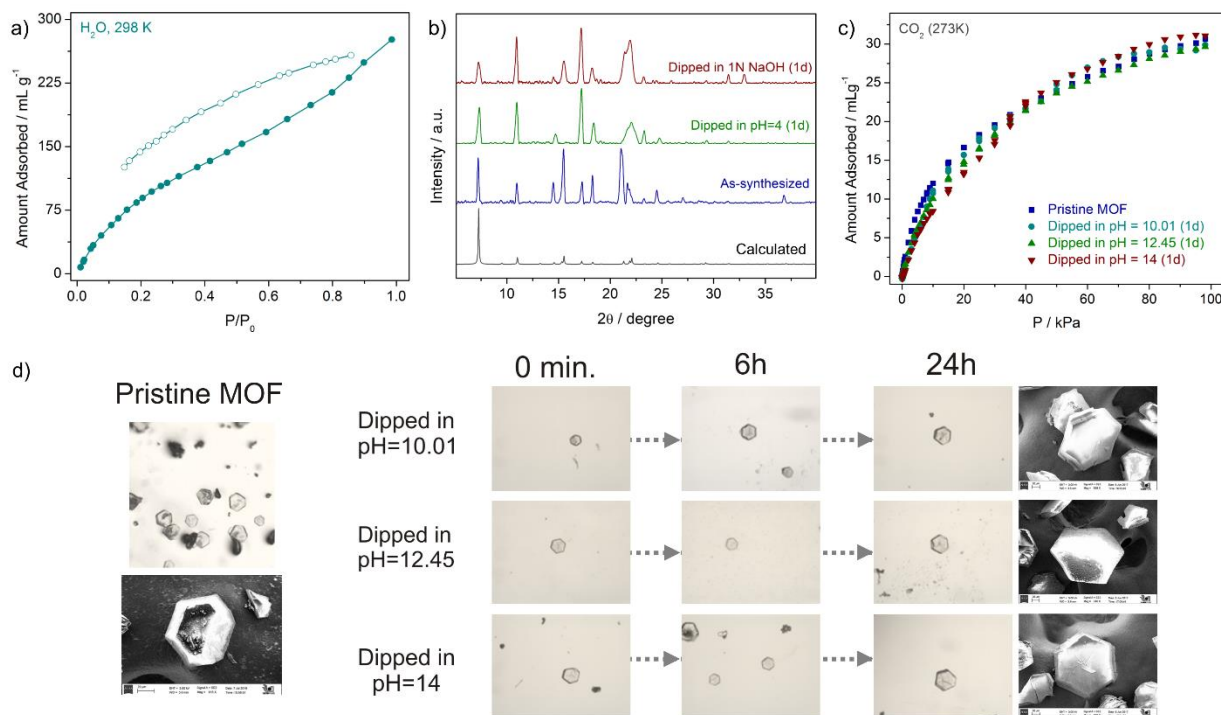


Figure 5.2 a) Water adsorption isotherm for IPM-MOF-201 at 298K (closed & open symbols denote adsorption & desorption respectively), b) PXRD patterns of pH=4 & pH=14 dipped phases, c) CO<sub>2</sub> adsorption profiles (273 K) of base-treated phases of IPM-MOF-201, d) Photographs of different phases recorded by optical microscope and corresponding FESEM images.).

Unit-cell parameters were recorded for the crystals recovered after 1 day treatment at pH = 4 and 1N NaOH. In both the cases the parameters were found to be in close proximity of that of the as-synthesized phase (Appendix Table S3), suggesting negligible effect of the pH environment. Upon lowering the pH further, we found dissociation of the framework which is typically observed for frameworks built from neutral N-donor linkers. Encouraged from these preliminary observations we then tested this behaviour on the bulk scale. Crystals of IPM-MOF-201 were dispersed in separate pH solutions under stirring for 24 hours. The compounds recovered after these treatments were characterized using PXRD, SEM and gas adsorption measurements. PXRD patterns confirmed the retention of bulk-phase purity (Figure 5.2b, Appendix 5.24), along-with supplementary evidence from FT-IR spectra SEM images and EDX profiles (Figure 5.2d, Appendix 5.25-5.29). Also, ICP-AES analysis for the supernatant collected after dipping in pH = 4 and 1N NaOH validated that the compound did not undergo disintegration (Appendix Table S1). CO<sub>2</sub> adsorption



measurements at 273 K (Figure 5.2c, Appendix 5.30) and 298 K (Appendix 5.31) substantiated the resistance of the compound, with almost similar uptakes in all the treated phases, without perturbing the structural integrity (Appendix 5.34). As additional evidence to the above observations, we performed NMR studies using deuterated solvents. Crystals of IPM-MOF-201 were dispersed in a solution of NaOD/D<sub>2</sub>O for 1 day (Scheme S3). The solution was centrifuged to separate the filtrate and CDCl<sub>3</sub> was added to the residue and rinsed thoroughly. The solution was centrifuged once again and the supernatant collected for recording the NMR spectra (Appendix 5.32). The lack of peaks corresponding to the ligand in the spectra corroborated with the observed base resistance of IPM-MOF-201. In addition the SEM images of the residue were recorded which showed retention of the hexagonal morphology (Appendix 5.33). The residue was subjected to CO<sub>2</sub> adsorption (298 K) and we found similar uptakes, substantiating the resistance feature (Appendix 5.31). It is noteworthy that the present compound marks an extremely rare example of a MOF exhibiting base resistance and an even rarer case of a cationic MOF retaining integrity under basic conditions.

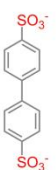
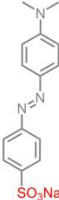
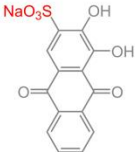
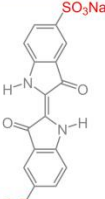
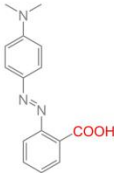
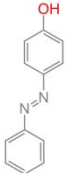
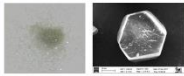
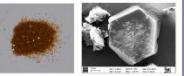
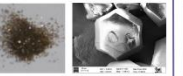
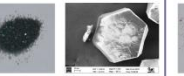
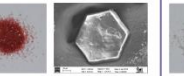
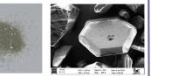
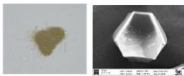
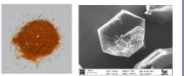
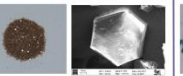
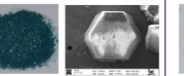
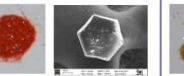
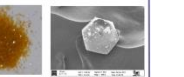
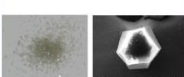
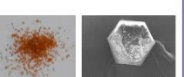
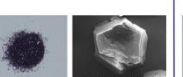

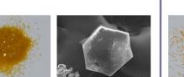
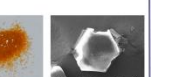
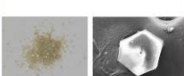

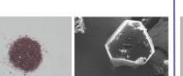
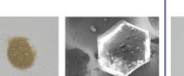
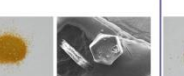
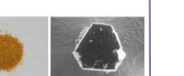
Phase Condition	 Only MOF (IPM-MOF-201)	 Methyl Orange exchange	 Alizarin Red S exchange	 Indigo Carmine exchange	 Methyl Red exchange	 4-phenylazophenol exchange
pH = 4						
pH = 7						
pH = 10.01						
pH = 12.45						

Figure 5.3 Summary showing photographs of all the phases of compound IPM-MOF-201 and the dye-exchange phases under different conditions. The corresponding SEM images are shown along-side.

We believe that the structure of the compound affords significant hydrolytic stability owing to the shielding of the metal nodes in the non-planar 2D sheets (Appendix 5.7), as all the coordination sites are occupied by the ligands. The utilization of the tridentate ligand with strongly coordinating terminal units can afford enhanced stability to the packing. Also Ni(II) based MOFs are known to be hydrolytically stable, and in certain cases even stable under extreme chemical conditions, providing additional stability to the resulting framework.

As a control experiment to examine the efficacy of the design strategy, we synthesized an isostructural Co(II) MOF keeping all the other reagents and their ratios same. The bulk phase purity of the thus synthesized MOF viz. IPM-MOF-201(Co) was validated using PXRD patterns (Appendix 5.35). Although Co-based MOF has been previously reported with ligand (L), 19b but owing to the bulky anion, the structure obtained is subtly different (Appendix 5.35). Upon primary characterization, the compound was activated in an analogous manner to the Ni(II) compound and then checked for its stability in different pH. Crystals of IPM-MOF-201(Co) were dipped in different pH solutions and monitored under optical microscope at incremental time intervals (Appendix 5.36). Unlike the previous case, the crystals were found to disintegrate with increasing time intervals. This observation was substantiated in the PXRD patterns recorded for the bulk-phase after dipping in different conditions (Appendix 5.35). Further control experiments with previously reported MOFs having similar structures<sup>19b,19e</sup> were checked and in both the cases we observed complete breakdown of the framework under high basic conditions (Appendix 5.37-5.38). These results further support the validity of design strategy in the choice of metal nodes and employment of higher dentate neutral ligands.

Along with the critical issue of stability, suitability of MOFs for real-time application in varying chemical environments is a focussed aspect of research in this domain. Although only as a consequence of stability, the effective utilization of porosity across wide pH range remains a challenge for this class of materials. Thus to tap the resistance of IPM-MOF-201 across wide pH range and the accessible porosity to foreign species, we sought to investigate the ability of the compound to capture small organic dye molecules. Capture and degradation of dye molecules is an important research problem owing to the serious hazards caused by the release of these compounds in water streams.<sup>21</sup> Most of these contaminants have high absorption which blocks the passage of sunlight to living species in water media.<sup>22</sup> Also on account of high consumption of dissolved oxygen, the aquatic ecosystem is imbalanced. These issues have compounded in recent years owing to the extent and growth of dye-manufacturing industries. It is reckoned that the annual production scale of commercial dyes is close to a million tons.<sup>23</sup> The allied industries, which include textiles, are estimated to release 10% of the total dyestuffs as industrial wastewaters. Thus given the gravity of this issue, researches have trialled several techniques such as adsorption, coagulation, membrane separation and

photocatalysis among others.<sup>24</sup> Owing to simplicity, ease of handling, sensitivity and relative lower cost of operation, adsorption-based methods have commanded greater attention. Thus the development of newer sorbents which can overcome the bottlenecks of existing/conventional adsorbents such as poor selectivity, slow kinetics and stability are desired. Notably majority of the reports using ionic-MOFs as sorbent of dyes have been performed in organic solvents or water at neutral pH.<sup>25</sup> Dyes released as industrial wastewaters can have varying pH and hence the stability and investigation of MOF-based adsorption at varying pH is more pertinent for seeking real-time applicability.

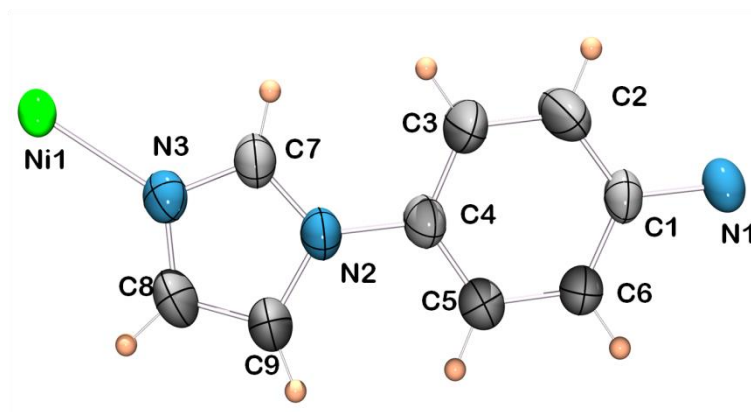
The cationic nature of IPM-MOF-201 and the shape of the pores actuated us to test its trapping ability for anionic dye with linear shape methyl orange (MO). When crystals of IPM-MOF-201 were dipped in an aqueous MO solution (1 mM), the supernatant underwent decolouration over 48 hours, while the colour of the crystals changed to orange during the same period (Appendix 5.39). PXRD patterns and the SEM images of this ion-exchanged phase suggested retention of structural integrity (Appendix 5.40, 5.42). UV-Vis spectra were recorded at increasing time intervals to corroborate with the naked-eye observation. As anticipated the UV-vis spectra of the supernatant showed gradual decrease in intensity with passage of time (Appendix 5.41, 5.56). This behaviour was retained across different pH of 4.01, 10.01 and 12.45 as well (Appendix 5.44). The PXRD patterns corresponding to these phases demonstrated that the ion-exchange at different pH did not affect the structure (Appendix 5.60). To substantiate that the ion-exchange process was charge selective, a cationic dye of similar size viz. methylene blue (MB) was chosen. The colour of the compound did not change upon addition to an aqueous solution of MB and the colour of the supernatant did not undergo any change in intensity (Appendix 5.43), as evidenced using UV-vis experiments. This hypothesis of charge-selectivity was further supported when the compound was added to an equimolar mixture of MO and MB. The colour of the compound turned orange and the UV-vis spectra of the supernatant confirmed the selective uptake of only MO (Appendix 5.45-5.47). A prototype column experiment was executed wherein this charge-selective separation of dyes could be monitored in a short time (Appendix 5.64). Additionally, MB did not entrap even at pH = 10.01, confirming the effect of charge selectivity of the compound (Appendix 5.48). The mixtures of cationic and anionic dyes could be separated over wide pH ranges as well (Appendix 5.65). In addition to charge selectivity, we observed that the ion-exchange was size selective. A bulky dye viz. bromothymol blue was chosen for this study and no noticeable change was observed in the time-dependent UV-vis spectra (Appendix 5.53). For real-time applicability, recycling of the adsorbent is highly desired. The cycling efficiency of IPM-MOF-201 for MO dye was checked over 3 cycles and the performance was found to be retained (Appendix 5.63).

To extent this behaviour even further, we checked the efficacy of IPM-MOF-201 to entrap anionic dyes of similar sizes viz. Indigo carmine (IC) and alizarin red S (ARS). It has been observed in the literature that

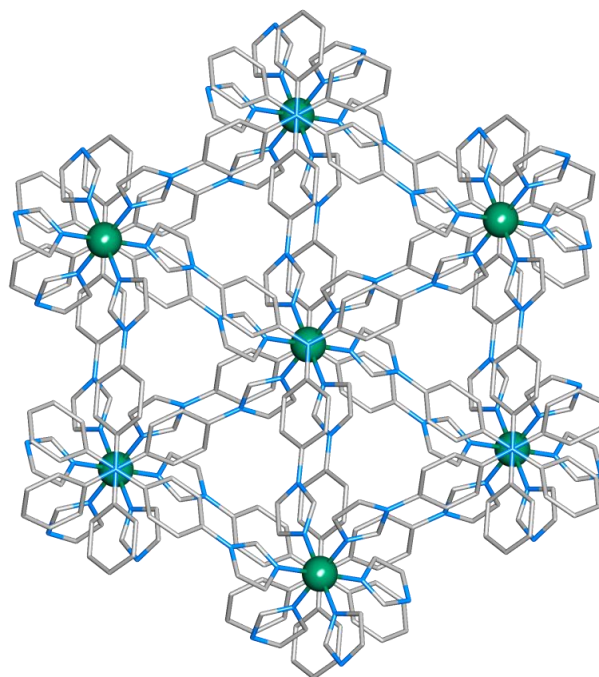
the dye molecules with dimensions between the minimum and maximum pore windows in porous frameworks can undergo ion-exchange.<sup>25</sup> Thus linear ions having suitable dimensions can be expected to undergo uptake. In both the cases the colour of the compound changed drastically upon addition of the MOF to aqueous solution of the dyes (Appendix 5.49). PXRD patterns for these phases suggested retention of the structural integrity without change to the overall framework (Appendix 5.50). Like the previous case, we recorded time-dependent UV-Vis spectra at different pH and a similar pattern was observed for both IC and ARS (Appendix 5.51, 5.54). Crystals of IPM-MOF-201 were added to an equimolar mixture of two blue dyes (IC and MB). As anticipated, only the peak corresponding to IC underwent decrement without any noticeable change to the peak for MB (Appendix 5.55). As a control experiment, time-dependent UV-vis spectra of blank dye solutions were recorded to validate the ion-exchange process (Appendix 5.52). The anionic dye capture tendency was retained even for dye molecules with carboxylic acid (methyl red - MR) and phenolic functionalities (4-phenylazophenol - PAP) (Appendix 5.57, 5.59). As observed previously, the structural integrity was not perturbed during the exchange at different pH (Appendix 5.58, 5.60). For the dyes studied in this work, the ion-exchange process was also observed under high basic conditions at pH=14 (Appendix 5.61-5.62). Figure 3 summarizes the naked-eye dye capture process at different pH along-with the corresponding morphology of the compound. These results suggest that the feature of differential colour of the dyes at different pH is carried unabatedly into the MOF-encapsulated phases as well, making this MOF as a potentially useful marker for capture of dyes at specific pH.

## 5.4 Conclusions

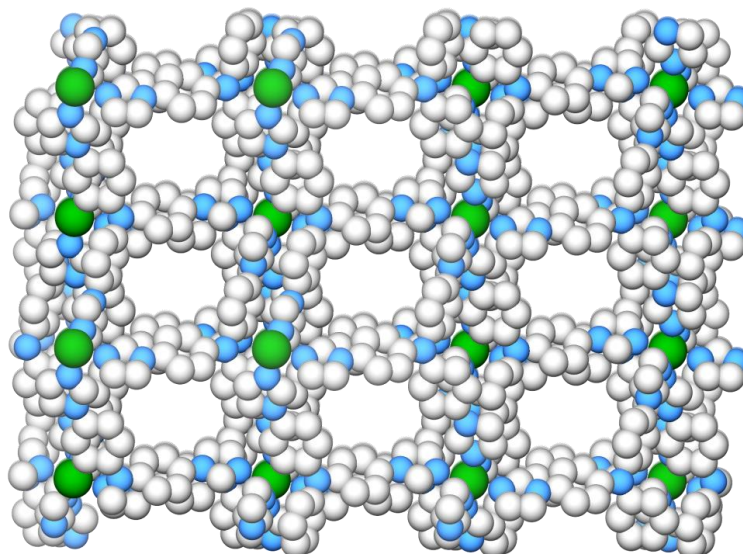
In summary, we have developed a hydrolytically stable cationic MOF which exhibits remarkably high resistance across wide pH range. To the best of our knowledge this is an extremely rare example of a porous MOF exhibiting base resistance and an even rarer case of a porous cationic MOF retaining structural integrity even under high basic pH. Control experiments were executed to validate the choice of the building blocks and the design strategy. The stability and the accessible porosity were harnessed for the function of trapping small organic dyes over wide pH range. Notably, hitherto systematic investigation of dye capture over wide pH range has not been investigated systematically in the literature of MOFs. We believe that the results obtained from this work will contribute significantly to the development of design principles for ionic-MOFs which offer stability over varying chemical environments.

**5.5 Appendix Section**

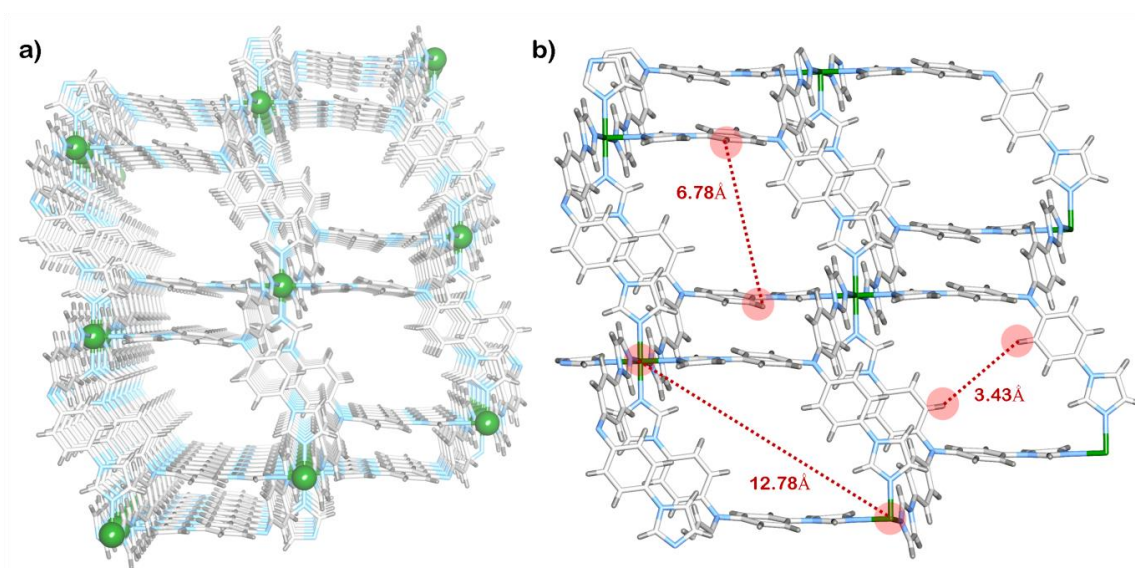
**Appendix 5.1:** ORTEP diagram of asymmetric unit of **IPM-MOF-201** in thermal ellipsoids.



**Appendix 5.2:** Appendix 5.howing packing of **IPM-MOF-201** along crystallographic *c*-axis. (Hydrogen atoms and disordered anions have been omitted for clarity, colour: Gray - C, Blue - N, Green - Ni).

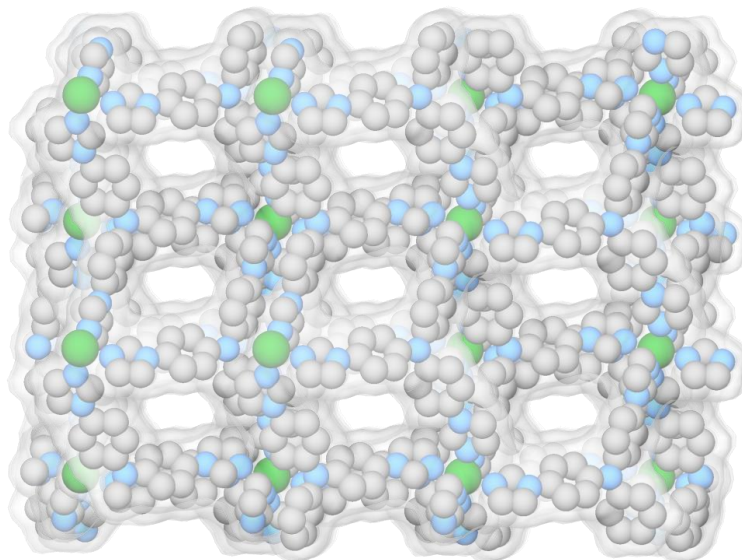


**Appendix 5.3:** Packing diagram of **IPM-MOF-201** showing porous channel. (Hydrogen atoms and disordered anions have been omitted for clarity, colour: Gray - C, Blue - N, Green - Ni).

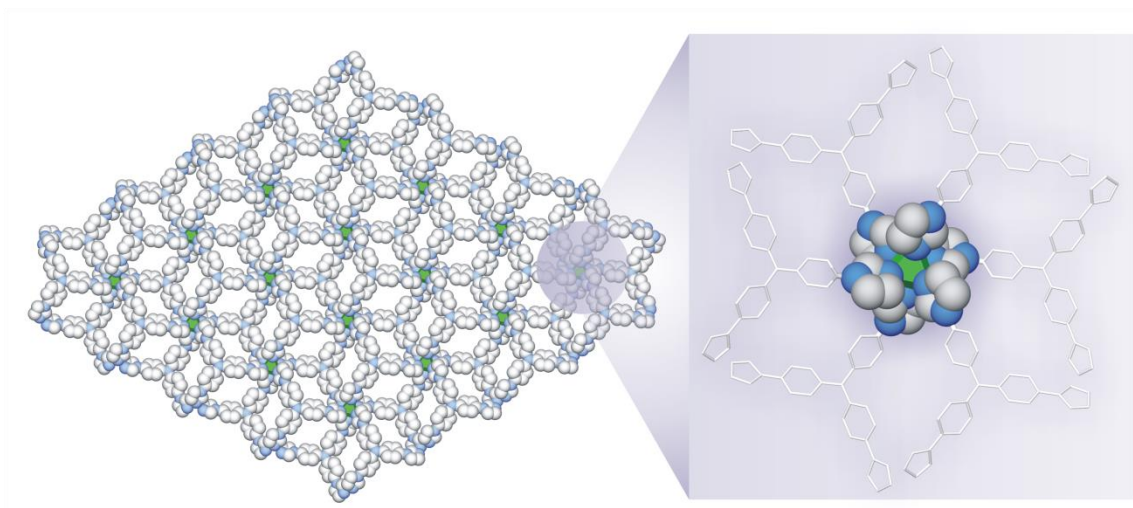


**Appendix 5.4:** a) Packing diagram of **IPM-MOF-201** showing porous channels, b) View of a single net adopted from the packing diagram showing the dimensions of the pore. The dimensions have included the Van der Waal radii of the atoms chosen for measurement. The measurements suggest that the  $d_{\min}$  and  $d_{\max}$  for the compound is 3.43Å and 12.78Å respectively. (Disordered anions have been omitted for clarity, colour: Light Gray - C, Dark Gray - H, Blue - N, Green - Ni).

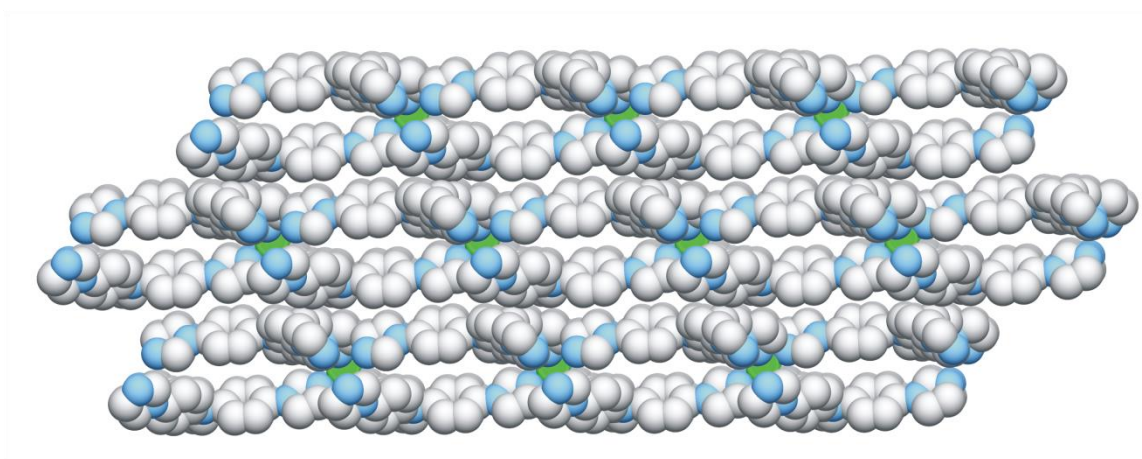




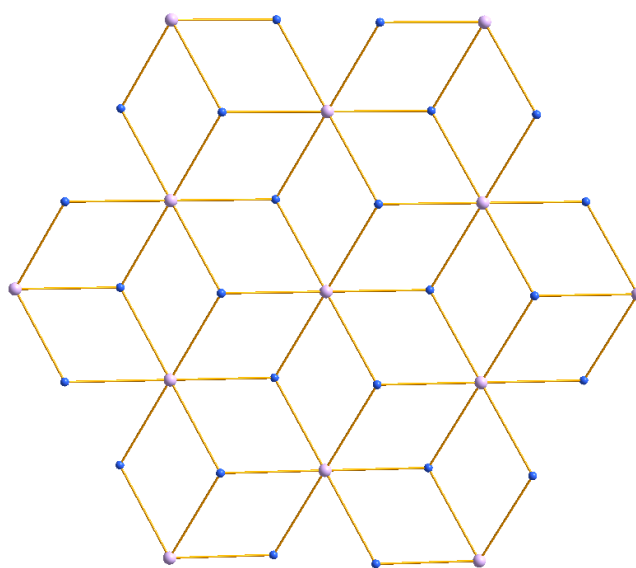
**Appendix 5.5:** Packing diagram of **IPM-MOF-201**. (Hydrogen atoms and disordered anions have been omitted for clarity, colour: Gray - C, Blue - N, Green - Ni).



**Appendix 5.6:** Packing diagram of **IPM-MOF-201** and zoomed view of the coordination environment of the metal node. (Hydrogen atoms and disordered anions have been omitted for clarity, colour: Gray - C, Blue - N, Green - Ni).

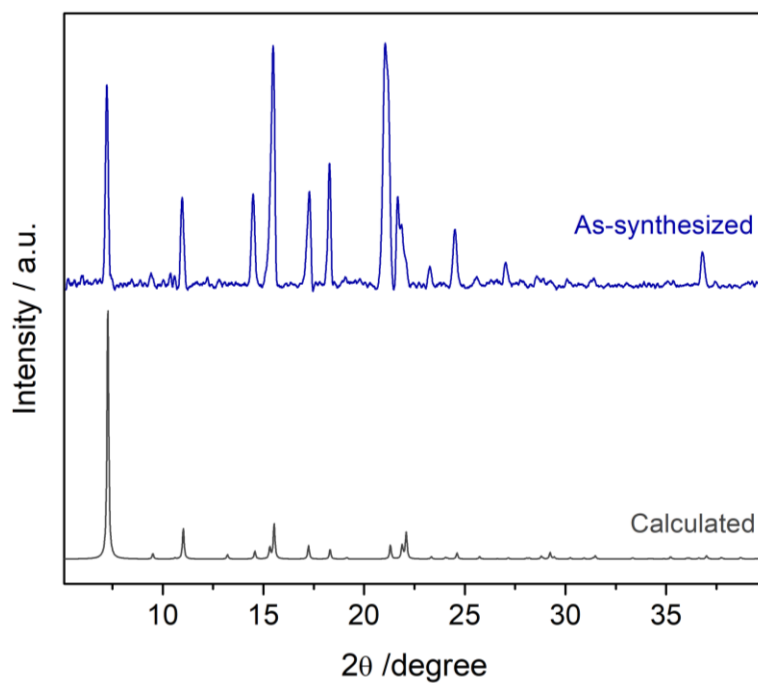


**Appendix 5.7:** Packing diagram of **IPM-MOF-201** showing depicting the metal nodes are buried in the 2D layer stacking arrangement. (Hydrogen atoms and disordered anions have been omitted for clarity, colour: Gray - C, Blue - N, Green - Ni).

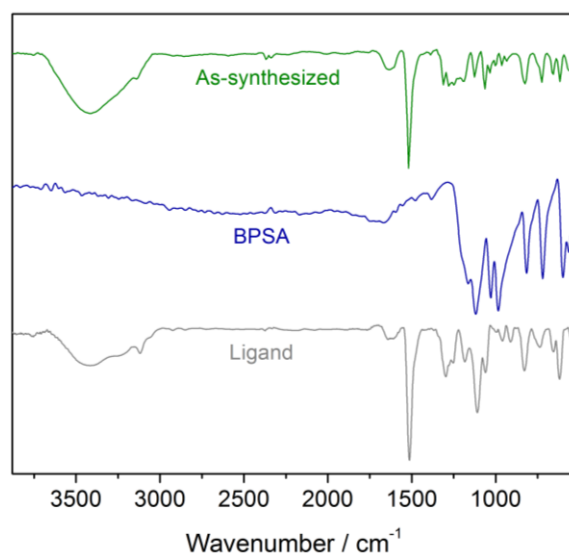


**Appendix 5.8:** Simplified topological representation of **IPM-MOF-201** having kgd topology.

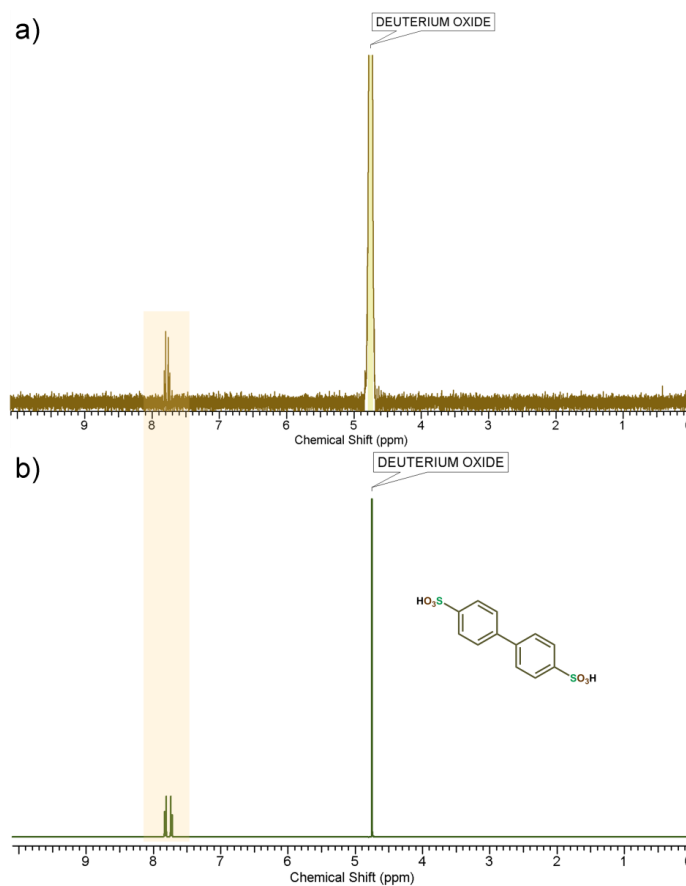




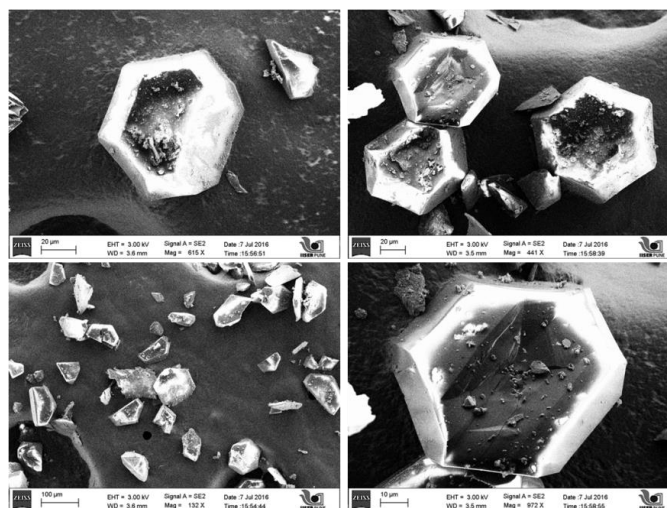
**Appendix 5.9:** Powder X-ray diffraction patterns of **IPM-MOF-201** - calculated (gray), as-synthesized (blue).



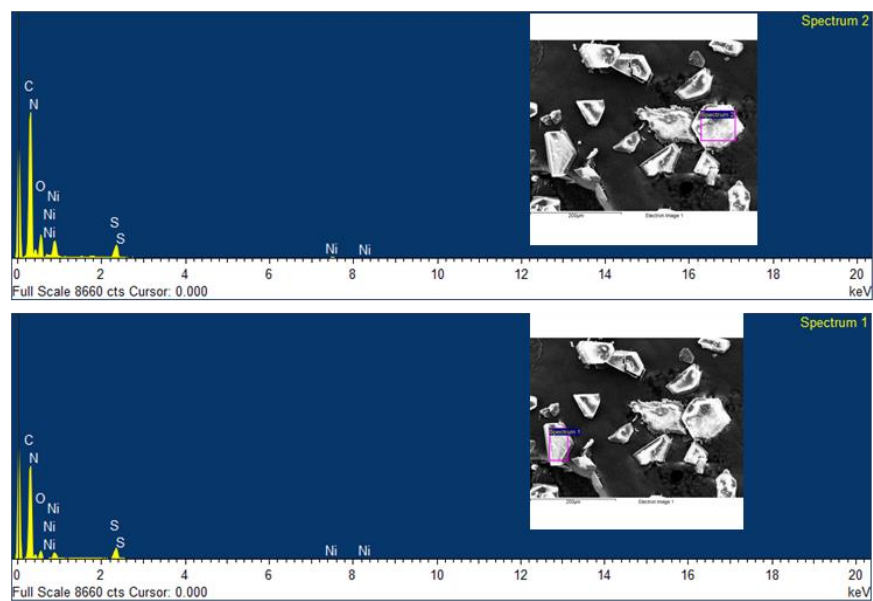
**Appendix 5.10:** FT-IR spectra for compound **IPM-MOF-201** (green), BPSA (blue) and ligand (gray).



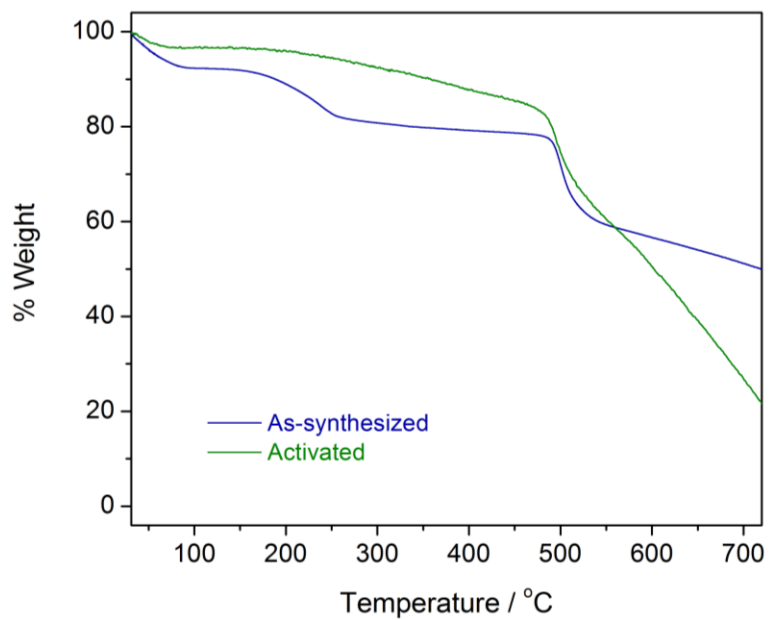
**Appendix 5.11:** a)  $^1\text{H-NMR}$  after digesting **IPM-MOF-201** in  $\text{D}_3\text{PO}_4/\text{D}_2\text{O}$  followed by neutralization with  $\text{NaOD}$ . b)  $^1\text{H-NMR}$  of commercially available BPSA in  $\text{D}_2\text{O}$ .



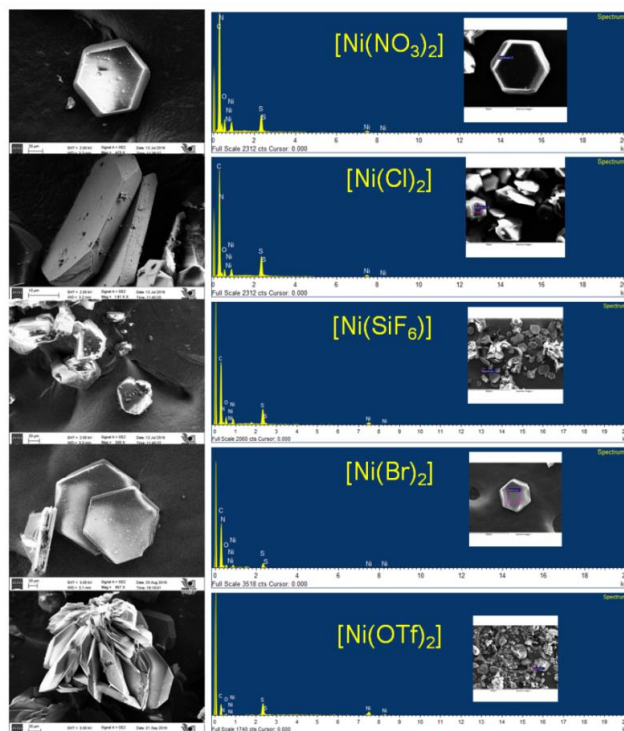
**Appendix 5.12:** FESEM images for compound **IPM-MOF-201**.



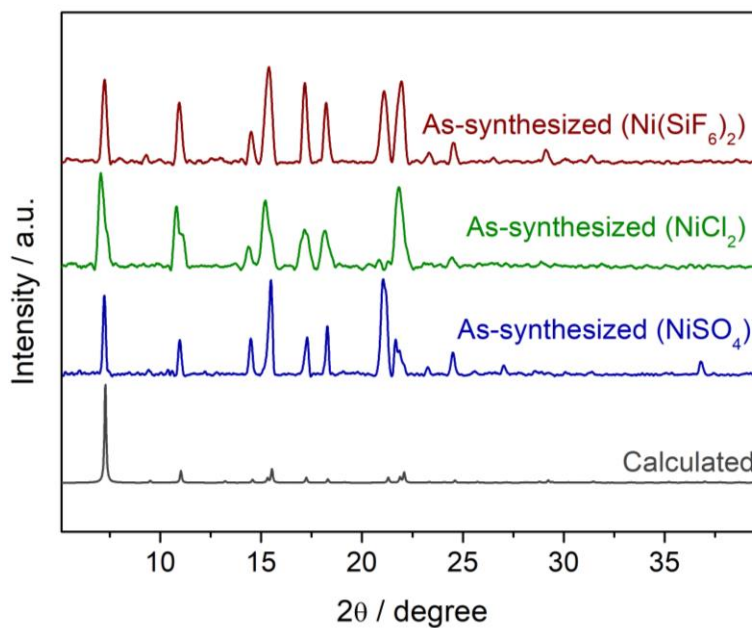
**Appendix 5.13:** EDX spectra for compound IPM-MOF-201.



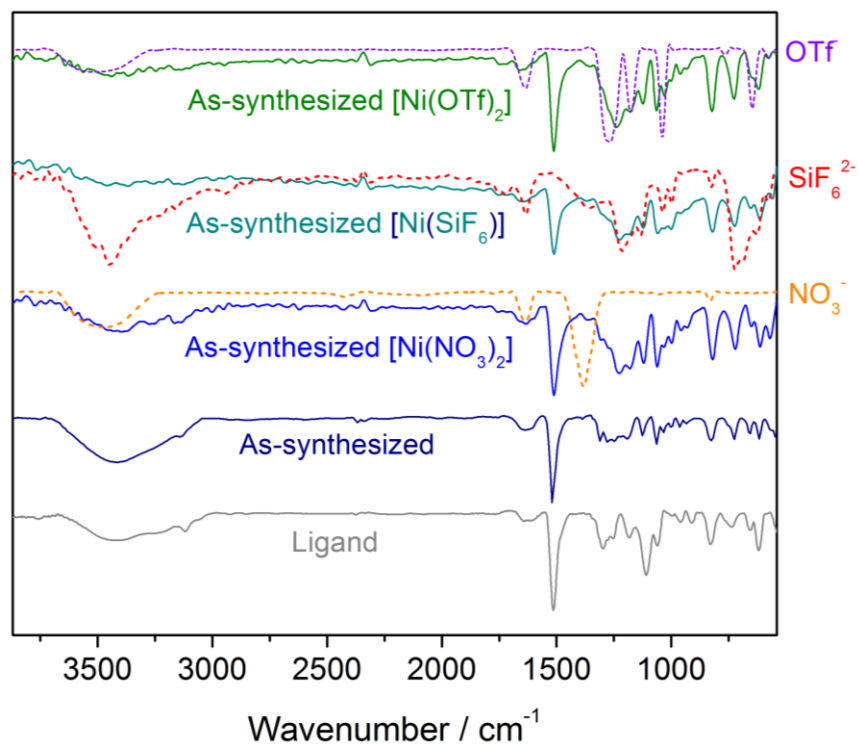
**Appendix 5.14:** TGA profiles for compound IPM-MOF-201.



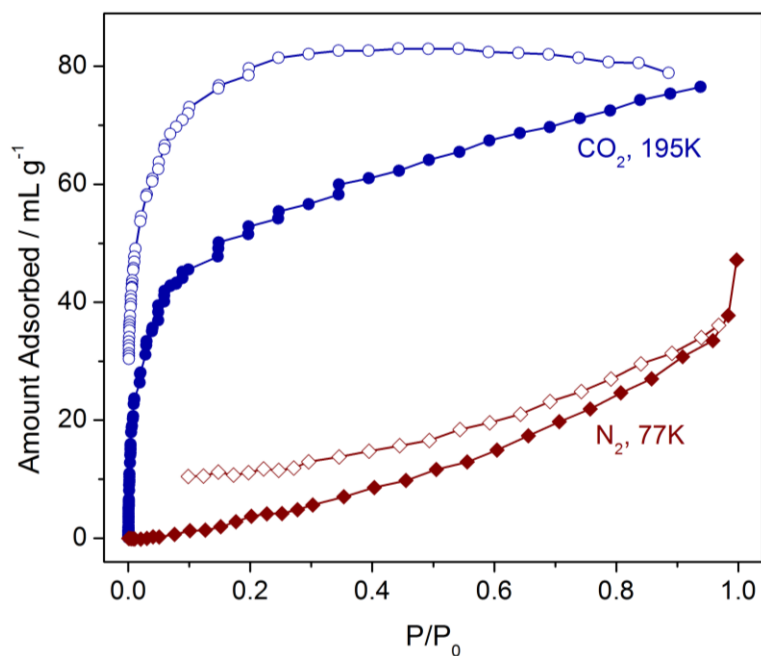
**Appendix 5.15:** EDX spectra for compounds synthesized using different salts of  $\text{Ni}^{2+}$  and BPSA (excess).



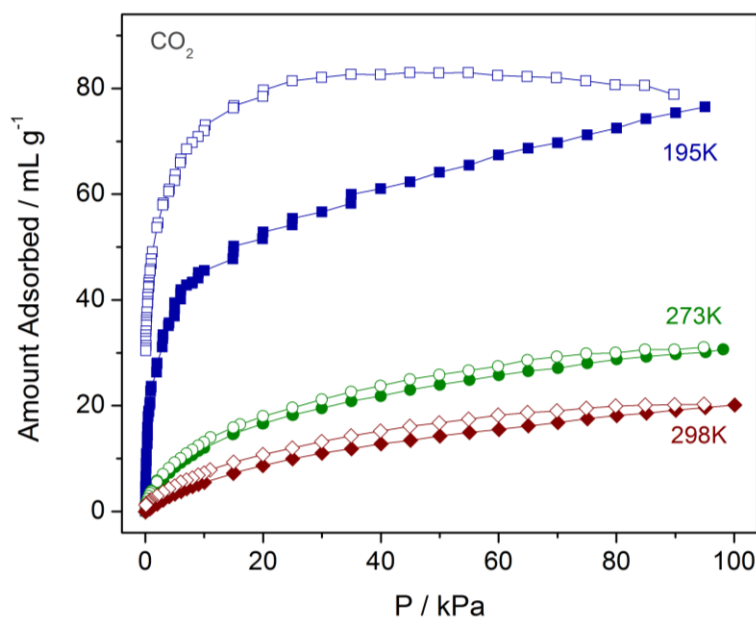
**Appendix 5.16:** Powder X-ray diffraction patterns for compounds synthesized using different salts of  $\text{Ni}^{2+}$  and BPSA (excess).



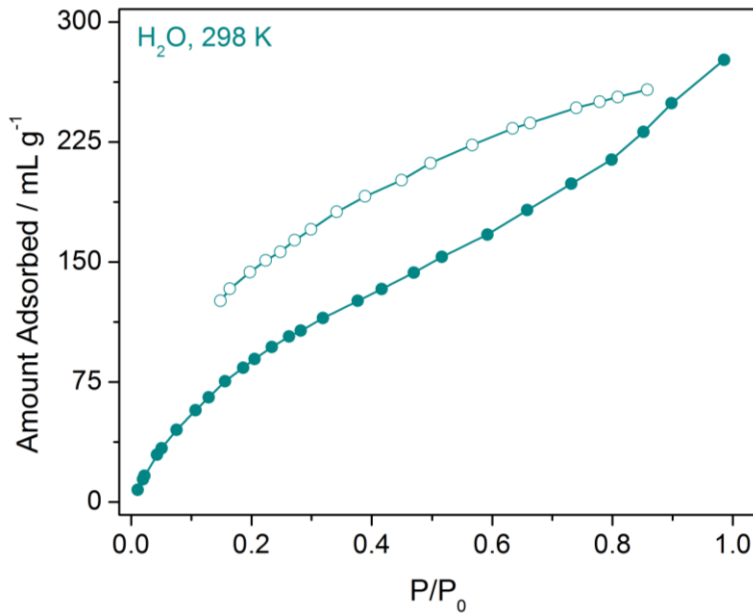
**Appendix 5.17:** FT-IR spectra for compounds synthesized using different salts of  $\text{Ni}^{2+}$  and BPSA (excess). Dotted lines represent spectra for salts of respective anions.



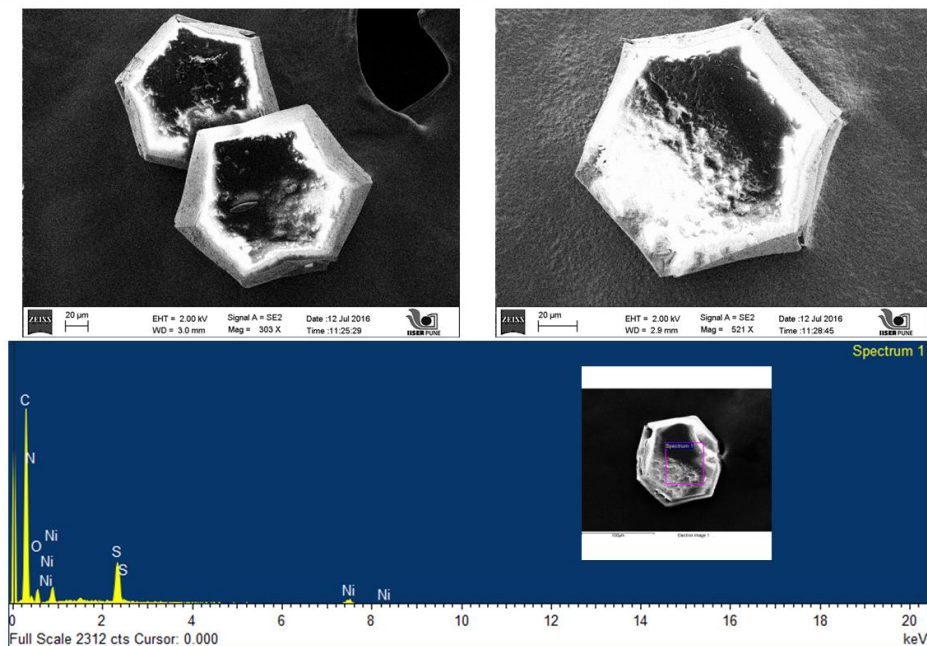
**Appendix 5.18:** Low temperature gas adsorption isotherms for compound IPM-MOF-201. Closed symbols denote adsorption while open symbols denote desorption.



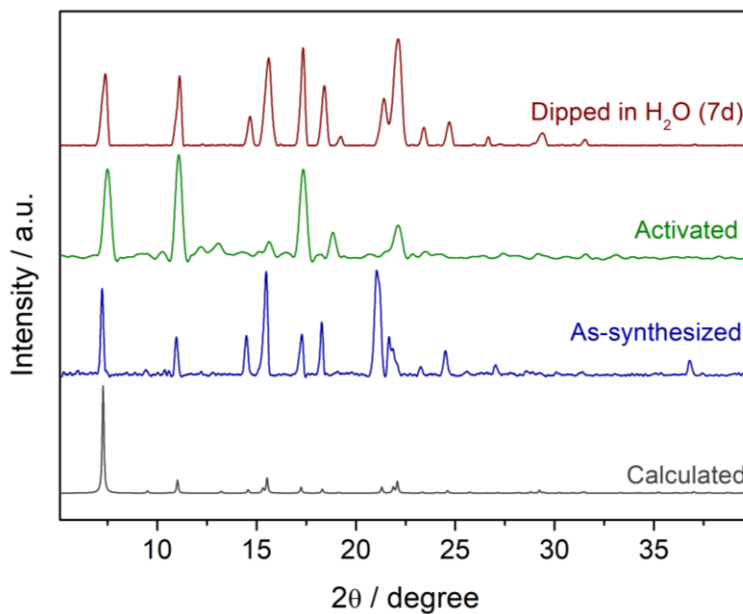
**Appendix 5.19:** CO<sub>2</sub> adsorption isotherms for compound **IPM-MOF-201** at different temperatures; 195K (blue), 273K (green), 298K (wine red). Closed symbols denote adsorption while open symbols denote desorption.



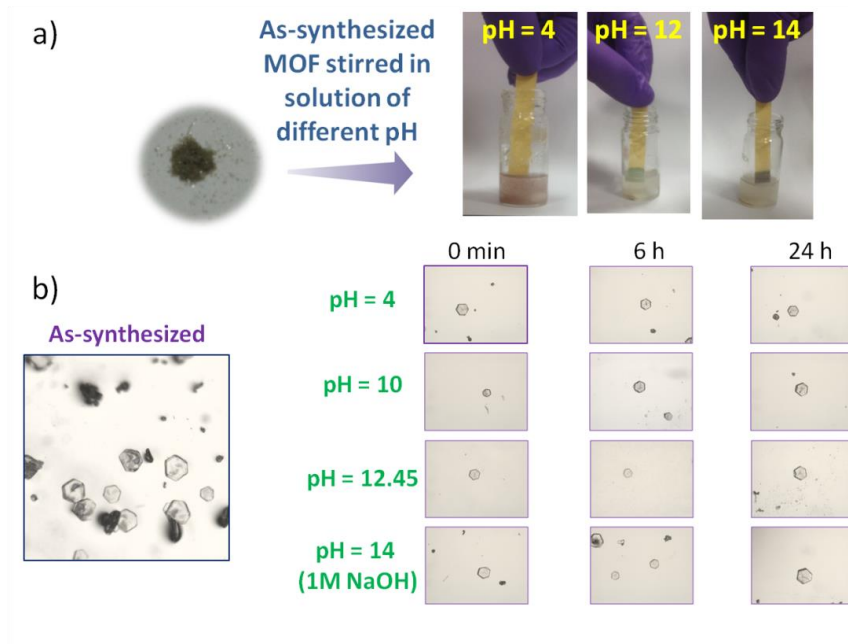
**Appendix 5.20:** Water adsorption isotherm for compound **IPM-MOF-201** at 298K. Closed symbols denote adsorption while open symbols denote desorption.



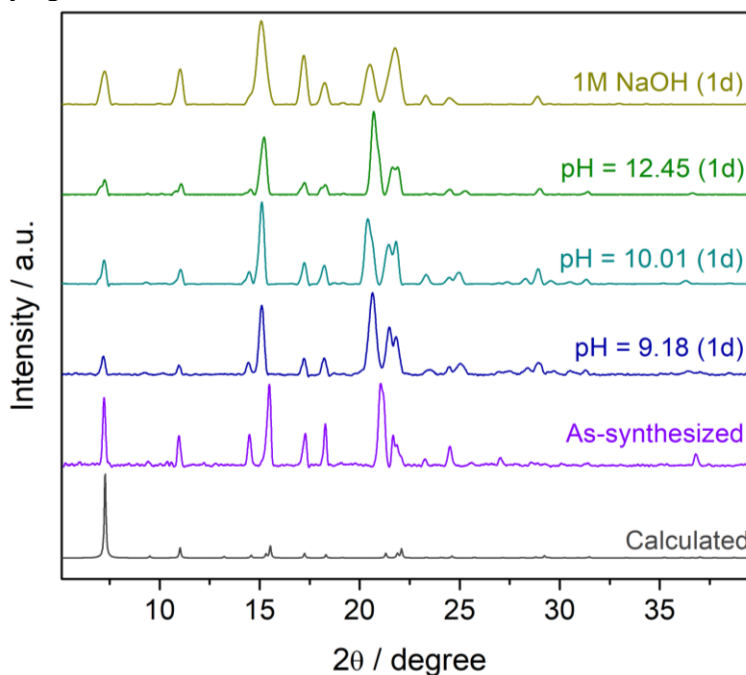
**Appendix 5.21:** FESEM images (top) and EDX spectra (below; inset sample chosen for recording the EDX spectra) for compound **IPM-MOF-201** dipped in D.I. water for 1 month.



**Appendix 5.22:** PXRD patterns for calculated (grey), as-synthesized (blue), activated (green) and water-dipped phases (wine red).

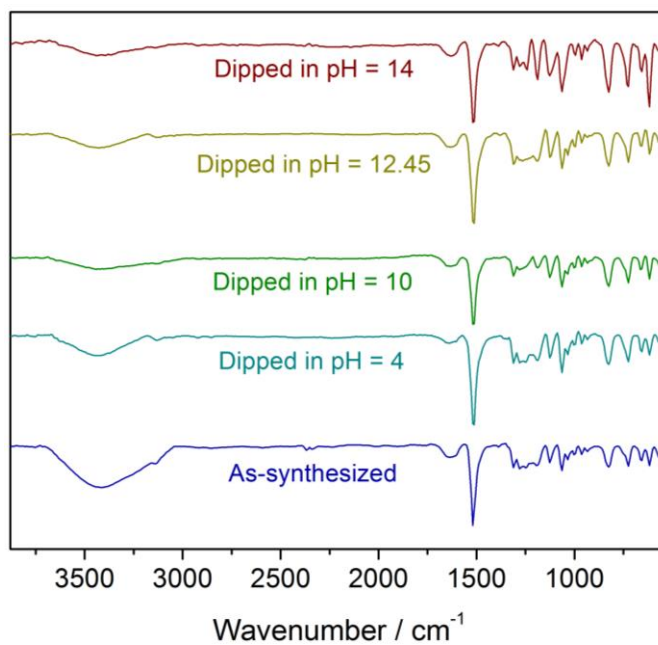


**Appendix 5.23:** a) Photographs showing the experiment performed to check pH resistance, b) photographs taken under microscope for as-synthesized phase and the crystals upon dipping in solutions of different pH at varying time intervals.

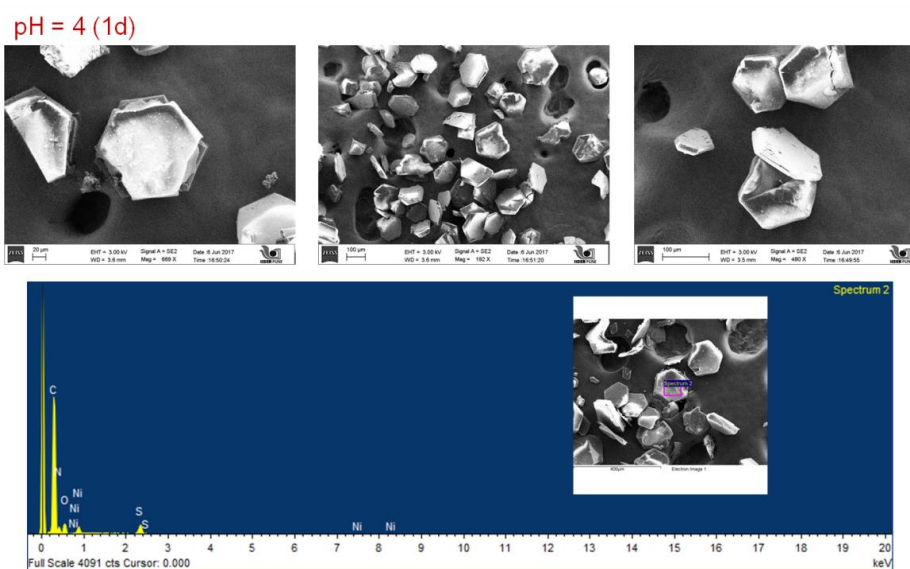


**Appendix 5.24:** Powder x-ray diffractions patterns for calculated (grey), as-synthesized (purple), and compound IPM-MOF-201 dipped in different pH conditions.

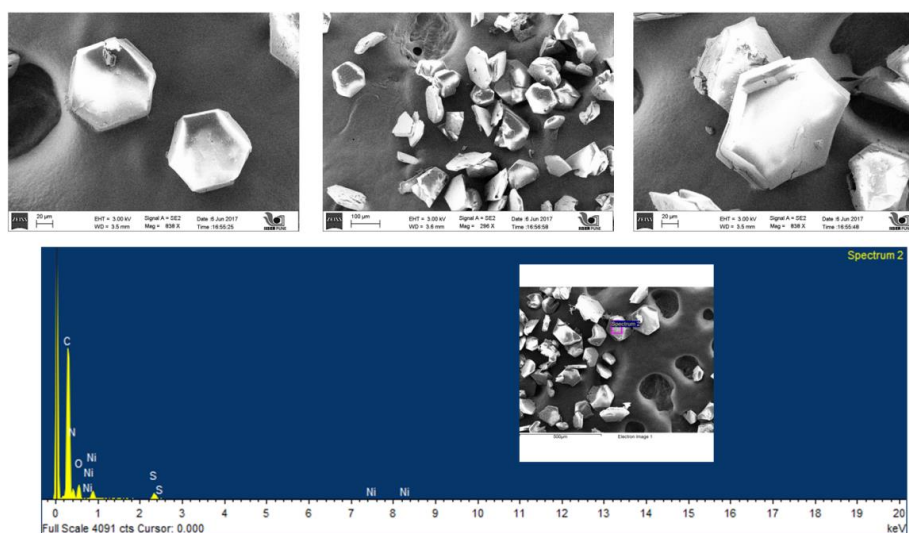




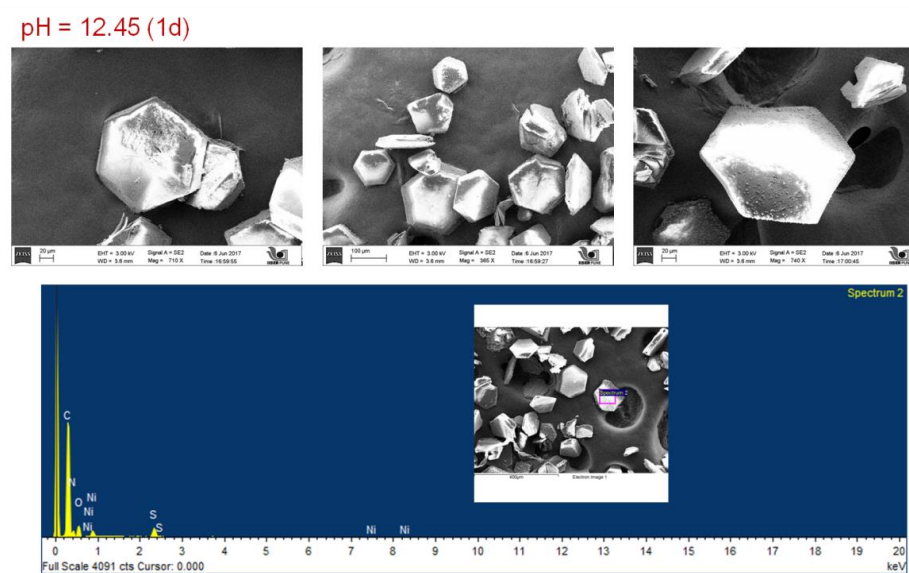
**Appendix 5.25:** FT-IR spectra for **IPM-MOF-201** dipped in different pH solutions.



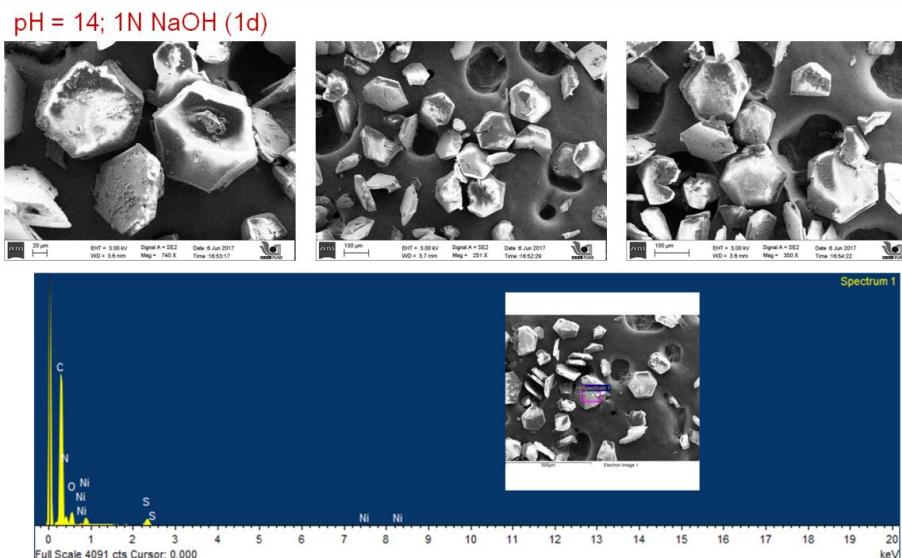
**Appendix 5.26:** FESEM images of compound **IPM-MOF-201** dipped in solution of pH = 4 & corresponding EDX profile.



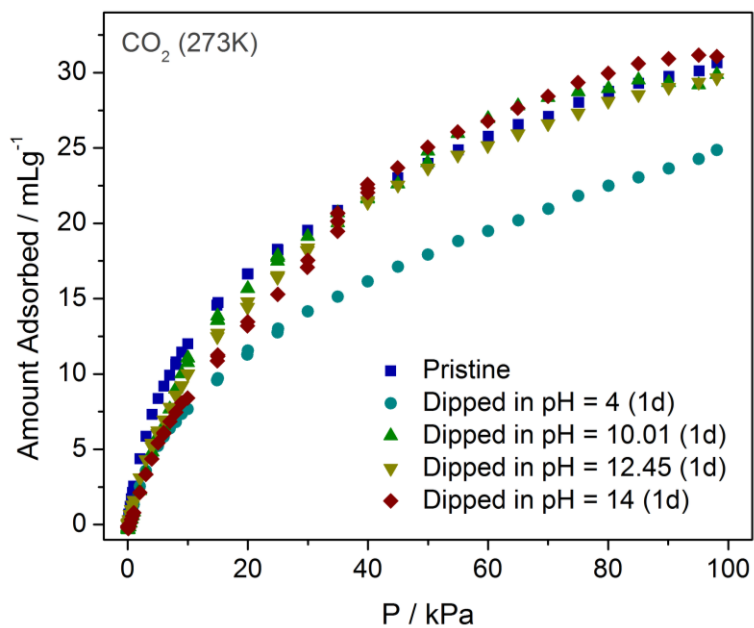
**Appendix 5.27:** FESEM images of compound **IPM-MOF-201** dipped in solution of pH = 10.01 & corresponding EDX profile.



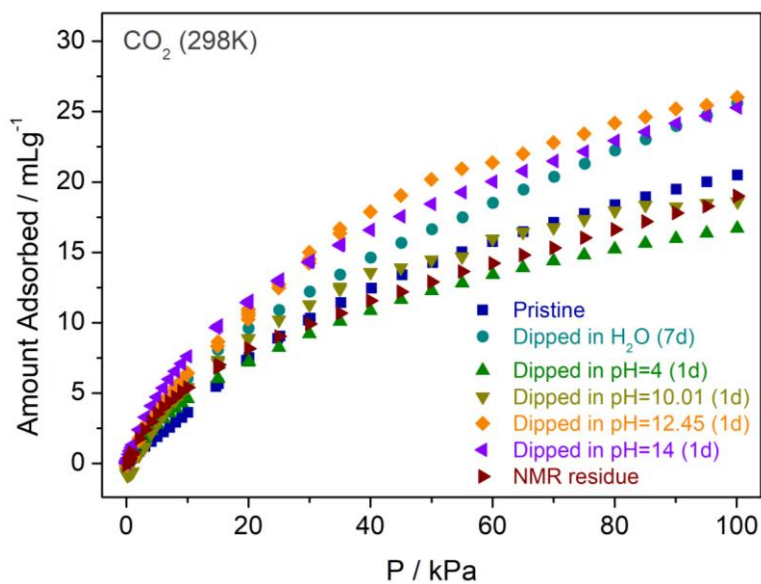
**Appendix 5.28:** FESEM images of compound **IPM-MOF-201** dipped in solution of pH = 12.45 & corresponding EDX profile.



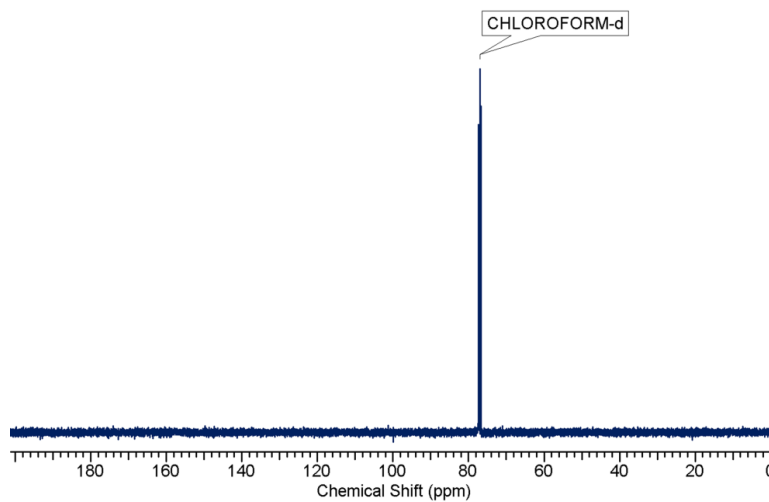
**Appendix 5.29:** FESEM images of compound **IPM-MOF-201** dipped in solution of pH = 14 (1N NaOH) & corresponding EDX profile.



**Appendix 5.30:** CO<sub>2</sub> adsorption isotherms at 273K for compound **IPM-MOF-201** dipped in different conditions.

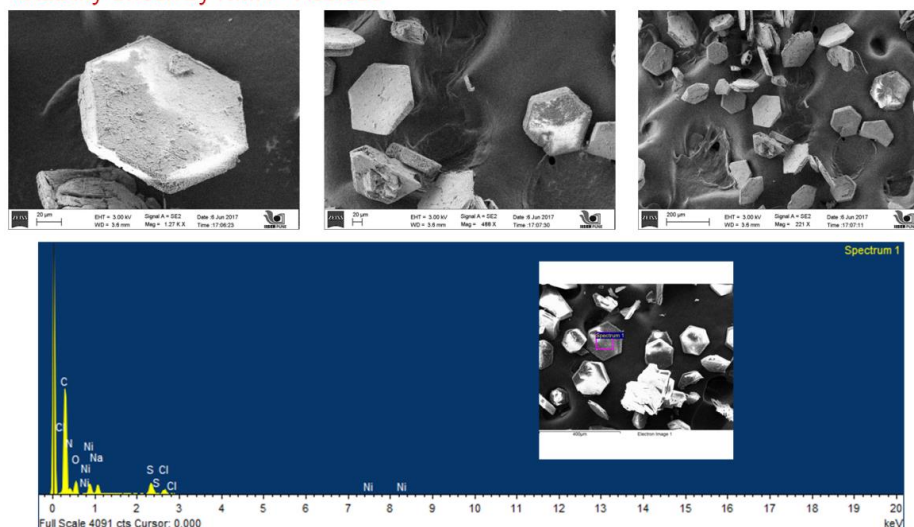


**Appendix 5.31:** CO<sub>2</sub> adsorption isotherms at 298K for compound **IPM-MOF-201** dipped in different conditions.

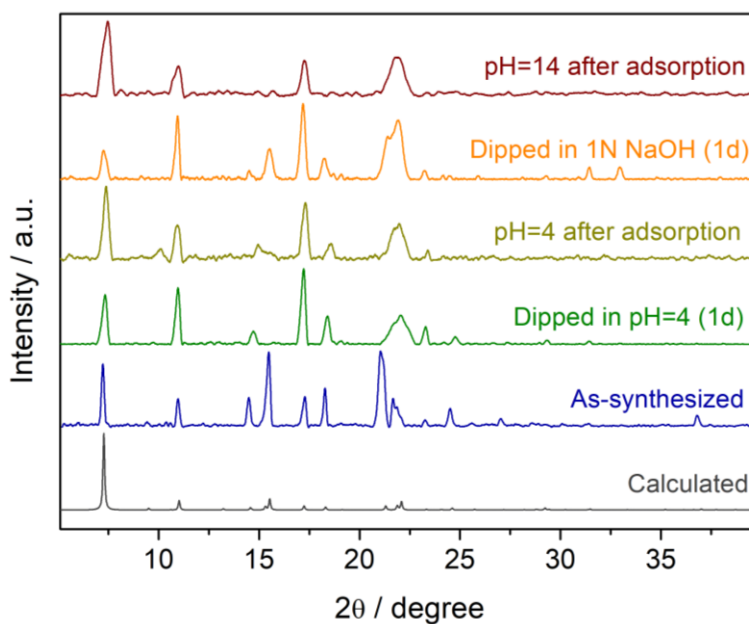


**Appendix 5.32:** <sup>13</sup>C-NMR of the supernatant obtained after treating **IPM-MOF-201** in solution of NaOD/D<sub>2</sub>O for 1 day.

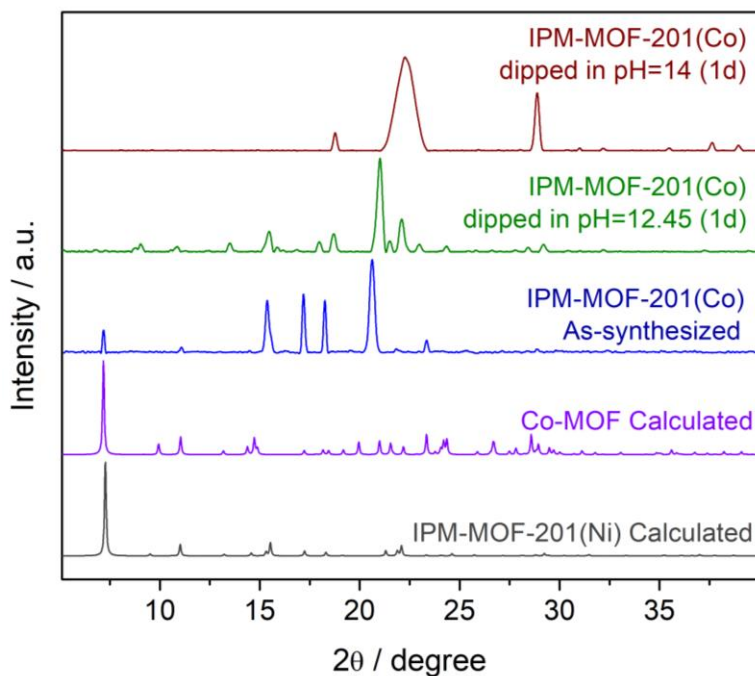
## Stability Check by NMR - Residue



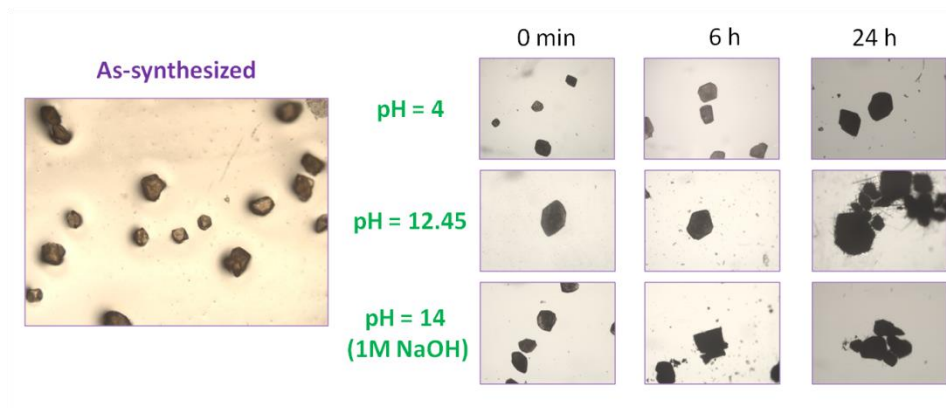
**Appendix 5.33:** FESEM images of compound **IPM-MOF-201** & corresponding EDX profile after performing the NMR characterization experiment.



**Appendix 5.34:** PXRD patterns for the pH dipped conditions and the post-adsorption phases.

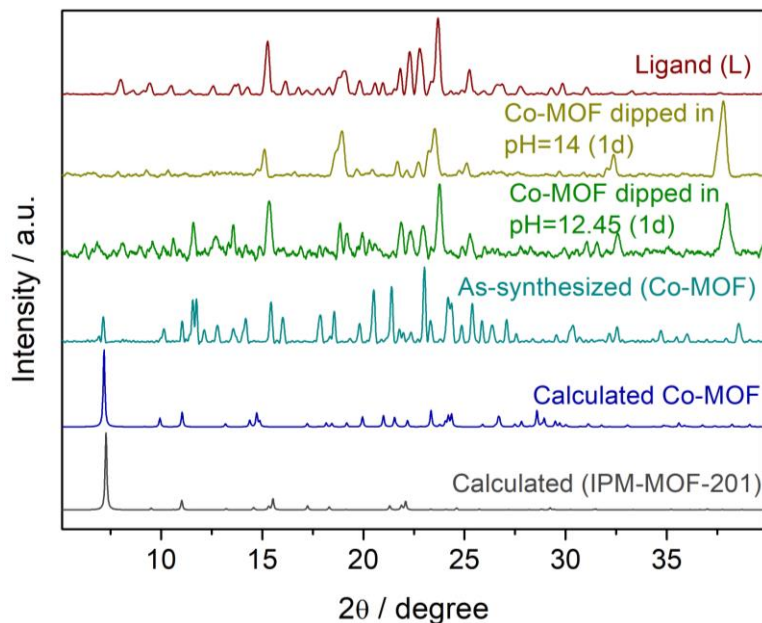


**Appendix 5.35:** Powder diffraction patterns for compound **IPM-MOF-201(Ni)** (calculated, grey), Co-MOF (calculated, purple) [calculated pattern adapted from ref. 2], as-synthesized **IPM-MOF-201(Co)** (blue) and phase dipped in pH=12.45 (green) and pH=14 (wine red).

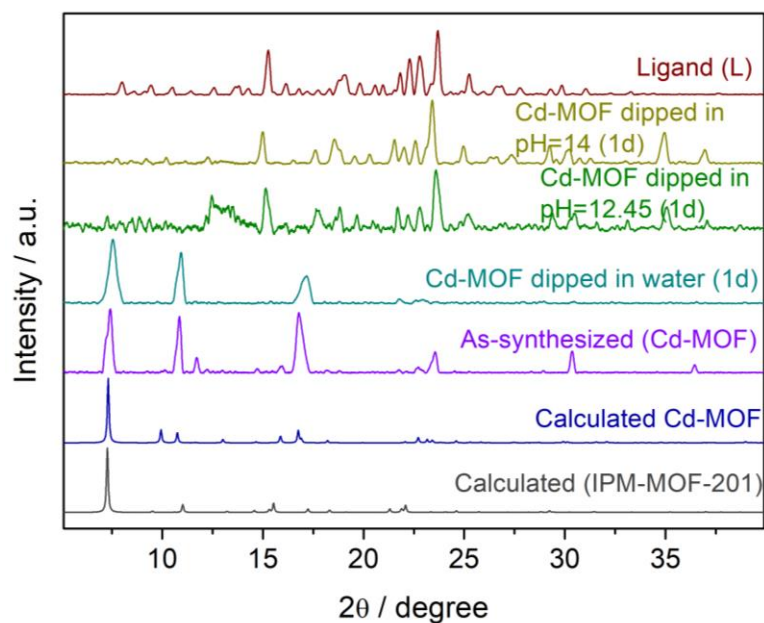


**Appendix 5.36:** Photographs of Co-IPM-MOF when dipped in pH solutions of 4, 12.45 and 14 at different time intervals.

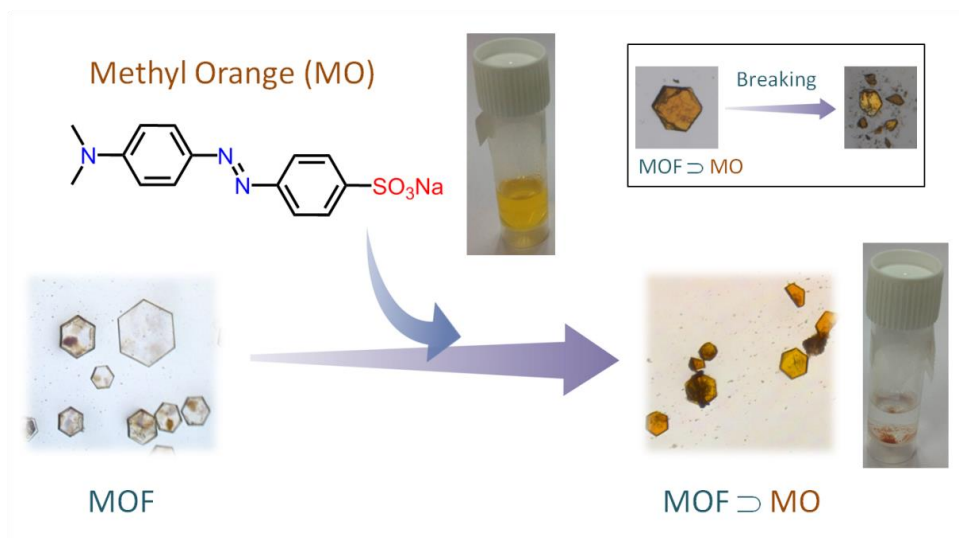




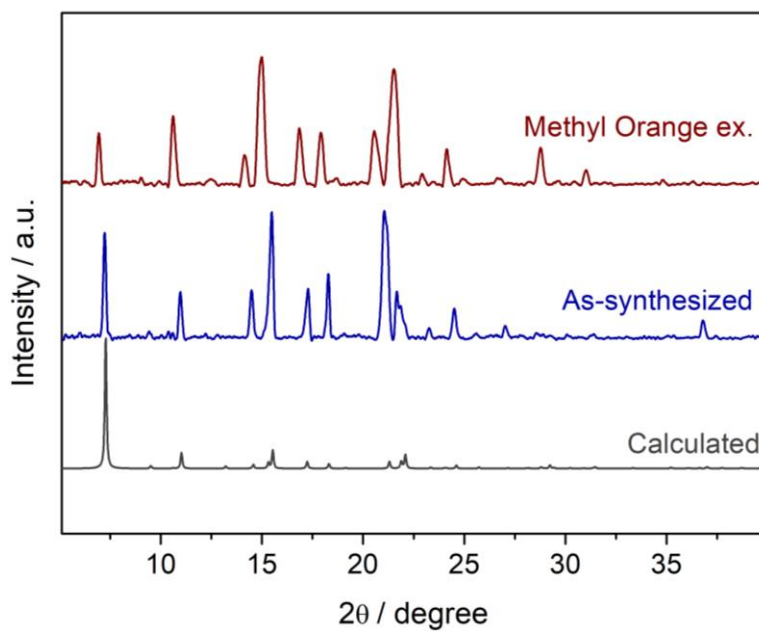
**Appendix 5.37:** Powder diffraction patterns for compound **IPM-MOF-201(Ni)** (calculated, grey), Co-MOF (calculated, blue) [calculated pattern adapted from ref. 19b], as-synthesized Co-MOF (cyan), phase dipped in pH=12.45 (green) and pH=14 (yellow), and ligand (wine red).



**Appendix 5.38:** Powder diffraction patterns for compound **IPM-MOF-201(Ni)** (calculated, grey), Cd-MOF (calculated, blue) [calculated pattern adapted from ref. 19e], as-synthesized Cd-MOF (purple), dipped in water (cyan), phase dipped in pH=12.45 (green) and pH=14 (yellow), and ligand (wine red).

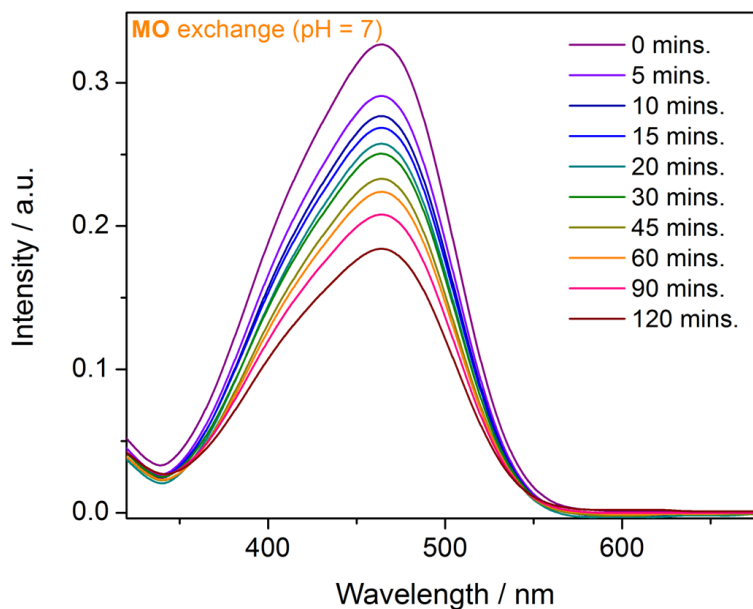


**Appendix 5.39:** Schematic illustration of dye inclusion (Methyl Orange - MO) in compound **IPM-MOF-201**. The corresponding photographs of the crystals under the microscope have been shown alongside. (Inset) The photograph of MO-exchanged crystals and the fragments after breaking it randomly.

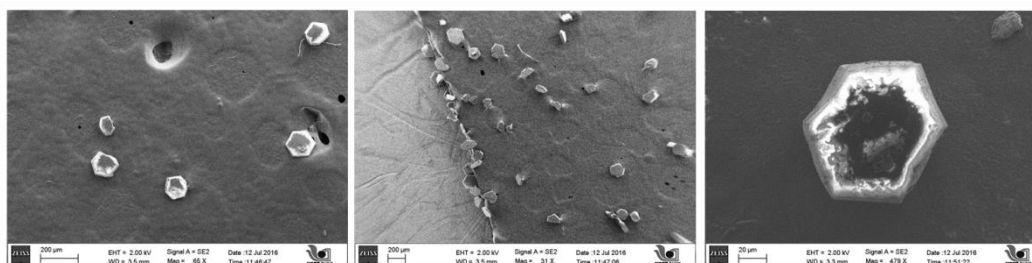


**Appendix 5.40:** Powder diffraction patterns for compound **IPM-MOF-201** (calculated, grey), as-synthesized (blue) and MO-exchange phase (wine red).

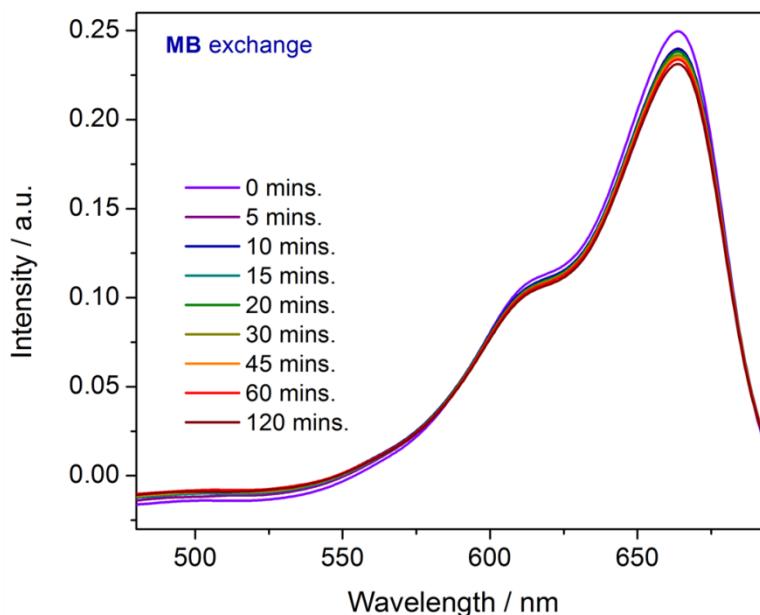




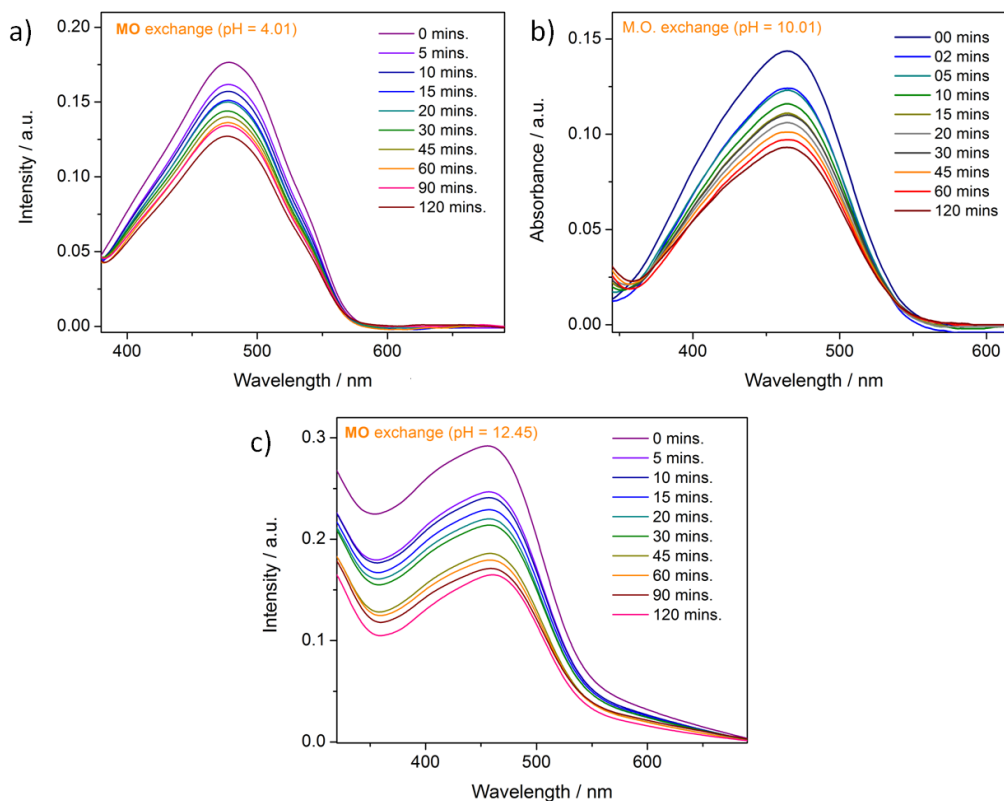
**Appendix 5.41:** UV-Vis spectra of the supernatant aqueous MO solution after addition of compound **IPM-MOF-201** at different time intervals.



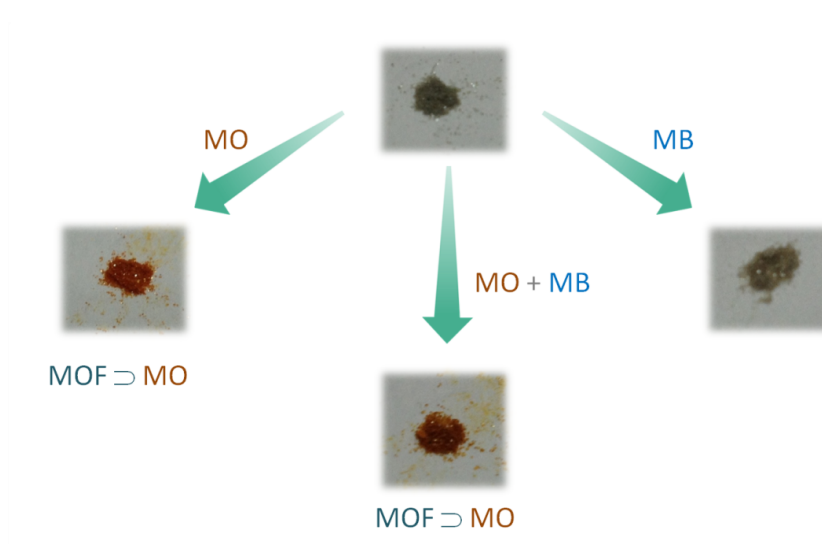
**Appendix 5.42:** FESEM images of compound **IPM-MOF-201** dipped in aqueous MO solution.



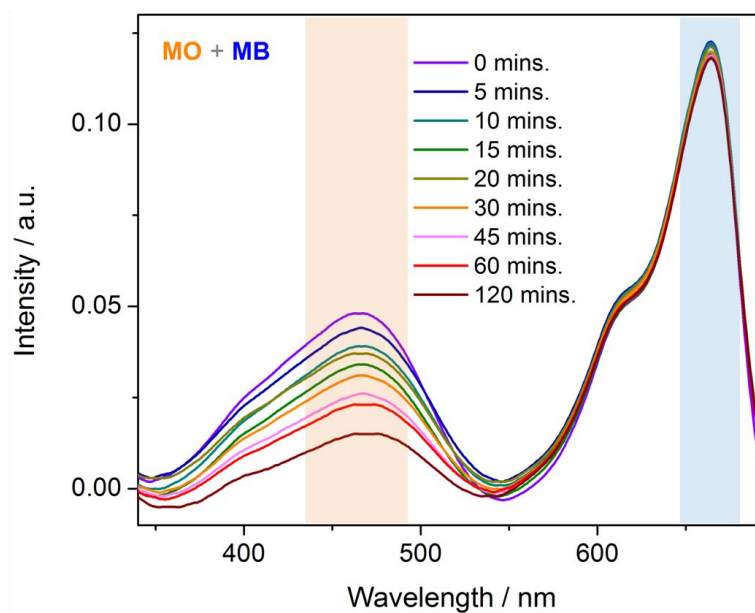
**Appendix 5.43:** UV-Vis spectra of the supernatant aqueous MB solution after addition of compound IPM-MOF-201 at different time intervals.



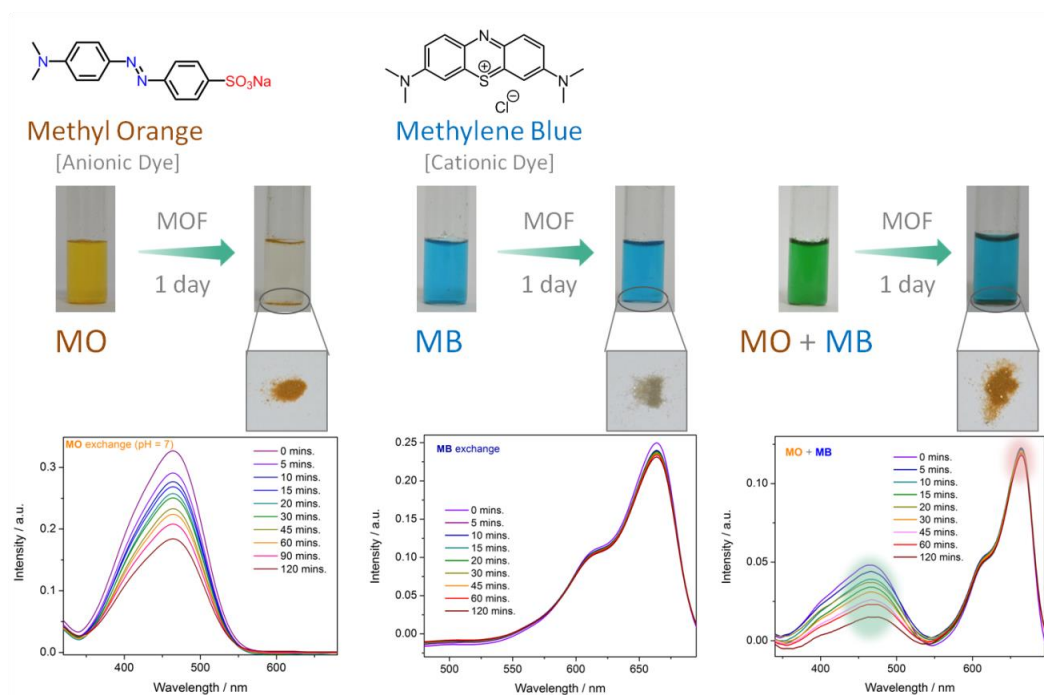
**Appendix 5.44:** UV-Vis spectra of the supernatant MO solution having pH a) 4.01, b) 10.01 and c) 12.45, after addition of compound IPM-MOF-201 to respective phases at different time intervals.



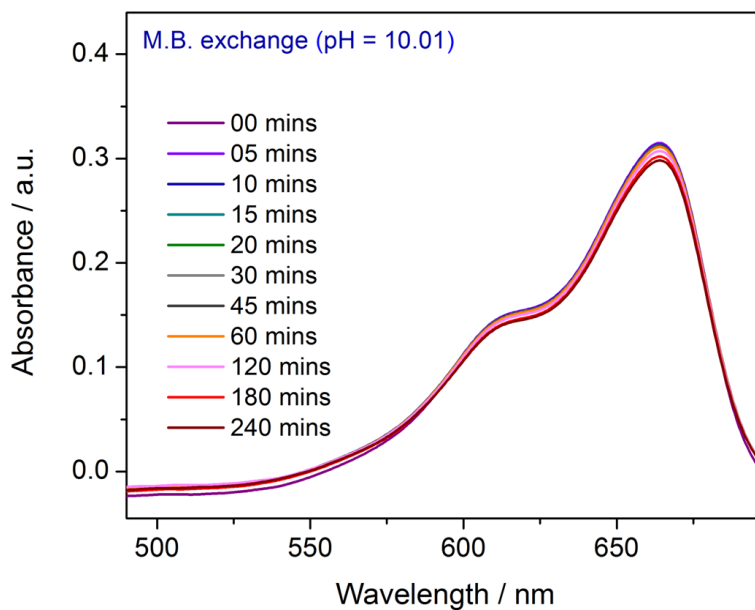
**Appendix 5.45:** Photographs showing preferential capture of anionic dye over cationic dye, even in presence of equimolar mixture of both dyes.



**Appendix 5.46:** UV-Vis spectra of the supernatant solution of equimolar mixture of MB & MO after addition of compound **IPM-MOF-201** recorded at different time intervals.



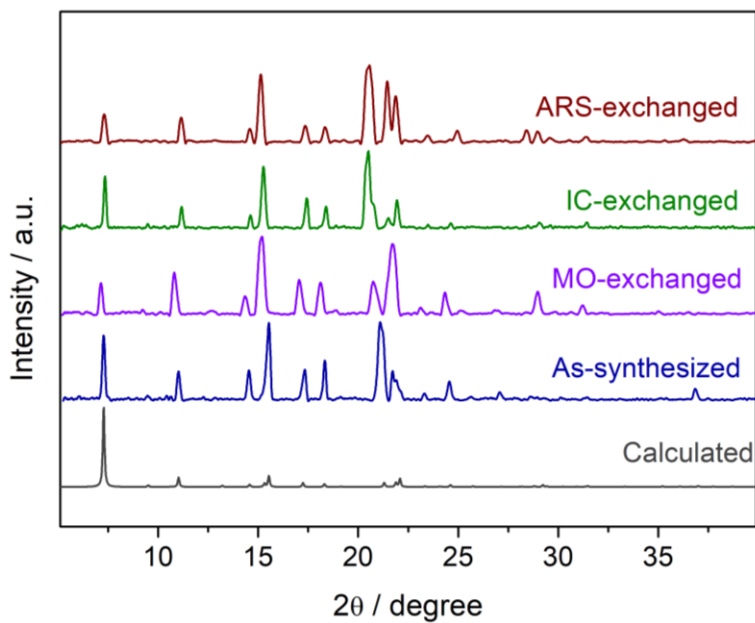
**Appendix 5.47:** Overall representation of the charge selective dye capture by IPM-MOF-201.



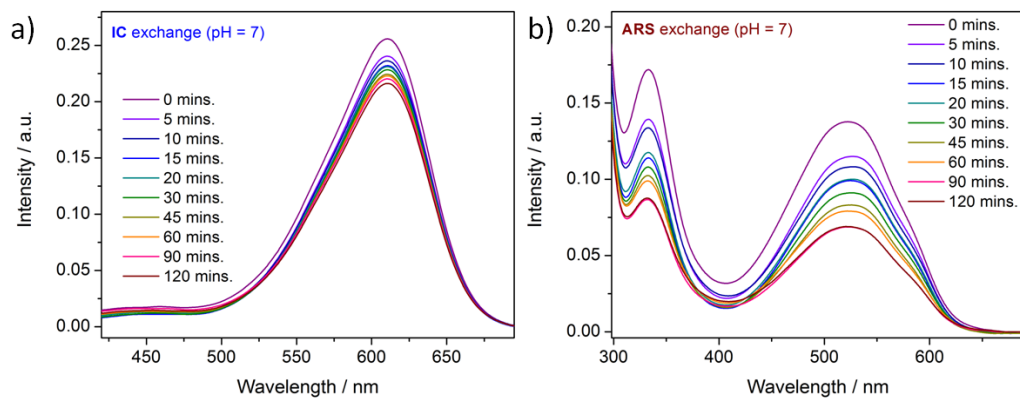
**Appendix 5.48:** UV-Vis spectra of the supernatant MB solution of pH = 10.01 after addition of compound IPM-MOF-201 recorded at different time intervals.



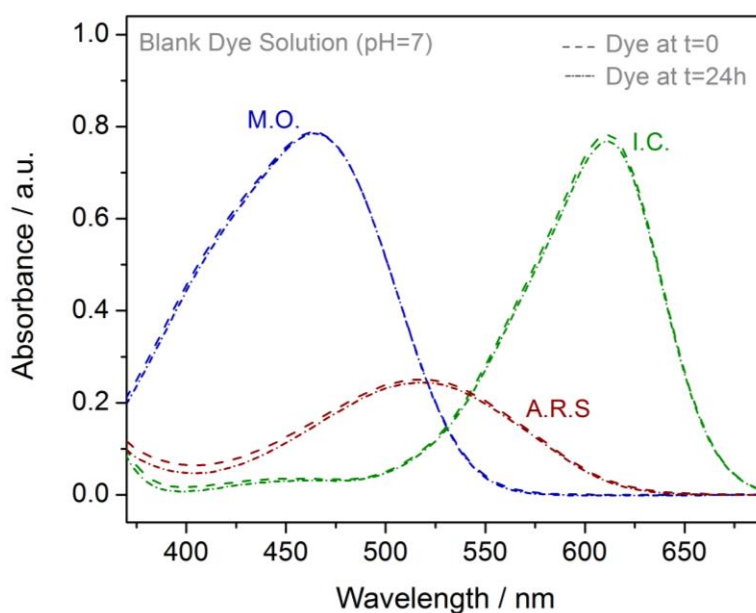
**Appendix 5.49:** Illustration showing capture of anionic dyes (IC & ARS) by compound **IPM-MOF-201**.



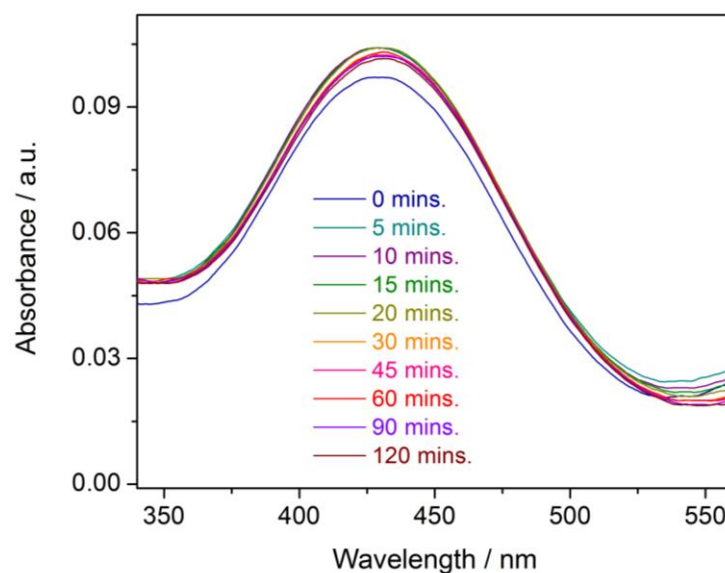
**Appendix 5.50:** Powder x-ray diffraction patterns of calculated (grey), as-synthesized (blue), and aqueous phase dye exchanged phases (MO - purple, IC - green, ARS - wine red).



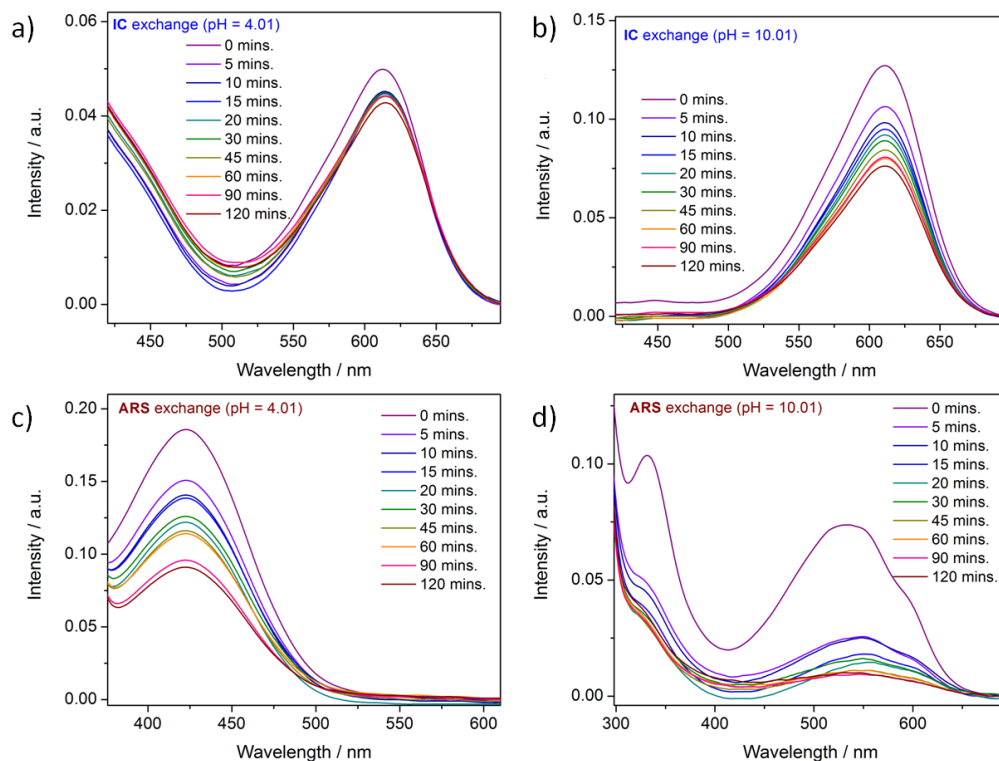
**Appendix 5.51:** UV-Vis spectra of the supernatant aqueous solution of a) IC and b) ARS, after addition of compound **IPM-MOF-201** at different time intervals.



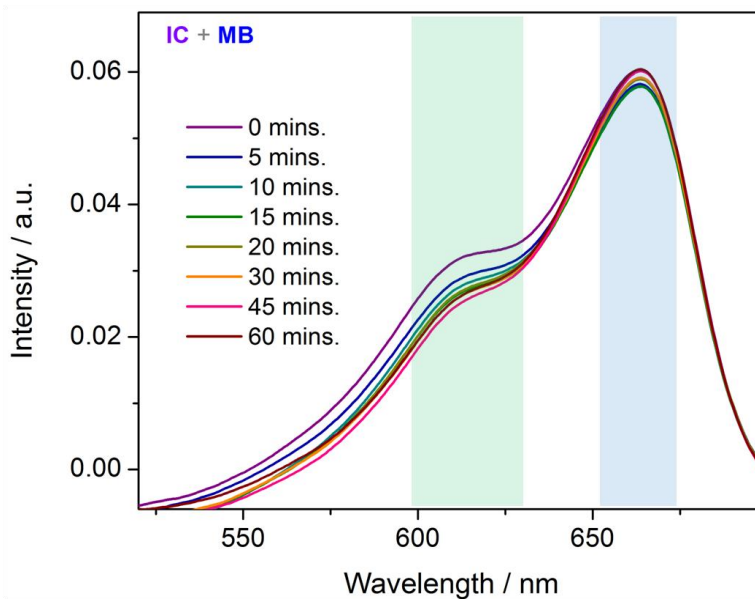
**Appendix 5.52:** UV-Vis spectra of blank aqueous dye solutions at different time intervals.



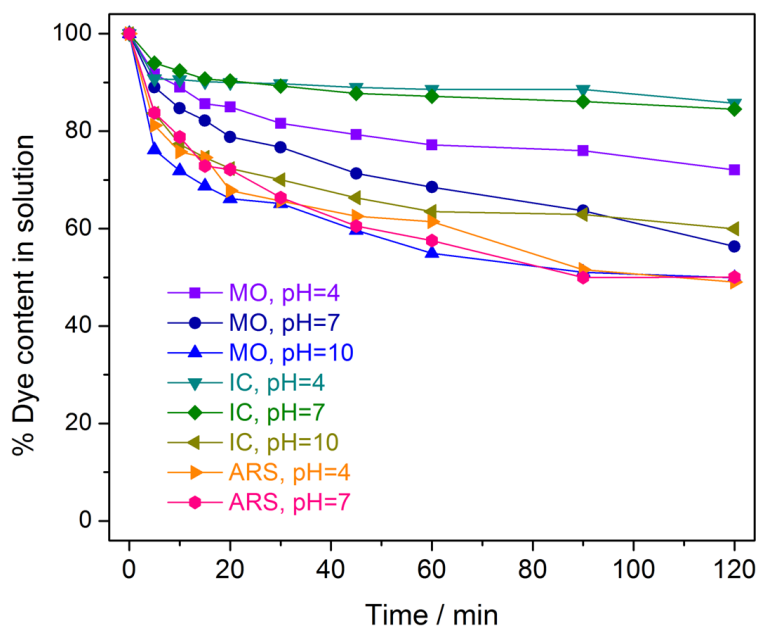
**Appendix 5.53:** UV-Vis spectra of the supernatant aqueous solution of bromothymol blue (BTB) at pH=7 after addition of compound **IPM-MOF-201** at different time intervals.



**Appendix 5.54:** UV-Vis spectra of the supernatant solution of a) IC (pH=4.01), b) IC (pH =10.01), c) ARS (pH=4.01) and d) ARS (pH=10.01), after addition of compound **IPM-MOF-201** to respective phases at different time intervals.

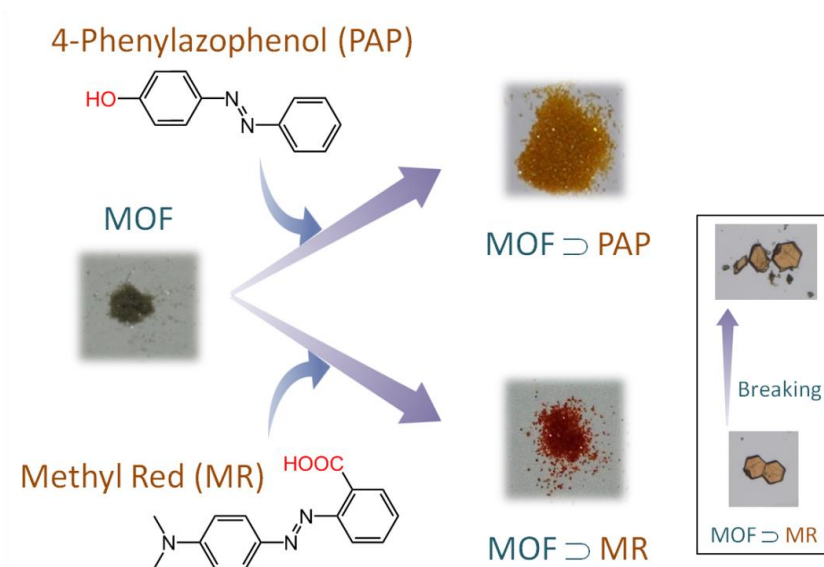


**Appendix 5.55:** UV-Vis spectra of the supernatant solution of equimolar mixture of MB & IC after addition of compound **IPM-MOF-201** recorded at different time intervals.

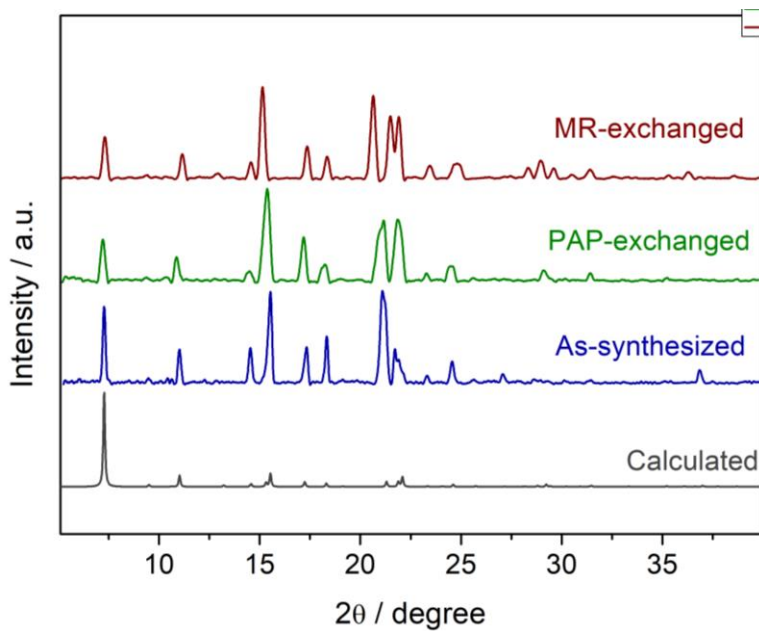


**Appendix 5.56:** Plot showing the rate of decrement in the concentration of the supernatant solution upon addition of compound **IPM-MOF-201**, recorded at different time intervals.

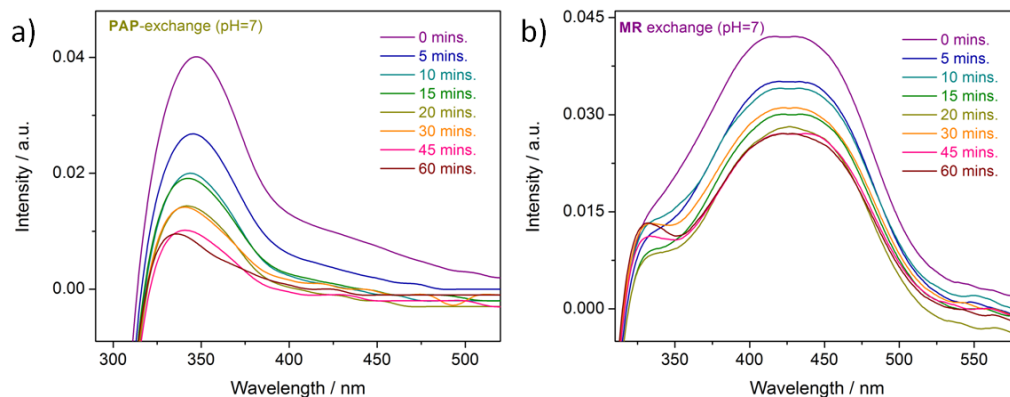




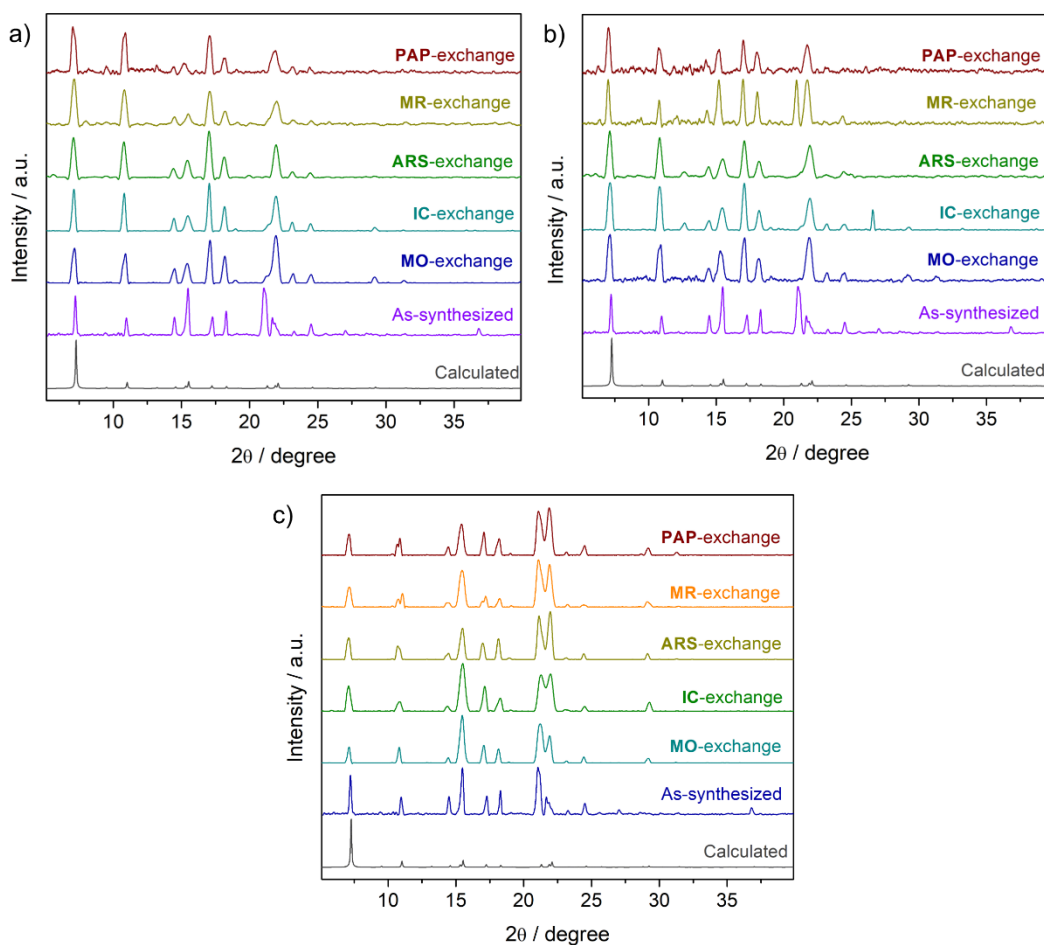
**Appendix 5.57:** Illustration showing capture of anionic dyes (PAP & MR) by compound **IPM-MOF-201**. (Inset): The photograph of MR-exchanged crystals and the fragments after breaking it randomly.



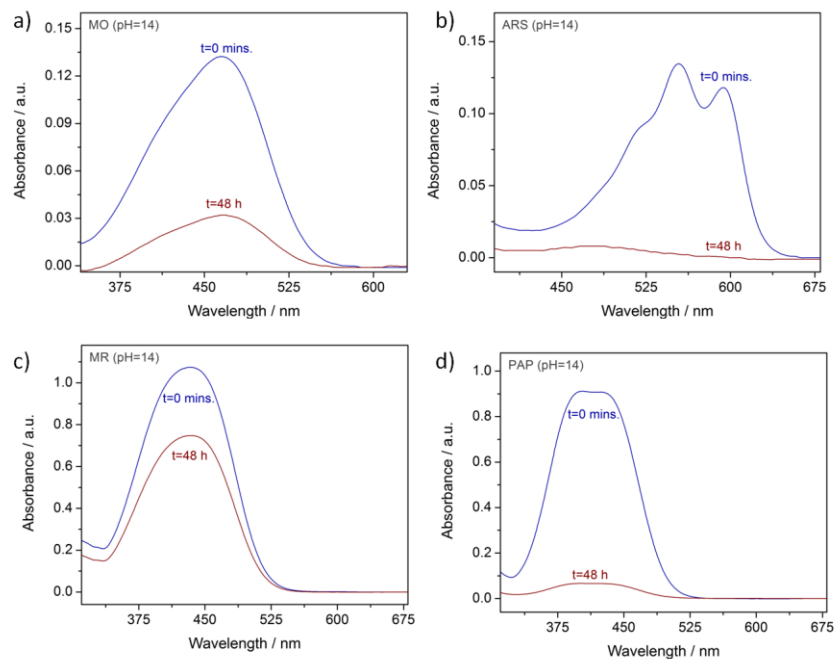
**Appendix 5.58:** Powder x-ray diffraction patterns of calculated (grey), as-synthesized (blue), and aqueous phase dye exchanged phases (PAP - green, MR - wine red).



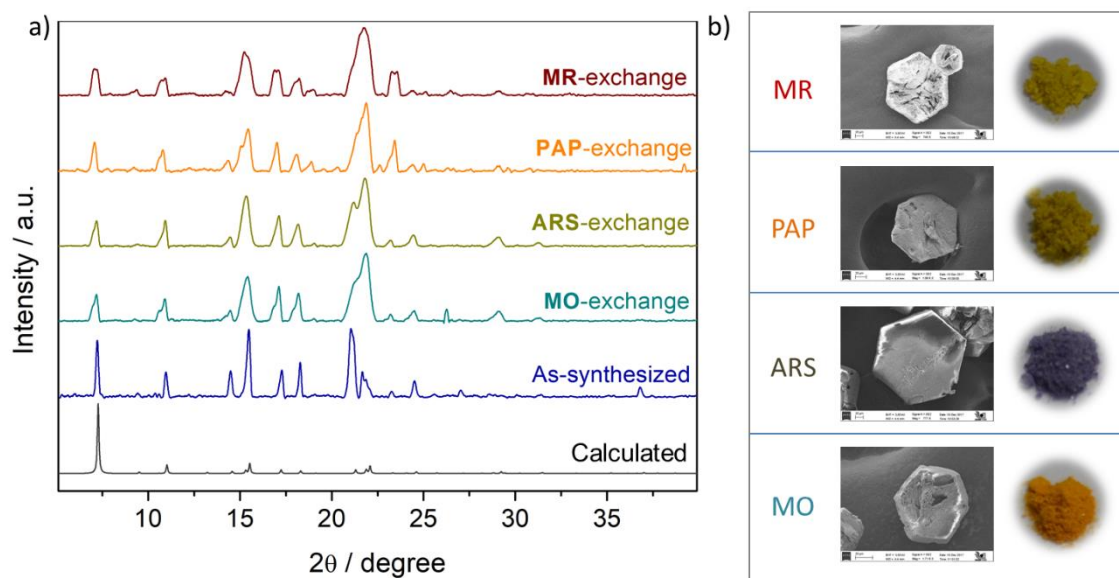
**Appendix 5.59:** UV-Vis spectra of the supernatant aqueous solution of a) PAP and b) MR, after addition of compound IPM-MOF-201 at different time intervals.



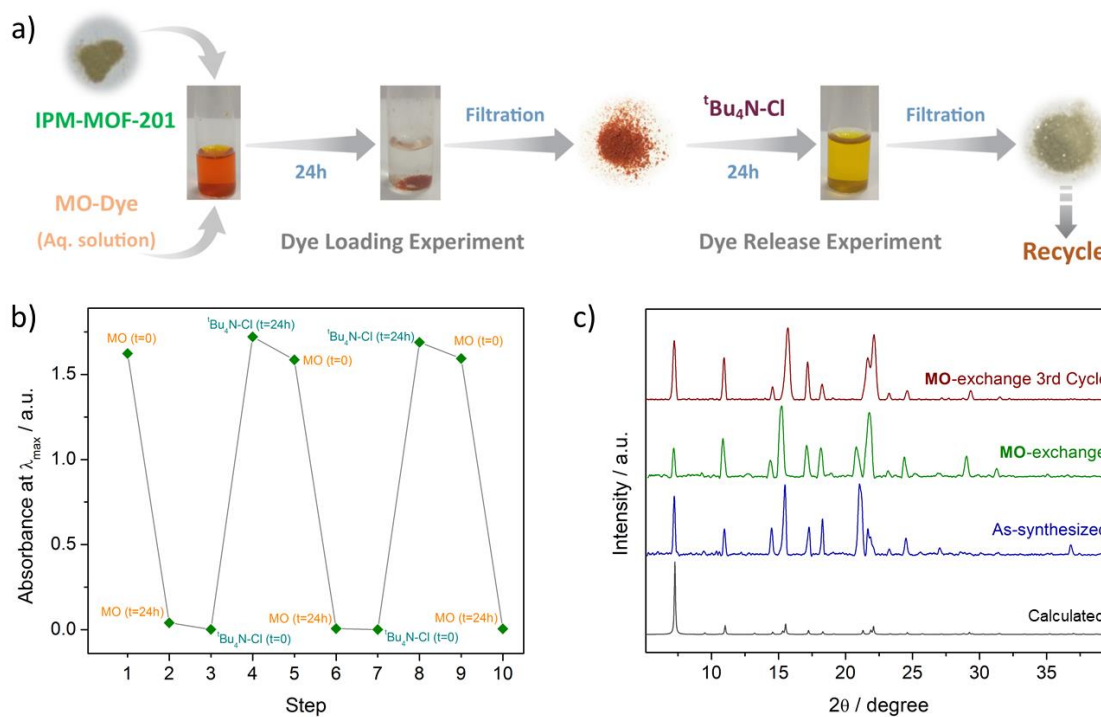
**Appendix 5.60:** Powder x-ray diffraction patterns of dye-exchanged phases at different pH, a) pH = 4.01, b) pH = 10.01 and c) pH = 12.45.



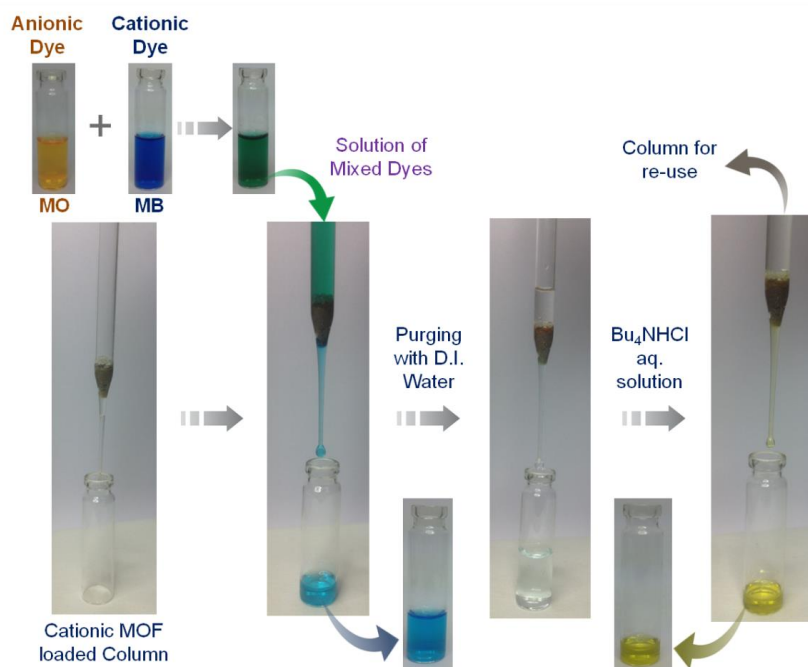
**Appendix 5.61:** UV-vis spectra of the supernatant at pH = 14, after addition of compound **IPM-MOF-201** at two time intervals.



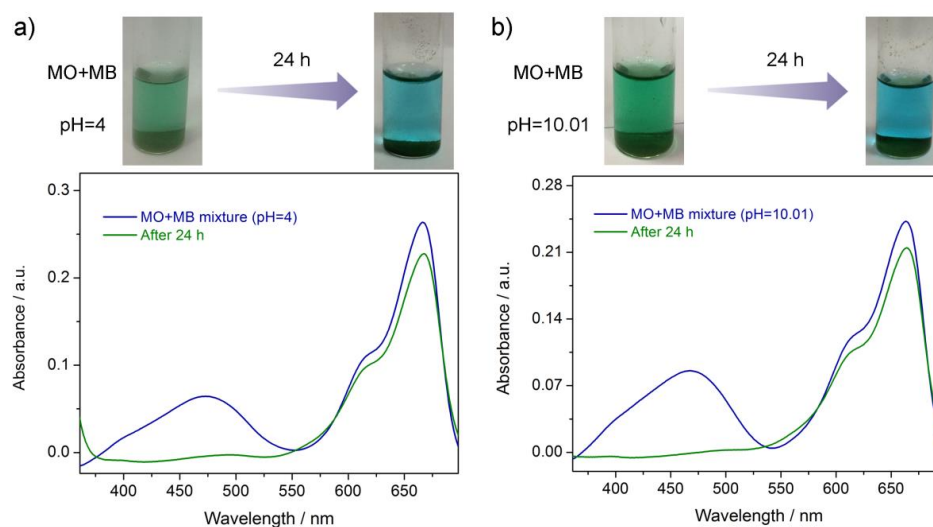
**Appendix 5.62:** a) Powder x-ray diffraction patterns of dye-exchanged phases at pH = 14, b) corresponding SEM images and naked-eye photographs.



**Appendix 5.63:** a) Schematic depiction of the cyclic experiment for capture of MO-dye, b) absorbance of the supernatant during the adsorption-desorption cycles; c) PXRD patterns of the phase recovered after the 3<sup>rd</sup> adsorption cycle.



**Appendix 5.64:** Representation of the selective dye capture process by a MOF-loaded column.



**Appendix 5.65:** Naked-eye changes and corresponding UV-Vis spectral profiles for mixtures of methyl orange (MO) [anionic] and methylene blue [cationic] at different time intervals for a) pH=4 and b) pH=10.01.

**Appendix Table S1:** Content of Ni (in ppm) in the supernatant solution recorded using ICP-AES.

Phase	Ni(ppm)
pH = 4 (2 days)	1.85
1N NaOH (1day)	0.485
NMR Supernatant (1 day)	0.033

**Appendix Table S2.** Crystal data and structure refinement for **IPM-MOF-201**.

Identification code	IPM-MOF-201 (CCDC 1561299)	
Empirical formula	C <sub>54</sub> H <sub>42</sub> N <sub>14</sub> Ni	
Formula weight	945.72	
Temperature	100(2) K	
Wavelength	0.71073 Å	
Crystal system	Trigonal	
Space group	R-3	
Unit cell dimensions	a = 16.0448 (10) Å	α = 90°
	b = 16.0448 (10) Å	β = 90°
	c = 25.0057 (18) Å	γ = 120°
Volume	5574.9 (8) Å <sup>3</sup>	
Z	3	
Density (calculated)	0.845 Mg/m <sup>3</sup>	
Absorption coefficient	0.30 mm <sup>-1</sup>	
F(000)	1476	
Crystal size	0.17 x 0.12 x 0.10 mm <sup>3</sup>	
Theta range for data collection	2.2 to 28.4°.	
Index ranges	-19 ≤ h ≤ 21, -21 ≤ k ≤ 21, -33 ≤ l ≤ 33	
Reflections collected	46123	
Independent reflections	3119 [R(int) = 0.131]	
Completeness to theta = 28.42°	0.999	
Refinement method	Full-matrix least-squares on F <sup>2</sup>	
Data / restraints / parameters	3119 / 0 / 105	
Goodness-of-fit on F <sup>2</sup>	1.164	
Final R indices [I > 2σ(I)]	R <sub>I</sub> = 0.090, wR <sub>2</sub> = 0.2959	
R indices (all data)	R <sub>I</sub> = 0.1542, wR <sub>2</sub> = 0.334	
Largest diff. peak and hole	0.43 and -0.37 e.Å <sup>-3</sup>	

**Appendix Table S3:** Comparison of unit cell parameters of the compound treated under different

conditions.

<b>Cell Parameters</b>	<b>As-synthesized</b>	<b>Dipped in pH=4</b>	<b>Dipped in 1N NaOH</b>
<i>a</i>	16.0448(10)	15.95±0.05	15.96±0.07
<i>b</i>	16.0448(10)	15.95±0.05	15.96±0.07
<i>c</i>	25.0057(18)	25.12±0.09	25.02±0.012
$\alpha=\beta$	90	90	90
$\gamma$	120	120	120
Volume ( $\text{\AA}^3$ )	5574.9(8)	5540±30	5520±50

## 5.6 References

1. (a) Long, J. R.; Yaghi, O. M., *Chem. Soc. Rev.* **2009**, *38*, 1213-1214. (b) Horike, S.; Shimomura, S.; Kitagawa, S., *Nat. Chem.* **2009**, *1*, 695-704. (c) Furukawa, H.; Cordova, K. E.; O’Keeffe, M.; Yaghi, O. M., *Science*, **2013**, DOI: 10.1126/science.1230444. (d) Zhou, H. C.; Kitagawa, S., *Chem. Soc. Rev.* **2014**, *43*, 5415-5418. (e) Howarth, A. J.; Peters, A. W.; Vermeulen, N. A.; Wang, T. C.; Hupp, J. T.; Farha, O. K., *Chem. Mater.* **2017**, *29*, 26-39. (f) Maurin, G.; Serre, C.; Cooper, A.; Ferey, G., *Chem. Soc. Rev.* **2017**, *46*, 3104-3107.
2. (a) Farrusseng, D.; Aguado, S.; Pinel, C., *Angew. Chem. Int. Ed.* **2009**, *48*, 7502-7513. (b) Horcajada, P.; Gref, R.; Baati, T.; Allan, P. K.; Maurin, G.; Couvreur, P.; Ferey, G.; Morris, R. E.; Serre, C., *Chem. Rev.* **2012**, *112*, 1232-1268. (c) Cui, Y.; Yue, Y.; Qian, G.; Chen, B., *Chem. Rev.* **2012**, *112*, 1126-1162. (d) Sen, S.; Nair, N. N.; Yamada, T.; Kitagawa, H.; Bharadwaj, P. K., *J. Am. Chem. Soc.* **2012**, *134*, 19432-19437. (e) Li, S. L.; Xu, Q., *Energy Environ. Sci.* **2013**, *6*, 1656-1683. (f) Ramaswamy, P.; Wong, N. E.; Shimizu, G. K. H., *Chem. Soc. Rev.* **2014**, *43*, 5913-5932. (g) Falcaro, P.; Ricco, R.; Doherty, C. M.; Liang, K.; Hill, A. J.; Styles, M. J., *Chem. Soc. Rev.* **2014**, *43*, 5513-5560. (h) Howarth, A. J.; Liu, Y.; Hupp, J. T.; Farha, O. K., *CrystEngComm* **2015**, *17*, 7245-7253. (i) Sun, L.; Campbell, M. G.; Dinca, M., *Angew. Chem. Int. Ed.* **2016**, *55*, 3566-3579. (j) Li, B.; Chrzanowski, M.; Zhang, Y.; Ma, S., *Coord. Chem. Rev.* **2016**, *307*, 106-129. (k) Aguilera-Sigalat, J.; Bradshaw, D., *Coord. Chem. Rev.* **2016**, *307*, 267-291. (l) Bao, Z.; Chang, G.; Xing, H.; Krishna, R.; Ren, Q.; Chen, B., *Energy Environ. Sci.* **2016**, *9*, 3612-3641. (m) Lustig, W. P.; Mukherjee, S.; Rudd, N. D.; Desai, A. V.; Li, J.; Ghosh, S. K., *Chem. Soc. Rev.* **2017**, *46*, 3242-3285.
3. (a) Karmakar, A.; Desai, A. V.; Ghosh, S. K., *Coord. Chem. Rev.* **2016**, *307*, 313-341. (b) Li, P.; Vermeulen, N. A.; Gong, X.; Malliakas, C. D.; Stoddart, J. F.; Hupp, J. T.; Farha, O. K., *Angew. Chem. Int. Ed.* **2016**, *55*, 10358-10362.
4. (a) Canivet, J.; Fateeva, A.; Guo, Y.; Coasne, B.; Farrusseng, D., *Chem. Soc. Rev.* **2014**, *43*, 5594-5617. (b) Burtch, N. C.; Jasuja, H.; Walton, K. S., *Chem. Rev.* **2014**, *114*, 10575-10612. (c) Qadir, N.; Said, S. A. M.; Bahaidarah, H. M., *Microporous Mesoporous Mater.* **2015**, *201*, 61-90. (d) Hendon, C. H.; Reith, A. J.; Korzyński, M. D.; Dinca, M., *ACS Cent. Sci.* **2017**, *3*, 554-563.
5. (a) Ferey, G.; Mellot-Draznieks, C.; Serre, C.; Millange, F.; Dutour, J.; Surble, S.; Margiolaki, I., *Science* **2005**, *309*, 2040-2042. (b) Park, K. S.; Ni, Z.; Cote, A. P.; Choi, J. Y.; Huang, R.; Uribe-Romo, F. J.; Chae, H. K.; O’Keeffe, M.; Yaghi, O. M., *Proc. Natl. Acad. Sci. U.S.A.*, **2006**, *103*, 10186-10191. (c) Cavka, J. H.; Jabosken, S.; Olsbye, U.; Guillou, N.; Lamberti, C.; Bordiga, S.; Lillerud, K. P., *J. Am. Chem. Soc.* **2008**, *130*, 13850-13851. (d) Howarth, A. J.; Liu, Y.; Li, P.; Li, Z.; Wang, T. C.; Hupp, J. T.; Farha, O. K., *Nat. Rev. Mater.* **2016**, DOI: 10.1038/natrevmats.2015.18. (e) Wang, B.; Lv, X.-L.; Feng, D.; Xie,



L.-H.; Zhang, J.; Li, M.; Xie, Y.; Li, J.-R.; Zhou, H.-C., *J. Am. Chem. Soc.* **2016**, *138*, 6204-6216. (f) Liu, T.-F.; Feng, D.; Chen, Y.-P.; Zou, L.; Bosch, M.; Yuan, S.; Wei, Z.; Fordham, S.; Wang, K.; Zhou, H.-C., *J. Am. Chem. Soc.* **2015**, *137*, 413-419. (g) Wang, C.; Liu, X.; Demir, N. K.; Chen, J. P.; Li, K.; *Chem. Soc. Rev.* **2016**, *45*, 5107-5134. (h) Duan, J.; Jin, W.; Kitagawa, S., *Coord. Chem. Rev.* **2017**, *332*, 48-74. (i) Wang, K.; Lv, X.-L.; Feng, D.; Li, J.; Chen, S.; Sun, J.; Song, L.; Xie, Y.; Li, J.-R.; Zhou, H.-C., *J. Am. Chem. Soc.* **2016**, *138*, 914-919. (j) Bai, Y.; Dou, Y.; Xie, L.-H.; Rutledge, W.; Li, J.-R.; Zhou, H.-C., *Chem. Soc. Rev.* **2016**, *45*, 2327-2367.

6. (a) Oliver, S. R. J., *Chem. Soc. Rev.* **2009**, *38*, 1868-1881. (b) Banerjee, D.; Kim, D.; Schweiger, M. J.; Kruger, A. A.; Thallapally, P. K., *Chem. Soc. Rev.* **2016**, *45*, 2724-2739. (c) Kumar, P.; Pournara, A.; Kim, K.-H.; Bansal, V.; Rapti, S.; Manos, M. J., *Prog. Mater. Sci.* **2017**, *86*, 25-74.

7. (a) Fei, H.; Rogow, D. L.; Oliver, S. R. J., *J. Am. Chem. Soc.* **2010**, *132*, 7202-7209. (b) Schoedel, A.; Wojtas, L.; Kelley, S. P.; Rogers, R. D.; Eddaoudi, M.; Zaworotko, M. J., *Angew. Chem. Int. Ed.* **2011**, *50*, 11421-11424. (c) Ma, J.-P.; Yu, Y.; Dong, Y.-B., *Chem. Commun.* **2012**, *48*, 2946-2948. (d) Manna, B.; Chaudhari, A. K.; Joarder, B.; Karmakar, A.; Ghosh, S. K., *Angew. Chem. Int. Ed.* **2013**, *52*, 998-1002. (e) Chen, Y.-Q.; Li, G.-R.; Chang, Z.; Qu, Y.-K.; Zhang, Y.-H.; Bu, X.-H., *Chem. Sci.* **2013**, *4*, 3678-3682. (f) Hou, S.; Liu, Q.-K.; Ma, J.-P.; Dong, Y.-B., *Inorg. Chem.* **2013**, *52*, 3225-3235. (g) Manna, B.; Desai, A. V.; Ghosh, S. K., *Dalton Trans.* **2016**, *45*, 4060-4072. (h) Sheng, D.; Zhu, L.; Xu, C.; Xiao, C.; Wang, Y.; Wang, Y.; Chen, L.; Diwu, J.; Chen, J.; Chai, Z.; Albrecht-Schmitt, T. E.; Wang, S., *Environ. Sci. Technol.* **2017**, *51*, 3471-3479.

8. (a) Colombo, V.; Galli, S.; Choi, H. J.; Han, G. D.; Maspero, A.; Palmisano, G.; Masciocchi, N.; Long, J. R., *Chem. Sci.* **2011**, *2*, 1311-1319. (b) Zhang, J.-P.; Zhang, Y.-B.; Lin, J.-B.; Chen, X.-M., *Chem. Rev.* **2012**, *112*, 1001-1033. (c) Pettinari, C.; Tabacaru, A.; Galli, S., *Coord. Chem. Rev.* **2016**, *307*, 1-31. (d) He, T.; Zhang, Y.-Z.; Wang, B.; Lv, X.-L.; Xie, L.-H.; Li, J.-R., *ChemPlusChem*, **2016**, *81*, 864-871. (e) Rieth, A. J.; Tulchinsky, Y.; Dinca, M., *J. Am. Chem. Soc.*, **2016**, *138*, 9401-9404.

9. Chen, S.-S., *CrystEngComm* **2016**, *18*, 6543-6565.

10. (a) Desai, A. V.; Manna, B.; Karmakar, A.; Sahu, A.; Ghosh, S. K., *Angew. Chem. Int. Ed.* **2016**, *55*, 7811-7815. (b) Lv, X.-L.; Wang, K.; Wang, B.; Su, J.; Zou, X.; Xie, Y.; Li, J.-R.; Zhou, H.-C., *J. Am. Chem. Soc.* **2017**, *139*, 211-217.

11. (a) Fei, H.; Rogow, D. L.; Oliver, S. R. J., *J. Am. Chem. Soc.* **2010**, *132*, 7202-7209. (b) Fei, H.; Oliver, S. R. J., *Angew. Chem. Int. Ed.* **2011**, *50*, 9066-9070. (c) Fei, H.; Han, C. S.; Robins, J. C.; Oliver, S. R. J., *Chem. Mater.* **2013**, *25*, 647-652. (d) Sergo, K. M.; Han, C. S.; Bresler, M. R.; Citrak, S. C.;

Abdollahian, Y.; Fei, H.; Oliver, S. R. J., *Inorg. Chem.* **2015**, *54*, 3883-3888. (e) Yang, H.; Fei, H., *Chem. Commun.* **2017**, *53*, 7064-7067.

12. *SAINT Plus*, version 7.03; Bruker AXS Inc.: Madison, WI, **2004**.
13. Krause, L.; Herbst-Irmer, R.; Sheldrick, G. M.; Stalke, D., *J. Appl. Cryst.* **2015**, *48*, 3-10.
14. Sheldrick, G. M., *Acta. Cryst.*, **2008**, *A64*, 112-122.
15. Sheldrick, G. M., *Acta. Cryst.*, **2015**, *C71*, 3-8.
16. Farrugia, L., *WinGX*, version 1.80.05; University of Glasgow: Glasgow, Scotland, **2009**.
17. Spek, A. L., *Acta. Cryst.*, **2015**, *C71*, 9-18.
18. Blatov, V. A., *TOPOS*. Samara State University, Russia, **2004**.
19. (a) Zheng, S.-R.; Yang, Q.-Y.; Liu, Y.-R.; Zhang, J.-Y.; Tong, Y.-X.; Zhao, C.-Y.; Su, C.-Y., *Chem. Commun.*, **2008**, *0*, 356-358. (b) Yao, X.-Q.; Cao, D.-P.; Hu, J.-S.; Li, Y.-Z.; Guo, Z.-J.; Zheng, H.-G., *Cryst. Growth Des.* **2011**, *11*, 231-239. (c) Mitina, T. G.; Blatov, V. A., *Cryst. Growth Des.* **2013**, *13*, 1655-1664. (d) Wang, R.; Wang, Z.; Xu, Y.; Dai, F.; Zhang, L.; Sun, D., *Inorg. Chem.* **2014**, *53*, 7086-7088. (e) Liu, S.-S.; Yuan, S.; Li, X.-Y.; Miao, S.; Yu, Z.-W.; Wang, X.-P.; Sun, D., *Inorg. Chim. Acta* **2014**, *416*, 195-199. (f) Guillermin, V.; Kim, D.; Eubank, J. F.; Luebke, R.; Liu, X.; Adil, K.; Lah, M. S.; Eddaoudi, M., *Chem. Soc. Rev.* **2014**, *43*, 6141-6172.
20. (a) Li, B.; Zhang, Y.; Krishna, R.; Yao, K.; Han, Y.; Wu, Z.; Ma, D.; Shi, Z.; Pham, T.; Space, B.; Liu, J.; Thallapally, P. K.; Liu, J.; Chrzanowski, M.; Ma, S., *J. Am. Chem. Soc.* **2014**, *136*, 8654-8660. (b) Samanta, P.; Desai, A. V.; Anothumakkool, B.; Shirolkar, M. M.; Karmakar, A.; Kurungot, S.; Ghosh, S. K., *J. Mater. Chem. A* **2017**, *5*, 13659-13664.
21. Wang, C.-C.; Li, J.-R.; Lv, X.-L.; Zhang, Y.-Q.; Guo, G., *Energy Environ. Sci.* **2014**, *7*, 2831-2867.
22. Allen, S.; Koumanova, B., *J. Univ. Chem. Technol. Metall.* **2005**, *40*, 175-192.
23. (a) Robinson, T.; McMullan, G.; Marchant, R.; Nigam, P., *Biores. Technol.* **2001**, *77*, 247-255. (b) Rawat, D.; Mishra, V.; Sharma, R. S., *Chemosphere* **2016**, *155*, 591-605.
24. (a) Crini, G., *Bioresour. Technol.* **2006**, *97*, 1061-1085. (b) Ayati, A.; Ahmadpur, A.; Bamoharram, F. F.; Tanhaei, B.; Manttari, M.; Lahtinen, M.; Sillanpaa, M., *Sep. Purif. Technol.* **2014**, *133*, 415-420. (c) Sarkka, H.; Bhatnagar, A.; Sillanpaa, M., *J. Electroanal. Chem.* **2015**, *754*, 46-56. (d) Singh, R. L.; Singh,

P. K.; Singh, R. P., *Int. Biodeter. Biodegr.* **2015**, *104*, 21-31. (e) Samanta, P.; Chandra, P.; Desai, A. V.; Ghosh, S. K., *Mater. Chem. Front.* **2017**, *1*, 1384-1388.

25. (a) Nickerl, G.; Notzon, A.; Heitbaum, M.; Senkovska, I.; Glorius, F.; Kaskel, S., *Cryst. Growth Des.* **2013**, *13*, 198-203. (b) Zhao, X.; Bu, X.; Wu, T.; Zheng, S.-T.; Wang, L.; Feng, P., *Nat. Commun.* **2013**, DOI: 10.1038/ncomms3344. (c) Chen, D.-i.; Shi, W.; Cheng, P., *Chem. Commun.* **2015**, *51*, 370-372. (d) Song, B.-Q.; Wang, X.-L.; Zhang, Y.-T.; Wu, X.-S.; Liu, H.-S.; Shao, K.-Z.; Su, Z.-M., *Chem. Commun.* **2015**, *51*, 9515-9518. (e) Gao, C.-Y.; Yang, Y.; Ai, J.; Tian, H.-R.; Li, L.-J.; Yang, W.; Dang, S.; Sun, Z.-M., *Chem. Eur. J.* **2016**, *22*, 11652-11659. (f) Yu, P.; Li, Q.; Hu, Y.; Liu, N.; Zhang, L.; Su, K.; Qian, J.; Huang, S.; Hong, M., *Chem. Commun.* **2016**, *52*, 7978-7981. (g) Jia, Y.-Y.; Ren, G.-J.; Li, A.-L.; Zhang, L.-Z.; Feng, R.; Zhang, Y.-H.; Bu, X.-H., *Cryst. Growth Des.* **2016**, *16*, 5593-5597. (h) Li, C.-P.; Zhou, H.; Wang, S.; Yuan, H.-H.; Zhang, S.-Z.; Du, M., *Chem. Commun.* **2017**, *53*, 4767-4770. (i) Zhao, N.; Sun, F.; Zhang, N.; Zhu, G., *Cryst. Growth Des.* **2017**, *17*, 2453-2457. (j) Nath, K.; Maity, K.; Biradha, K., *Cryst. Growth Des.* **2017**, *17*, 4437-4444. (k) Li, Q.; Xue, D.-X.; Zhang, Y.-F.; Zhang, Z.-H.; Gao, Z.; Bai, J., *J. Mater. Chem. A* **2017**, *5*, 14182-14189.

---

## *Chapter 6*

---

### **Summary and Perspectives**

## 6.1 Summary and Perspectives

In a nutshell, the work carried out in this thesis demonstrates the feasibility of MOFs built from neutral N-donor based linkers as effective solid sorbents for the recognition and capture of toxic environmental pollutants present in air and water. Also, the feature of structure-property correlation in MOFs has been further emphasized with developing systems which can be applied for specific targeted species. Hitherto, owing to weak stability of frameworks constructed from neutral donor ligands, application studies were severely limited; in particular the lack of stable compounds had stalled the development of cationic MOFs which offer several unique advantages inaccessible by other MOF compounds. Especially, the rational approaches to afford stable compounds is a take-away outcome from the present findings. This is highly important as very few MOF compounds have been found to present resistance to chemical extremities, strongly restricting the progress towards practical implementation.

Although stability at the molecular level is one crucial aspect, the subsequent challenges include converting these materials into workable form, as MOFs which are obtained as dispersed powders are uneasy to be applied as solid sorbents directly. Apart from this, the retention of performance from particle scale to the level of workable form along-with their toxicity studies in real-time conditions are some vital aspects which need to be examined for practical implementation of these materials. In addition to these challenges, cost considerations and scalability are some of the issues which are being currently investigated thoroughly by researchers working in the domain of MOFs. Thus the simultaneous development of functional MOFs for remediation of targeted environmental species, which are stable under operating conditions and can be applied in workable forms is expected to be line of research over the next few years.